CORA Cork Open Research Archive
Cartlann Taighde Oscailte Chorcaí

Title	Computational studies on metal-organic frameworks as catalysts
Authors	Pareras, Gerard
Publication date	2021-12-16
Original Citation	Pareras, G. 2021. Computational studies on metal-organic frameworks as catalysts. PhD Thesis, University College Cork.
Type of publication	Doctoral thesis
Rights	© 2021, Gerard Pareras. - https://creativecommons.org/licenses/by-nc-nd/4.0/
Download date	2026-11-15 13:39:04
Item downloaded from	https://hdl.handle.net/10468/13186



UCC
University College Cork, Ireland
Coláiste na hOllscoile Corcaigh

Ollscoil na hÉireann, Corcaigh

National University of Ireland, Cork



Computational Studies on Metal-Organic Frameworks as Catalysts

Thesis presented by

Gerard Pareras, MSc

https://orcid.org/0000-0002-8435-3297

for the degree of

Doctor of Philosophy

University College Cork

School of Chemistry

Head of School/Department: Dr. Humphrey Moynihan

Supervisor(s): Dr. Davide Tiana

2021

Table of Contents

Declaration III
Acknowledgments IV
Abstract VI
Full list of publications VIII
List of Figures IX
List of tables XVII
Chapter 1. Introduction 23
Section 1. Catalysis 24
Section 2. Metal-Organic Frameworks 26
2.1 Structural properties of MOFs 27
2.2 Applications of MOFs 29
2.2.1 Gas adsorption, storage and separation. 29
2.2.2 Catalysis 30
Section 3. Catalysis and MOFs 32
3.1 Metal inorganic nodes as active sites 33
3.2 Organic and pseudo-organic linkers as active sites 36
3.3 Encapsulation of active sites 38
3.4 Post-synthetic active site modifications 39
3.5 Unique catalytic applications 42
Section 4. Computational chemistry and molecular modelling 45
4.1 Electronic structure calculations on MOFs 45
4.2 Molecular cluster calculations 45
4.3 Periodic Boundary Conditions (PBC) 47
4.4 Computational methods used in this thesis 48
Section 5. Bibliography 50
Chapter 2. General objectives 64
Section 1. The manuscript 65

Section 2. Objectives.....66

Chapter 3. Computationally aided design of defect-appended aliphatic amines for CO_2 activation within UiO-66.....68

Chapter 4. UiO-66 mediated methyl acrylate formation from the direct electrophilic nickelalactone ring opening with methyl iodate 76

Chapter 5. Metal-organic frameworks as kinetic modulators for branched selectivity in hydroformylation.....92

Annex: author's contribution and unpublished data 111

Chapter 6. MOF encapsulation of Ru olefin metathesis catalysts to block catalyst decomposition 120

Chapter 7. Conclusions and Future Work.....142

Conclusions.....143

Future Work 145

Supplementary material for chapter 3 147

Supplementary material for chapter 4 155

Supplementary material for chapter 5 159

Supplementary material for chapter 6 196

Annex 1: Computational chemistry 285

Declaration

This is to certify that the work I am submitting is my own and has not been submitted for another degree, either at University College Cork or elsewhere. All external references and sources are clearly acknowledged and identified within the contents. I have read and understood the regulations of University College Cork concerning plagiarism and intellectual property.

Acknowledgments

I will start apologising myself as for sure I will forget someone; it is difficult to remember everyone that walked next to me at some point during this journey we call Ph.D. where we do not only grow as researched but more important as persons. I will take the freedom to say thank you to all my friends and family from Catalunya, my homeland, in our lovely language, the Catalan. Where to begin?

I think I will start saying thank you to this person that gave me the opportunity to start my career as a researcher and stayed next to me, being extremely patient with me, and this is my supervisor Davide, that more than a supervisor is a friend. I remember the though moments at the beginning of the Ph.D. UCC was a new place and they had strange ways to do things (at least for me), however we managed to finally obtain that card, I was finally able to get in and out of that office between two labs freely! Now that I am writing this, I remember all the setbacks we had to overcome during these four years, like finding extra funding for the project, writing proposals to get some computational time and do not forget the biggest one called COVID… No matter which was the problem that we always had time to go for a pint on Friday's evening. And we finally got it to the end and pretty well indeed. Davide, I wish you the best in your future projects as well as in you future time in Cork.

Following with that person that was there also, maybe not from the beginning, but I can say you were my big brother in Ireland. Adrià, el tio que quan el vaig conèixer els divendres feia classe de fer el pi, quin màquina. Podria explicar mil histories de tots els dies (perquè sí, ens veiem cada dia), però encara no se com et vaig liar per jugar a handbol i vas acabar al comitè i tot, be també t'agrada el marro eh! Com no oblidar les cheese and wine parties i tots els socials, els dos catalanets per allà fent de les seves. Ara et serè sincer, i molt podria dir que sort en tinc que et vaig conèixer, molt segurament el meu temps a Irlanda no hagués estat ni de bon tros la meitat de divertit, però no tot era diversió, també ens em vist en apures i podria dir que ens tenim l'un a l'altre (amb permís de la Sílvia). Espero que podem celebrar el conferring junts i tancar aquesta etapa amb un últim dinar al sicilià, o una altre hamburguesa al son of a bun o, una pizza al tom barris o una pinta al mardyke, buf masses llocs per no oblidar, crec que ens hi haurem d'estar una bona temporada!

No em puc deixar a les persones més importants, que amb el seu amor incondicional han fet de mi la persona que soc. Mama, Papa, Anna, se que soc capaç de marxar a mes de 1000 km de casa i estar dies sense dir res però perquè sé que sabeu que tot va bé. Tot i així no vol dir que no pensi amb vosaltres i que no fos un fet que enyorés estar a casa, tots aquets dies que he estat fora us he dut al cor i ha sigut una empenta per aquells dies en que la ciència, i res en general funciona, per seguir endavant. Tenia ganes de tornar a casa essent doctor, però mira al final serè doctor estant a casa, que millor? Mama, Papa, Anna us estimo molt.

Parlant d'amor incondicional, hi ha una persona que ha arribat fa relativament poquet a la meva vida, un any o potser dos ja? Coral, ja saps que m'agrada arrodonir a l'alça per tant posem-ne dos! Vas aparèixer com per art de màgia diguem-ne, però t'has convertit en algú especial, no hi ha decisió que prengui que no l'hagi comentat amb tu i t'has convertit en un recolze essencial de la meva vida que fa que no es trontolli a cada segon. Com tot hem tingut alts i baixos però ens en sortim força bé. Ja saps que no soc gaire hàbil a l'hora de fer grans demostracions d'amor, recorda que encara soc molt català! T'estimo.

Last but no least, com no mencionar la colla d'amics que baix deixar enrere quan vaig emprendre aquest camí però sempre s'han mantingut al meu costat, Sergi, Xavier, Frede, Comas, Josep i un llarg etc. La colla de la uni, Edu, Joel, Tarru, Nuria i com no els del despatx, Silvia, Martí que vam començar tota aquesta historia junts ara farà molts anys enrere. En certa manera també sou partícips d'aquesta tesis. I would like to remember also all the people from the handball club in UCC, in special Jan, they left us a kind of handball team, and we built up a proper club, that was the perfect distraction from all the Ph.D. life issues.

Finalment, també m'agradaria agrair-li tot el suport durant aquets anys tot i no essent el meu supervisor a l'Albert Poater, segurament podríem dir que ets una mica el salvador d'aquesta tesis. Espero que això només hagi estat el principi de molts projectes fructífers en un futur no gaire llunyà!

Abstract

Metal-Organic Frameworks (MOFs) are nanoporous materials containing three-dimensional (3D) periodic networks of metal clusters held together by bridging organic linkers. They are thermally stable, crystalline, and characterized by high porosities and record-breaking surface. Moreover, their stability and perfect crystalline net offer the possibility to perform catalytic processes within its framework as well as intervening as catalysts themself. The applicability of MOFs within the branch of catalysis is immense and makes an impossible task to experimentally explore and test all the possible applications. However, computational chemistry can help in to predict such catalytic behaviour reducing the number of test-and-error experiments by preliminary discarding those that theoretically show no catalytic performance. This manuscript gathers four works (two published, two to be submitted) where computational methodologies have been applied to predict and unveil catalytic applications in different reaction processes. In the first chapter is reported CO_2 activation over defective UiO-66 functionalized with amino acids. DFT calculations confirms not only the activation of CO_2 but also the formation of carbamic acid due to a cooperative effect between the amino acid chains. Following to the second chapter, it has been described that MOF UiO-67 can be functionalized with a TMEDA like homogenous catalyst, to enhance CO_2-ethylene direct coupling reaction. The third chapter is a multidisciplinary work that shows how micropores in metal-organic frameworks (MOFs) push homogeneous catalytic reactions into kinetic regimes inaccessible under standard conditions. Such property allows branched selectivity up to 90% in the Co-catalysed hydroformylation of olefins without directing groups. Finally, chapter 4 describes the encapsulation of Ru olefin catalysts within MOF MIL-101, such encapsulation is a strategy not only for avoiding catalyst decomposition but also to enhance reactivity. All this works apart from studying catalytic performance, selected MOFs have been studied under different computational approaches (molecular cluster and periodic boundary conditions simulations) and using different computational tools (NCI plots, steric maps, frontier molecular orbital, etc.).

Full list of publications

1. Bauer, G., Ongari, D., Tiana, D., Gäumann, P., Rohrbach, T., Pareras, G., Tarik, M., Smit, B. & Ranocchiari, M. *Nat. Commun.* **11**, 1–8 (2020).

2. Pareras, G., Tiana, D. & Poater, A. *Catalysts* **10**, 687 (2020).

Other publications by the author not included in this thesis

3. Gharajedaghi, S., Mohamadnia, Z., Ahmadi, E., Marefat, M., Pareras, G., Simon, S., Poater, A. & Bahri-Laleh, N. *Mol. Catal.* **509**, 111636 (2021).

4. Tabrizi, M., Sadjadi, S., Pareras, G., Nekoomanesh-Haghighi, M., Bahri-Laleh, N. & Poater, A. *J. Colloid Interface Sci.* **581**, 939–953 (2021).

5. Karimi, S., Bahri-Laleh, N., Pareras, G., Sadjadi, S., Nekoomanesh-Haghighi, M. & Poater, A. *J. Ind. Eng. Chem.* **97**, 441–451 (2021).

6. Sadjadi, S., Koohestani, F., Pareras, G., Nekoomanesh-Haghighi, M., Bahri-Laleh, N. & Poater, A. *J. Mol. Liq.* **331**, 115740 (2021).

7. Pareras, G., Szczepanik, D. W., Duran, M., Solà, M. & Simon, S. *J. Org. Chem.* **84**, 15538–15548 (2019).

8. Pareras, G., Palusiak, M., Duran, M., Solà, M. & Simon, S. *J. Phys. Chem. A* **122**, 2279–2287 (2018).

List of Figures

Chapter 1

Figure 1.1 From left to right, visual exemplification of homogeneous, heterogeneous and heterogenized homogeneous catalyst. 25

Figure 1.2 Representation of the different parts of a MOF (MOF-5), from left to right, building blocks (organic linker and metal node), periodic unit cell and crystalline structure. 26

Figure 1.3 Representation of (A) UiO-66, (B) UiO-67, (C) UMCM-1 and (D) MiL-101.....27

Figure 1.4 Schematic representation of, from left to right, MOF-5, IRMOF-3, and IRMOF-10. Adapted from: Ranocchiari, M. & Bokhoven, J. A. Van. *Phys. Chem. Chem. Phys.* 13, 6388–6396 (2011).[12] 29

Figure 1.5 Representations of different gases absorption within MOF-520; (A) CO_2, (B) H_2, (C) CH_4 and (D) N_2O. Wireframe corresponds to carbon and hydrogen atoms (relevant carbon and hydrogen atoms are in grey and white colour respectively), blue colour for nitrogen atoms and red colour for oxygen atoms. 30

Figure 1.6 Example of a portion of the microporous MOF $Mn_3[(Mn_4Cl)_3BTT_8(CH_3OH)_{10}]_2$ (1, H_3BTT = 1,3,5-benzenetristetrazol-5-yl) showing the two different types of Mn^{II} active sites exposed within the three-dimensional pore. Also represented the Cyanosilation reaction catalysed by the crystal. Orange, green, gray, and blue spheres represent Mn, Cl, C, and N atoms, respectively; H atoms and bound MeOH molecules are omitted for clarity. Adapted from: Horike, S., Dincă, M., Tamaki, K. & Long, J. R. *J. Am. Chem. Soc.* 130, 5854–5855 (2008).[104] 35

Figure 1.7 Example of organic linker as an active site. Top: The large cage involved in MIL-101-SO_3H with the readily accessible acid sites. The grey ball highlights the large void inside the cage. b) Schematic illustration for the two types of cages in MIL-101-SO_3H with Brønsted and Lewis acid sites. Bottom: Proposed mechanism for the ring opening of styrene oxide in MeOH catalyzed by the Brønsted acid sites in MIL-101-SO_3H. Adapted from: Zhou, Y. X.,

Chen, Y. Z., Hu, Y., Huang, G., Yu, S. H. & Jiang, H. L. *Chem. - A Eur. J.* 20, 14976–14980 (2014).[121] 38
Figure 1.8 Example of a post modified MOF. Nu-1000 supporting a dihydride iridium pincer complex able to catalyse condensed phase hydrogenation of liquid alkene. Adapted from Rimoldi, M., Nakamura, A., Vermeulen, N. A., Henkelis, J. J., Blackburn, A. K., Hupp, J. T., Stoddart, J. F. & Farha, O. K. *Chem. Sci.* 7, 4980–4984 (2016).[159] 42
Figure 1.10 (Left) Extended structure of MIL-101. (Right) Molecular cluster containing 112 atoms obtained from the periodic geometry and designed to reproduce the environment nearby the metal node (it includes the metal cluster and the six organic linkers attached to it). Cr, C, O and H atoms are represented as dark blue, grey, red, and white spheres, respectively. 47
Figure 1.11 (Left) Extended structure for UiO-66, highlighted the primitive cell. (Right) Represented the geometry used to perform the calculations with the UiO-66 primitive cell under PBC. Zr, C, O and H atoms are represented as blue, grey, red, and white spheres, respectively.....48

Chapter 3

Figure 3.1 Reaction mechanism for the CO_2 activation and posterior carbamic acid obtention.....69
Figure 3.2 Aliphatic amino acids chosen to functionalise UiO-66. 70
Figure 3.3 Optimized geometries for systems; (A) UiO-66_ava_HOUT_3 and (B) UiO-66_gaba_HOUT_3 UiO-66_ava_HOUT_3. Hydrogen bonds are highlighted with block dotted lines. Colour scheme: C = grey, H = white, N = blue. The organic ligand and inorganic node of the MOF are represented as black line and black polyhedral for clarity reason. 71
Figure 3.4 Geometry optimization for system UiO-66_ava_2. Hydrogen bonds highlighted in black dotted lines. Colour scheme: C = grey, H = white, O = red, N =blue. The organic ligand and inorganic node of the MOF are represented as black line and black polyhedral for clarity reason. 72
Figure 3.5 Geometry optimization for system UiO-66_ava_HOUT_6. Hydrogen bonds highlighted in black dotted lines. Colour scheme: C = grey, H = white, O = red, N = blue. The organic ligand and inorganic node of the MOF are represented as black line and black polyhedral for clarity reason. 73

Figure 3.6 Geometry optimization for systems; (A) UiO-66_ava_2_H-tran, (B) UiO-66_ava_HOUT_6_H-tran and (C) UiO-66_ava_HOUT_6_H-back. Colour scheme: C = grey, H = white, O = red, N = blue. The organic ligand and inorganic node of the MOF are represented as black line and black polyhedral for clarity reason. 74

Chapter 4

Figure 4.1 Zero-valent metal mediated acrylic acid formation via direct coupling of carbon dioxide and ethylene.....77

Figure 4.2 First reaction step resulting in the metallacycle formation.....78

Figure 4.3 Hypothetical catalytic cycle for the nickel mediated synthesis of methyl acrylate from the CO_2-ethylene direct coupling and assisted with the methylating agent MeI. 79

Figure 4.4 Left: commercial Bis(dimethylamino)chlorophosphine. Centre: suggested coordination with MOFs. Right: posterior chelation of the Ni centre. 81

Figure 4.5 Reaction energy profile (in $kcal \cdot mol^{-1}$) corresponding to the synthesis of methyl acrylate starting with the electrophilic attack of CH_3I to the nickelalactone. Represented energies from TMEDA (continuous red) and UiO-67 (dot blue) systems. 81

Figure 4.6 Optimized geometry for; UiO-67-DMAP step A, UiO-67-DMAP step TS_AB and UiO-67-DMAP step B. Colour scheme: C = grey, H = white, O = red, N = blue I = purple, P = orange and Ni = green. The organic ligand and inorganic node of the MOF are represented as black line and black polyhedral for clarity reason. 82

Figure 4.7 Optimized geometry for; UiO-67-DMAP step TS_BC and UiO-67-DMAP step C. Colour scheme: C = grey, H = white, O = red, N = blue I = purple, P = orange and Ni = green. The organic ligand and inorganic node of the MOF are represented as black line and black polyhedral for clarity reason. 83

Figure 4.8 Optimized geometry for; UiO-67-DMAP step TS_CD and UiO-67-DMAP step D. Colour scheme: C = grey, H = white, O = red, N = blue I = purple, P = orange and Ni = green. The organic ligand and inorganic node of

the MOF are represented as black line and black polyhedral for clarity reason. 84
Figure 4.9 Structure of the molecular cluster from the UiO-66, the terephthalic acid dimethyl aminophosphine ligand (TFA-DMAP). 84

Chapter 5

Figure 5.1 a) General scheme for the Co-catalysed hydroformylation of olefins. For 1-hexene R = C_4H_9, R1=C_3H_7. b) Accepted mechanism for the Co-catalysed hydroformylation of olefins. 94
Figure 5.2 Structures and molecular formulas of the MOFs used in hydroformylation. a MixUMCM-1-NH_2. b MOF-74(Zn). bdc = 1,4-benzenedicarboxylate; abdc = 2-amino-1,4-benzenedicarboxylate, btb = 4,4′,4″,-benzene-1,3,5-triyl-trisbenzoate and dobdc = 2,5-dioxido-1,4-benzenedicarboxylate. Hydrogen and nitrogen atoms are omitted for clarity. 96
Figure 5.3 a) Experimental branched to linear ratios (B/L) with MixUMCM-1-NH2 (28%) and MOF-74(Zn) relative to the homogeneous B/L as function of syngas pressure (Table S9). b) Calculated relative rates of formation of the branched and linear aldehydes (RB/RL) in the MOFs UMCM-1-NH2 and MOF-74(Zn) and homogeneous phase referenced to the homogeneous system as function of syngas pressure. 103
Figure 5.4 From top to bottom: Optimised adsorption geometry of $HCoCO_4$ with UMCM-1. Optimised adsorption geometry of HCoCO4 and UMCM-1-NH_2. Optimised adsorption geometry of $HCoCO_4$ and MOF-74(Zn). Colour scheme: Co = blue, O = red, C = brown, H = beige, N = pale blue. The organic ligand and inorganic node of the MOF are represented as black line and grey polyhedral for clarity.....112
Figure 5.5 Top left: optimised binding geometry of $HCoCO_3$ and UMCM-1. Top right: optimised binding geometry of $HCoCO_3$ and UMCM-1-NH_2. Bottom: optimised binding geometry of $HCoCO_3$ and MOF-74(Zn). Colour scheme: Co = blue, O = red, C = brown, H = beige, N = pale blue. The organic ligand and inorganic node of the MOF are represented as black line and grey polyhedral for clarity reason. 113

Figure 5.6 On the top, optimized geometry of $HCoCO_4$ and MixUMCM-1- PPh_2 (50%). On the bottom, optimized binding geometry of $HCoCO_3$ and MixUMCM-1-PPh_2 (50%). Colour scheme: Co = blue, O = red, C = brown, H = beige, P = bright blue. The organic ligand and inorganic node of the MOF are represented as black line and grey polyhedral for clarity reason. 113
Figure 5.7 Accepted catalytic cycle for the Co-catalysed hydroformylation of olefines. 115
Figure 5.8 Relative energy profile in kcal/mol for the Co-catalysed hydroformylation of olefines, considering as zero the 18e specie ($Co(CO)_4H$). Represented in blue colour the reaction pathway of the linear product and in red colour the branched product.....115
Figure 5.9 The 2-(diphenylphosphino) terephthalic acid is the specie used as a rough approximation of the organic linker of UMCM-1.....117
Figure 5.10 Relative energy profile in kcal/mol for the Co-catalysed hydroformylation of olefines, considering as zero the activated 16e specie (PPh_2-$Co(CO)_2H$). Represented in blue colour the reaction pathway of the linear product and in red colour the branched product. 118
Figure 5.11 Left: zoom out of the optimised MOF-P-$Co(CO)_3H$ structure, it is observable the different active sites spread along the framework. Right: zoom in on the active site MOF-P-$Co(CO)_3H$ optimised geometry. Colour scheme: Co = pink, O = red, C = grey, H = white, P = orange. The organic ligand and inorganic node of the MOF are represented as black line and black polyhedral for clarity reason. 119

Chapter 6

Figure 6.1 (a) Snapshot of the X-ray for the metal organic framework (MOF) (Cr)MIL-101-SO_3^-(Na·15-crown-5)$^+$,[26] and (b) with the addition of the catalyst AquaMet^{TM} as part of the MOF. 122
Figure 6.2 Three-dimensional (3D) Lewis structure of the olefin metathesis catalysts studied: (a) Hoveyda-type catalyst (HOV); (b) AquaMet^{TM}; (c) MOF-AquaMet^{TM}.....123
Figure 6.3 Calculated reaction profile for the initiation of the neutral HOV catalyst (free energies in kcal/mol). Blue lines correspond the concerted bonding of

ethylene together with the Ru–O bond cleavage (free energies in solvent given in kcal/mol). 124
Figure 6.4 Transition state TS_Ci2 of the opening of the metallacycle for (a) HOV, (b) AquaMet^{TM+} and (c) AquaMet^{TM} (selected distances in Å). 125
Figure 6.5 Snapshot of the MOF from the X-Ray with an inserted ammonium NHC-tagged olefin metathesis catalyst AquaMet^{TM} in a cavity. 129
Figure 6.6 Topographic steric maps of the section of the MOF (plane xy) from the X-ray: (a) orientation of the axis; (b) HOV with a radius of 3.5 Å; (c) MOF with a radius of 10 Å and (d) MOF-AquaMet^{TM} with a radius of 10 Å. The linking C atom of the NHC is on the z axis, and the metal atom is 2 Å below the plane described by the metal and both chloride atoms. The isocontour curves of the steric maps are given in Å. 131
Figure 6.7 NCI plot of the truncated MOF in combination with Precat. 132
Figure 1.9 Representation of the different parameters set within a force field. ...287

Supplementary material for chapter 3

Figure S1 Optimized geometries for systems; (A) UiO-66_gly, (B) UiO-66_ala and (C), UiO-66_gaba and (D) UiO-66_ava. Colour scheme: C = grey, H = white, N = Blue. The organic ligand and inorganic node of the MOF are represented as black line and black polyhedral for clarity reason. 148
Figure S2 Optimized geometries for; (A) UiO-66_ava, (B) UiO-66_ava_NonFun_1 and (C) UiO-66_ava_NonFun_2. Colour scheme: C = grey, H = white, N = Blue. The organic ligand and inorganic node of the MOF are represented as black line and black polyhedral for clarity reason. 151

Supplementary material for chapter 5

Figure S1 Structure of MixUMCM-1-PPh2 (29%).....160
Figure S2 Powder X-Ray pattern of the MOFs used in this work. MixUMCM-1-PPh2 (29%), MOF-74(Mg), MOF-74(Ni) and MOF-74(Co) when starting from top left and going clockwise.....162
Figure S3 Powder X-Ray pattern of the MOFs used in this work. MixUMCM-1-PPh2 (29%), MOF-74(Mg), MOF-74(Ni) and MOF-74(Co) when starting from top left and going clockwise.....163

Figure S4 Powder X-Ray pattern of MixUMCM-1-NH2 (28%) (left) and MOF74(Zn) (right) after (red) and before (black) catalysis respectively. ...163
Figure S5 Nitrogen Physisorption curves of MixUMCM-1-NH2 (28%). Blue and red symbols representing the adsorption and desorption branch respectively. Circles show the values before and triangles the ones after catalysis. 165
Figure S6 Nitrogen Physisorption curves of MOF-74(Zn). Blue and red symbols representing the adsorption and desorption branch respectively. Circles show the values before and triangles the ones after catalysis. 166
Figure S7 Calculated by Horvath-Kawwazoe model for MixUMCM-1-NH2 (28%) before (top) and after (bottom) catalysis. 167
Figure S8 Calculated by Horvath-Kawwazoe model for MOF-74(Zn) before (top) and after (bottom) catalysis. 168
Figure S9 FT-IR spectra. Pristine MOF (top), catalyst-loaded MOF (middle) and catalyst (bottom) for MixUMCM-1-NH2 (28%) (top spectrum) and MOF-74(Zn) (bottom spectrum). 173
Figure S10 Extracted ion chromatogram for the mass of the aldol product (210 u) and mass spectra of the two found compounds compared to the best fitting substance in the database. The two products are likely isomers of the depicted aldol product.....175
Figure S11 Optimised adsorption geometry of HCoCO4 with UMCM-1. Colour scheme: Co = blue, O = red, C = brown, H = white. The organic ligand and inorganic node of the MOF are represented as black line and grey polyhedral for clarity. 181
Figure S12 Optimised adsorption geometry of HCoCO4 and UMCM-1-NH2. Colour scheme: Co = blue, O = red, C = brown, H = white. The organic ligand and inorganic node of the MOF are represented as black line and grey polyhedral for clarity. 181
Figure S13 Optimised adsorption geometry of HCoCO4 and MOF-74(Zn). Colour scheme, Co = blue, O = red, C = brown, H = beige. The organic ligand and inorganic node of the MOF are represented as black line and grey polyhedral for clarity. 181
Figure S14 Optimised binding geometry of HCoCO3 and UMCM-1. Colour scheme: Co = blue, O = red, C = brown, H = beige. The organic ligand and

inorganic node of the MOF are represented as black line and grey polyhedral for clarity.....182
Figure S15 Optimised binding geometry of HCoCO3 and UMCM-1-NH2. Colour scheme: Co = blue, O = red, C = brown, H = beige, N = pale blue. The organic ligand and inorganic node of the MOF are represented as black line and grey polyhedral for clarity.....182
Figure S16 Optimized binding geometry of HCoCO3 and MOF-74(Zn). Colour scheme: Co = blue, O = red, C = brown, H = beige. The organic ligand and inorganic node of the MOF are represented as black line and grey polyhedral for clarity.....182
Figure S17 On the top, optimized geometry of HCoCO4 and MixUMCM-1-PPh2 (50%). On the bottom, optimized binding geometry of HCoCO3 and MixUMCM-1-PPh2 (50%). Colour scheme: Co = blue, O = red, C = brown, H = beige, P = bright blue. The organic ligand and inorganic node of the MOF are represented as black line and grey polyhedral for clarity reason. 183
Figure S18 Torsional scan of the carbonyl group in a representative model for branched aldehydes. The torsional potential was computed using the MP2/6-31G* method and used to fit the parameters for the TraPPE force field. The plot shows the agreement of the fitting and the conformation of the molecule in the maximum and minimum points 184

Supplementary material for chapter 6

Figure S1 NCIplots 231

List of tables

Chapter 4

Table 4.1 Relative energies in kcal·mol^{-1} for the reaction mechanism and the three systems under study. Reaction step A is considered the relative zero. 85

Chapter 5

Table 5.1 Influence of MOFs on the selectivity and reactivity of the Co-catalysed hydroformylation. [a] 98

Table 5.2 Affinity of the different species with the frameworks is reported as percentage occupancy (%occup.) which is related to the average number of molecules of that species in the MOF's simulation box. The error is computed as standard deviation over ten independent simulations. The first column reports the relative density of 1-hexene (Rel. density) computed in the pore volume with respect to the density observed in the homogeneous simulation box (see also Table S17and Table S18). 101

Table 5.3 Substrate scope of the Co-catalysed hydroformylation of olefins without directing groups with MOF additives and comparison with the homogeneously catalysed reaction[a,b].....104

Table 5.4 DFT interaction energy of $HCo(CO)_4$. M-Co (MOF–$COCo(H)(CO)_3$ in the main text) is the adsorption of $HCoCO_4$ to the metal node via its axial carbonyl. M-H (MOF–H-$Co(CO)_4$ in the main text) is the adsorption of $HCoCO_4$ to the metal node via its hydride. L-CO = adsorption of $HCoCO_4$ to the function via its axial carbonyl. 112

Table 5.5 DFT binding energies. M-Co (MOF–$Co(H)(CO)_3$ in the main text) is the binding energy between the metal of the MOF and the Co of $HCoCO_3$. L-Co (MOFFunc–$Co(H)(CO)_3$ in the main text) is the binding energy between the functional group of the MOF and the Co of $HCoCO_3$. 114

Chapter 6

Table 6.1 Relative energies of the reaction profile of the initiation in olefin metathesis with ethylene as a substrate for the Hoveyda catalysts (HOV), with the tagged N-heterocyclic carbene (NHC) ligand, including the chloride

counteranion (AquaMet^{TM}) or not (AquaMet^{TM+}). Energy values in kcal/mol. 125
Table 6.2 Main distances for catalysts HOV, AquaMet^{TM} and MOF-AquaMet^{TM} (in Å). 126
Table 6.3 Conceptual density functional theory (DFT) analysis (μ = chemical potential, η = chemical hardness, ε = Parr electrophicity; in a.u.) for Precat, Act and I14e. 127
Table 6.4 Natural bond orbital (NBO) charge analysis on the metal, oxygen, two Cylidene, CNHC and two chlorides (in e^-).....128
Table 6.5 Relative energies in gas phase (in kcal/mol) of the intermediates for catalysts HOV, AquaMet^{TM} and MOF-AquaMet^{TM}, and including the model of MOF.....129

Supplementary material for chapter 3

Table S1 Protonation of the 1st amine group. Only configurations in which a H bond can be formed between the protonated and the unprotonated amines are favourable. Values are in kcal·mol^{-1}. 148
Table S2 Protonation of the 2nd and 3rd ammine. Values are in kcal·mol^{-1}. The 3rd protonation was not calculated if the 2nd was already energetically unfavourable.....149
Table S3 Binding energy (BE) and geometrical parameters for the adsorption of CO_2 at the inorganic node of UiO-66. Energies in kcal·mol^{-1}; Bond distances in Angstrom; Angle in degree. CO_2 is considered activated when there is an elongation of the CO bond compared to 1.18 Ang, the calculated value for isolated CO_2. 149
Table S4 Binding energy (BE) and geometrical parameters for the adsorption of CO_2. Energies in kcal·mol^{-1}; Bond distances in Angstrom; Angle in degree. CO_2 is considered activated when there is an elongation of the CO bond compared the calculated value for isolated CO_2 = 1.18 Ang. Calculated CN distance in carbamic acid = 1.37 Ang. 150
Table S5 Binding energy (BE) and geometrical parameters for the adsorption of CO_2 in protonated UiO-66_ala. HIN indicates that the transfer is from an OH group of the same inorganic node of the amine, HOUT the H is from another OH. Energies in kcal·mol^{-1}; Bond distances in Angstrom; Angle in degree.

CO_2 is considered activated when there is an elongation of the CO bond compared the calculated value for isolated CO_2 = 1.18 Ang. Calculated CN distance in carbamic acid = 1.37 Ang. 151
Table S6 Binding energies in kcal·mol^{-1} for the CO_2 activated system with different amount of defect functionalisation for the active configurations of unprotonated UiO-66_gaba and UiO-66_ava. 152
Table S7 Binding energies in kcal·mol^{-1} for the CO_2 activated system with different amount of defect functionalisation for the active configurations of protonated UiO-66_ava. 152
Table S8 Hydrogen transfer relative energies for the active unprotonated UiO-66_gaba and UiO-66_ava. Values in kcal·mol^{-1}. 152
Table S9 Hydrogen transfer relative energies for the active protonated UiO-66_ava. Values in kcal·mol^{-1}. 153
Table S10 Relative energies for the active unprotonated UiO-66_gaba and UiO-66_ava with only two amines for the hydrogen transfer. Values in kcal·mol^{-1}. 153
Table S11 Relative energies for the active protonated UiO-66_ava for the hydrogen transfer to the hydroxyl group. Values in kcal·mol^{-1}. 153
Table S12 Relative energies for the active protonated UiO-66_ava with only two amines for the hydrogen transfer to the hydroxyl group. Values in kcal·mol^{-1}. 154

Supplementary material for chapter 4

Table S1 Relevant distances in Angstroms (Å) for step A of the three different systems under study. 155
Table S2 Relevant distances in Angstroms (Å) for step TS_AB of the three different systems under study. 155
Table S3 Relevant distances in Angstroms (Å) for step B of the three different systems under study. 156
Table S4 Relevant distances in Angstroms (Å) for step TS_BC of the three different systems under study. 156
Table S5 Relevant distances in Angstroms (Å) for step C of the three different systems under study. 157

Table S6 Relevant distances in Angstroms (Å) for step TS_CD of the three different systems under study. 157
Table S7 Relevant distances in Angstroms (Å) for step D of the three different systems under study. 157
Table S8 Negative frequency values for the three different transition states and systems. 158
Table S9 HOMO-LUMO gap values in electronolts (eV) for the different reaction steps and the three systems under study. 158

Supplementary material chapter 5

Table S1 BET numbers of the MOFs used in this work. 164
Table S2 Overview incipient-wetness impregnated samples. 171
Table S3 Co-Loading in MixUMCM-1-NH2 (28%) after catalysis dependent on the pressure. 174
Table S4 Co-Loading in MOF-74(Zn) after catalysis dependent on the pressure. 174
Table S5 Screening of reaction conditions in the homogeneous reaction. 176
Table S6 Screening of reaction conditions with MixUMCM-1-NH2 (28%). Variation of MOF loading and pressure.[a] 176
Table S7 Blank reaction with different Zn sources.[a] 177
Table S8 Blank reaction with different MOFs.[a] 177
Table S9 Reactions at different pressures.[a] 178
Table S10 Aldehyde yields in Table 5.3 of the main text determined by GCFID with p-cymene as external standard.[a] 178
Table S11 Reactions with incipient-wetness impregnated MOFs.[a] 179
Table S12 Reactions with recycled incipient-wetness impregnated MOFs.[a] 179
Table S13 Reactions with recycled, washed MOFs.[a] 180
Table S14 DFT interaction energy of $HCo(CO)_4$. M-Co (MOF–$COCo(H)(CO)_3$ in the main text) is the adsorption of $HCoCO_4$ to the metal node via its axial carbonyl. M-H (MOF–H-$Co(CO)_4$ in the main text) is the adsorption of $HCoCO_4$ to the metal node via its hydride. L-CO = adsorption of $HCoCO_4$ to the function via its axial carbonyl. Optimised geometries reported in supplementary notes (Figure S11 to Figure S17). 187

Table S15 DFT binding energies. M-Co (MOF–Co(H)$(CO)_3$ in the main text) is the binding energy between the metal of the MOF and the Co of $HCoCO_3$. L-Co (MOFFunc–Co(H)$(CO)_3$ in the main text) is the binding energy between the functional group of the MOF and the Co of $HCoCO_3$. Optimised geometries reported in supplementary notes (Figure S11 to Figure S17). 187
Table S16 Grand Canonical Monte Carlo (GCMC) simulations. For each framework the first column lists the 1-hexene uptake measured from Grand Canonical Monte Carlo (GCMC) simulations (average and standard deviation over 5 blocks). The second column shows the rounded number of 1-hexene molecules that were used for the following simulations and to compute the size of the paired homogenous box that contains the same number of solvent molecules, reported in the third column.....188
Table S17 Affinity of the different species with the frameworks. This is reported as percentage occupancy (%occup.) which is related to the average number of molecules of that species in the MOF's simulation box. The error is computed as standard deviation over ten independent simulations. The last column reports the relative density of 1- hexene computed in the pore volume with respect to the density observed in the homogeneous simulation box (see also Table S16). 188
Table S18 The affinity of the different species with UMCM-1 and MOF- 74(Zn). as setting to zero the Coulomb interactions. is reported with its standard deviation. The difference in the %occup. with the charged model shown in Supplementary Table S19 is also reported.....189
Table S19 Molar solubilities of H2 and CO in 1-hexene at 100 °C in function of pressure. 190
Table S20 Correction factors Z used to calculate the modified concentration of the reactants within the pores of the MOFs. 190
Table S21 Concentration of H_2 and CO at different syngas pressures. (H_2:CO = 1) Their effect on the rate of formations of the branched aldehyde RB and of the linear one RL for homogeneous catalysis is shown. 191
Table S22 Concentration of H_2 and CO at different syngas pressures. (H_2:CO = 1) Their effect on the rate of formations of the branched aldehyde RB and of the linear one RL for catalysis within the pores of UMCM-1-NH2 is also shown. 192

Table S23 Concentration of H_2 and CO at different syngas pressures. (H_2:CO = 1) Their effect on the rate of formations of the branched aldehyde RB and of the linear one RL for catalysis within the pores of MOF-74(Zn) is also shown. 193

Supplementary material chapter 6

Table S1 NCI plots of the truncated MOF in combination with the Precat. Previously optimised geometries have been evaluated using the promolecular approach suitable for large structures. 231

Table S2 Coordinates data set, absolute energies (a.u.) for all DFT optimized neutral complexes.....232

Table S3 Coordinates data set, absolute energies (a.u.) for DFT all the optimized ammonium tagged complexes (AquaMet^{TM}). 242

Table S4 Coordinates data set, absolute energies (a.u.) for DFT all the optimized ammonium tagged complexes (AquaMet^{TM+}). 255

Table S5 Coordinates data set, absolute energies (a.u.) for DFT optimized ionic complex (Cluster (Cr)Mil-101-AquaMet^{TM}).....269

Table S6 Coordinates data set, absolute energies (a.u.) for DFT optimized cluster (Cr)Mil-101 and (Cr)Mil-101-$SO3^-$. 282

Chapter 1. Introduction

Section 1. Catalysis

The first time that the term catalyst is used was in 1794 in the book An Essay on Combustion with a View to a New Art of Dying and Painting, where in the Phlogistic and Antiphlogistic Hypotheses are Proven Erroneous by Elizabeth Fulhame. However, it is not until 1836 that one of the founders of the modern chemistry Jöns Jacob Berzelius defines the term as: "a catalyst is a substance that has the power to awake affinities that are asleep at a given temperature by their mere presence and not by their own affinity". A definition closer to our times was made by Friedrich Wilhelm Ostwald in 1900: "a catalyst is substance that modifies (usually accelerates) the rate to achieve the chemical equilibrium without self-modification or self-consumption". Indeed W. Ostwald received the Nobel Prize in 1909 for his contribution to the fields of catalysis, chemical equilibrium, and reaction velocities. Basically, a chemical reaction happens faster in presence of a catalyst as this provides an alternative reaction pathway with a lower activation energy. Catalytic technology is not only applied on the synthesis of a wide range of products such as fuels, fertilizers, plastics, and pharmaceuticals, but also used to clean emissions from cars, power plants and industrial production. Catalysis is clearly ubiquitous in our day-to-day life and it is estimated that more than 20% of manufacturing in the industrialized world is dependent on it.[1] Depending on the phase where the catalysts is allocated, they can be classified as either homogeneous (including here the emergent biocatalysts) or heterogeneous.

In homogeneous catalysis the catalyst, reactants and products are dispersed in the same phase (usually gaseous or liquid). Homogeneous catalysis represents only the 10-15% of all the catalytic processes in industry, manly focused on fine chemistry. Apart from its undeniable advantages which are all the catalyst is considered as an active centre, high selectivity, absence of diffusion problems and a well-defined structure. It also presents some disadvantages, such as the difficult separation of catalyst, products and reactants and the contamination of products with catalyst waste which, in addition, can cause some secondary reactions unwanted during the reaction process, highly undesirable, especially when it is considered an industrial process.

In heterogeneous catalysis the catalyst acts in a different phase than reactants and products, in this case the phases distinguish not only solid, liquid and

gas components but also immiscible mixtures such as oil and water. Nowadays the 85-90% of all chemical processes are run by heterogeneous catalysts, with a ratio of applications of heterogeneous to homogeneous catalysis of approximately 75:25.[2] Indeed, most catalysts used in industry are solids and the catalysis takes place only on the surface of the active material.[3] Some of the advantages of the heterogeneous catalysis are the high concentration of catalyst, the easily recovery of it, its medium-high selectivity, and thermal stability. Even though heterogeneous catalysis is well stabilised in industrial processes, as mentioned before, it also presents some disadvantages such as that only the surface of the catalyst is considered an active site, the reactions are controlled by diffusion and the possibility of activity loss due to poisoning.

Both large groups of catalysts show advantages and disadvantages, but it would be possible to merge only the advantages of both types by means of a heterogenization of the homogeneous catalyst. This process would create a homogeneous catalyst supported on a solid phase which is insoluble. Thus, one will not only obtain a catalyst where all the compound itself would be considered as an active centre, with a high selectivity, and a well-defined structure but also with a high concentration, an easily recovery and a high thermal stability. Nevertheless, some of the drawbacks would still be present such as, the catalyst decomposition by side-reactions and the fact that reactions would still be controlled by diffusion.[4–8] Over the past several years, metal−organic frameworks (MOFs) have been targeted as particularly attractive supports for such molecular catalysts because of their well-defined and highly tuneable pore structures and high porosities.[9–12]

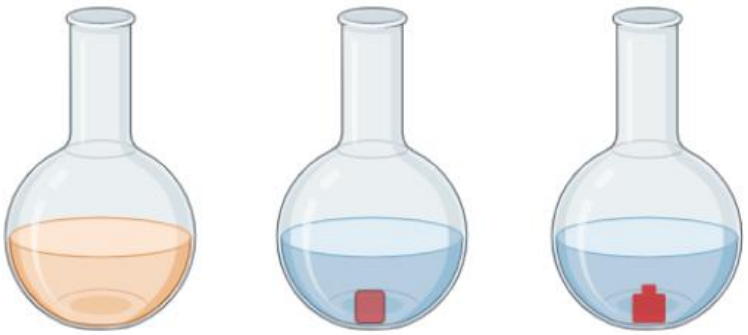


Figure 1.1 From left to right, visual exemplification of homogeneous, heterogeneous and heterogenized homogeneous catalyst.

Section 2. Metal-Organic Frameworks

Metal-Organic Frameworks (MOFs) are a class of nanoporous materials containing three-dimensional (3D) and periodic networks of metals, metal clusters, or metals oxide clusters held together by bridging organic linkers.[9,13] One can also find them referred in the literature as coordination polymers, coordination networks or porous coordination polymers (PCP) (see Figure 1.2). MOFs have relevant properties from a technology point-of-view: they are thermally stable, crystalline, and characterized by high porosities (up to 90% free volume) and record-breaking surface areas (in excess of 6000 m^2/g).[14,15] These properties make them perfect candidates as gas adsorbents. Moreover, the functional groups in their pores and the shapes and sizes of those pores can be tuned improving their capacities. Mainly by increasing the organic linkers one can tune MOF's porosities.[16–21] The existence of many metals, metal clusters, metal oxides, metal oxide clusters and organic linkers that can be combined to form an almost infinite spectrum of MOFs having different topologies makes this logical tuneability an intrinsic property of them. As a result, the rational design, synthesis, and characterization of MOFs is, nowadays, still a focus of significant scientific research. The large number of possible combinations of metal clusters and organic linkers makes almost impossible to compile a list of all existing MOFs. Moreover, the difference on the metallic components, makes MOFs differ not only in their atomic compositions but also in their symmetry and the number of available sites for coordination to the organic linker. Thus, different MOFs show completely different topologies as well as physical properties.

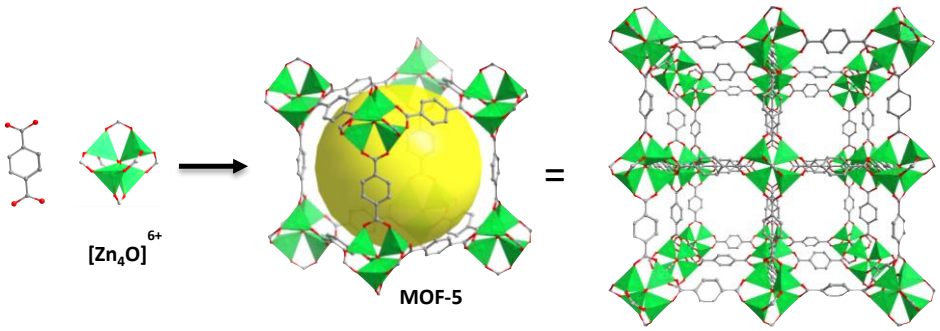


Figure 1.2 Representation of the different parts of a MOF (MOF-5), from left to right, building blocks (organic linker and metal node), periodic unit cell and crystalline structure.

2.1 Structural properties of MOFs

As mentioned before, MOFs are crystalline structures build up as a conjunction of multi-functionalized organic molecules binded to metal clusters through coordinating moieties. These crystalline materials can give one-, two-, or three-dimensional structures, showing pores with sizes that can vary from microporous (smaller than 2 nm) to mesoporous (between 2 and 50 nm). The fact that the organic building blocks can combine with various inorganic building blocks, makes them especially tuneable generating almost an infinity of possible structures (see Figure 1.3 for a representation of different MOF crystalline structures).

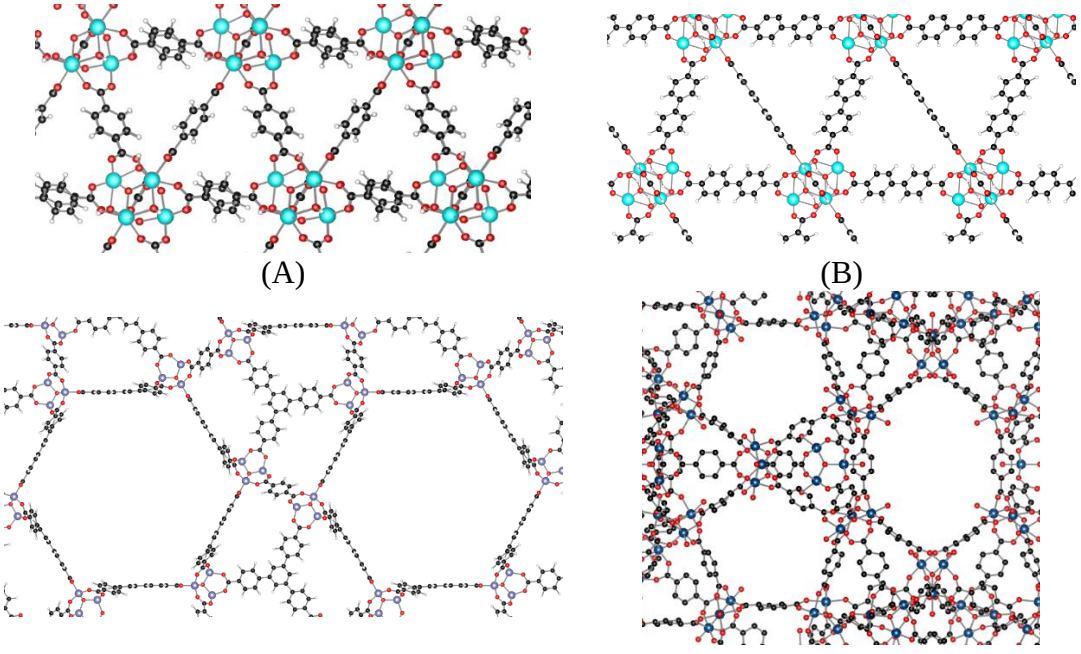


Figure 1.3 Representation of (A) UiO-66, (B) UiO-67, (C) UMCM-1 and (D) MiL-101.

The chemistry of polymers coordination did it first steps relatively long time ago, first publications dated from the fifties. However, it is not until fifty years later that the applications of such materials were demonstrated, showing to be perfect candidates in areas such as catalysis, photocatalysis, gas separation and storage and materials chemistry.[22–26] Even though the existence of different pioneering works on the field,[27–29] it is not actually until the nineties that the chemistry of porous coordination polymers gets a relevant impact on the scientific world with the publication by Yaghi et al. reporting the synthesis and characterization of

$[Zn_4O(tpa)_3]_n$ (MOF-5, tpa = terephthalic acid).[30] MOF-5 is a 3D cubic-shaped framework in which, the inorganic fragments are tetrahedral Zn_4O clusters bind to six carboxylate moieties of different terephthalate organic building blocks in an octahedral shape.

MOF-5 is the coordinate polymer that helped the most in the discovery and development of new concepts that in the future enhanced the research on the design of new PCPs based on their tunability. Later studies of Yaghi *et al.* were focused on the synthesis of new materials based on the same geometry of MOF-5. The only differences were the presence of functional groups, such as halogens, alkyloxy, hydroxyl, and amino groups and the size of the building-blocks.[31] The MOFs synthetised from the geometry of MOF-5 were so called IRMOFs as they are isoreticular to MOF-5. The ability of synthetise those IRMOFs not only demonstrated the principle of geometrical design and tunability of the pore size by using a known material as prototype, but also opened new perspectives on the synthesis of coordinated materials with functional groups, this feature was crucial for the future application of MOFs to catalysis.

However, the unique structural features of MOFs do not end here, the concept of multivariable or mixed MOFs (MTV-MOFs or MIXMOFs) extends they tunability by means of the synthesis of frameworks with two or more isoreticular organic linkers which are randomly and homogeneously distributed within the framework. First examples of MTV-MOFs were reported by Richardson[32] and Baiker[33] and later extended by Yaghi and co-workers.[34] By mixing up to seven different functionalized terephthalate derivatives they synthesized a several number of MTV-MOF-5 materials. Moreover, it is also possible to synthesize MOFs mixing organic building blocks with a different overall geometry while assembled with the same inorganic unit.[35] Nevertheless, it is difficult to assure the homogeneity of the material while mixing organic linkers and that could induce to obtain separate solid phases.

Organic starting materials and inorganic units can be modelled increasing the number of possible combinations. Each new connection could be a new structure, this versatility creates an almost infinite combinations, thus, and almost infinite catalogue of MOFs, impossible to synthetize and study experimentally each of one. A simple example using MOF-5 could be; If one exchanges the terephthalic

acid building block with 1,3,5-tris(4-carboxyphenyl)benzene, MOF-177 is obtained.[36] And if then the Zn_4O clusters are changed with hexanuclear $Zr_6O_4(OH_4)$ ones, one can obtain UiO-66 which actually presents a completely different connection of the metal cluster with the organic linker.[37] Finally, it is even possible to synthetise MOFs with similar structural cages than zeolites, such as the zeolite imidazole frameworks (ZIFs).[38] MOFs present a unique structural flexibility difficult to be achieved by other solid materials not only because of the possibility of design and modelling but also due to the large structural diversity, matter of fact, it makes them perfect candidates for a large vast of applications.[12]

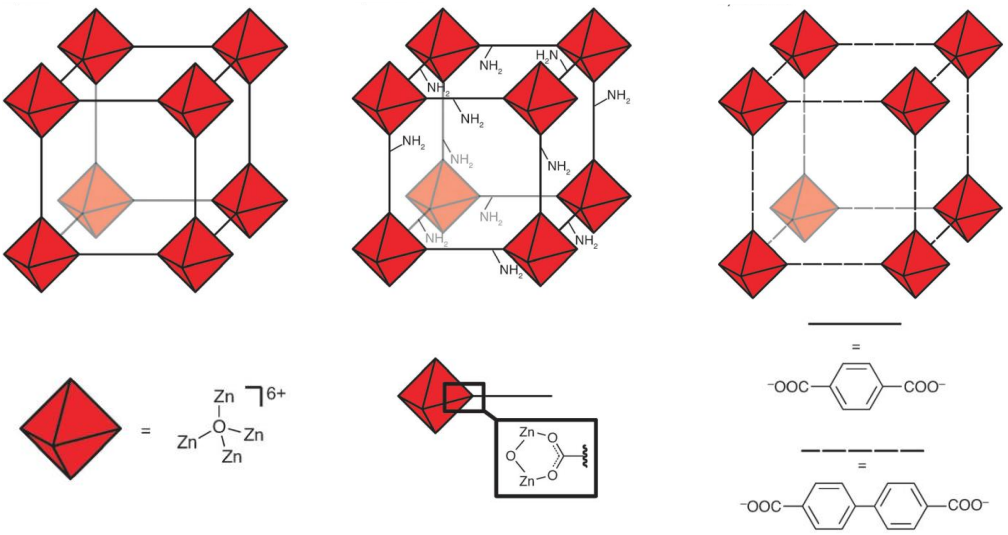


Figure 1.4 Schematic representation of, from left to right, MOF-5, IRMOF-3, and IRMOF-10. Adapted from: Ranocchiari, M. & Bokhoven, J. A. Van. *Phys. Chem. Chem. Phys.* **13**, 6388–6396 (2011).[12]

2.2 Applications of MOFs

The chemistry of MOFs can be applied in many different fields, here they will be gathered and discussed only for the two major applications: gas adsorption, storage and separation and, catalysis. As mentioned before, the potential applications of MOFs are much greater and it exists relevant research work in other applications which will not be described here such as luminescent[22,39,48,49,40–47] and magnetic MOFs.[43,50,59–62,51–58]

2.2.1 Gas adsorption, storage and separation.

One of the earliest promising properties of MOFs was gas adsorption due to their high porosity and surface areas.[63] Moreover, its thermal stability allows to

remove the guest allocated within the MOF through a thermal reactivation process. This fact makes them suitable for gas capture, separation, and purification.[64,65,74–76,66–73] One of the most relevant examples is the capture of carbon dioxide (CO_2), from industrial emissions as it is the principal agent of the greenhouse effect contributing to the climate change.[68,71,74,77,78]

Moreover, MOFs with very large surface areas and high affinities for different gasses such as hydrogen (H_2) are perfect candidates for capturing, storing, and delivering those gases. Many research works have been focused indeed on the development of MOFs with very large surfaces permitting the capture of more gas molecules at high H_2 pressure. The development of a container where to store safely molecular H_2 would likely significantly accelerate the commercialization of hydrogen-fuelled automobiles. Nevertheless, the ability of MOFs to capture, store and delivery is extended to many other gases, including natural gas.[79–86]

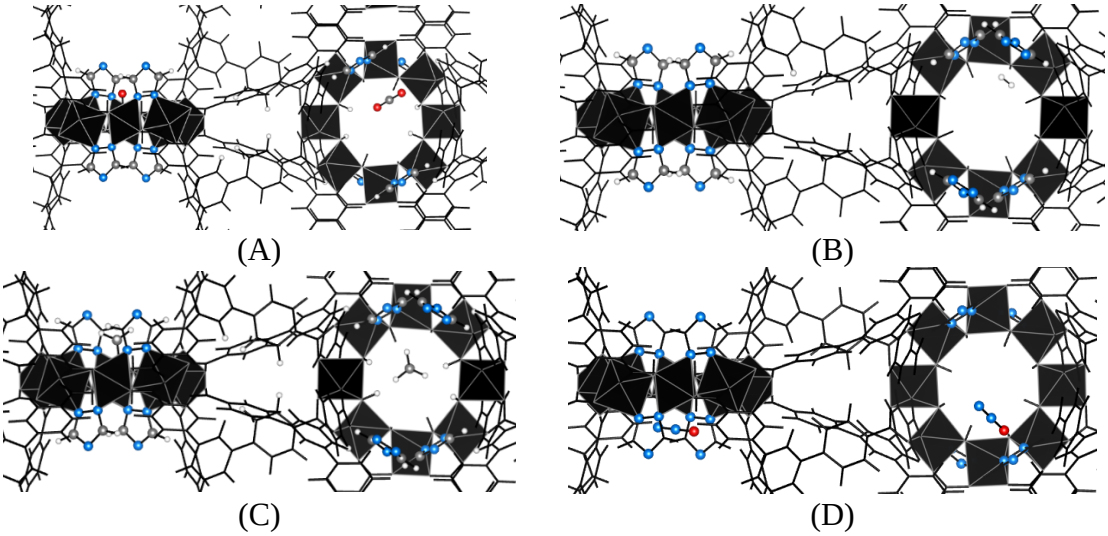


Figure 1.5 Representations of different gases absorption within MOF-520; (A) CO_2, (B) H_2, (C) CH_4 and (D) N_2O. Wireframe corresponds to carbon and hydrogen atoms (relevant carbon and hydrogen atoms are in grey and white colour respectively), blue colour for nitrogen atoms and red colour for oxygen atoms.

2.2.2 Catalysis

It is clear that MOFs can absorb, storage and delivery a huge number of gases, and that the porosity, thermal stability and high crystallinity are key factors. However, they also have a high concentration of metals organized at regular distances and in long arrays. The sum of these qualities makes them highly desirable

in industrial catalysis. MOFs not only present the typical advantages of heterogenous catalysts such as the easy separation of products from the reaction mixture and the easy recyclability of the catalyst. But they also have the advantage of holding the catalytic metal sites apart with no danger of sintering. Many reports achieved efficient reaction catalysis by using MOFs containing catalytically active metal sites.[12,87–95] The versatility of MOFs towards catalysis is that extent that one can control the reaction by controlling the size and shapes of the pores.[43] In addition, this tuneability opens the door to the heterogenization of homogenous catalysts by means of a simple interaction in between MOF and catalyst or a directly functionalization of the organic linker of the MOF with the catalyst.[96,97] As this work focuses on the computational study of MOFs as catalysts further investigations on this topic will be discussed below in an extended section.

Section 3. Catalysis and MOFs

When one refers to MOFs as catalysts it is impossible not to mention their closest catalytic porous materials predecessors, the aluminosilicate zeolites. Zeolites are among the most commercially important class of heterogeneous catalysts.[98] They are purely inorganic materials and, extraordinary robust making them suitable for catalysis under extreme conditions. As porous materials they internal surface areas are relatively large, enhancing their catalytic reactivity. Moreover, the uniformity of their pore and channel size help on improving their catalytic selectivity.

MOFs can be considered as relatives to the zeolites as they share some catalytically relevant features such as the large internal surface areas and uniform pore sizes. Moreover, MOFs contain organic components exhibiting an almost infinity of geometrical possibilities, they can be synthesized in a greater chemical variety. Even though, MOFs show a good thermal stability, this cannot be compared to the stability of zeolites, most of the MOFs cannot handle temperatures above the 500 ºC.[99,100] For this reason, one could consider MOFs not competitive with zeolites as catalysts for reactions requiring extreme conditions because of their lower thermal stability. However, they can be used for a different type of catalysis requiring milder conditions such as production of fine chemicals, individual enantiomers, etc. Finally, many MOFs show permanent microporosity as zeolites, however they can collapse when solvent is removed. This persistence microporosity is essential for gas-phase catalysis, as well as for other applications as gas separation and storage. However, it may not be required for condensed-phase reactions.[101]

In order to understand how the catalytical reaction proceeds it is vital to determine which are the active sites and their origin. The catalytic active sites of MOFs can be situated in two places: the coordinatively unsaturated metal sites (CUSs or open metal sites) as Lewis acid sites and, the acid/base sites on the organic linkers. Functional molecular catalysts such as metalloporphyrins or Schiff-base complexes among others can be used as building units to enhance catalytical reactivity of MOFs. In fact, MOFs present a limited type of active sites, and one could believe that this actually restricts the applicable scope of reactions and performance improvement. Fortunately, the before mentioned large structural tuneability of MOFs greatly extends these weaknesses and enrich the origin of

active sites. The tailoring of metal clusters and organic linkers in addition to the pore space engineering of MOFs together extend their opportunities towards catalysis. Their pores make possible to encapsulate diverse catalytically active species, such as metal-based nanoparticles (NPs), molecular catalysts, enzymes, etc. for efficient catalysis. Moreover, they have been employed as precursors for the synthesis of derived porous materials, including porous carbon metal-based compounds and their composites, upon thermal/chemical conversion, showing to be also very promising candidates for catalysis. In fact, one could consider that MOFs do not have theoretical pores size limitations, meaning that is possible to have a homogeneous distribution of one or more active sites due to their high crystallinity and, at the same time, to overcome diffusion and pore size limitations. The modelling of MOFs is such that even the fine structure and the nature of the active site can be controlled. However, MOFs can have limitations concerning to their stability and the synthetic cost related to the components of the materials. The right combination between cost, stability, and chemical applications should be chosen accordingly.

There are different technologies to create active sites in PCPs and it is possible to categorize the class of MOFs depending on the situation where the active site is considered within it.

3.1 Metal inorganic nodes as active sites

The earliest reports about catalytic activity of MOFs are those where the active site is an intrinsic part of the framework, in fact, one could also consider it as opportunistic catalysis. The presence of coordinatively unsaturated metal sites (CUSs) of metal nodes/clusters give rise to Lewis acid sites.

Among the earliest reports it is worth to mention, because of its nobility at that time, the description made by Fujita and co-workers in 1994 on the cyanosilylation of aldehydes by a 2D MOF (layered square grids) of formula $Cd(4,4'\text{-bpy})_2(NO_3)_2$, (bpy = bipyridine) in which the cadmium centre is the active Lewis-acid site. The investigation was first focused mainly on the size- and shape selective encapsulation, however, it was also reported the catalytic cyanosilylation of aldehydes.[101] MOFs with cooper paddle wheel dimers as inorganic unit such as HKUST-1 or MOF-199 have shown similar Lewis acid catalytic activity

([$Cu_3(btc)_2(H2O)_3$]n btc = 1,3,5-benzenetricarboxylate). In this case they bear H_2O molecules that complete the coordination sphere of Cu(II) atoms.[102] Upon activation of these frameworks by heating in vacuum, the water molecules are removed, and the material goes through the Lewis acid-catalysed cyanosilylation of carbonyl groups. However, recent investigations have shown that HKUST-1 loses its activity under humid conditions due to water re-occupation of the open Cu sites. Surfaces hydrophobic modifications could be able to inhibit the water attack and prevent its decease of activity.[103]

Unsaturated metal centres can be generated not only by Cu and Mg but also by other metals, e.g.Mn, Cr, Ni, Co, Zr, Fe, Zn.[72,104–106] For instance MIL-101 ([$Cr_3X(H_2O)_2O(1,4\text{-bdc})_3$]; X = F, OH; bdc = benzene-1,4-dicarboxylate)) is a perfect stable MOF for applications in heterogeneous catalysis attributed to its Lewis acid activity,[107] and is able to catalyse the same reaction mentioned before avoiding the pre-treatment heating as it is more reactive. The open trimeric chromium (III) clusters accessible after water removal offer a significantly higher catalytic activity than HKUST-1 since Cr(III) has a greater Lewis acidity than Cu(II).[108,109] Recent works have reported another MOF (NU-1000) with Lewis-acidic Zr^{IV} ions as active sites that showed to be effective for the degeneration of nerve agents and their simulants.[110]

Another set of PCPs with catalytic activity at the inorganic nodes are the ones presenting an intrinsic Brønsted-acid catalytic activity such as, MIL-100 ([$M_3OF_{0.85}(OH)_{0.15}(H_2O)_2(btc)_2]_n$ M = Fe, Cr) which is able to catalyse the Friedel-Crafts benzylation reaction.[111] Ravon *et al.* have extended the studies of Friedel-Crafts tert-butylation catalysis by using MOF-5.[112] This material presents coordinatively saturated Zn_4O nodes and bdc as organic linkers (bdc =benzene-1,4-dicarboxylate). In this case the para-alkylation is favoured over the ortho-alkylation, this behaviour is due to the encapsulation of the reactant within the well-defined pores of MOF-5. This example shows how MOFs can not only catalyse a reaction but also be selective in between two isomers. Another outstanding example is the framework [$Pd(2\text{-ymo})_2]_n$ (2-pymo = 2-hydroxypyrimidolate), that is able to catalyse the Suzuki-Miyaura cross coupling of *p*-bromoanisole with phenylboronic acid showing good conversion and selectivity.[88]

It is clear that the discovery of the nodes as active sites for catalysis was transcendental for the research in MOFs as catalysts and that, nowadays, there is still promising research focused on this approach. However, nodes play a very important role on the construction of MOFs as they hold together all the structure. By using them as active sites the structure of the cluster is being stressed with the possibility of experience a rearrangement of the coordination geometry during catalysis. That could lead to the collapse of the structure with negative consequences in activity, reproducibility and recycling due to the deactivation of the catalyst. Thus, active sites designed in the same position where all the framework is supported makes their reactivity more limited compared to a position with less structural charge. A clear example of the possible collapse of a MOF structure due to its catalytic activity on the metal node is reported by LLabrés i Xamena *et al*. in its work based on a two-dimensional, square-grid MOF containing Pd(II) ions in the nodes.[88] The palladium centres in this MOF can catalyse alcohol oxidation, olefin hydrogenation and Suzuki C-C coupling. However, these reactions go through a redox oscillation of the metal nodes between Pd(II) and Pd(0) followed by a drastic change in its coordination number which could lead to a destabilization and potential destruction of the original framework.

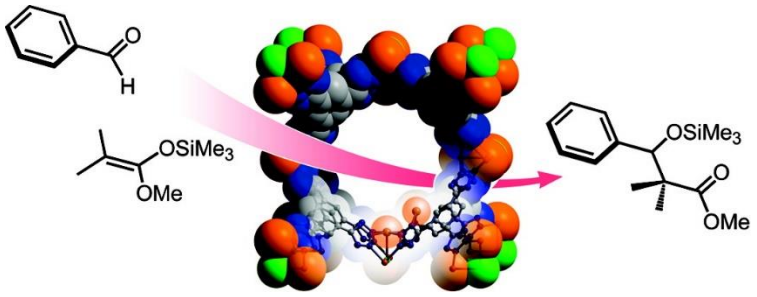


Figure 1.6 Example of a portion of the microporous MOF $Mn_3[(Mn_4Cl)_3BTT_8(CH_3OH)_{10}]_2$ (1, H_3BTT = 1,3,5-benzenetristetrazol-5-yl) showing the two different types of Mn^{II} active sites exposed within the three-dimensional pore. Also represented the Cyanosilation reaction catalysed by the crystal. Orange, green, gray, and blue spheres represent Mn, Cl, C, and N atoms, respectively; H atoms and bound MeOH molecules are omitted for clarity. Adapted from: Horike, S., Dincă, M., Tamaki, K. & Long, J. R. *J. Am. Chem. Soc.* **130**, 5854–5855 (2008).[104]

3.2 Organic and pseudo-organic linkers as active sites

Building blocks such as metal complexes with functionalized organic ligands can also perform catalytically. First reports were focused on Mn(III) and Zn(II) porphyrincarboxylate frameworks which successfully catalyse the epoxidation of olefins[113] and the acyl transfer to pyridylcarbinols[114] respectively. These MOFs show to bear the metal at both the inorganic node and coordinated to the porphyrin nitrogen, it is indeed this last metal position the one performing the catalytic activity. Amino-functionalized MOFs such as IRMOF-3 ($(Zn_4O)(atpa)_3$ atpa = 2-aminoterepthalate) which acts as an active basic catalyst for the Knoevenagel condensation of benzaldehyde with ethyl cyanoacetate[115] are also an example of this methodology. Moreover, asymmetric catalysis has been achieved by using this method. By assembling a chiral pyridino-functionalized Mn(III)-salen complex with Zn(II) paddle-wheel dimers and biphenyldicarboxylic acid, one is able to catalyse the epoxidation of 2,2-dimethyl-2H-chromene with up to 82% ee, which is slightly lower than the homogeneous analogue that shows a 88% ee.[116] Due to the harsh conditions needed to synthesis the crystalline materials described above this methodology is moving to the use of materials with organocatalytic properties such as amino functionalized PCPs or crystalline structures produced only with stable metal-porphyrins and metal-salen complexes.[115]

Vermoortele et al. showed that the presence of functional groups on the aromatic linkers can strongly influence the intrinsic catalytic activity of the metal nodes through inductive effects, in addition to the metal nodes they can perform activity as acid and basic catalysts.[117,118] Brønsted acidic groups can be added to the organic linkers. An example of how is possible to functionalize the organic linker by changing the preparation method is the observed in UiO-66 $[Zr_6O_4(OH)_4(BDC)_6]$ where a free carboxylic acid group was attached on the organic linker by using H_2BDC-COOH instead of H_2BDC for the preparation of UiO-66.[119] It is possible to obtain MOFs with stronger Brønsted acids by functionalizing them with sulfonic acid. Kitagawa et al. synthetised MIL-101 (Cr) functionalized with partially protonated $-SO_3Na$ by solvothermal reaction of chromium (VI) oxide, monosodium 2-sulfotherapthalic acid, and hydrochloric acid in water.[120] Following this reaction process, it has been possible to synthetise sulfonic acid functionalized MIL-101 (Cr), MIL-101-SO_3H, by a hydrothermal

process followed by a HCl treatment strategy.[121] MIL-101-SO_3H showed exceptionally high activity, excellent selectivity and recyclability towards alcoholysis of epoxides under ambient conditions. Other examples are acidic MOFs which contain Brønsted acidic sites from a protonated phosphonates and Lewis acidic sites from open lanthanide sites.[122] They are able to behave as enantioselective acid catalysts for cyanosilylation of benzaldehyde and ring opening of meso-carboxylic anhydrides.

Moreover, basic sites can also be grafted onto organic linkers by using N-containing ligands as building blocks.[123–126] N-containing groups can be introduced to the MOF directly during the synthesis process as seen before with the sulphonate containing MOFs. For instance, IRMOF-1 also known as MOF-5 is constructed from the ligand BDC, whereas the replacement of BDC with NH_2-BDC leads to IRMOF-3, showing a basic character.[127] A different strategy to obtain such basic active sites on the organic linker is by a partial substitution of original ligands with functional N-containing groups. The synthesis using mixed ligands consisting of both BDC and NH_2-BDC leads to the formation of MIXMOFs.[128,129,138–143,130–137] As mentioned before the most used ligands to obtain basic active sites are the N-containing ones concretely the NH_2-functionalized MOFs. Examples of their catalytic activity are seen in the Knoevenagel condensation reaction between benzaldehyde and malononitrile reported using Fe-MIL-101-NH_2 and Al-MIL-101-NH_2, observing 90 % yield of the expected condensation product at 80ºC.[144] Another example is the homochiral MOF D-POST-1 which has pyridyl groups exposed in the channels which perform the enantioselective transesterification of racemic 2,4-dinitrophenyl acetate.[145]

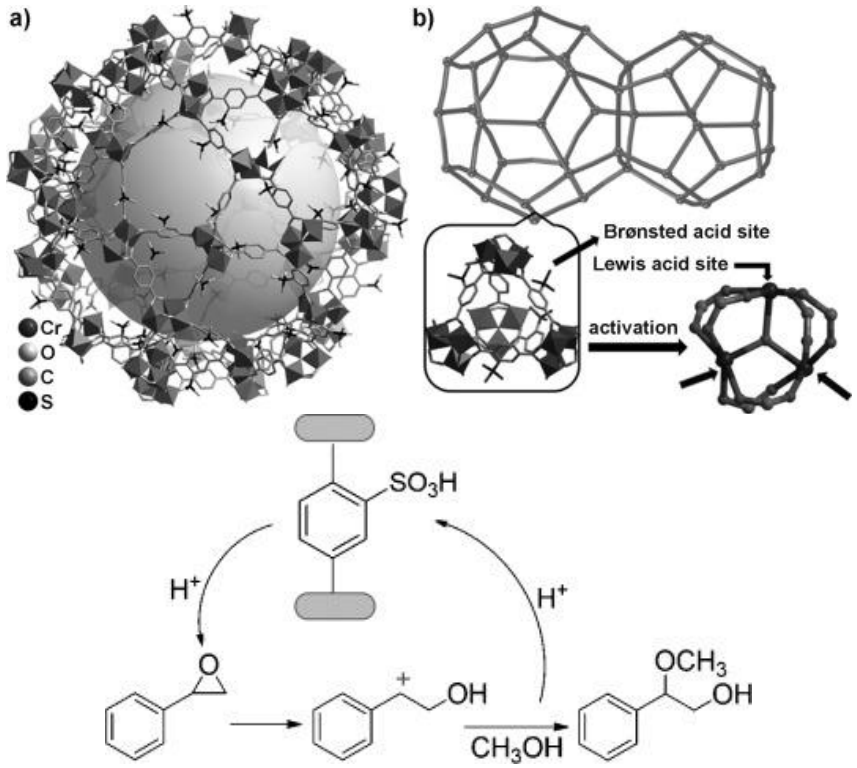


Figure 1.7 Example of organic linker as an active site. Top: The large cage involved in MIL-101-SO_3H with the readily accessible acid sites. The grey ball highlights the large void inside the cage. b) Schematic illustration for the two types of cages in MIL-101-SO_3H with Brønsted and Lewis acid sites. Bottom: Proposed mechanism for the ring opening of styrene oxide in MeOH catalysed by the Brønsted acid sites in MIL-101-SO_3H. Adapted from: Zhou, Y. X., Chen, Y. Z., Hu, Y., Huang, G., Yu, S. H. & Jiang, H. L. *Chem. - A Eur. J.* **20**, 14976–14980 (2014).[121]

3.3 Encapsulation of active sites

Until now it has been considered only the framework of the MOF itself as an active site, however, one must not forget about the pores and the capacity of the MOF to allocate molecules within it. As mentioned before encapsulation of molecules within their pores was indeed their very first application. Basically, encapsulation means that the active site is positioned within the pores of the MOF structure by a non-covalent interaction. Here the framework is used as a support for the catalyst and its main function is to provide a stable pore structure and surface area. Metal particles, complexes, and clusters supported within a PCP are examples of this category, which is growing interest in the scientific community due to the

large variety of pores that are available in MOFs. Different investigations are focused in using MOF-5 in gas storage and purification,[146] and as support for palladium, platinum, copper, and gold nanoparticles. Once the material is supporting the nanoparticles within the pore, it can be used for different applications, such as the hydrogenation of cyclooctane (Pd@MOF-5), the synthesis of methanol from syngas (Cu@MOF-5), and H_2O_2 synthesis (Pt@MOF-5).[147,148] MOF-101 can adsorb polyoxometalates $[PW_{11}TiO_{40}]^{5-}$ and $[PW_{11}CoO_{39}]^{5-}$ catalysing the oxidation of α-pinene to the corresponding alcohol and ketone using hydrogen peroxide and oxygen as oxidants.[149]

One could observe that the catalysts mentioned before could also be supported to other materials that also have porosity, surface area, and stability. Nevertheless, MOFs are attractive for their primordial features, the tuneable por size as well as the high surface area, and crystallin ordering that enhance the shape selective catalysis. There is an important drawback to consider when dealing with encapsulating catalysts and that is the possibility of losing particles or clusters during the reaction process. It is necessary to run a leaching test after the processes consisting of the filtration of the mother liquor under reaction conditions to check whether the catalysis persists even in absence of the MOF catalyst.[150]

3.4 Post-synthetic active site modifications

One of the greatest properties of MOFs is their chemical versatility. One can produce functionalized materials, subsequently modifying them and even including active sites, such as metal complexes, thought covalent interactions. Thus, allowing scientists to design the catalytic site accordingly to the reaction. Moreover, it enhances the process of design, optimizing and rationalizing the structure of heterogeneous catalysts which their possibilities are extended by a heterogenization of the homogeneous catalyst. It is indeed this heterogenization of known homogeneous catalysts the main strategy followed to add active sites through post-synthetic modifications (PSM). For example, a heterogeneous vanadyl-iminophenol complex was synthetized in two steps from IRMOF-3, an amino-functionalized MOF-5. This material effectively catalyses the oxidation of cyclohexene.[151] Similarly, it is the post-synthetic approach to produce a gold-iminophenol functional material, that effectively catalyses the selective hydrogenation of butadiene.[152]

Enantiomerically pure MOFs have been post-functionalized with metal complexes and then applied in catalysis. One of the most representative examples was published by Lin and co-workers in 2005, they structurally characterized a 2D cadmium MOF bearing binaphthol moieties. After being post-functionalized with $Ti(O^iPr)_4$, the resulting complex catalysed the alkylation of aldehydes with diethylzinc. If one goes deeper on this example. The active site is considered being the titanium (IV) complex with two isopropanolate ligands and two alcoholate ligands coming from the binaphthol groups on the framework. The enantioselectivity seen on this example suggests that the catalysis is heterogeneous. This example shows how it is possible to perform asymmetric transformations with crystalline metal-organic frameworks.[153]

These PSM can be carried out in different parts of the structure of the MOF, until now it has been only mentioned the very first modifications reported that where indeed performed on the organic linker. However, it exists a large spectrum of research works on this ambit. For instances, many efforts have been made to functionalize the metal nodes/clusters of MOFs with active transition metals (metal oxides), inorganic acidic sites and molecular catalysts to afford MOF-based catalysts with high performance. Promising approaches have been done by constructing bimetallic clusters in a MOF by means of metal-oxo nodes/clusters as structural supports and other transition metals as active sites. By using atomic layer deposition (ALD) it has been possible to install Ni ions uniformly and precisely on the node of NU-1000, naming it as Ni-AIM showing great performance on the hydrogenation catalysis.[154] Following the same methodology it has been possible to add Mo(VI) oxide on the Zr_6 nodes of Nu-1000 via solvothermal deposition of the MOF, showing higher activity for the epoxidation of cyclohexene than that of Mo(VI) oxide powder and was comparable to that of a zirconia-supported analogue ($Mo\text{-}ZrO_2$) similarly prepared.[155] Following with the modifications on Nu-1000, a highly electrophilic single-site d0 Zr-benzyl catalytic centre was successfully attached to the nodes of a Hf-Nu-1000, subsequently forming a Hf-NU-1000-ZrBn. This material showed to catalyse ethylene and stereoregular 1-hexene polymerization.[156]

Another approach to induce PSM on the metal node is by adding inorganic acidic sites. MOF-808 was successfully modified treating it with aqueous sulfuric

acid and subsequently adding a sulphate site on the metal node being MOF-808-2.5SO_4 showing a stronger Brønsted acidity. MOF-808-2.5SO_4 is able to catalyse various acid-catalysed reactions such as Friedel-Crafts acylation, esterification, and isomerization.[157]

Following the different methods to treat the metal nodes/clusters in order to add PSM one can also modify them with molecular catalysts. Ethylenediamine (ED) and diethylenetriamine (DETA) were successfully coordinated to the nodes of MIL-101(Cr). The resulting material exhibits catalytic activity for the Knoevenagel condensation. Banerjee et al. attached L-proline-based chiral ligands to the open metal coordination sites of MIL-101 by PSM.[158] Which presents higher enantioselectivity in asymmetric aldol reactions than the chiral ligands themselves. Finally, recent work from Rimoldi et al. immobilised iridium pincer complex in NU-1000 by solvent-assisted ligand incorporation, the resulting Ir-pincer MOF is catalytic active for the condensed phase hydrogenation of liquid alkene and operated as an efficient heterogeneous catalyst under flow conditions.[159]

As mentioned before, one must consider that the node is a key position in terms of MOF structure, and all the modifications that stress this position could lead to the destruction of the framework. Moreover, as also observed in catalysis with encapsulation of active sites, a careful investigation must be carried out after the reaction process. Structure of the active site, thermal and chemical stability of the framework, and the crystallinity of the sample can be distorted after the catalytic process. Apart from the possible changes observed on the catalyst and/or framework itself, it is important to understand if the catalyst is indeed heterogeneous, or the active site is breaking the coordination with the framework and becomes homogeneous as well as, if the reaction is happening on the surface or within the pore. Leaching, surface vs. pores catalysis, and re-use are the most effective tests to understand how the reaction has performed and the evolution of the different components during the reaction process.

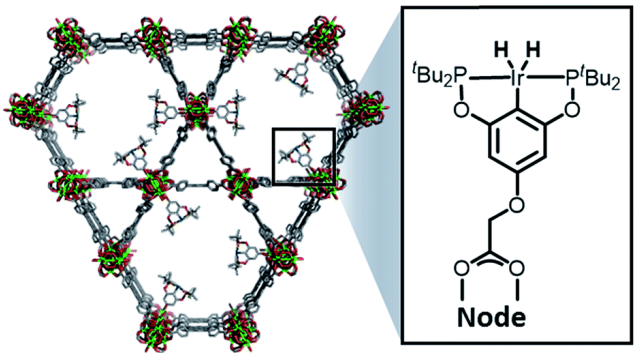


Figure 1.8 Example of a post modified MOF. Nu-1000 supporting a dihydride iridium pincer complex able to catalyse condensed phase hydrogenation of liquid alkene. Adapted from Rimoldi, M., Nakamura, A., Vermeulen, N. A., Henkelis, J. J., Blackburn, A. K., Hupp, J. T., Stoddart, J. F. & Farha, O. K. *Chem. Sci.* **7**, 4980–4984 (2016).[159]

3.5 Unique catalytic applications

The large applicability of MOFs combines the benefits of heterogeneous and homogeneous catalysis for liquid phase heterogeneous catalysis, enantioselective transformations, and solvent-free reactions, etc…. However, their applicability can be further extended to a different than homogeneous or heterogeneous catalysis as they have shown to perform also as photocatalysts.

Photocatalysis is one of the most important methods to address the essential energy into clean fuel and/or chemicals.[160] The different characteristics of MOFs that makes them ideal candidates for photocatalysis are:[161–167]

- The structural defects are avoided due to its crystallinity, these defects are usually recombination centres of charge carriers.
- Both metal ions and organic linkers can be designed as light-harvesting centres with a wide spectrum absorption.
- Metal clusters reassemble inorganic semiconductors.
- High surface areas and porous structures ensure the possibility of introducing photosensitizers or cocatalysts such as, polyoxometalates (POMs), metal NPs, semiconductors, etc. It is possible to achieve an enhanced photocatalytic efficiency by the addition of the abovementioned species as they lead to a spatial separation of charge carriers.

Apart from the abovementioned characteristics there are some common advantages with the heterogeneous catalysis described earlier such as the understanding of structure-property relationship. Moreover, MOFs structural versatility gives the possibility to perform different approaches where to perform the photocatalysis depending again on which position the reaction is performed.

Metal nodes/clusters of MOFs are perfect to perform photocatalysis. They are often open metal sites and electron-deficient centres that can interact with electron-rich reagents. MOFs containing open metal sites can also be doped with external metal ions and active species to perform photocatalytic reactions. Garcia and co-workers[168] reported that MOF-5 behaves as a semiconductor, as they observed charge separation (electrons and holes). This semiconductor-like behaviour made MOFs as promising candidates for the hydrogen production by water splitting. Since then, metal-node engineering has been successfully developed for different MOF to promote their photocatalytic performance in water splitting.[169–172] Moreover, MOFs containing redox-active metal clusters can be used for photocatalytic reduction of CO_2. First works reported that NH_2-MIL-125(Ti), was able to phototactically reduce CO_2 to obtain $HCOO^-$ under light irradiation. Via ligand-to-metal charge transfer is photo-generated the Ti^{3+} moiety which is responsible for the formation of $HCOO^-$.[173] Following these studies it has been possible to perform CO_2 reduction using different metals such as Zr and Fe.[174–177] Post-synthetic modifications have been also applied in order to improve MOFs' photocatalytic efficiency. For example, partial substitution of Zr in NH 2 -UiO-66(Zr) by a Ti moiety via a post- synthetic metal exchange method leads to the mixed metal NH2-UiO-66(Zr/Ti) with enhanced photocatalytic performance for CO2 reduction under visible light irradiation.[178]

As observed in traditional catalytic opportunities, MOFs can also be functionalized with homogeneous photocatalysts. Furthermore, it has been observed that they can drive photocatalysis more efficiently after being incorporated or embedded into MOFs. For instances, MOF-253-Pt material was synthetized through immobilizing a platinum complex into the framework of MOF-253 using a post-synthesis modification strategy.[179] The modified MOF served both as a photosensitizer and a photocatalytic H_2 evolution catalyst. The photocatalytic activity of MOF-253-Pt was approximately five times higher than that of the

corresponding complex. However, studies with UiO-67 doped with Ir complexes have shown lower photocatalytic performance due to the decrease of porosity of the material furnished with the Ir complexes [196-197]. Same strategy has been adopted in reactions of CO_2 reduction. The first heterogenization of molecular complexes onto MOFs for CO_2 photoreduction was reported in 2011.[180] By successfully incorporating $Re^{I}(CO)_3$(dcbpy)Cl(dcbpy=(2,2-bipyridine)-5,5-dicarboxylic acid, H_2L) into UiO- 67(dcppy), they obtained a Re complex-doped MOF heterogeneous photocatalyst that is active for CO_2 reduction under visible light. Further studies have improved the photocatalytic performance of the before mentioned MOF catalysts,[181–183] however this branch within the framework of MOFs as catalyst is still in its early stages.

Section 4. Computational chemistry and molecular modelling

MOFs have proven their large spectrum of applications and their versatility towards catalysis, either being a catalyst them self or supporting catalytic species within them. Nowadays, it exists an extensive bibliography of MOFs with possible applications for catalysis and others[12]. However, such versatility it makes almost impossible to experimentally study all the candidates and all the possible applications. The number of try-and-error tests that should be done to study all the possible combinations of metals and nodes for a given reaction or application it is unmanageable. Computational chemistry and molecular modelling give the possibility to avoid this bottle-neck situation as well as to reduce the waste generated by the experimentation (use of solvents, side reactions, by-products, etc.). By applying computational methodologies, it is possible to preliminary study the different candidates with possible potential for a determined process and predict which materials are more suitable. Moreover, it permits to tailor-made and model the already existent materials to enhance their capacities and explore new applications. A further description of the theoretical chemistry behind computational calculations are collected in Annex 1.

4.1 Electronic structure calculations on MOFs

As described at the beginning of the Introduction, MOFs are crystalline systems which possess a repeating unit (unit cell) composed of tens to hundreds of atoms, sometimes belonging to space groups exhibiting a high degree of symmetry. Electronic calculations of MOFs can be carried out in three different ways, by constructing a smaller molecular cluster which is sufficiently larger for a region of central interest to behave as though it were embedded in the bulk solid, by using the unit cell exploiting periodic boundary conditions (PBC) to model an infinite solid and by combining quantum mechanical and molecular mechanical methods (this las one will not be further discussed as it was not implemented in this manuscript).

4.2 Molecular cluster calculations

MOFs can be approximate by a subnanomolecular cluster or even a nanoscale cluster, referred as a molecular cluster model. One can physically justify the use of cluster models when studying MOFs as the phenomena of interest

(catalysis, gas separation, etc.) are usually localized. By truncating an extended solid-state MOF into a molecular cluster significantly reduces the computational cost. However, such truncation can introduce unphysical edge effects and spatial anisotropy in the model clusters, and if the cluster is too small non-negligible dispersion interaction can be missed in some cases, truncated models must be constructed with special attention to such details.

Supronowicz et al.[184] studied interactions of small gases with Cu-BTC. In such study they used a cluster of Cu-BTC which contains a binuclear copper Cu paddle-wheel unit that is connected to four BTC (benzene tricarboxylate ligands). Two different sizes molecular clusters were constructed. The first one only incorporated a dicopper tetraformate ($Cu_2(HCOO)_4$), which captures the bimetallic nature of the paddle wheel but assumes that the four BTC ligands can be truncated into formate ions. Since the small gas molecules can also interact with portions of the organic linker, the second model contained dicopper tetrabenzene tricarboxylate $Cu_2(BTC)_4$. It is important to consider that the overall charge of the unit cell of Cu-BTC is zero, but the original clusters cut from the periodic crystalline structure are highly charged. Almost all the clusters must be protonated in order to ensure that they reach charge neutrality, as in the MOF's unit cell, being the size of the cluster chosen to minimise the chemical impacts of such local charge adjustments.

Here, Supronowicz et al. study has been selected as an illustrative example, however many electronic structure calculations on MOFs are carried out at the cluster model level.[185–188] A significant advantage of cluster models is that many levels of electronic structure theory are widely available for molecular cluster calculations but not for calculations employing periodic boundary conditions (PBC).

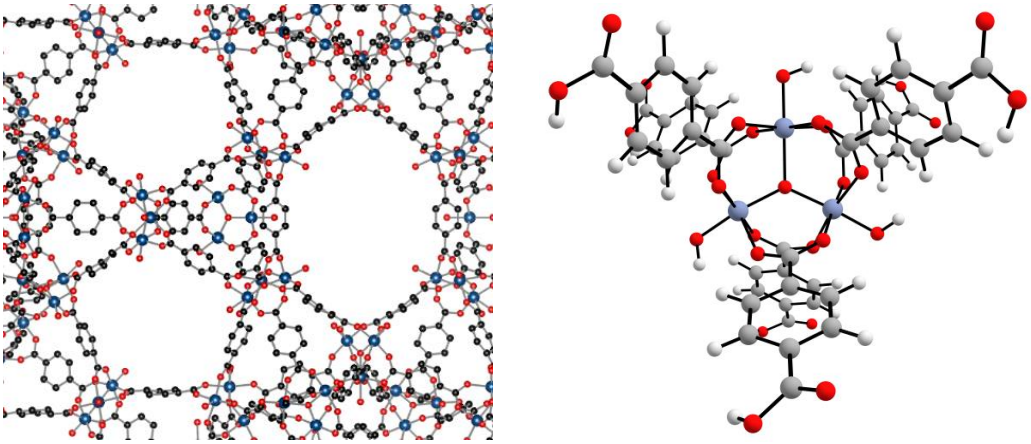


Figure 1.9 (Left) Extended structure of MIL-101. (Right) Molecular cluster containing 112 atoms obtained from the periodic geometry and designed to reproduce the environment nearby the metal node (it includes the metal cluster and the six organic linkers attached to it). Cr, C, O and H atoms are represented as dark blue, grey, red, and white spheres, respectively.

4.3 Periodic Boundary Conditions (PBC)

DFT calculations on the unit cell or also called supercell of MOFs, considering Periodic Boundary Conditions (PBC), are becoming increasingly used (usually referred as periodic DFT calculations) as the necessary computational machinery to perform such calculations has been implemented in several software packages. These calculations are usually performed with plane wave basis sets.[189] The use of plane wave basis sets makes simple to evaluate forces, stresses, and force constants, allowing the optimization of the atomic positions in the unit cell as well as the shape and volume of the unit cell. The construction of plane wave basis sets permits the use of fast Fourier techniques to speed solution of the electronic structure equations and also ensures completeness and orthonormality. Plane waves can treat all the electrons of a system or can be used in conjunction with atomic pseudopotentials that replace the core electrons. All-electron calculations are extremely demanding as the core orbitals vary rapidly and therefore require high frequencies in the plane wave basis. Pseudopotentials simplify the description of the atoms by constructing pseudoatoms in which subset of typically valence electrons is involved in self-consistent calculations and the remaining electrons are replaced with pseudopotentials mimicking their influence on the overall electronic structure.[190] The implementation of pseudopotentials results in significant savings

in computational costs moreover, they are consistent as the most physical and chemical properties are defined by the electrons in valence orbitals. Faster calculations are possible when working with pseudopotentials as the cutoff energy and basis set size are reduced dramatically. Since the quality of plane wave basis sets is uniform at every point space, a very large number of basis functions are needed to properly describe extended but sparsely packed systems (such as MOFs and zeolites) in which the density is both nonuniform and strongly dependent on the local chemical environment. Nevertheless, many plane waves periodic DFT calculations on MOFs have used the pseudopotential approach and works described in this manuscript will not be an exception.

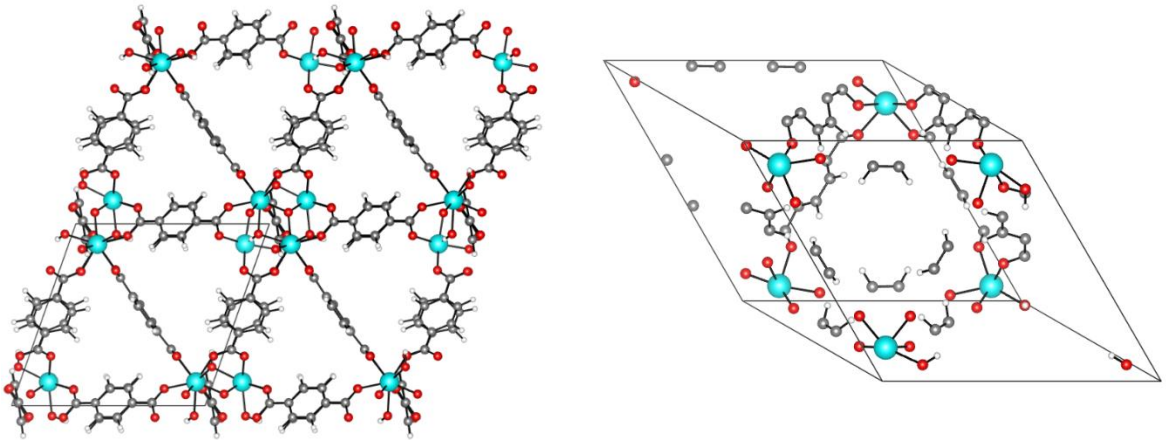


Figure 1.10 (Left) Extended structure for UiO-66, highlighted the primitive cell. (Right) Represented the geometry used to perform the calculations with the UiO-66 primitive cell under PBC. Zr, C, O and H atoms are represented as blue, grey, red, and white spheres, respectively.

4.4 Computational methods used in this thesis

This last subsection summarizes the methods used on the basis of what has been previously discussed in general terms, however it will be accurately depicted in each project section the details of the computational methods used in the correspondent work.

All calculations considering PBC (chapters 3, 4 and 5) were performed using the code CP2K[191] at density functional level of theory. The semi-local PBEsol[192] functional was adopted using the DZVP-MOLOPT-SR-GTH gaussian basis set for all the atom types.[193] The cut-off for the plane wave auxiliary basis set used is depicted in each work. MOF structures are obtained from IR data base. In

order to relieve the computational cost of the calculations, all the systems were studied using the primitive cell. Full geometry optimization i.e., both atomic positions and cell parameters were performed to optimize the MOF-catalyst system considering periodic conditions.

In project developed in chapter 6 it was used a molecular cluster model. The unit cell of the MOF under study was excessively large for periodic DFT calculations, therefore, the calculations were done on a cluster representing the MOF. All the simulations of the cluster were performed with CP2K[191] at density functional level of theory. The semi-local PBE functional of Perdew, Burke and Ernzerhof was adopted[192] using the DZVP-MOLOPT-SR-GTH Gaussian basis set for all the atom types,[193] and a cutoff of 450 Ry for the plane wave auxiliary basis set. The cubic simulation box size was set to 25 × 25 × 25 $Å^3$ ensuring isolated molecule simulation.

In the same chapter 6 it was performed molecular calculations in order to understand the effect of the confinement when performing the reaction. Such calculations were performed using the Gaussian09 set of programs.[194] In these calculations, the BP86 of Becke and Perdew was employed.[195,196] The electronic configuration of the studied molecules was described with the standard split valence basis set with a polarization function for H, C, Cl, N and O (Def2SVP keyword in Gaussian) of Ahlrichs and co-workers.[197] The quasi relativistic, small-core, effective core potential of Stuttgart/Dresden, with an associated valence basis set (SDD keyword in Gaussian) was used for Ru atom.[198] Solvent effects on the potential energy surfaces of the oligomerization cycle were estimated based on the polarizable continuum solvation model (PCM) using dimethyl carbonate (DMC) as solvent,[199,200] the B3LYP, hybrid GGA functional of Becke-Lee, Parr, and Yang[201] and triple-ζ basis set (cc-pVTZ keyword in Gaussian),[202] together with the Grimme D3 correction term for the electronic energy.[203]

Section 5. Bibliography

1. Maxwell, I. E. *Stud. Surf. Sci. Catal.* **101 A**, 1–9 (1996).
2. Cornils, B. & Herrmann, W. A. *J. Catal.* **216**, 23–31 (2003).
3. Nørskov, J. K., Scheffler, M. & Toulhoat, H. *MRS Bull.* **31**, 669–674 (2006).
4. Jones, C. W. *Top. Catal.* **53**, 942–952 (2010).
5. Margelefsky, E. L., Zeidan, R. K. & Davis, M. E. *Chem. Soc. Rev.* **37**, 1118–1126 (2008).
6. Collis, A. E. C. & Horváth, I. T. *Catal. Sci. Technol.* **1**, 912–919 (2011).
7. End, N. & Schöning, K. *Immobilized Catalysts in Industrial Research and Application*. Springer: Berlin, Heidelberg, 2004.
8. Wang, Z., Chen, G. & Ding, K. *Chem. Rev.* **109**, 322–359 (2009).
9. Eddaoudi, M., Moler, D. B., Li, H., Chen, B., Reineke, T. M., O'Keeffe, M. & Yaghi, O. M. *Acc. Chem. Res.* **34**, 319–330 (2001).
10. Furukawa, H., Cordova, K. E., O'Keeffe, M. & Yaghi, O. M. *Science* **341**, 974 (2013).
11. Zhou, H. C., Long, J. R. & Yaghi, O. M. *Chem. Rev.* **112**, 673–674 (2012).
12. Ranocchiari, M. & Bokhoven, J. A. Van. *Phys. Chem. Chem. Phys.* **13**, 6388–6396 (2011).
13. Rowsell, J. L. C. & Yaghi, O. M. *Microporous Mesoporous Mater.* **73**, 3–14 (2004).
14. Jun, C. H. *Chem. Soc. Rev.* **33**, 610–618 (2004).
15. Todd A. Keith, T. G. **2014**, 2017 (2014).
16. Chen, B., Ockwig, N. W., Millward, A. R., Contreras, D. S. & Yaghi, O. M. *Angew. Chemie - Int. Ed.* **44**, 4745–4749 (2005).
17. Chui, S. S. Y., Lo, S. M. F., Charmant, J. P. H., Orpen, A. G. & Williams, I. D. *Science* **283**, 1148–1150 (1999).
18. Eddaoudi, M., Kim, J., Wachter, J. B., Chae, H. K., O'Keeffe, M. & Yaghi,

O. M. *J. Am. Chem. Soc.* **123**, 4368–4369 (2001).

19. Lin, X., Jia, J., Zhao, X., Thomas, K. M., Blake, A. J., Walker, G. S., Champness, N. R., Hubberstey, P. & Schröder, M. *Angew. Chemie* **118**, 7518–7524 (2006).

20. Lin, X., Telepeni, I., Blake, A. J., Dailly, A., Brown, C. M., Simmons, J. M., Zoppi, M., *et al. J. Am. Chem. Soc.* **131**, 2159–2171 (2009).

21. Moulton, B., Lu, J. & Zaworotko, M. J. *J. Am. Chem. Soc.* **123**, 9224–9225 (2001).

22. Allendorf, M. D., Bauer, C. A., Bhakta, R. K. & Houk, R. J. T. *Chem. Soc. Rev.* **38**, 1330–1352 (2009).

23. Bordiga, S., Bonino, F., Petter Lillerud, K. & Lamberti, C. *Chem. Soc. Rev.* **39**, 4885–4927 (2010).

24. Corma, A., García, H. & Llabrés I Xamena, F. X. *Chem. Rev.* **110**, 4606–4655 (2010).

25. Farrusseng, D., Aguado, S. & Pinel, C. *Angew. Chemie - Int. Ed.* **48**, 7502–7513 (2009).

26. Lee, J. Y., Roberts, J. M., Farha, O. K., Sarjeant, A. A., Scheidt, K. A. & Hupp, J. T. *Inorg. Chem.* **48**, 9971–9973 (2009).

27. Johnson, J. W., Jacobson, A. J., Butler, W. M., Rosenthal, S. E., Brody, J. F. & Lewandowski, J. T. *J. Am. Chem. Soc.* **111**, 381–383 (1989).

28. Drumel, S., Janvier, P., Barboux, P., Bujoli-Doeuff, M. & Bujoli, B. *Inorg. Chem.* **34**, 148–156 (1995).

29. Riou, D., Roubeau, O. & Férey, G. *Microporous Mesoporous Mater.* **23**, 23–31 (1998).

30. Li, H., Eddaoudi, M., O'Keeffe, M. & Yaghi, O. M. *Nature* **402**, 276–279 (1999).

31. Eddaoudi, M., Kim, J., Rosi, N., Vodak, D., Wachter, J., O'Keeffe, M. & Yaghi, O. M. *Science* **295**, 469–472 (2002).

32. Burrows, A. D., Frost, C. G., Mahon, M. F. & Richardson, C. *Angew. Chemie* **120**, 8610–8614 (2008).

33. Kleist, W., Jutz, F., Maciejewski, M. & Baiker, A. *Eur. J. Inorg. Chem.* **2009**, 3552–3561 (2009).

34. Deng, H., Doonan, C. J., Furukawa, H., Ferreira, R. B., Towne, J., Knobler, C. B., Wang, B. & Yaghi, O. M. *Science* **327**, 846–850 (2010).

35. Koh, K., Wong-Foy, A. G. & Matzger, A. J. *Angew. Chemie - Int. Ed.* **47**, 677–680 (2008).

36. Chae, H. K., Siberio-Pérez, D. Y., Kim, J., Go, Y. B., Eddaoudi, M., Matzger, A. J., O'Keeffe, M. & Yaghi, O. M. *Nature* **427**, 523–527 (2004).

37. Garibay, S. J. & Cohen, S. M. *Chem. Commun.* **46**, 7700–7702 (2010).

38. Wang, B., Côté, A. P., Furukawa, H., O'Keeffe, M. & Yaghi, O. M. *Nature* **453**, 207–211 (2008).

39. Cui, Y., Xu, H., Yue, Y., Guo, Z., Yu, J., Chen, Z., Gao, J., Yang, Y., Qian, G. & Chen, B. *J. Am. Chem. Soc.* **134**, 3979–3982 (2012).

40. Chandler, B. D., Cramb, D. T. & Shimizu, G. K. H. *J. Am. Chem. Soc.* **128**, 10403–10412 (2006).

41. Bauer, C. A., Timofeeva, T. V., Settersten, T. B., Patterson, B. D., Liu, V. H., Simmons, B. A. & Allendorf, M. D. *J. Am. Chem. Soc.* **129**, 7136–7144 (2007).

42. Chen, B., Yang, Y., Zapata, F., Qian, G., Luo, Y., Zhang, J. & Lobkovsky, E. B. *Inorg. Chem.* **45**, 8882–8886 (2006).

43. Kuppler, R. J., Timmons, D. J., Fang, Q. R., Li, J. R., Makal, T. A., Young, M. D., Yuan, D., Zhao, D., Zhuang, W. & Zhou, H. C. *Coord. Chem. Rev.* **253**, 3042–3066 (2009).

44. Rocha, J., Carlos, L. D., Paz, F. A. A. & Ananias, D. *Chem. Soc. Rev.* **40**, 926–940 (2011).

45. Cui, Y., Yue, Y., Qian, G. & Chen, B. *Chem. Rev.* **112**, 1126–1162 (2012).

46. Lan, A., Li, K., Wu, H., Olson, D. H., Emge, T. J., Ki, W., Hong, M. & Li, J. *Angew. Chemie* **121**, 2370–2374 (2009).

47. Chen, B., Wang, L., Xiao, Y., Fronczek, F. R., Xue, M., Cui, Y. & Qian, G. *Angew. Chemie* **121**, 508–511 (2009).

48. Chen, B., Yang, Y., Zapata, F., Lin, G., Qian, G. & Lobkovsky, E. B. *Adv. Mater.* **19**, 1693–1696 (2007).

49. Della Rocca, J., Liu, D. & Lin, W. *Acc. Chem. Res.* **44**, 957–968 (2011).

50. Zeng, M. H., Wang, B., Wang, X. Y., Zhang, W. X., Chen, X. M. & Gao, S. *Inorg. Chem.* **45**, 7069–7076 (2006).

51. Xu, G. C., Ma, X. M., Zhang, L., Wang, Z. M. & Gao, S. *J. Am. Chem. Soc.* **132**, 9588–9590 (2010).

52. Jia, Q. X., Sun, W. W., Yao, C. F., Wu, H. H., Gao, E. Q. & Liu, C. M. *J. Chem. Soc. Dalt. Trans.* **0**, 2721–2730 (2009).

53. Jia, H. P., Li, W., Ju, Z. F. & Zhang, J. *Eur. J. Inorg. Chem.* **2006**, 4264–4270 (2006).

54. Habib, H. A., Sanchiz, J. & Janiak, C. *Inorganica Chim. Acta* **362**, 2452–2460 (2009).

55. Coronado, E. & Espallargas, G. M. *Chem. Soc. Rev.* **42**, 1525–1539 (2013).

56. Black, C. A., Costa, J. S., Fu, W. T., Massera, C., Roubeau, O., Teat, S. J., Aromí, G., Gamez, P. & Reedijk, J. *Inorg. Chem.* **48**, 1062–1068 (2009).

57. Ricco, R., Malfatti, L., Takahashi, M., Hill, A. J. & Falcaro, P. *J. Mater. Chem. A* **1**, 13033–13045 (2013).

58. Maurice, R., Verma, P., Zadrozny, J. M., Luo, S., Borycz, J., Long, J. R., Truhlar, D. G. & Gagliardi, L. *Inorg. Chem.* **52**, 9379–9389 (2013).

59. Maspoch, D., Ruiz-Molina, D. & Veciana, J. *J. Mater. Chem.* **14**, 2713–2723 (2004).

60. Li, Q., Tian, C., Zhang, H., Qian, J. & Du, S. *CrystEngComm* **16**, 9208–9215 (2014).

61. Li, Q. & Du, S. *RSC Adv.* **5**, 9898–9903 (2015).

62. Biswas, C., Mukherjee, P., Drew, M. G. B., Gómez-García, C. J., Clemente-Juan, J. M. & Ghosh, A. *Inorg. Chem.* **46**, 10771–10780 (2007).

63. James, S. L. *Chem. Soc. Rev.* **32**, 276–288 (2003).

64. Ju, P., Jiang, L. & Lu, T. B. *Chem. Commun.* **49**, 1820–1822 (2013).

65. Pan, L., Olson, D. H., Ciemnolonski, L. R., Heady, R. & Li, J. *Angew. Chemie - Int. Ed.* **45**, 616–619 (2006).

66. Mason, J. A., Sumida, K., Herm, Z. R., Krishna, R. & Long, J. R. *Energy Environ. Sci.* **4**, 3030–3040 (2011).

67. Li, K., Olson, D. H., Seidel, J., Emge, T. J., Gong, H., Zeng, H. & Li, J. *J. Am. Chem. Soc.* **131**, 10368–10369 (2009).

68. Li, J. R., Ma, Y., McCarthy, M. C., Sculley, J., Yu, J., Jeong, H. K., Balbuena, P. B. & Zhou, H. C. *Coord. Chem. Rev.* **255**, 1791–1823 (2011).

69. Li, J. R., Kuppler, R. J. & Zhou, H. C. *Chem. Soc. Rev.* **38**, 1477–1504 (2009).

70. Lee, J. Y., Olson, D. H., Pan, L., Emge, T. J. & Li, J. *Adv. Funct. Mater.* **17**, 1255–1262 (2007).

71. Keskin, S., van Heest, T. M. & Sholl, D. S. *ChemSusChem* **3**, 879–891 (2010).

72. Dietzel, P. D. C., Besikiotis, V. & Blom, R. *J. Mater. Chem.* **19**, 7362–7370 (2009).

73. Chen, B., Liang, C., Yang, J., Contreras, D. S., Clancy, Y. L., Lobkovsky, E. B., Yaghi, O. M. & Dai, S. *Angew. Chemie - Int. Ed.* **45**, 1390–1393 (2006).

74. Britt, D., Furukawa, H., Wang, B., Glover, T. G. & Yaghi, O. M. *Proc. Natl. Acad. Sci. U. S. A.* **106**, 20637–20640 (2009).

75. Bae, Y. S., Mulfort, K. L., Frost, H., Ryan, P., Punnathanam, S., Broadbelt, L. J., Hupp, J. T. & Snurr, R. Q. *Langmuir* **24**, 8592–8598 (2008).

76. Babarao, R., Hu, Z., Jiang, J., Chempath, S. & Sandler, S. I. *Langmuir* **23**,

659–666 (2007).

77. McDonald, T. M., Mason, J. A., Kong, X., Bloch, E. D., Gygi, D., Dani, A., Crocellà, V., *et al. Nature* **519**, 303–308 (2015).

78. McDonald, T. M., Lee, W. R., Mason, J. A., Wiers, B. M., Hong, C. S. & Long, J. R. *J. Am. Chem. Soc.* **134**, 7056–7065 (2012).

79. Millward, A. R. & Yaghi, O. M. *J. Am. Chem. Soc.* **127**, 17998–17999 (2005).

80. Rosi, N. L., Eckert, J., Eddaoudi, M., Vodak, D. T., Kim, J., O'Keeffe, M. & Yaghi, O. M. *Science* **300**, 1127–1129 (2003).

81. Rowsell, J. L. C., Millward, A. R., Park, K. S. & Yaghi, O. M. *J. Am. Chem. Soc.* **126**, 5666–5667 (2004).

82. Morris, R. E. & Wheatley, P. S. *Angew. Chemie - Int. Ed.* **47**, 4966–4981 (2008).

83. Liu, C., Li, F., Lai-Peng, M. & Cheng, H. M. *Adv. Mater.* **22**, E28–E62 (2010).

84. Choi, S., Drese, J. H. & Jones, C. W. *ChemSusChem* **2**, 796–854 (2009).

85. Ma, S. & Zhou, H. C. *Chem. Commun.* **46**, 44–53 (2010).

86. Yaghi, O. M., O'Keeffe, M., Ockwig, N. W., Chae, H. K., Eddaoudi, M. & Kim, J. *Nature* **423**, 705–714 (2003).

87. Llabrés i Xamena, F. X., Casanova, O., Galiasso Tailleur, R., Garcia, H. & Corma, A. *J. Catal.* **255**, 220–227 (2008).

88. Llabrés i Xamena, F. X., Abad, A., Corma, A. & Garcia, H. *J. Catal.* **250**, 294–298 (2007).

89. Mueller, U., Schubert, M., Teich, F., Puetter, H., Schierle-Arndt, K. & Pastré, J. *J. Mater. Chem.* **16**, 626–636 (2006).

90. Dang, D., Wu, P., He, C., Xie, Z. & Duan, C. *J. Am. Chem. Soc.* **132**, 14321–14323 (2010).

91. Dhakshinamoorthy, A. & Garcia, H. *Chem. Soc. Rev.* **41**, 5262–5284 (2012).

92. Czaja, A. U., Trukhan, N. & Müller, U. *Chem. Soc. Rev.* **38**, 1284–1293 (2009).

93. Carson, F., Agrawal, S., Gustafsson, M., Bartoszewicz, A., Moraga, F., Zou, X. & Martín-Matute, B. *Chem. - A Eur. J.* **18**, 15337–15344 (2012).

94. Beier, M. J., Kleist, W., Wharmby, M. T., Kissner, R., Kimmerle, B., Wright, P. A., Grunwaldt, J. D. & Baiker, A. *Chem. - A Eur. J.* **18**, 887–898 (2012).

95. Lee, J., Farha, O. K., Roberts, J., Scheidt, K. A., Nguyen, S. T. & Hupp, J. T. *Chem. Soc. Rev.* **38**, 1450–1459 (2009).

96. Canivet, J., Aguado, S., Schuurman, Y. & Farrusseng, D. *J. Am. Chem. Soc.* **135**, 4195–4198 (2013).

97. Zhang, D., Guan, Y., Hensen, E. J. M., Chen, L. & Wang, Y. *Catal. Commun.* **41**, 47–51 (2013).

98. Davis, M. E. *Acc. Chem. Res.* **26**, 111–115 (1993).

99. Farha, O. K., Spokoyny, A. M., Mulfort, K. L., Hawthorne, M. F., Mirkin, C. A. & Hupp, J. T. *J. Am. Chem. Soc.* **129**, 12680–12681 (2007).

100. Cavka, J. H., Jakobsen, S., Olsbye, U., Guillou, N., Lamberti, C., Bordiga, S. & Lillerud, K. P. *J. Am. Chem. Soc.* **130**, 13850–13851 (2008).

101. Fujita, M., Washizu, S., Ogura, K. & Kwon, Y. J. *J. Am. Chem. Soc.* **116**, 1151–1152 (1994).

102. Schlichte, K., Kratzke, T. & Kaskel, S. *Microporous Mesoporous Mater.* **73**, 81–88 (2004).

103. Zhang, W., Hu, Y., Ge, J., Jiang, H. L. & Yu, S. H. *J. Am. Chem. Soc.* **136**, 16978–16981 (2014).

104. Horike, S., Dincă, M., Tamaki, K. & Long, J. R. *J. Am. Chem. Soc.* **130**, 5854–5855 (2008).

105. Deng, H., Grunder, S., Cordova, K. E., Valente, C., Furukawa, H., Hmadeh, M., Gándara, F., *et al. Science* **336**, 1018–1023 (2012).

106. Hu, Z., Faucher, S., Zhuo, Y., Sun, Y., Wang, S. & Zhao, D. *Chem. - A Eur.*

J. **21**, 17246–17255 (2015).

107. Férey, C., Mellot-Draznieks, C., Serre, C., Millange, F., Dutour, J., Surblé, S. & Margiolaki, I. *Science* **309**, 2040–2042 (2005).

108. Henschel, A., Gedrich, K., Kraehnert, R. & Kaskel, S. *Chem. Commun.* **35**, 4192 (2008).

109. Hwang, Y. K., Hong, D.-Y., Chang, J.-S., Jhung, S. H., Seo, Y.-K., Kim, J., Vimont, A., Daturi, M., Serre, C. & Férey, G. *Angew. Chemie* **120**, 4212–4216 (2008).

110. Mondloch, J. E., Katz, M. J., Isley, W. C., Ghosh, P., Liao, P., Bury, W., Wagner, G. W., *et al. Nat. Mater.* **14**, 512–516 (2015).

111. Horcajada, P., Surblé, S., Serre, C., Hong, D. Y., Seo, Y. K., Chang, J. S., Grenèche, J. M., Margiolaki, I. & Férey, G. *Chem. Commun.* **27**, 2820–2822 (2007).

112. Ravon, U., Domine, M. E., Gaudillère, C., Desmartin-Chomel, A. & Farrusseng, D. *New J. Chem.* **32**, 937–940 (2008).

113. Suslick, K. S., Bhyrappa, P., Chou, J. H., Kosal, M. E., Nakagaki, S., Smithenry, D. W. & Wilson, S. R. *Acc. Chem. Res.* **38**, 283–291 (2005).

114. Shultz, A. M., Farha, O. K., Hupp, J. T. & Nguyen, S. T. *J. Am. Chem. Soc.* **131**, 4204–4205 (2009).

115. Gascon, J., Aktay, U., Hernandez-Alonso, M. D., van Klink, G. P. M. & Kapteijn, F. *J. Catal.* **261**, 75–87 (2009).

116. Morris, G. A., Nguyen, S. B. T. & Hupp, J. T. *J. Mol. Catal. A Chem.* **174**, 15–20 (2001).

117. Kang, X., Zhu, Q., Sun, X., Hu, J., Zhang, J., Liu, Z. & Han, B. *Chem. Sci.* **7**, 266–273 (2016).

118. Jiang, J. & Yaghi, O. M. *Chem. Rev.* **115**, 6966–6997 (2015).

119. Biswas, S., Zhang, J., Li, Z., Liu, Y. Y., Grzywa, M., Sun, L., Volkmer, D. & Van Der Voort, P. *Dalt. Trans.* **42**, 4730–4737 (2013).

120. Akiyama, G., Matsuda, R., Sato, H., Takata, M. & Kitagawa, S. *Adv. Mater.* **23**, 3294–3297 (2011).

121. Zhou, Y. X., Chen, Y. Z., Hu, Y., Huang, G., Yu, S. H. & Jiang, H. L. *Chem. - A Eur. J.* **20**, 14976–14980 (2014).

122. Evans, O. R., Ngo, H. L. & Lin, W. *J. Am. Chem. Soc.* **123**, 10395–10396 (2001).

123. Gotthardt, M. A., Grosjean, S., Brunner, T. S., Kotzel, J., Gänzler, A. M., Wolf, S., Bräse, S. & Kleist, W. *Dalt. Trans.* **44**, 16802–16809 (2015).

124. Aguilera-Sigalat, J. & Bradshaw, D. *Chem. Commun.* **50**, 4711–4713 (2014).

125. Dong, X. W., Liu, T., Hu, Y. Z., Liu, X. Y. & Che, C. M. *Chem. Commun.* **49**, 7681–7683 (2013).

126. Jiang, D., Keenan, L. L., Burrows, A. D. & Edler, K. J. *Chem. Commun.* **48**, 12053–12055 (2012).

127. Gascon, J., Aktay, U., Hernandez-Alonso, M. D., van Klink, G. P. M. & Kapteijn, F. *J. Catal.* **261**, 75–87 (2009).

128. Xiao, J., Chen, C. X., Liu, Q. K., Ma, J. P. & Dong, Y. Bin. *Cryst. Growth Des.* **11**, 5696–5701 (2011).

129. Hasegawa, S., Horike, S., Matsuda, R., Furukawa, S., Mochizuki, K., Kinoshita, Y. & Kitagawa, S. *J. Am. Chem. Soc.* **129**, 2607–2614 (2007).

130. Wu, P., Wang, J., Li, Y., He, C., Xie, Z. & Duan, C. *Adv. Funct. Mater.* **21**, 2788–2794 (2011).

131. Jin, R., Bian, Z., Li, J., Ding, M. & Gao, L. *Dalt. Trans.* **42**, 3936–3940 (2013).

132. Tran, U. P. N., Le, K. K. A. & Phan, N. T. S. *ACS Catal.* **1**, 120–127 (2011).

133. Vaesen, S., Guillerm, V., Yang, Q., Wiersum, A. D., Marszalek, B., Gil, B., Vimont, A., *et al. Chem. Commun.* **49**, 10082–10084 (2013).

134. Chen, X. Y., Hoang, V. T., Rodrigue, D. & Kaliaguine, S. *RSC Adv.* **3**, 24266–24279 (2013).

135. Zhang, F., Zou, X., Gao, X., Fan, S., Sun, F., Ren, H. & Zhu, G. *Adv. Funct. Mater.* **22**, 3583–3590 (2012).

136. Rodenas, T., Van Dalen, M., García-Pérez, E., Serra-Crespo, P., Zornoza, B., Kapteijn, F. & Gascon, J. *Adv. Funct. Mater.* **24**, 249–256 (2014).

137. Timofeeva, M. N., Panchenko, V. N., Jun, J. W., Hasan, Z., Matrosova, M. M. & Jhung, S. H. *Appl. Catal. A Gen.* **471**, 91–97 (2014).

138. Vermoortele, F., Vimont, A., Serre, C. & De Vos, D. *Chem. Commun.* **47**, 1521–1523 (2011).

139. Toyao, T., Saito, M., Horiuchi, Y. & Matsuoka, M. *Catal. Sci. Technol.* **4**, 625–628 (2014).

140. Kleist, W., Jutz, F., Maciejewski, M. & Baiker, A. *Eur. J. Inorg. Chem.* **2009**, 3552–3561 (2009).

141. Zhang, C., Xiao, Y., Liu, D., Yang, Q. & Zhong, C. *Chem. Commun.* **49**, 600–602 (2013).

142. Sun, D., Ye, L. & Li, Z. *Appl. Catal. B Environ.* **164**, 428–432 (2015).

143. Long, J., Wang, S., Ding, Z., Wang, S., Zhou, Y., Huang, L. & Wanga, X. *Chem. Commun.* **48**, 11656–11658 (2012).

144. Hartmann, M. & Fischer, M. *Microporous Mesoporous Mater.* **164**, 38–43 (2012).

145. Seo, J. S., Whang, D., Lee, H., Jun, S. I., Oh, J., Jeon, Y. J. & Kim, K. *Nature* **404**, 982–986 (2000).

146. Mueller, U., Schubert, M., Teich, F., Puetter, H., Schierle-Arndt, K. & Pastré, J. *J. Mater. Chem.* **16**, 626–636 (2006).

147. Hermes, S., Schröter, M. K., Schmid, R., Khodeir, L., Muhler, M., Tissler, A., Fischer, R. W. & Fischer, R. A. *Angew. Chemie - Int. Ed.* **44**, 6237–6241 (2005).

148. Czaja, A. U., Trukhan, N. & Müller, U. *Chem. Soc. Rev.* **38**, 1284–1293 (2009).

149. Maksimchuk, N. V., Kovalenko, K. A., Arzumanov, S. S., Chesalov, Y. A., Melgunov, M. S., Stepanov, A. G., Fedin, V. P. & Kholdeeva, O. A. *Inorg. Chem.* **49**, 2920–2930 (2010).

150. Sheldon, R. A., Wallau, M., Arends, I. W. C. E. & Schuchardt, U. *Acc. Chem. Res.* **31**, 485–493 (1998).

151. Ingleson, M. J., Perez Barrio, J., Guilbaud, J. B., Khimyak, Y. Z. & Rosseinsky, M. J. *Chem. Commun.* **0**, 2680–2682 (2008).

152. Zhang, X., Llabrés i Xamena, F. X. & Corma, A. *J. Catal.* **265**, 155–160 (2009).

153. Wu, C. De, Hu, A., Zhang, L. & Lin, W. *J. Am. Chem. Soc.* **127**, 8940–8941 (2005).

154. Li, Z., Schweitzer, N. M., League, A. B., Bernales, V., Peters, A. W., Getsoian, A. B., Wang, T. C., *et al. J. Am. Chem. Soc.* **138**, 1977–1982 (2016).

155. Noh, H., Cui, Y., Peters, A. W., Pahls, D. R., Ortuno, M. A., Vermeulen, N. A., Cramer, C. J., Gagliardi, L., Hupp, J. T. & Farha, O. K. *J. Am. Chem. Soc.* **138**, 14720–14726 (2016).

156. Klet, R. C., Tussupbayev, S., Borycz, J., Gallagher, J. R., Stalzer, M. M., Miller, J. T., Gagliardi, L., *et al. J. Am. Chem. Soc.* **137**, 15680–15683 (2015).

157. Jiang, J., Gándara, F., Zhang, Y. B., Na, K., Yaghi, O. M. & Klemperer, W. G. *J. Am. Chem. Soc.* **136**, 12844–12847 (2014).

158. Banerjee, M., Das, S., Yoon, M., Hee, J. C., Myung, H. H., Se, M. P., Seo, G. & Kim, O. *J. Am. Chem. Soc.* **131**, 7524–7525 (2009).

159. Rimoldi, M., Nakamura, A., Vermeulen, N. A., Henkelis, J. J., Blackburn, A. K., Hupp, J. T., Stoddart, J. F. & Farha, O. K. *Chem. Sci.* **7**, 4980–4984 (2016).

160. Lewis, N. S. & Nocera, D. G. *Proc. Natl. Acad. Sci. U. S. A.* **103**, 15729–15735 (2006).

161. Xiao, J. D. & Jiang, H. L. *Acc. Chem. Res.* doi:10.1021/acs.accounts.8b00521 (2018).

162. Dhakshinamoorthy, A., Li, Z. & Garcia, H. *Chem. Soc. Rev.* **47**, 8134–8172 (2018).

163. Zhu, J., Li, P. Z., Guo, W., Zhao, Y. & Zou, R. *Coord. Chem. Rev.* **359**, 80–101 (2018).

164. Li, R., Zhang, W. & Zhou, K. *Adv. Mater.* **30**, 1705512 (2018).

165. Fang, Y., Ma, Y., Zheng, M., Yang, P., Asiri, A. M. & Wang, X. *Coord. Chem. Rev.* **373**, 83–115 (2018).

166. Dhakshinamoorthy, A., Asiri, A. M. & García, H. *Angew. Chemie - Int. Ed.* **55**, 5414–5445 (2016).

167. Zhang, T. & Lin, W. *Chem. Soc. Rev.* **43**, 5982–5993 (2014).

168. Alvaro, M., Carbonell, E., Ferrer, B., Llabrés I Xamena, F. X. & Garcia, H. *Chem. - A Eur. J.* **13**, 5106–5112 (2007).

169. Silva, C. G., Luz, I., Llabrés I Xamena, F. X., Corma, A. & García, H. *Chem. - A Eur. J.* **16**, 11133–11138 (2010).

170. Horiuchi, Y., Toyao, T., Saito, M., Mochizuki, K., Iwata, M., Higashimura, H., Anpo, M. & Matsuoka, M. *J. Phys. Chem. C* **116**, 20848–20853 (2012).

171. Dong, X.-Y., Zhang, M., Pei, R.-B., Wang, Q., Wei, D.-H., Zang, S.-Q., Fan, Y.-T. & Mak, T. C. W. *Angew. Chemie* **128**, 2113–2117 (2016).

172. Yuan, S., Qin, J. S., Xu, H. Q., Su, J., Rossi, D., Chen, Y., Zhang, L., *et al. ACS Cent. Sci.* **4**, 105–111 (2018).

173. Fu, Y., Sun, D., Chen, Y., Huang, R., Ding, Z., Fu, X. & Li, Z. *Angew. Chemie - Int. Ed.* **51**, 3364–3367 (2012).

174. Chen, D., Xing, H., Wang, C. & Su, Z. *J. Mater. Chem. A* **4**, 2657–2662 (2016).

175. Xu, H. Q., Hu, J., Wang, D., Li, Z., Zhang, Q., Luo, Y., Yu, S. H. & Jiang, H. L. *J. Am. Chem. Soc.* **137**, 13440–13443 (2015).

176. Wang, D., Huang, R., Liu, W., Sun, D. & Li, Z. *ACS Catal.* **4**, 4254–4260 (2014).

177. Sun, D., Fu, Y., Liu, W., Ye, L., Wang, D., Yang, L., Fu, X. & Li, Z. *Chem. - A Eur. J.* **19**, 14279–14285 (2013).

178. Sun, D., Liu, W., Qiu, M., Zhang, Y. & Li, Z. *Chem. Commun.* **51**, 2056–2059 (2015).

179. Zhou, T., Du, Y., Borgna, A., Hong, J., Wang, Y., Han, J., Zhang, W. & Xu, R. *Energy Environ. Sci.* **6**, 3229–3234 (2013).

180. Wang, C., Xie, Z., Dekrafft, K. E. & Lin, W. *J. Am. Chem. Soc.* **133**, 13445–13454 (2011).

181. Ryu, U. J., Kim, S. J., Lim, H. K., Kim, H., Choi, K. M. & Kang, J. K. *Sci. Rep.* **7**, (2017).

182. Choi, K. M., Kim, D., Rungtaweevoranit, B., Trickett, C. A., Barmanbek, J. T. D., Alshammari, A. S., Yang, P. & Yaghi, O. M. *J. Am. Chem. Soc.* **139**, 356–362 (2017).

183. Li, D., Xu, H.-Q., Jiao, L. & Jiang, H.-L. *EnergyChem* **1**, 100005 (2019).

184. Supronowicz, B., Mavrandonakis, A. & Heine, T. *J. Phys. Chem. C* **117**, 14570–14578 (2013).

185. Verma, P., Xu, X. & Truhlar, D. G. *J. Phys. Chem. C* **117**, 12648–12660 (2013).

186. Valenzano, L., Civalleri, B., Sillar, K. & Sauer, J. *J. Phys. Chem. C* **115**, 21777–21784 (2011).

187. Planas, N., Dzubak, A. L., Poloni, R., Lin, L. C., McManus, A., McDonald, T. M., Neaton, J. B., Long, J. R., Smit, B. & Gagliardi, L. *J. Am. Chem. Soc.* **135**, 7402–7405 (2013).

188. Bordiga, S., Vitillo, J. G., Ricchiardi, G., Regli, L., Cocina, D., Zecchina, A., Arstad, B., Bjørgen, M., Hafizovic, J. & Lillerud, K. F. *J. Phys. Chem. B* **109**, 18237–18242 (2005).

189. Kresse, G. & Furthmüller, J. *Phys. Rev. B - Condens. Matter Mater. Phys.*

54, 11169–11186 (1996).

190. Joubert, D. *Phys. Rev. B - Condens. Matter Mater. Phys.* **59**, 1758–1775 (1999).

191. Hutter, J., Iannuzzi, M., Schiffmann, F. & Vandevondele, J. *Wiley Interdiscip. Rev. Comput. Mol. Sci.* **4**, 15–25 (2014).

192. Perdew, J. P., Ruzsinszky, A., Csonka, G. I., Vydrov, O. A., Scuseria, G. E., Constantin, L. A., Zhou, X. & Burke, K. *Phys. Rev. Lett.* **100**, 136406 (2008).

193. Wilhelm, J. & Hutter, J. *Phys. Rev. B* **95**, 235123 (2017).

194. Frisch, M., Trucks, G., Schlegel, H. & Scuseria, G. *Inc., Wallingford CT* (2009).

195. Becke, A. D. *Phys. Rev. A* **38**, 3098–3100 (1988).

196. Perdew, J. P. *Phys. Rev. B* **33**, 8822–8824 (1986).

197. Schäfer, A., Horn, H. & Ahlrichs, R. *J. Chem. Phys.* **97**, 2571–2577 (1992).

198. Küchle, W., Dolg, M., Stoll, H. & Preuss, H. *J. Chem. Phys.* **100**, 7535–7542 (1994).

199. Barone, V. & Cossi, M. *J. Phys. Chem. A* **102**, 1995–2001 (1998).

200. Tomasi, J. & Persico, M. *Chem. Rev.* **94**, 2027–2094 (1994).

201. Stephens, P. J., Devlin, F. J., Chabalowski, C. F. & Frisch, M. J. *J. Phys. Chem.* **98**, 11623–11627 (1994).

202. Kendall, R. A., Dunning, T. H. & Harrison, R. J. *J. Chem. Phys.* **96**, 6796–6806 (1992).

203. Grimme, S., Antony, J., Ehrlich, S. & Krieg, H. *J. Chem. Phys.* **132**, 154104 (2010).

Chapter 2. General objectives

Section 1. The manuscript

In a previous chapter it has been discussed the chemical features of Metal-Organic frameworks as well as summarized their state-of-the-art applications, focusing mainly on their role as catalysts. Moreover, since this work is purely computational, all the data discussed in the following sections will be obtained by means of theoretical chemistry calculations, thus a brief description of the theory behind those calculations has been also previously included.

MOFs shown to be very promising materials not only for adsorbing and capturing different gases but also for acting as a catalyst. The Introduction chapter, apart from being a description of the most relevant and transcendental works with MOF in the branch of catalytic processes, it was also an intention to demonstrate the vast spectrum of applicability of these materials. Their tunability and the versatility in terms of performing catalytic processes in and on their framework creates an infinity of possibilities impossible to study and test all of them, at least experimentally. Apart from being an impossible task to perform in terms of human time, the number of resources needed to at least study a portion of these possibilities is unimaginable, to say nothing of the derivative amount of waste that would generate. However, it exists a tool that would help in going over through this bottle-neck situation, a tool that is able to study multiple structures and test different features at the same time, not only reducing the time needed to obtain preliminary results but also the resources consumption. Computational chemistry is the tool, by performing computational studies one can select the perfect candidates among all the possibilities for a same process, avoiding all the trial-and-error tests and saving time and resources.

The general idea behind the present manuscript is the use of computational chemistry as a tool to predict and reproduce catalytic activity with MOFs as catalytic species. This thesis collects four works (published or to be published) demonstrating that computational methods can predict and reproduce catalytic capacities for different MOFs and reaction processes. Moreover, these works explore different techniques and approaches on how MOFs can be computationally studied, from how the material is represented (molecular clusters or periodic boundary conditions) until how their features can be depicted (NCI plots, Molecular Orbital calculations, and reactivity calculations among others).

Chapters 3 to 6 collect all the results, and they are defined as the published (or to be) works. Since they are published in scientific journals, they will present the standard organization, each chapter will contain introduction, results and discussion, conclusion, methodology and references sections (not always in this strict order). All the data represented in chapters 3, 4 and 6 has been fully obtained by the author, data represented in chapter 5 arises from an interdisciplinary collaboration between two computational groups and one experimental. For this strict reason in chapter 5 there will be added and extra section specifying the work performed by the author as well as including data omitted on the final published work. Finally, chapter 7 contains general conclusions and perspectives of the work described in previous chapters. Supporting materials for chapters 3 to 6 are gathered after the conclusions chapter.

Section 2. Objectives

The following section will describe one by one the objectives under study in each following chapter in order to contextualize them with the main objective of the thesis.

Chapter 3, the main objective in this project was to perform the DFT calculations prior the experimental studies in order to understand first the CO_2 adsorption within the amino acid functionalized defective-UiO-66. And followed with the rationalization of the CO_2 activation and subsequent carbamic acid formation. All this including the possibility that the defective-UiO-66 would be functionalized with 4 different amino acids. This project was in principle a collaboration with the experimental group of Dr. Marco Taddei, however for technical problems in their labs it will be published only the computational data in a communications format. In context with the thesis, DFT calculations were performed to select the system able to first activate the CO_2 and second perform the formation of the carbamic acid as well as understanding the whole process, prior the experimental study began.

Chapter 4, consists in a pure computational work where UiO-66 has been functionalized with a TMEDA Ni catalyst in order to explore a better performance of the methyl acrylate synthesis from the direct CO_2-ethylen coupling. Performing an heterogenization of homogeneous catalysts is a good technique in order to avoid

catalyst decomposition, however the objective in this work is to explore new reaction pathways and mechanistical aspects to seek for a better performance in the CO_2-ethylen coupling reaction.

Chapter 5, as mentioned before the data from this work arises from an interdisciplinary collaboration between different research groups. The objective here is to demonstrate that by functionalizing MOFs UMCM-1 and MOF-74 with the relevant Co catalyst it is possible to perform selective catalytic transformations. Concretely, allowing branched selectivity in the Co-catalysed hydroformylation of olefines. In the context of the thesis, calculations were performed prior the experimental analysis in order to understand how the catalyst was supported within the structure of the MOF, and how this would affect over the linear/branched selectivity.

Chapter 6, this project is born during a research stay of the author in the research group of Dr. Albert Poater in Girona and intends to explain the role of the supported ruthenium catalyst within the MOF MIL-101 as well as the type of confinement of this catalyst within the cavity of the MOF. This work follows a different trend as intends to explain and unveil the features of an experimental work previously published, differently than the works described in previous chapters where computational calculations were carried out in order to predict catalytic capacities. Nevertheless, this work is in line with the objective of the thesis as demonstrates that computational studies can be useful in both ways, by predicting possible applications as well as by helping in to understand processes already known.

Chapter 3. Computationally aided design of defect-appended aliphatic amines for CO_2 activation within UiO-66

Data reproduced from the article planned to be submitted to *Physical Chemistry Chemical Physics* (*Phys. Chem. Chem. Phys*) journal under the communications format.

Abstract

We report CO_2 adsorption and posterior formation of carbamate acid within the defective UiO-66 functionalized with aliphatic amines. First principle calculations confirms the activation of CO_2 with at minimum two equivalents of aliphatic amines in the system, and the mechanism followed to obtain the final carbamic acid, the key point in this process is the formation of hydrogen bonding between the aliphatic amines.

Reproduced with permission from:

Pareras, G., Taddei, M. & Tiana, D. *Phys. Chem. Chem. Phys. Commun.* (TBC).

Introduction

The use of aliphatic amines to capture CO_2 is one of the oldest and more successful methods, via either chemical absorption (amine scrubbing) or chemical adsorption (solid supported amines). In the case of primary and secondary amines in anhydrous conditions, the mechanism involves the formation of a C-N bond between CO_2 and one amine group, yielding a carbamic acid. This species is then turned into a more stable ammonium carbamate upon proton transfer to a second, neighbouring amine group. In this mechanism, two amine groups are required to capture one CO_2 and proximity of these groups is key to reach the most stable state (see Figure 3.1). In the presence of water, the ammonium carbamate can further react with water, forming a bicarbonate ion and freeing one of the amine groups. Thus, the amine efficiency, i.e., the number of amine groups necessary to bind one CO_2, is doubled when water is involved. The chemisorptive nature of the phenomenon leads to high heat of adsorption and makes it possible to capture CO_2 even in ultradilute conditions, including directly from the air (415 ppm CO_2, 0.0415%).

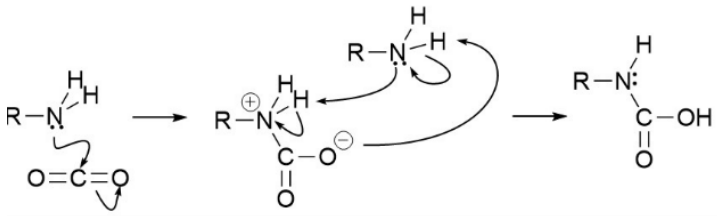


Figure 3.1 Reaction mechanism for the CO_2 activation and posterior carbamic acid obtention.

In this work, we computationally explore the possibility of forming a carbamate from CO_2 and aliphatic amines grafted onto the pore surface of metal-organic frameworks (MOFs). Grafting of aliphatic amines within MOFs is not common, due to the difficulty to introduce these groups in the organic linkers usually employed for the construction of MOFs. A notable example is the introduction of ethyleneimine groups on the aromatic ring of the linker in a pore expanded MOF-74 analogue.[1] A few strategies have been proposed that exploit modifications of the inorganic unit, such as grafting of diamines on the open metal

sites found in MOF-74 analogues[2] or in MIL-101,[3] and installation of ethanolamine in place of μ_3-OH groups on the metal clusters of UiO-66.[4]

We here propose to include aliphatic amines in the internal surface of Zr-based UiO-66 using a defect-engineering approach. In fact, after having created missing cluster defects in UiO-66, functionalisation with a range of monocarboxylic acids, including amino acids, such as serine, is relatively simple.[5] Four aliphatic amino acids were chosen to functionalise the internal surface of UiO-66: glycine (gly), beta-alanine (ala), gamma-aminobutyric acid (gaba) and 5-aminovaleric acid (ava) (see Figure 3.2). The rationale behind this choice is to evaluate the effect of increasing degrees of freedom in the amino acid chain and to see if, by increasing its length, it is possible to promote some cooperative effect between amine groups that lead to formation of carbamates.

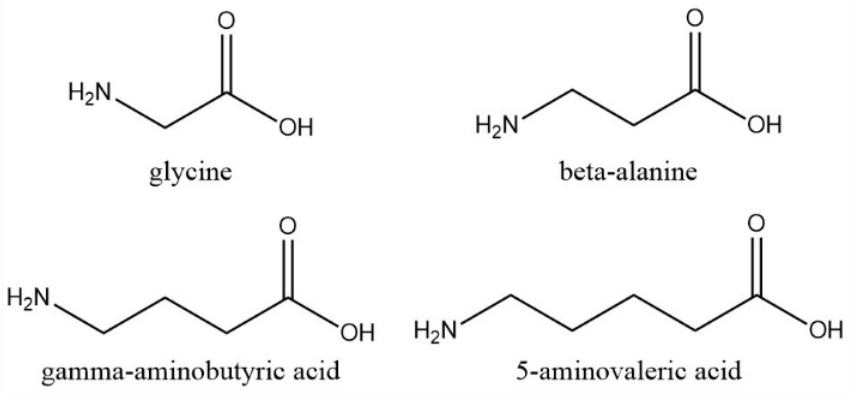


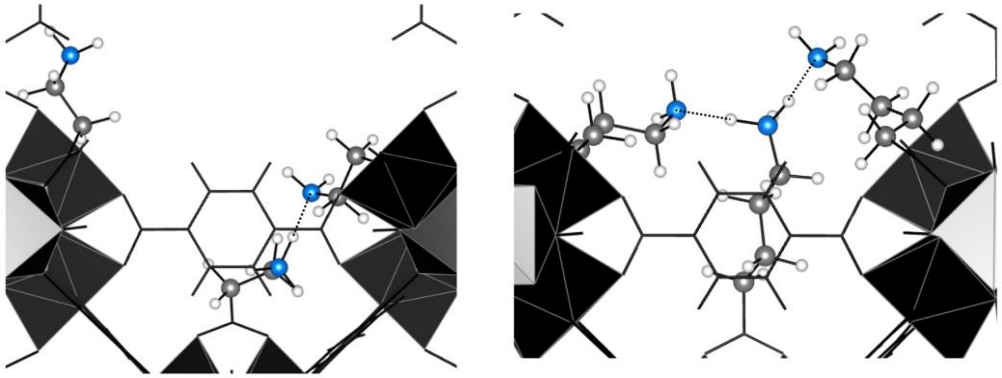
Figure 3.2 Aliphatic amino acids chosen to functionalise UiO-66.

Results and Discussion

Defective MOFs optimization. Standard MOFs scaffolds are quite stiff and, normally, their structures can be approximated as rigid. The situation changes when aliphatic amino acid groups are inserted into the framework, because the aliphatic chains are flexible and fluctuate due to thermal motions. To partially account for this effect, we analysed several configurations for each defect-engineered MOF (see Figure S1). Note that it has been considered initially the functionalization of the defective MOF with three amino acid chains as the geometry under study contains three neighbour exposed clusters able to be functionalized. In fact, there are twelve exposed clusters in the pore of a missing-cluster defect UiO-66. After having optimised the geometry of the four defect-

engineered UiO-66, we checked the possibility of having protonated -NH_3^+ groups in the pore (all the energies are collected in Table S1). This is motivated by the pK_a of the μ_3-OH groups in the clusters (about 3.5)[6] being much lower than the one of the primary amine groups (9.6 for gly, 10.3 for ala, 10.2 for both gaba and ava). Two different simulations were performed: a) the calculation is done in vacuum and the MOF is considered as it is, simulating the situation of the MOF after crystallisation and desiccation; b) the solvent and its dielectric effect are considered using the continuum approximation, which simulates the MOF when in solution during its synthesis. We found that for the systems in vacuum, the protonation is always energetically unfavourable. For the systems in solution, we found that the protonation of the amine is favourable for UiO-66_ava. Two different possibilities have been considered on this process, in systems named (HIN) the H responsible for the amine protonation is coming from the same cluster where the amino acid is bound and in systems named (HOUT) it comes from a neighbour cluster.

On top of the effect of the solvent, which is present and partially stabilises also the other functionalised MOFs (UiO-66_gly, UiO-66_ala, UiO-66_gaba), the reason why the amine is protonated in the solvated UiO-66_ava is the formation of hydrogen bonding between the protonated -NH_3^+ and the two neighbouring, neutral -NH_2 groups (see Figure 3.3). For these systems, we checked if further amine could be protonated. As expected, we found that further protonations are not favourable (see Table S2).



(A) (B)

Figure 3.3 Optimized geometries for systems; (A) UiO-66_ava_HOUT_3 and (B) UiO-66_gaba_HOUT_3 UiO-66_ava_HOUT_3. Hydrogen bonds are highlighted with block dotted lines. Colour scheme: C = grey, H = white, N = blue. The organic ligand and inorganic node of the MOF are represented as black line and black polyhedral for clarity reason.

CO_2 adsorption and activation. We calculated the CO_2 adsorption energy with the inorganic node and with the amie groups (Table S3 and Table S4). As previously found in literature, CO_2 has only physisorptive interactions with μ_3-OH groups in the inorganic node.[4] In UiO-66_gly and UiO-66_ala the amine groups are only slightly more preferable as adsorption sites. This is in line with the experimental observation of Shearer et al. that the isosteric heat of adsorption is only marginally increased when serine is grafted in missing cluster defects in UiO-66.[5] On the other hand, the calculations revealed that CO_2 can be chemically adsorbed in UiO-66_gaba and UiO-66_ava. A geometrical analysis of the chemically adsorbed configurations (i.e., configurations in which N···C distance is within the order of a chemical bond and there is an elongation of the C=O bond distance) indicates that this is promoted by a cooperative effect between the amine groups that create a network of H bonds (see Figure 3.4).

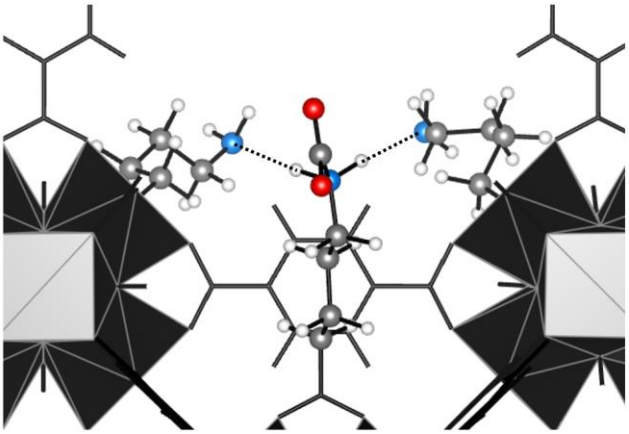


Figure 3.4 Geometry optimization for system UiO-66_ava_2. Hydrogen bonds highlighted in black dotted lines. Colour scheme: C = grey, H = white, O = red, N =blue. The organic ligand and inorganic node of the MOF are represented as black line and black polyhedral for clarity reason.

Following the previous consideration on protonation, we considered the option for one amine group of UiO-66_ava to be protonated prior to exposure to CO_2. This simulates the possibility that the amino group remains quenched in the protonated form during the crystallisation. The results showed that, if one of the amine groups is protonated, the adsorption of CO_2 becomes stronger (average of ca -56 kcal mol^{-1} and interactions up to ca -100 kcal mol^{-1} for the protonated UiO-66_ava compared to an average of ca 20 kcal mol^{-1}, max -50 kcal mol^{-1} for the non-

protonated form) (see Table S5). A geometrical analysis of the configurations reveals again that the interaction is facilitated by the hydrogen bond network that exists between the amino acids present (see Figure 3.5).

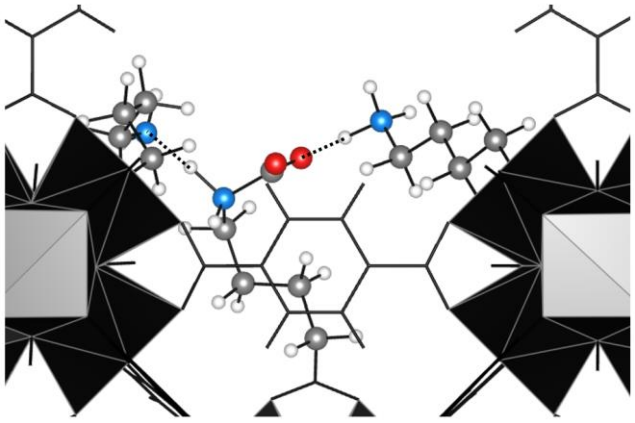


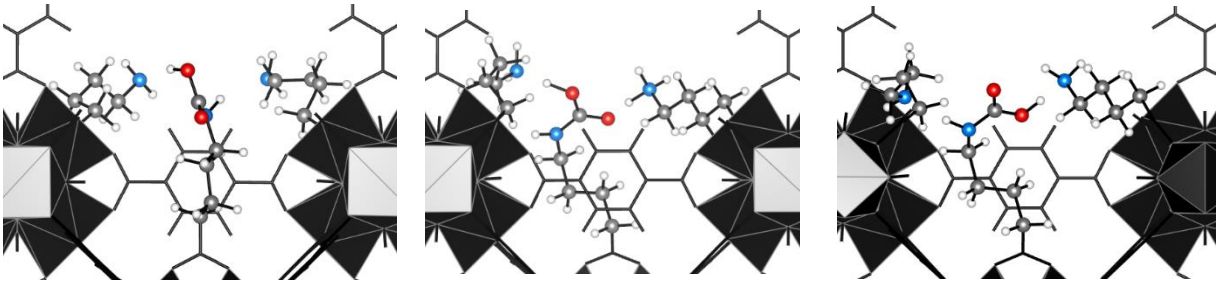
Figure 3.5 Geometry optimization for system UiO-66_ava_HOUT_6. Hydrogen bonds highlighted in black dotted lines. Colour scheme: C = grey, H = white, O = red, N = blue. The organic ligand and inorganic node of the MOF are represented as black line and black polyhedral for clarity reason.

At this stage, we also considered the possibility that not all the defect sites are functionalised with amino acids. This situation might be realistic for the pendant amino acids with the longest chains, due to steric constraints within the confined pore space that might prevent reaching full functionalisation. We simulated the adsorption of CO_2 for UiO-66_gaba and UiO-66_ava and protonated UiO-66_ava with only two or one amino acid moieties (see Figure S2). The results corroborate the idea that a cooperative effect between amine groups is necessary to activate CO_2 (Table S6 and Table S7). The adsorption energies are smaller for all the configurations with only two amines and become of the order of magnitude of physisorption when there is only one amino acid.

Hydrogen transfer and subsequent carbamate formation. Following the reaction scheme of figure 1, for the activated systems we simulated the proton transfer step that leads to the formation of carbamate (see Figure 3.6) (see Table S8, Table S9 and Table S10). As for the standard reaction (mechanism a), this step is characterised by a H transfer from $N1^+$ to N2 followed by the migration of another H from N2 to O^-. This is the mechanism that can occur for UiO-66_gaba and UiO-66_ava (see Figure 3.6 (A) and (B)). An analysis of the atoms confirmed that this

step is an intramolecular process involving two different hydrogens and not an intermolecular H migration were checked and confirmed. Regarding protonated UiO-66_ava, another mechanism could be possible and was tested (mechanism b), i.e., the transfer of the H from $N1^+$ back to the inorganic node. Regardless of the mechanism, we found that the formation of the C-N bond was energetically favourable for all the activated UiO-66_gaba and UiO-66_ava configurations (see Figure 3.6 (C)) (see

Table S11 and Table S12). We note, however, that in the real case of a MOF exposed to a dry stream containing CO_2 the proton back transfer might as well not be relised due to the lack of a suitable proton carrier, such as the solvent during the initial proton transfer from the cluster to the amine group occurring during synthesis.



(A) (B) (C)

Figure 3.6 Geometry optimization for systems; (A) UiO-66_ava_2_H-tran, (B) UiO-66_ava_HOUT_6_H-tran and (C) UiO-66_ava_HOUT_6_H-back. Colour scheme: C = grey, H = white, O = red, N = blue. The organic ligand and inorganic node of the MOF are represented as black line and black polyhedral for clarity reason.

Conclusions

To conclude a computationally aided design procedure was used to engineer the internal surface of UiO-66 to promote CO_2 activation. The internal surface was decorated functionalising missing cluster defects with amino acids with increasing chain length: glycine (gly), beta-alanine (ala), gamma-aminobutyric acid (gaba) and 5-aminovaleric acid (ava). It was found that to promote CO_2 activation hydrogen bonds are required between the different amine groups which can occur only if the amino acid chain is at least as long as gaba (cooperative effect). Furthermore, at least and two of the exposed cluster sites must be functionalised in the same pore

(corresponding to ca 16.66 %). With these concepts in mind the synthesis of UiO-66_gaba and UiO-66_ava, and the experimental verification of the reaction, are under progress.

Notes and references

1. Kim, H. & Hong, C. S. *CrystEngComm* **23**, 1377–1387 (2021).

2. Choe, J. H., Kim, H. & Hong, C. S. *Mater. Chem. Front.* **5**, 5172–5185 (2021).

3. Wang, S., Bromberg, L., Schreuder-Gibson, H. & Hatton, T. A. *ACS Appl. Mater. Interfaces* **5**, 1269–1278 (2013).

4. Usman, M., Helal, A., Abdelnaby, M. M., Alloush, A. M., Zeama, M. & Yamani, Z. H. *Chem. Rec.* **21**, 1771–1791 (2021).

5. Shearer, G. C., Vitillo, J. G., Bordiga, S., Svelle, S., Olsbye, U. & Lillerud, K. P. *Chem. Mater.* **28**, 7190–7193 (2016).

6. Klet, R. C., Liu, Y., Wang, T. C., Hupp, J. T. & Farha, O. K. *J. Mater. Chem. A* **4**, 1479–1485 (2016).

Chapter 4. UiO-66 mediated methyl acrylate formation from the direct electrophilic nickelalactone ring opening with methyl iodate

Data reproduced from the article planned to be submitted to *Molecular Catalysis* (*Mol. Cat.*) journal.

Abstract

Methyl acrylate synthesis from the direct coupling of CO_2-ethylene is a controversial reaction process as the reaction mechanism proposed show relatively high transition states. The functionalization of Metal-Organic Frameworks (MOFs) with homogeneous catalysts not only showed advantages on a better performing by avoiding catalyst decomposition but it has also been observed that are able to modify reaction mechanisms, discovering new reaction pathways. Here we report a full computational work were MOF UiO-67 has been functionalized with an adaptation of the Tetramethylethylenediamine (TMEDA) existent homogeneous catalyst in order to explore a possible alternative pathway. Computational results reported here show a slight improvement of the reaction mechanism and more interestingly it has been observed structural changes in the catalyst itself that could not happen under homogeneous conditions.

Reproduced with permission from:

Pareras, G. & Tiana, D. *Mol. Cat.* (TBC).

Introduction

The world energy consumption in the last decade has almost double compared to 2010. The demand for fuels has grown, driven by natural gas which led to an increase in carbon dioxide emissions, that reached a record growth of 1.7% in 2018. With this trend it is clear that the Paris agreement on the climate change, i.e. to reduce greenhouse gas emissions by at least 40% by 2030 compared to 1990, will not be met.

CO_2 is normally considered as a waste product to be capture and store somewhere, this has produced the research field of Carbon Capture and Storage (CCS).[1–6] However it is a source of C1 building block and could become a cheap raw material for different bulk chemicals giving us the chance of turning this spent-CO_2 in to working CO_2.[7] That is the concept of CCS can be upgraded to a more economically interesting idea of Carbon Capture and Reutilisation (CCR).[8–10]

Acrylic acid and acrylate derivatives are ubiquitous in our daily life as hygiene products, coatings and food preservatives, presenting a global market volume of approximately four millions tons.[11] One of the most promising reactions is the direct coupling between CO_2 and ethylene (C_2H_4) to form acrylic acid and acrylates, this is one of the most rising concepts for the large-scale utilization of CO_2.[12] The synthesis of acrylates from CO_2 and C_2H_4 has been broadly discussed and investigated exhibiting promising outcomes.[13–17] First investigations were particularly focused on the synthesis of high-demanded acrylic acid through the zero-valent transition-metal assisted coupling of CO_2 and ethylene (see Figure 4.1).[18–23]

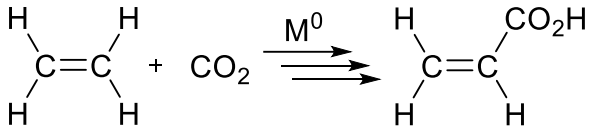


Figure 4.1 Zero-valent metal mediated acrylic acid formation via direct coupling of carbon dioxide and ethylene.

However, all the reactions involving the oxidative coupling between olefins and CO_2 in presence of transition metal centres, such as Ni, Pd and Mo lead to the formation of a five-membered metallacycle, first evidences of the formation of

these species were reported by Hoberg and co-workers[24] in the 1980s. These compounds also referred to as metallalactones are stable and they could be isolated (Figure 4.2). Consequently, the following β-hydride elimination required to yield acrylic acid is not allowed, turning this step the most challenging one. The difficulty to cleave this rigid planar five-membered ring results in a long distance between the metal centre and the β-H atoms. Different mechanistic studies[25–27] have been carried out in order to spread some light on this controversial catalytic process, nevertheless the endergonic nature of the overall reaction and the high energetic barrier required for the β-hydride elimination (ΔG = 164 kJ/mol)[14,19] have been fazing the researchers.

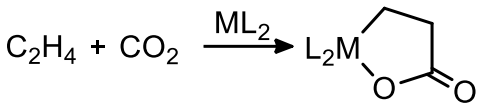


Figure 4.2 First reaction step resulting in the metallacycle formation.

Last investigations based on the metal-assisted coupling of CO_2 with alkenes for the formation of acrylates are based on the use of Ni^0 following the first steps of Hoberg and co-workers. Hoberg studies reported that the coupling reaction between CO_2 and C_2H_4 was mediated by a stoichiometric amount of Ni(DBU).[30] Subsequently, a theoretical study of Graham et al.[28] reported some insights with regard to these experimental observations, concluding that the direct β-hydride elimination is unlikely due to the high energy barrier that this step presents (ΔG = 147.4 kJ/mol). They also relied in the fact that a possible elongation of the Ni-O bond on the nickelalactone could help in decreasing the ring strain reducing the energy required to perform this β-H elimination. The idea of introducing an external reagent is the best way of clearing this obstacle. Several research groups focused their efforts in studying different compounds with the capacity of activate the Ni-O bond, the most promising promotors are methylating agents, Lewis acidic reagents and sodium-containing promotors[17,31–36].

Despite of the success in obtaining the relevant acrylates by the promotion of Lewis acids and sodium-containing reagents, methylating agents showed to be the best candidates as promotors for the nickelalactone cleavage. The first methylating agent tasted was the methyl iodate (MeI) by Rieger et al[35]. The aim is to activate the Ni-O bond by an electrophilic attack of the Me cation of MeI,

followed by the β-hydride transfer and closing the cycle with the reductive elimination of HI (see Figure 4.3). Studies by Rieger and co-workers confirmed that the in situ methylation of nickelalactone enables both the β-hydride elimination and the subsequent release of methyl acrylate, however yields obtained for this process were quite moderate (max.33%)[35]. Khün et al.[34] deepened into this reaction extending their studies in to analyse various methylating agents in order to achieve a complete catalytic cycle. Their preliminary screening goes from milder and stronger reagents such as dimethyl carbonate, sulphur-containing reagents such us MeOTf and the toxic dimethyl sulphate. MeOTf is the most effective in the electrophilic ring opening of the nickelalactone and the subsequent release of methyl acrylate, being even far more efficient than the overriding methylating agent MeI. However, MeI is still the best candidate, as MeOTf can coordinate to the Ni centre blocking the coordinating site necessary for the β-hydride elimination leading to the cease of the reaction process.

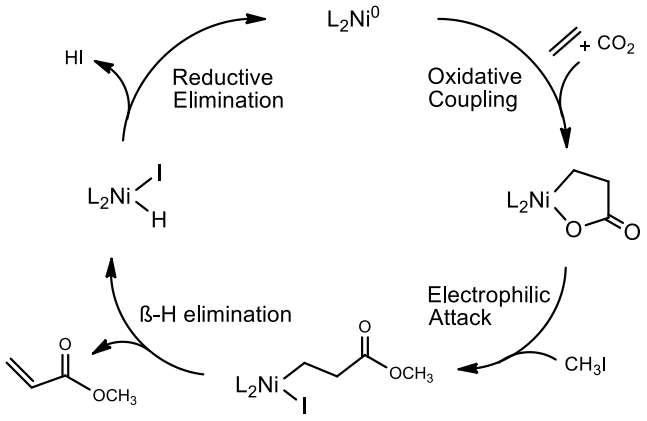


Figure 4.3 Hypothetical catalytic cycle for the nickel mediated synthesis of methyl acrylate from the CO_2-ethylene direct coupling and assisted with the methylating agent MeI.

Apart from the methylating agent screening, Khün and co-workers study was further extended focusing on the influence of different ligands at the nickel center.[17] A range of different ligands was studied finally concluding that chelating diamine/diphosphine ligands facility the β-hydride elimination. Moreover, flexible bound ligands, due to a partial disassociation of the ligand, stimulate the approach of the β-H toward the Ni centre. The conjunction between the methylating agent

MeI and the most reactive TMEDA nickelalactone is the best approach and the reagent of choice to yield methyl acrylate.

The mechanism proposed for the synthesis of methyl acrylate from the reaction between CO_2, C_2H_4 and MeI mediated by Ni complexes has been detailed and different ligands and methylating agents have been exhaustively studied.[23,33,37–42] Although all the efforts and promising results obtained from academia, it has not been possible to reduce the required energy for the nickelalactone ring opening allowing the β-hydride elimination. Hereby, it is necessary to keep investigating on new candidates for ring-opening reagents. In this work a new Ni complex has been developed and computationally tested in order to improve the methyl acrylate synthesis by reducing the energy required for the MeI electrophilic attack and the subsequent β-hydride elimination.

Metal-Organic Frameworks (MOFs) have shown being promising materials for catalysis. Their potential as catalysts goes beyond mere supporting materials. They have shown the capacity not only to encapsulate reactants, and perform catalytic reactions within a confined space but also to interact with the reactants, becoming part of the it opening new reaction pathways.[43–55] Following the methodology of a heterogenization of a homogeneous catalysis, in this work we design a new catalyst starting from UiO-67, a mesoporous MOF stable at high temperature.[56] It is composed 4,4′biphenyl-dicarboxylate as organic linker while the inorganic node consists of $Zr_6O_4(OH)_4$ clusters, in which the triangular faces of the Zr_6-octahedron are alternatively capped by μ3-O and μ3-OH groups. Due to its relatively larger pore size, it has been reported several works with UiO-67 as a material supporter for catalysts.[57–61] As demonstrated in previous works the organic ligands can be functionalised to create active catalytic sites.[62,63] Furthermore, recent works reported that by attaching different substituents to those linkers one can modulate the catalytic activity of the MOF.[64,65] For this reason in this work we explored the opportunity of having a new functionalised ligand based on the commercially known as Bis(dimethylamino)chlorophosphine (DMAP, see Figure 4.4).

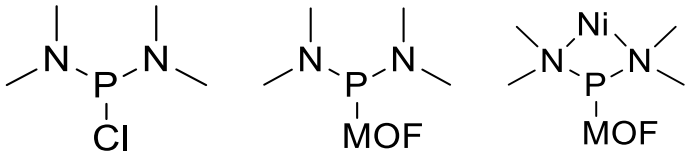


Figure 4.4 Left: commercial Bis(dimethylamino)chlorophosphine. Centre: suggested coordination with MOFs. Right: posterior chelation of the Ni centre.

Results and discussion

Figure 4.5 reports the reaction energy profile for TMEDA and for our new proposed catalyst UiO-67-DMAP

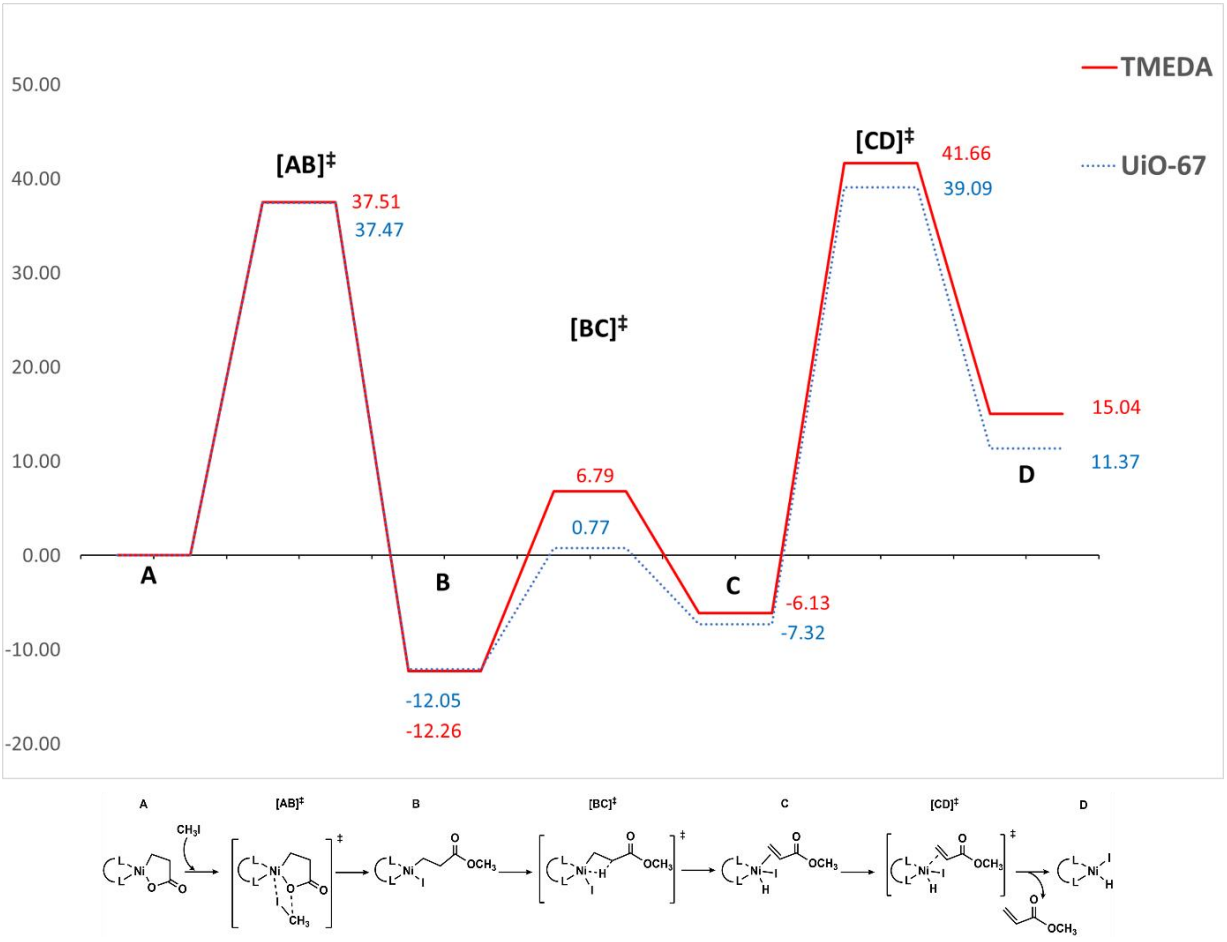
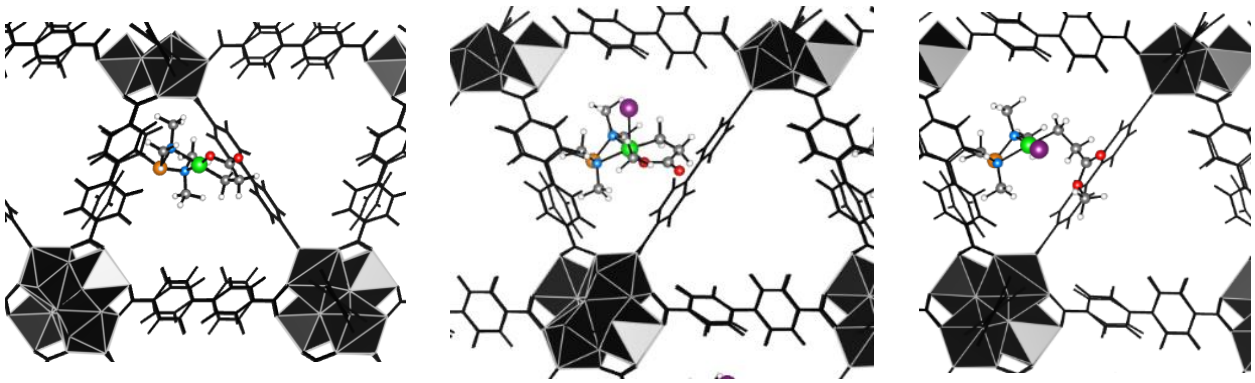


Figure 4.5 Reaction energy profile (in kcal·mol^{-1}) corresponding to the synthesis of methyl acrylate starting with the electrophilic attack of CH_3I to the nickelalactone. Represented energies from TMEDA (continuous red) and UiO-67 (dot blue) systems.

The 1st step of the reaction involves the electrophilic attack of CH_3I to the metallacycle leading to the cleavage of the lactone ring the square planar complex

B. In this step CH_3I elongates from of ca 0.5 Angstrom (see the SI for all the geometrical parameters). At this stage there is no difference in the reaction energy profile reaction of the classical ligand TMEDA and our new proposed UiO-67-DMAP. An analysis of the bond distances and of the angles confirms the reactions follow exactly the same path when going from A to TS_AB and then B (see from Table S1 to Table S3).

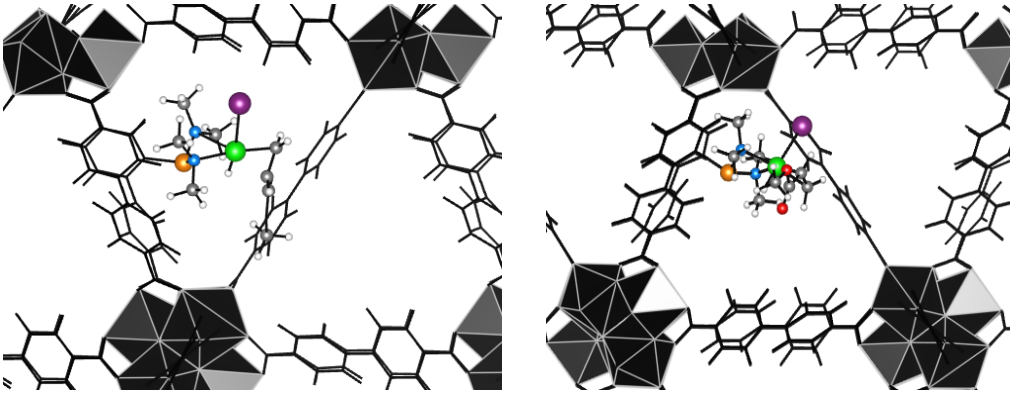


A TS_AB B

Figure 4.6 Optimized geometry for; UiO-67-DMAP step A, UiO-67-DMAP step TS_AB and UiO-67-DMAP step B. Colour scheme: C = grey, H = white, O = red, N = blue I = purple, P = orange and Ni = green. The organic ligand and inorganic node of the MOF are represented as black line and black polyhedral for clarity reason.

The 2nd step of the reaction involves the β-hydrogen migration via the formation of a 4-member ring between NiCαCβHβ (TS_BC) and the following formation of a CC double bond coordinated to the Ni (complex C). Here the positive effect of our proposed catalyst can be seen as the TS_BC activation energy decreases of ca 6 kcal·mol^{-1}. To rationalise this difference in energies we need to look at what happens in this transition state. The analysis of the geometrical parameters reveals that in UiO-67-DMAP there is a big elongation of the N1··Ni (from 1.88 to 2.95 Ang) compared to TMEDA (from 1.97 to 2.35 Ang) (see Table S4 and Table S5). This can be attributed to a temporary breaking of the Ni bond with N1. That is, in UiO-67-DMAP, Ni maintains its coordination number as 4 (instead of 5). For this reason, Ni is more prone to accept electrons from the β-H resulting in a bigger activation of the βC··βH bond in UiO-67-DMAP compared to TMEDA (the former elongates from 1.10 to 1.90 Ang, the latter from 1.10 to 1.65

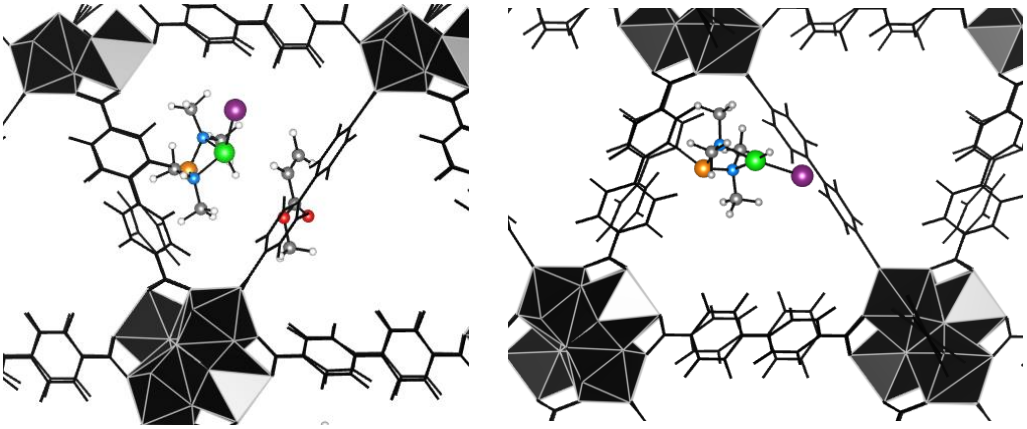
Ang). The β-hydride elimination leads to the formation of intermediate C, where the acrylate η2-coordinates with the nickel centre.



TS_BC C

Figure 4.7 Optimized geometry for; UiO-67-DMAP step TS_BC and UiO-67-DMAP step C. Colour scheme: C = grey, H = white, O = red, N = blue I = purple, P = orange and Ni = green. The organic ligand and inorganic node of the MOF are represented as black line and black polyhedral for clarity reason.

The last step of the reaction, a ligand dissociation in which the product leaves, involves the removal of the methyl acrylate after the elongation of the Ni – alkene group interaction. As for the previous step, a slightly different mechanism is present for UiO-67-DMAP compared to TMEDA. In fact, as for TS_BC when getting to the transition state configuration, there is a distortion in how Ni coordinates with the ligands. Ni is chelated by TMEDA Ni-N1 = 2.04 Ang, Ni-N2 = 2.00 Ang whilst it can be considered as sigma coordinated by UiO-67-DMAP (Ni-N1 = 2.36 Ang, Ni-N2 = 1.91 Ang). In this case, this changing in the Ni N interactions have only a small effect in lowering the activation energy to get to TS_CD (ca 2 kcal·mol^{-1}). Finally, it was found that UiO-67_DMAP has an important role in stabilising complex D (see Table S6 and Table S7).



TS_CD D

Figure 4.8 Optimized geometry for; UiO-67-DMAP step TS_CD and UiO-67-DMAP step D. Colour scheme: C = grey, H = white, O = red, N = blue I = purple, P = orange and Ni = green. The organic ligand and inorganic node of the MOF are represented as black line and black polyhedral for clarity reason.

To verify that our assumption about the indirect effect of the MOF scaffold to the reaction was correct, we calculated the reaction energy profile of an isolated organic ligand similar to the one we used in UiO-67, i.e. terephthalic acid dimethyl aminophosphine (TFA-DMAP), see Figure 4.9. The results (see Table 4.1) confirmed that UiO-67 has a role in the energetic profile, particularly in lowering the activation energy of TS_BC (see the SI for all the geometrical parameters).

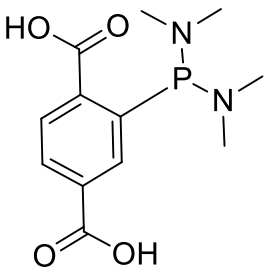


Figure 4.9 Structure of the molecular cluster from the UiO-66, the terephthalic acid dimethyl aminophosphine ligand (TFA-DMAP).

Table 4.1 Relative energies in kcal·mol^{-1} for the reaction mechanism and the three systems under study. Reaction step A is considered the relative zero.

Step	TMEDA	UiO-67-DMAP	TFA-DMAP
A	0.00	0.00	0.00
TS_AB	37.51	37.47	39.73
B	-12.26	-12.05	-7.40
TS_BC	6.79	0.77	7.74
C	-6.13	-7.32	-2.14
TS_CD	41.66	39.09	42.36
D	15.04	11.37	16.08

Conclusions

In this work it has been performed a computational study to tailor made a new brand catalyst by functionalizing UiO-67. Basically, the internal surface of UiO-67 is functionalized with the dimethylaminophospine (UiO-67-DMAP) and subsequently coordinating the Ni atom. Functionalized UiO-67 show an interesting role on the reaction of the formation of methyl acrylate from the CO_2-ethylene direct coupling. It is observed a stabilization of the reaction intermediates following the stabilisation of TS_BC. To be note how, despite at a small intensity, the new catalyst was also found to lower the rating determinant step (TS_CD). This is an important finding because, in principle, other small modifications to the MOF could lead to more pronounced lowering. However, TS_AB still shows a quit high energy barrier. It is interesting to mention that by attaching the catalyst to the MOF it has more grade of liberty, in other words, we observed a partial breaking of the chelating ligands that helps on performing the transition states, this would not be possible under homogeneous conditions as it will lead to the destruction of the catalyst. Calculations with the molecular cluster of UiO-66 show that there is no difference between the cluster and the TMEDA catalyst, reaffirming that is needed to perform the calculations considering the whole cavity of the MOF.

Computational details

All calculations were performed using the code CP2K[66] at density functional level of theory considering gas phase. The semi-local PBEsol functional was adopted[67] using the DZVP-MOLOPT-SR-GTH gaussian basis set for all the atom types,[68] and a cutoff of 500 Ry for the plane wave auxiliary basis set. MOF

structures were obtained from IR data base. In order to relieve the computational cost of the calculations, all the systems were studied using the primitive cell. Full geometry optimization i.e., both atomic positions and cell parameters were performed to optimize the MOF-catalyst system considering periodic conditions. Calculations using the molecular cluster of the MOF as well as calculations of the TMEDA system were carried out within a cubic simulation box size set to 25 × 25 × 25 $Å^3$ ensuring isolated molecule simulation. Posterior to the geometry optimization vibrational analysis have been carried out. All the intermediates show positive frequencies ensuring that are local minima while transition states show only one imaginary frequency that leads to the desired following minima on the reaction mechanism (see Table S8).

References

1. Gibbins, J. & Chalmers, H. *Energy Policy* **36**, 4317–4322 (2008).

2. Boot-Handford, M. E., Abanades, J. C., Anthony, E. J., Blunt, M. J., Brandani, S., Mac Dowell, N., Fernández, J. R., *et al. Energy Environ. Sci.* **7**, 130–189 (2014).

3. Bui, M., Adjiman, C. S., Bardow, A., Anthony, E. J., Boston, A., Brown, S., Fennell, P. S., *et al. Energy Environ. Sci.* **11**, 1062–1176 (2018).

4. Anderson, S. & Newell, R. *Annu. Rev. Environ. Resour.* **29**, 109–142 (2004).

5. Pires, J. C. M., Martins, F. G., Alvim-Ferraz, M. C. M. & Simões, M. *Chem. Eng. Res. Des.* **89**, 1446–1460 (2011).

6. Stuart Haszeldine, R. *Science* **325**, 1647–1652 (2009).

7. Plasseraud, L. *ChemSusChem* **3**, 631–632 (2010).

8. Ghiat, I., AlNouss, A. & Al-Ansari, T. *Comput. Aided Chem. Eng.* **50**, 695–701 (2021).

9. Al Baroudi, H., Awoyomi, A., Patchigolla, K., Jonnalagadda, K. & Anthony, E. J. *Appl. Energy* **287**, 116510 (2021).

10. Sedlar, D. K., Vulin, D., Krajačić, G. & Jukić, L. *Renew. Sustain. Energy Rev.* **108**, 159–174 (2019).

11. Aresta, M., Dibenedetto, A. & Quaranta, E. *J. Catal.* **343**, 2–45 (2016).

12. Cokoja, M., Bruckmeier, C., Rieger, B., Herrmann, W. A. & Kühn, F. E. *Angew. Chemie - Int. Ed.* **50**, 8510–8537 (2011).

13. Schubert, G. & Pápai, I. *J. Am. Chem. Soc.* **125**, 14847–14858 (2003).

14. Graham, D. C., Mitchell, C., Bruce, M. I., Metha, G. F., Bowie, J. H. & Buntine, M. A. *Organometallics* **26**, 6784–6792 (2007).

15. Drees, M., Cokoja, M. & Kühn, F. E. *ChemCatChem* **4**, 1703–1712 (2012).

16. Kirillov, E., Carpentier, J. F. & Bunel, E. *Dalt. Trans.* **44**, 16212–16223 (2015).

17. Lee, S. Y. T., Cokoja, M., Drees, M., Li, Y., Mink, J., Herrmann, W. A. & Kühn, F. E. *ChemSusChem* **4**, 1275–1279 (2011).

18. Sasaki, Y., Inoue, Y. & Hashimoto, H. *J. Chem. Soc. Chem. Commun.* **460**, 605–606 (1976).

19. Inoue, Y., Sasaki, Y. & Hashimoto, H. *Bull. Chem. Soc. Jpn.* **51**, 2375–2378 (2006).

20. Alvarez, R., Carmona, E., Galindo, A., Poveda, M. L., Cole-Hamilton, D. J., Gutiérrez-Puebla, E., Monge, A. & Ruiz, C. *J. Am. Chem. Soc.* **107**, 5529–5531 (1985).

21. Alvarez, R., Carmona, E., Galindo, A., Gutierrez, E., Marin, J. M., Monge, A., Poveda, M. L., Ruiz, C., Savariault, J. M. & Savariault, J. M. *Organometallics* **8**, 2430–2439 (1989).

22. Galindo, A., Pastor, A., Pérez, P. J. & Carmona, E. *Organometallics* **12**, 4443–4451 (1993).

23. Fischer, R., Langer, J., Malassa, A., Walther, D., Görls, H. & Vaughan, G.

Chem. Commun. 2510–2512 (2006).

24. Hoberg, H., Jenni, K., Angermund, K. & Krüger, C. *Angew. Chemie Int. Ed. English* **26**, 153–155 (1987).

25. Schubert, G. & Pápai, I. *J. Am. Chem. Soc.* **125**, 14847–14858 (2003).

26. Plessow, P. N., Weigel, L., Lindner, R., Schäfer, A., Rominger, F., Limbach, M. & Hofmann, P. *Organometallics* **32**, 3327–3338 (2013).

27. Aresta, M., Pastore, C., Giannoccaro, P., Kovács, G., Dibenedetto, A. & Pápai, I. *Chem. - A Eur. J.* **13**, 9028–9034 (2007).

28. Graham, D. C., Mitchell, C., Bruce, M. I., Metha, G. F., Bowie, J. H. & Buntine, M. A. *Organometallics* **26**, 6784–6792 (2007).

29. Pápai, I., Schubert, G., Mayer, I., Besenyei, G. & Aresta, M. *Organometallics* **23**, 5252–5259 (2004).

30. Hoberg, H., Peres, Y., Krüger, C. & Tsay, Y. -H. *Angew. Chemie Int. Ed. English* **26**, 771–773 (1987).

31. Zhang, Z., Guo, F., Kühn, F. E., Sun, J., Zhou, M. & Fang, X. *Appl. Organomet. Chem.* **31**, e3567 (2017).

32. Jin, D., Schmeier, T. J., Williard, P. G., Hazari, N. & Bernskoetter, W. H. *Organometallics* **32**, 2152–2159 (2013).

33. Lejkowski, M. L., Lindner, R., Kageyama, T., Bódizs, G. É., Plessow, P. N., Müller, I. B., Schäfer, A., *et al. Chem. - A Eur. J.* **18**, 14017–14025 (2012).

34. Lee, S. Y. T., Ghani, A. A., D'Elia, V., Cokoja, M., Herrmann, W. A., Basset, J. M. & Kühn, F. E. *New J. Chem.* **37**, 3512–3517 (2013).

35. Bruckmeier, C., Lehenmeier, M. W., Reichardt, R., Vagin, S. & Rieger, B. *Organometallics* **29**, 2199–2202 (2010).

36. Fischer, R., Langer, J., Malassa, A., Walther, D., Görls, H. & Vaughan, G. *Chem. Commun.* **23**, 2510–2512 (2006).

37. Stieber, S. C. E., Huguet, N., Kageyama, T., Jevtovikj, I., Ariyananda, P., Gordillo, A., Schunk, S. A., Rominger, F., Hofmann, P. & Limbach, M. *Chem. Commun.* **51**, 10907–10909 (2015).

38. Guo, W., Michel, C., Schwiedernoch, R., Wischert, R., Xu, X. & Sautet, P. *Organometallics* **33**, 6369–6380 (2014).

39. Huguet, N., Jevtovikj, I., Gordillo, A., Lejkowski, M. L., Lindner, R., Bru, M., Khalimon, A. Y., *et al. Chem. - A Eur. J.* **20**, 16858–16862 (2014).

40. Plessow, P. N., Schäfer, A., Limbach, M. & Hofmann, P. *Organometallics* **33**, 3657–3668 (2014).

41. Drees, M., Cokoja, M. & Kühn, F. E. *ChemCatChem* **4**, 1703–1712 (2012).

42. Li, Y., Liu, Z., Cheng, R. & Liu, B. *ChemCatChem* **10**, 1420–1430 (2018).

43. Bauer, G., Ongari, D., Xu, X., Tiana, D., Smit, B. & Ranocchiari, M. *J. Am. Chem. Soc.* **139**, 18166–18169 (2017).

44. Park, H. D., Dinca, M. & Román-Leshkov, Y. *ACS Cent. Sci.* **3**, 444–448 (2017).

45. Furukawa, H., Cordova, K. E., O'Keeffe, M. & Yaghi, O. M. *Science* vol. 341 1230444–1230444 (2013).

46. Corma, A. *Angewandte Chemie - International Edition* vol. 55 6112–6113 (2016).

47. Bernales, V., Ortuño, M. A., Truhlar, D. G., Cramer, C. J. & Gagliardi, L. *ACS Cent. Sci.* **4**, 5–19 (2018).

48. Metzger, E. D., Brozek, C. K., Comito, R. J. & Dinca, M. *ACS Cent. Sci.* **2**, 148–153 (2016).

49. Rogge, S. M. J., Bavykina, A., Hajek, J., Garcia, H., Olivos-Suarez, A. I., Sepúlveda-Escribano, A., Vimont, A., *et al. Chem. Soc. Rev.* **46**, 3134–3184 (2017).

50. Chughtai, A. H., Ahmad, N., Younus, H. A., Laypkov, A. & Verpoort, F. *Chem. Soc. Rev.* **44**, 6804–6849 (2015).

51. Cook, T. R., Zheng, Y. R. & Stang, P. J. *Chemical Reviews* vol. 113 734–777 (2013).

52. Corma, A., García, H. & Llabrés I Xamena, F. X. *Chem. Rev.* **110**, 4606–4655 (2010).

53. Hendon, C. H., Rieth, A. J., Korzyński, M. D. & Dincă, M. *ACS Cent. Sci*. **3**, 554–563 (2017).

54. Cooper, A. I. *ACS Cent. Sci.* **3**, 544–553 (2017).

55. Lee, J., Farha, O. K., Roberts, J., Scheidt, K. A., Nguyen, S. T. & Hupp, J. T. *Chem. Soc. Rev.* **38**, 1450 (2009).

56. Goodenough, I., Devulapalli, V. S. D., Xu, W., Boyanich, M. C., Luo, T. Y., De Souza, M., Richard, M., Rosi, N. L. & Borguet, E. *Chem. Mater*. **33**, 910–920 (2021).

57. Arrozi, U. S. F., Wijaya, H. W., Patah, A. & Permana, Y. *Appl. Catal. A Gen.* **506**, 77–84 (2015).

58. Ding, L. G., Yao, B. J., Jiang, W. L., Li, J. T., Fu, Q. J., Li, Y. A., Liu, Z. H., Ma, J. P. & Dong, Y. Bin. *Inorg. Chem.* **56**, 2337–2344 (2017).

59. Hester, P., Xu, S., Liang, W., Al-Janabi, N., Vakili, R., Hill, P., Muryn, C. A., Chen, X., Martin, P. A. & Fan, X. *J. Catal.* **340**, 85–94 (2016).

60. Benseghir, Y., Lemarchand, A., Duguet, M., Mialane, P., Gomez-Mingot, M., Roch-Marchal, C., Pino, T., *et al. J. Am. Chem. Soc.* **142**, 9428–9438 (2020).

61. Abazari, R., Esrafili, L., Morsali, A., Wu, Y. & Gao, J. *Appl. Catal. B Environ.* **283**, 119582 (2021).

62. Bauer, G., Ongari, D., Xu, X., Tiana, D., Smit, B. & Ranocchiari, M. *J. Am.*

Chem. Soc. **139**, 18166–18169 (2017).

63. Bauer, G., Ongari, D., Tiana, D., Gäumann, P., Rohrbach, T., Pareras, G., Tarik, M., Smit, B. & Ranocchiari, M. *Nat. Commun.* **11**, 1–8 (2020).

64. Vermoortele, F., Vandichel, M., Van De Voorde, B., Ameloot, R., Waroquier, M., Van Speybroeck, V. & De Vos, D. E. *Angew. Chemie - Int. Ed.* **51**, 4887–4890 (2012).

65. Santiago-Portillo, A., Navalón, S., Concepción, P., Álvaro, M. & García, H. *ChemCatChem* **9**, 2506–2511 (2017).

66. Hutter, J., Iannuzzi, M., Schiffmann, F. & Vandevondele, J. *Wiley Interdiscip. Rev. Comput. Mol. Sci.* **4**, 15–25 (2014).

67. Perdew, J. P., Ruzsinszky, A., Csonka, G. I., Vydrov, O. A., Scuseria, G. E., Constantin, L. A., Zhou, X. & Burke, K. *Phys. Rev. Lett.* **100**, 136406 (2007).

68. VandeVondele, J. & Hutter, J. *J. Chem. Phys.* **127**, 114105 (2007).

Chapter 5. Metal-organic frameworks as kinetic modulators for branched selectivity in hydroformylation

Data reproduced from the article published in *Nat. Commun.* **11**, 1–8 (2020).

Abstract

Finding heterogeneous catalysts that are superior to homogeneous ones for selective organic transformation is a major challenge in catalysis. Here we show how micropores in metal-organic frameworks (MOFs) push homogeneous catalytic reactions into kinetic regimes inaccessible under standard conditions. Such property allows branched selectivity up to 90% in the Co-catalysed hydroformylation of olefins without directing groups, not achievable with existing catalysts. This finding has a big potential in the production of aldehydes for the fine chemical industry. Monte Carlo and density functional theory simulations combined with kinetic models show that the micropores of MOFs with UMCM-1 and MOF-74 topologies selectively adsorb the olefins while partially preventing the adsorption of syngas leading to high branched selectivity. The easy experimental protocol and the chemical and structural flexibility of MOFs will attract the interest of the fine chemical industries towards the design of heterogeneous processes with unprecedented selectivity in organic reactions.

Reproduced with permission from:

Bauer, G., Ongari, D., Tiana, D., Gäumann, P., Rohrbach, T., Pareras, G., Tarik, M., Smit, B. & Ranocchiari, M. *Nat. Commun*. **11**, 1–8 (2020).

Introduction

The fine chemical industry is dominated by homogeneous molecular catalysts when high selectivity is desired such as in regioselective and in stereoselective transformations. The main strategy to introduce heterogeneous catalysts to the fine chemical industry has been to immobilize homogeneous molecular catalysts on mesoporous supports and insoluble nanoparticles or polymers to overcome diffusion limitation and to accommodate large molecular active sites. Although some immobilized catalysts show promising catalytic activity, this strategy is still not applied in the chemical industry since "heterogenization" is simply not enough.[1] There is a need to demonstrate how the use of heterogeneous catalysts can promote selectivity that are challenging or even impossible to be obtained with existing catalytic systems. This can be done only if the chemical properties of heterogeneous catalysts can go beyond easier separation and recycling.

Since the discovery of metal-organic frameworks (MOFs), many researchers have been looking for catalytic applications with unique performance.[2–5] The chemical-flexibility, tuneable pore size and chemical and structural stability of MOFs showed how they can be used to design active sites at molecular level to direct selectivity and performance of reactions.[6–12] In recent years, promising catalytic applications that use MOFs as precursors for novel materials[13] as well as model systems to understand heterogeneous catalysis processes have been described.[14,15] After several decades, the field of catalysis by MOFs is still in its infancy since most of the examples are proof-of-concepts and do not offer attractive advantages to existing catalysts.[1,16] MOFs are widely known for their ability to selectively adsorb different molecules depending on their structure. This is a unique feature available only to microporous materials.[17–19] Here we demonstrate how adsorption properties can be exploited in catalysis to get otherwise inaccessible kinetics under standard conditions.

The hydroformylation of olefins – or oxo synthesis – (Figure 5.1a) is one of the most important reactions catalysed by homogeneous catalysts to obtain aldehydes from olefins in the presence of syngas.[20] The atom economic process yields linear aldehydes and branched ones. The linear isomers are key intermediates

for the detergent and polymer industry and are formed with Rh catalysts, which are generally more selective than Co ones.[21] Branched aldehydes are a powerful tool for the fine chemical industry with potential applications in the formation of enantioenriched products. Rh catalysts with bidentate ligands dominate the scene, especially with substrates with directing groups.[22] At present, the branched-selective hydroformylation of olefins without directing groups is still challenging and can be achieved only by complex Rh catalysts with a selectivity for 2-methylhexanale from 1-hexene up to 75%[23,24] and up to 86% for 2-methylbutanale from 1-butene.[25] Supramolecular chemistry has also been used to tune regioselectivity in Rh-catalysed hydroformylation.[26–28] The chemistry of Co-catalysed "branched-selective" hydroformylation is rare and yields at best moderate selectivity of acetal-protected products.[29] In this contribution, we show that the micropores of MOFs push the Co-catalysed hydroformylation of olefins without directing groups to kinetic regimes that favour high branched selectivity.

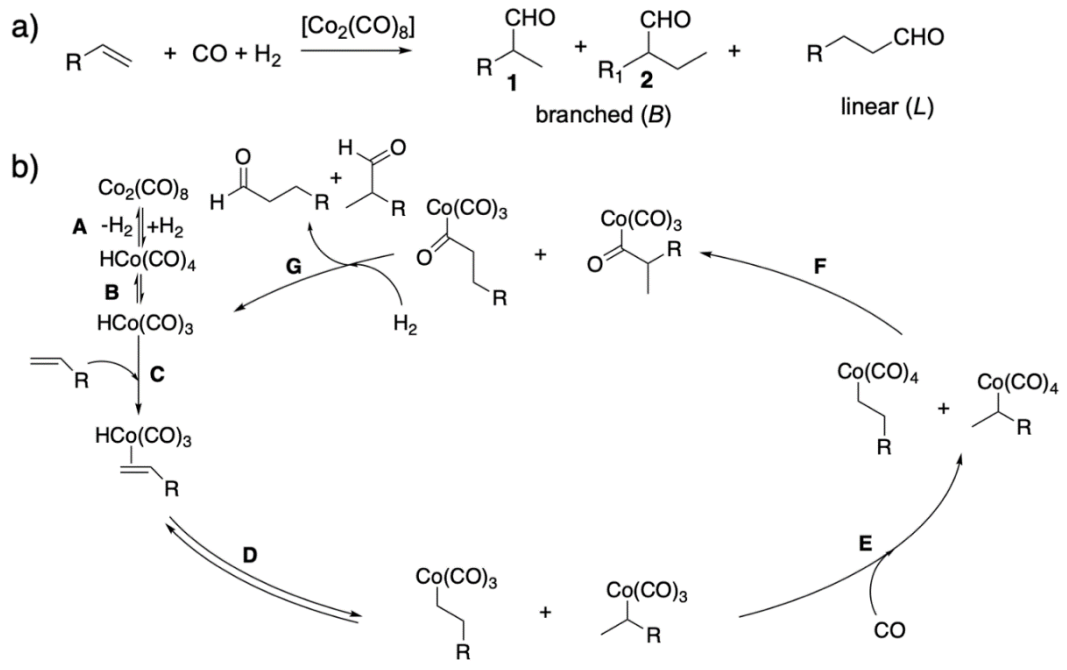


Figure 5.1 a) General scheme for the Co-catalysed hydroformylation of olefins. For 1-hexene R = C_4H_9, R1=C_3H_7. b) Accepted mechanism for the Co-catalysed hydroformylation of olefins.

Results and Discussion

The selectivity limit of homogeneous hydroformylation. Several catalytic conditions were screened, aiming to maximize the yield of the branched product with 1-hexene as substrate and $Co_2(CO)_8$ as pre-catalyst to identify the highest branched selectivity that may be obtained in homogeneous catalysis (Table S5). Preliminary reactions at different temperatures and pressures showed an optimum temperature at 100°C – at higher ones, a significant amount of the isomerization of the olefin was observed – and 30 bar syngas due to the lower branched selectivity at higher pressures. The reaction mixture without MOF showed a conversion of 40% with branched:linear ratio (B/L) of 49:51. The only way to exceed the 50% selectivity threshold was to reduce the pressure to 19 bar, which resulted in 15% conversion with 66% selectivity towards the branched products, 2-methylhexanal (1) and 2-ethylpentanal (2) (Figure 5.1a), which were formed in a 3:1 ratio. Increasing the catalyst loading to 0.47 molCo %, 1.19 molCo %, and 2.38 molCo % led to 61%, >99%, and >99% conversion, respectively with a B/L of 1:1 (Table S5). Only a narrow range of experimental conditions led to moderate branched selectivity at low conversion rate, which is consistent with kinetic studies.[30,31] In homogeneous catalysis, the limit to achieve high branched selectivity is to work in neat 1-hexene at 100 °C and 19 bar syngas pressure. As demonstrated below, we can go beyond this limit and achieve much higher branched selectivity by adding MOFs to the reaction mixture.

The addition of MOFs enhances branched selectivity. Our group has previously shown that MOFs with UMCM-1 topology can fully adsorb chiral Rh complexes within the pores of the frameworks leading to an increased performance in the asymmetric hydrogenation of olefins.[32] The addition of UMCM-1 and UMCM-1-NH_2 (fully or partially functionalized, Figure 5.2a) in the hydroformylation of 1-hexene with $Co_2(CO)_8$ (0.23 molCo%) was tested (Table 1). All screening was performed at the conditions that gave around 40% conversion and 50% selectivity in the pure homogeneous system (Table 1, entry 1) at 100 °C, 30 bar syngas, under neat 1-hexene. MOFs with UMCM-1 topology (Fig. 2a) gave 60%, 76%, and 76% branched selectivity, respectively for UMCM-1 (Table 5.1), MixUMCM-1-NH_2 (28%) (Table 5.1), and UMCM-1-NH_2 (Table 5.1), all at around 30% conversion.

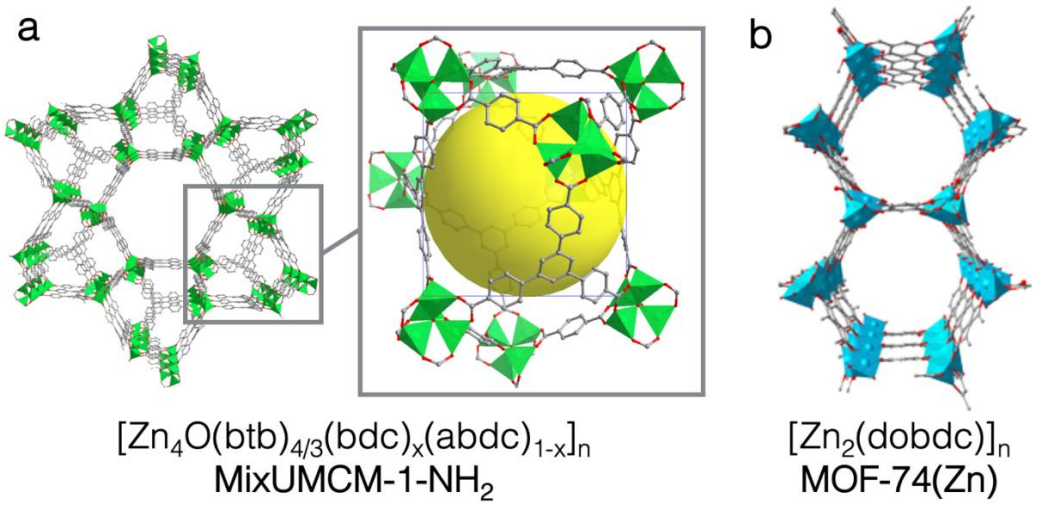


Figure 5.2 Structures and molecular formulas of the MOFs used in hydroformylation. a MixUMCM-1-NH_2. b MOF-74(Zn). bdc = 1,4-benzenedicarboxylate; abdc = 2-amino-1,4-benzenedicarboxylate, btb = 4,4′,4″,-benzene-1,3,5-triyl-trisbenzoate and dobdc = 2,5-dioxido-1,4-benzenedicarboxylate. Hydrogen and nitrogen atoms are omitted for clarity.

We investigated further the effect of MixUMCM-1-NH_2 (28%) additive. A screening of the amount of MOF was performed by keeping constant the Co catalyst concentration at 0.23 mol_{Co}% (Table S6), which revealed that there is an optimal MOF/Co molar ratio of 0.8. The branched products can be obtained in 75:25 B/L ratio with a 1 and 2 ratio of 3:1 and 36% conversion (Table 5.1, entry 5). This is a remarkable improvement showing that good branched selectivity can be achieved while maintaining the conversion levels of homogeneous catalysis. ICP-MS showed that MixUMCM-1-NH_2 (28%) adsorbed 73% of the Co after reaction under the conditions in Table 5.1 entry 5 (Table S3). The enhanced branched selectivity obtained by adding MixUMCM-1-NH_2 (28%) compared to the homogeneous reaction is observed at all pressures ranging from 19 bar to 78 bar. The higher the pressure the lower the overall branched selectivity, though (Table S6). One can increase the Co adsorption (up to 85%) with pressures up to 72 bar, whereas the cobalt adsorbed in the MOF decreases to 67% at 94 bar (Table S3). A series of blank experiments with additives such as the linkers in the MOFs and different Zn sources were done to rule out that leached species and defects enhance branched selectivity (Table S7).

We tested different MOF topologies that have been synthesised in our labs aimed at understanding the role of the MOF environment in such a change in selectivity. MOF-74(Zn) is superior to MixUMCM-1-NH_2 (28%) giving 25% conversion and 85% selectivity (Table 5.1 entry 6) while absorbing 60% of the Co. Both MixUMCM-1-NH_2 (28%) and MOF-74(Zn) retained crystallinity after catalysis as shown by powder X-ray diffraction (Figure S4). The BET number of MixUMCM-1-NH_2 (28%) changed from 2870 m^2/g to 2980 m^2/g after catalysis (Figure S5 and Figure S7), whereas the one of MOF-74(Zn) decreased from 1000 m^2/g to 150 m^2/g (Figure S6 and Figure S8). The lower surface area in MOF-74 after catalysis is caused by the adsorption of the catalyst and of organic products such as aldol compounds (Figure S10), which could not be removed by extensive washing, as also evidenced by pore size distributions before and after catalysis and by the recycling experiments below.

We attempted incipient wetness impregnation of the $Co_2(CO)_8$ pre-catalyst in dichloromethane at MOF/Co molar ratio of 0.7 and 0.3 with UMCM-1-NH_2 and MOF-74(Zn), respectively, to check whether the pre-adsorbed metal would lead to higher selectivity. Once 1-hexene was added to the impregnated MOF, a strong coloration of the homogeneous solution to dark brown was observed in all experiments indicating that the Co complex was preferentially in solution. Catalytic results under such conditions showed up to 41% conversion and 68% branched selectivity 0.46 molCo% for UMCM-1-NH_2 and up to 63% conversion and 68% branched selectivity with a 0.6 molCo% loading in the case of MOF-74(Zn) (Table S11), showing that higher selectivity can be obtained by adding the MOF to the reaction mixture rather than with pre-formed impregnated pre-catalyst. This is attributed to the relatively low chemical stability of $Co_2(CO)_8$[33] and suggests that it is an intermediate of the catalytic cycle that preferentially adsorbs within MOFs rather than the pre-catalyst.

After the first catalytic runs in Table 5.1 Entries 5 and 6, we extensively washed the MOFs and tested their recyclability for a second catalytic run. MixUMCM-1-NH_2 (28%) showed 5% conversion and 64% branched selectivity, whereas MOF-74(Zn) exhibited 68% selectivity at 35% conversion (Table S13). Branched selectivity decreased in both recycling experiments compared to the first run, but it was still higher than in the homogeneous reaction. Higher conversion

could be obtained with MOF-74(Zn). All recycling results suggest that there are trace compounds that are hard to wash out and may modify the adsorption properties of the MOFs causing lower selectivity as suggested also by BET after catalysis (see above). The recycling of impregnated Co@MOF catalysts with minimal washing – to keep the Co inside the pores – resulted in inactive catalysts (Table S2 and Table S12).

Table 5.1 Influence of MOFs on the selectivity and reactivity of the Co-catalysed hydroformylation. [a]

Entry	Additive	Conversion (%) [b]	*B*/*L* [c]
1	None	40	49:51
2	UMCM-1	32	60:40
3	MixUMCM-1-NH_2 (28 %)	24	76:24
4	UMCM-1-NH_2	20	76:24
5	MixUMCM-1-NH_2 (28 %) [d]	36	75:25
6	MOF-74(Zn)[e]	25	85:15

[a] $Co_2(CO)_8$ (0.8 mg, 2.3 µmol) were dissolved in 1-hexene (250 µL, 2.0 mmol) and the MOF was added (mol_{MOF}/mol_{Co} = 1.7) the mixture was brought to 30 bar and 100°C for 17 h. [b] The final reaction mixture contained 1-hexene, 1, 2, *n*-heptanale and unknown compounds (~2%) as detected by GC-FID and GC-MS. [c] 1:2 ratio = 3:1. [d] mol_{MOF}/mol_{Co} = 0.8. [e] mol_{MOF}/mol_{Co} = 20.

MOF-74 with different metals (Figure S2 and Table S1) such as Mg gave 77% branched products at 8% conversion, whereas MOF-74(Co) and MOF-74(Ni) both yielded around 55% branched aldehydes at 90% and 44% conversion, respectively. While MOF-74(Mg) is of little use since it lowers dramatically conversion and adsorbs a little Co amount (~20%), MOF-74(Co) and MOF-74(Ni) are reactive towards syngas and did not increase branched selectivity. MIL-101-NH_2(Al), MIL-101(Cr) (Figure S3 and Table S1), and Zeolite-Y were also tested but they gave almost no conversion and killed catalytic activity (Table S8).

There are two possible reasons why this selectivity enhancement is observed by adding certain MOFs to homogeneous catalysis: (1) either there is a bond between the Co complex and the MOF leading to a coordinative interaction, which consequently changes the reactivity of the active site or (2) the micropores of the MOFs alter the kinetics and energetics along the reaction pathway.

Electronic interactions are unlikely. We performed a set of computational and experimental studies to investigate what could be the cause of the selectivity change. $Co_2(CO)_8$ forms the active pre-catalyst $HCo(CO)_4$ in the presence of syngas (Figure 5.1 step A) and upon decoordination of one carbonyl group the active catalyst $HCo(CO)_3$ (Figure 5.1 step B) is formed. We modelled interaction energies of both species within the pores of MOF with UMCM-1 and MOF-74(Zn) topologies with density functional level of theory (DFT) (Supplementary Information). The interaction energies between $HCo(CO)_4$ and the MOFs with UMCM-1 (Figure S11 and Figure S12) and MOF-74 (Figure S13) topologies are between +1.2 kcal/mol and –2.53 kcal/mol (Table S14) and therefore in the range of van der Waals interactions and not of a coordination bond. When inside the pores of the MOF the formation of a MOF-$Co(H)(CO)_3$ system can be envisioned, though (Table S15). The stabilization energy of unfunctionalized UMCM-1-$Co(H)(CO)_3$ is 3.5 kcal/mol (Figure S14) and therefore negligible to form a coordinative bond. The functionalized UMCM-1-NH_2 (Figure S15) and MOF-74(Zn) (Figure S16) stabilize the unsaturated complex $HCo(CO)_3$ with 20-35 kcal/mol stabilization energy. Such energies are significantly lower than the binding energy between CO-$Co(H)(CO)_3$ (-62.7 kcal/mol and -61.6 kcal/mol for the axial and equatorial CO respectively) and 1-hexene-$Co(H)CO_3$ (-52.8 kcal/mol), which are formed under reaction conditions. The DFT energies above suggest that it is unlikely that a coordinative bond between the unsaturated cobalt complex and the MOF is formed under catalytic conditions. This is supported by analysing the interaction of the pre-catalyst $Co_2(CO)_8$ with the MOFs by infrared spectroscopy of impregnate Co@MOFs (Figure S9). The inactivity of MIL-101 and Zeolite-Y might be explained by an electronic interaction between the metal open sites in the MOF and the Co catalyst. The detrimental effect of Al/amines and of Cr to the activity in Co-catalysed hydroformylation is described in the literature.[34,35]

Further evidence that no electronic interaction is responsible for the selectivity change was provided by preparing MOFs that feature strong coordinative bonds with Co such as phosphine MOFs (P-MOFs).[15,36–38] Such phosphine solid ligands can coordinate Co as supported by the literature[39] and by our DFT P-Co binding energies (Table S15). MixUMCM-1-PPh_2 (29 %) was synthesized (Figure S1) and further tested in catalysis. The pre-formed $HCo(CO)_3$(MixUMCM-1-PPh_2)

complex[40] formed 50% branched aldehydes at 9% conversion showing that the P-Co bond does not yield branched selectivity. The addition of such P-MOF to the hydroformylation of 1-hexene showed no significant change to the previous results obtained by other UMCM-1 derivatives giving 67% branched selectivity at 22% conversion (Table S8), while adsorbing 70% Co, three times the molar amount of phosphino groups in the MOF. In this case, the catalyst that gives high selectivity is mostly not bound to the MOF. The evidence coming from simulation and experiments with P-MOFs strongly suggests that the cause of the branched selectivity is not likely coming from a coordinative interaction between the Co catalyst and the MOF materials. This is also intuitively supported by the mechanism of Co-catalysed hydroformylation (Figure 5.1b). Since the formation of the linear aldehyde is kinetically driven, any coordinative interaction between the catalyst and the support increases the steric hindrance around the cobalt (Figure 5.1 Steps D and E) and favours the formation of the linear aldehyde.

Understanding how adsorption affects selectivity. The application of MOFs closest to industrial scale is gas storage. The reason why MOFs are so successful in storing gaseous molecules within their pores is because the surface interaction between the material and the gas makes the packing between the molecules more efficient in the MOF micropores than in the gas phase.[41] This principle can be applied to catalysis as well. In fact, many groups have claimed that adsorption effects can play a role in the enhanced activity of catalytic reactions within the pores of MOFs due to confinement,[42] a phenomenon that is known in zeolites catalysis.[43,44] To study the affinity of the reactants and products with the different MOFs we set up a series of Monte Carlo simulations where the homogeneous liquid solution is compared to the mixture inside the pores of the crystal.

For each simulation, two periodic boxes, a cubic empty one and another reproducing the bulk crystal, were saturated with 1-hexene molecules at 30 bar and 100 °C. The number of 1-hexene molecules inside the pores of the frameworks, was computed using grand canonical Monte Carlo simulations (Table S16). Reactants and products (CO, linear heptanal and branched 1) were added at infinite solution in the solvent, as one molecule per box.[45–50] During the simulation, all molecules were allowed to move according to the detailed balance at the imposed temperature,

but also to swap between the two simulation boxes: the pore volume of the crystal and the homogeneous system (Supplementary Information).[51] We could measure the affinity of the reactants and product with the MOF: An average occupancy higher than 50%, for a reactive component confined in the framework's pores shows that it is more stable in the pores than in the homogeneous phase. The smaller this probability, the more stable the component will be in the homogeneous solvent. Table 5.2 shows the probability related to each MOF and component and the ratio of the 1-hexene density inside the pores[52] and in the homogeneous phase.

Table 5.2 Affinity of the different species with the frameworks is reported as percentage occupancy (%occup.) which is related to the average number of molecules of that species in the MOF's simulation box. The error is computed as standard deviation over ten independent simulations. The first column reports the relative density of 1-hexene (Rel. density) computed in the pore volume with respect to the density observed in the homogeneous simulation box (see also Table S17and Table S18).

Entry	MOF	1-hexene Rel. density	H_2 %occup.	CO %occup.
1	UMCM-1	1.04 ± 0.01	40.0 ± 0.5%	41.3 ± 0.5%
2	UMCM-1-NH_2	1.04 ± 0.01	39.1 ± 0.1%	40.8 ± 0.5%
3	MOF-74(Zn)	1.14 ± 0.01	22.4 ± 0.7%	21.9 ± 1.4%

The MOFs confinement can affect the reaction in three ways: (1) an increase in the solvent density inside the pores, (2) a higher affinity with the products compared to the homogeneous phase (Table S17 and Table S18) and (3) a lower affinity with the gas reactants. Our calculations suggest that the first two effects are due to the stronger interactions of the solvent and the aldehydes with the framework while the third observation is caused by the formation of less interstices in the confined MOF phase, which cannot be filled with small gas molecules. One can also note that both the linear and branched products have a similar affinity with the framework in all MOFs. This evidence excludes that the branched selectivity is due to a relative stabilization of the different products in the pores, as observed in similar systems.[53]

The Monte Carlo simulations point out that the concentration of the reactants within the MOF micropores is different than that in the homogeneous

phase. We can achieve higher 1-hexene concentration within the pores of the MOF than under neat 1-hexene homogeneous conditions, which is remarkable. This is in line with gas storage findings and allows to access reaction conditions that are not usually achievable in homogeneous catalysis. Since the MOFs that increase branched selectivity adsorb most of the Co complex (see above), it is safe to assume that selectivity is determined within the micropores. We qualitatively identified the effect of such modified concentrations in the branched selective hydroformylation by using published kinetic laws for the rate of formation of the branched (R_B) and of the linear (R_L) aldehyde that have been empirically determined for the hydroformylation of propene.[30] The two kinetic laws are shown in equations (1) and (2) and depict the rate of formation of the branched and linear product, respectively, in the hydroformylation of propene with k_B (110 °C) = 2.12 x 10^{-7} (m^3/mol)/1.94 s, k_{BCO} (110 °C) = 1.35 x 10^{-3} m^3/mol, k_L (110 °C) = 2.01 x 10^{-7} (m^3/mol)/2.17 s, and k_{LCO} (110 °C) = 8.014 x 10^{-3} m^3/mol.

$$R_B = \frac{k_B[H_2]^{0.32}[CO][Co_2(CO)_8]^{0.62}[alkene]}{(1 + K_{BCO}[CO])^2}, \qquad (1)$$

$$R_L = \frac{k_L[H_2]^{0.55}[CO][Co_2(CO)_8]^{0.75}[alkene]^{0.87}}{(1 + K_{LCO}[CO])^2}. \qquad (2)$$

A qualitative assessment of the effect of concentration within the pores of the MOF can be done by calculating RB/RL rates relative to that calculated for standard homogeneous conditions assuming that the order on the different reactants and catalysts is the same using 1-hexene and propene as olefins under the same conditions, which is a good approximation since the overall rate is not dependent from the size of the linear terminal olefin.[54] The concentration of H2 and CO at different pressures in 1-hexene were calculated using the Soave modifications of the Redlich-Kwong equation (SRK) (Table S19).[55] We used the Monte Carlo simulation data presented above to calculate the concentrations of the reactants within the MOF pores by multiplying the concentrations found in the homogeneous reaction by a factor Z derived in the Monte Carlo simulations (from Table S20 to Table S23). Fig. 3b shows the syngas pressure dependence of RB/RL in UMCM-1-NH_2 (green) and MOF-74(Zn) (blue) compared to the homogeneous reaction (red)

and depicts how we can increase RB/RL at 15–25 bar within the pores of UMCM-1-NH_2 and MOF-74(Zn), the latter being superior as supported by experimental results. The local concentration of the different species and the – in part favoured – isomerization of the alkene influence the rate of formation of the branched and of the linear aldehydes. The MOF micropores create the right conditions to tune the concentration of the reactants and push the kinetic limit of the homogeneous reaction favouring the formation of the branched aldehydes. The correlation between experimental B/L ratio (Fig. 3a) and calculated data (Fig. 3b) as function of syngas pressure is evident. The deviations are more prominent in the MOF-74(Zn) case at high pressure and are caused by a lower Co uptake (36% at 61 bar, Table S4) and by higher conversion.

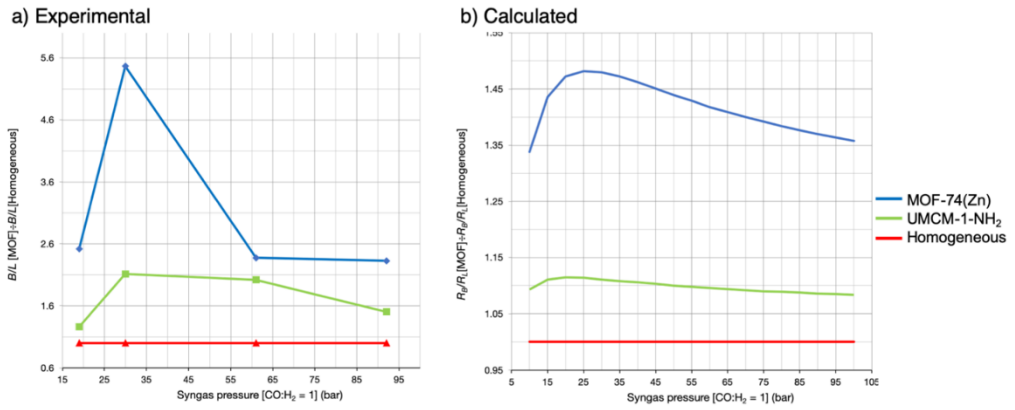
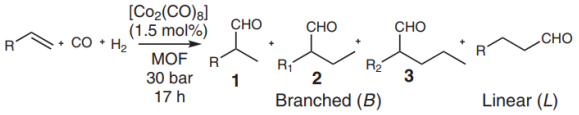


Figure 5.3 a) Experimental branched to linear ratios (B/L) with MixUMCM-1-NH2 (28%) and MOF-74(Zn) relative to the homogeneous B/L as function of syngas pressure (Table S9). b) Calculated relative rates of formation of the branched and linear aldehydes (RB/RL) in the MOFs UMCM-1-NH2 and MOF-74(Zn) and homogeneous phase referenced to the homogeneous system as function of syngas pressure.

In summary, MOFs can provide the right microporous environment to enhance branched selectivity by increasing the branched rate of formation while decreasing that of the linear because of concentration variations within their micropores. Not all microporous materials can push such limits since the material should adsorb the Co complex while minimizing the coordinative interaction with the catalyst and be inert towards syngas.

Substrate scope. Substrate scope was performed with screening aimed at achieving full conversion to show that this easy procedure can be applied to a range of non-functionalized branched aldehydes. Linear olefins with no directing groups from 1-hexene to 1-nonene and but-3-en-1-ylbenzene underwent hydroformylation at 100 °C, 35 bar under neat conditions and Co2CO8 (1.5 mol%) with high conversions and up to 90% branched selectivity in 17 h (Table 3). The comparison of the results in terms of selectivity with the homogeneous system is staggering. We observed in all cases an increase in branched selectivity – often between 30% and 40% increase – by simply adding a MOF to the reaction mixture showing that this protocol is flexible starting from olefins with no directing groups.

Table 5.3 Substrate scope of the Co-catalysed hydroformylation of olefins without directing groups with MOF additives and comparison with the homogeneously catalysed reaction[a,b].



Entry	Olefin	MixUMCM-1-NH_2 (28%)[a,c] B/L|Conv. (%) [Oxo yield (%)]	MOF-74(Zn)[a,d] B/L|Conv. (%) [Oxo yield (%)]	No MOF[a] B/L|Conv. (%) [Oxo yield (%)]
1	[e]	83/17|75 [60]	90/10|85 [70]	61/39|99 [95]
2	[f]	79/21|62 [55]	89/11|86 [75]	52/48|97 [95]
3	[g]	84/16|84 [80]	86/14|81 [75]	54/46|97 [95]
4	[h]	77/23|80 [75]	83/17|71 [65]	61/38|>99 [95]
5	Ph [i]	70/30|15 [10][j]	81/19|49 [40][k]	60/40|58 [50][l]

[a]Conv. = olefins conversion; Oxo yield = yield of oxo products. B/L and conversion were calculated using GC-FID with p-cymene as external standard. Oxo products yield was calculated by combining the mass of the raw product after reaction and the purity determined by GC-FID (see Supplementary Information). The oxo products were identified as aldehydes (Table S10) and aldol condensation products.
[b]$Co_2(CO)_8$ (1.5 mol%) were dissolved in olefin (500 µL) and the MOF was added. The mixture was brought to 30 bar and then heated to 100 °C for 17 h. [c]molMOF/molCo = 0.4.
[d]molMOF/molCo = 3.3.
[e]1:2:3 ratio (homogeneous and MixUMCM-1-NH2) = 3:1:0. 1:2 ratio (MOF-74(Zn)) = 2:1:0.
[f]1:2:3 ratio = 7:2:1.
[g]1:2:3 ratio = 7:2:1.
[h]1:2:3 ratio = 6:2:2.
[i]1:2:3 ratio = 7:1.5:1.5.
[j]Eleven per cent of hydrogenated olefin was detected by GC-FID and GC-MS.
[k]Ten per cent of hydrogenated olefin was detected by GC-FID and GC-MS.
[l]Five per cent of hydrogenated olefin was detected by GC-FID and GC-MS.

Conclusion

By combining experiments, classical, quantum, and kinetic simulations, the research shown here demonstrates the importance of micropores to push the kinetic limits and to drive the Co-catalysed hydroformylation of olefins without directing groups to unprecedented branched selectivity with good substrate scope. The micropores and the chemical flexibility of MOFs create a unique combination that can be exploited to tuning the concentration of the species within the pores, which basically act as microporous reactors. The easy reaction protocol, which consists in simply adding a MOF to a homogeneously catalysed reaction, should not be overlooked.

One of the most important consequence of this work is that the methodology can be used to predict the effect of microporous co-catalysts to increase selectivity in any homogeneous or heterogeneous catalytic reaction. The requirement is that the kinetic data for the different products of the reaction is known and that the order in (at least) one of the reactants is not the same for different products. One can choose the microporous material that has the best chances of increasing selectivity a) by appropriately selecting the ones that can adsorb the catalyst while being inert under reaction conditions and b) by using simulations to determine how the microporous materials can change the local concentration of the selectivity-determining reactant(s) within the micropores. It is therefore an extremely powerful tool for the design of uniquely selective catalytic heterogeneous processes in the fine chemical industry.

Methods

Synthesis of MOFs. Detailed experimental methods can be found in the Supplementary Information. MixUMCM-1-NH_2 (28%) was synthesized according to a published procedure.[10] MOF-74(Zn) was synthesized according to the following procedure: in a 20 mL microwave tube, 2,5-dihydroxyterephthalic acid (200 mg; 1.01 mmol) and $Zn(acac)_2{\cdot}H_2O$ (568 mg; 2.02 mmol) were dissolved in dimethyl- formamide (DMF) (19 mL) and H_2O (1 mL) to give a yellow solution. The reaction mixture was stirred at 130°C for 60 min in a Biotage Initiator+ microwave oven. The solid of the reaction mixture was filtered by membrane filter,

washed with DMF, H_2O and EtOH and dried in a vacuum oven. Yield: 388 mg (81%).

General hydroformylation procedure. Detailed experimental methods can be found in the Supplementary Information. $Co_2(CO)8$ (1.5 mol%) was dissolved in the olefin (500 μL), and the solution was added to the MOF in a 1 mL crimp vial. The vial was placed into a 50 mL Premex® autoclave and purged with Ar several times. Syngas pressure (CO:H2 1:1, 30 bar) was applied and the autoclaves heated at 100 °C for 17 h. The autoclave was allowed to cool down to room temperature before the pressure was released slowly over 15 min. The autoclave was flushed with nitrogen before it was opened to remove additional syngas for safety reasons. B/L and conversion were calculated using gas chromatography with flame ionization detector (GC-FID) with p-cymene as external standard. Oxo products yield was calculated by combining the mass of the raw product after reaction and the purity determined by GC-FID.

Molecular simulations. Detailed procedures for molecular simulations can be found in the Supplementary Information. DFT calculations were performed using the CP2K package[56] and adopting the PBEsol functional, considering gas phase.[57] Partial charges for the classical simulation have been computed using the REPEAT scheme.[58] The RASPA software[59] was used for Monte Carlo simulations, employing the DREIDING force field45 (extended with UFF [Universal force field] parameters[47] for Mg, Co, Ni and Mg) as dispersion parameters of the MOFs' atoms. TraPPE force field[48,49] was used to model the molecules, fitting from ab initio the missing parameters for the branched aldehydes. The pore volume of the frameworks has been computed using the software Zeo++.[60]

Kinetic analysis. The kinetic analysis was based on the empirical rate of formations of the branched and the linear aldehydes reported elsewhere.[30] The concentrations of 1-hexene, CO and H_2 within the pores of the MOFs were calculated by multiplying the concentration in the homogeneous phase by a factor Z derived from the Monte Carlo simulations (Table S20).

References

1. Hübner, S., De Vries, J. G. & Farina, V. *Adv. Synth. Catal.* **358**, 3–25 (2016).

2. Ranocchiari, M. & Bokhoven, J. A. Van. *Phys. Chem. Chem. Phys.* **13**, 6388–6396 (2011).

3. Furukawa, H., Cordova, K. E., O'Keeffe, M. & Yaghi, O. M. *Science* **341**, 1230444–1230444 (2013).

4. Gascon, J., Corma, A., Kapteijn, F. & Llabrés I Xamena, F. X. *ACS Catal.* **4**, 361–378 (2014).

5. Liu, J., Chen, L., Cui, H., Zhang, J., Zhang, L. & Su, C. Y. *Chem. Soc. Rev.* **43**, 6011–6061 (2014).

6. Zheng, M., Liu, Y., Wang, C., Liu, S. & Lin, W. *Chem. Sci.* **3**, 2623–2627 (2012).

7. Guo, Z., Xiao, C., Maligal-Ganesh, R. V., Zhou, L., Goh, T. W., Li, X., Tesfagaber, D., Thiel, A. & Huang, W. *ACS Catal.* **4**, 1340–1348 (2014).

8. Sawano, T., Lin, Z., Boures, D., An, B., Wang, C. & Lin, W. *J. Am. Chem. Soc.* **138**, 9783–9786 (2016).

9. Zhao, M., Yuan, K., Wang, Y., Li, G., Guo, J., Gu, L., Hu, W., Zhao, H. & Tang, Z. *Nature* **539**, 76–80 (2016).

10. Bauer, G., Ongari, D., Xu, X., Tiana, D., Smit, B. & Ranocchiari, M. *J. Am. Chem. Soc.* **139**, 18166–18169 (2017).

11. Huang, Y. B., Liang, J., Wang, X. S. & Cao, R. *Chem. Soc. Rev.* **46**, 126–157 (2017).

12. Liu, L., Zhou, T. Y. & Telfer, S. G. *J. Am. Chem. Soc.* **139**, 13936–13943 (2017).

13. Shen, K., Chen, X., Chen, J. & Li, Y. *ACS Catal.* **6**, 5887–5903 (2016).

14. Bloch, W. M., Burgun, A., Coghlan, C. J., Lee, R., Coote, M. L., Doonan, C. J. & Sumby, C. J. *Nat. Chem.* **6**, 906–912 (2014).

15. Beloqui Redondo, A., Morel, F. L., Ranocchiari, M. & Van Bokhoven, J. A.

ACS Catal. **5**, 7099–7103 (2015).

16. García-García, P., Müller, M. & Corma, A. *Chem. Sci.* **5**, 2979–3007 (2014).

17. He, Y., Zhou, W., Qian, G. & Chen, B. *Chem. Soc. Rev.* **43**, 5657–5678 (2014).

18. Peplow, M. *Nature* **520**, 148–150 (2015).

19. Silva, P., Vilela, S. M. F., Tomé, J. P. C. & Almeida Paz, F. A. *Chem. Soc. Rev.* **44**, 6774–6803 (2015).

20. Börner, A. & Franke, R. *Hydroformylation*; Wiley-VCH, Weinheim, 2016.

21. Franke, R., Selent, D. & Börner, A. *Chem. Rev.* **112**, 5675–5732 (2012).

22. Chikkali, S. H., Van Der Vlugt, J. I. & Reek, J. N. H. *Coord. Chem. Rev.* **262**, 1–15 (2014).

23. Noonan, G. M., Fuentes, J. A., Cobley, C. J. & Clarke, M. L. *Angew. Chemie* **124**, 2527–2530 (2012).

24. Dingwall, P., Fuentes, J. A., Crawford, L. E., Slawin, A. M. Z., Bühl, M. & Clarke, M. L. *J. Am. Chem. Soc.* **139**, 15921–15932 (2017).

25. Iu, L., Fuentes, J. A., Janka, M. E., Fontenot, K. J. & Clarke, M. L. *Angew. Chemie - Int. Ed.* **58**, 2120–2124 (2019).

26. Besset, T., Norman, D. W. & Reek, J. N. H. *Adv. Synth. Catal.* **355**, 348–352 (2013).

27. Wang, X., Nurttila, S. S., Dzik, W. I., Becker, R., Rodgers, J. & Reek, J. N. H. *Chem. - A Eur. J.* **23**, 14769–14777 (2017).

28. Jongkind, L. J., Elemans, J. A. A. W. & Reek, J. N. H. *Angew. Chemie - Int. Ed.* **58**, 2696–2699 (2019).

29. Li, B., Li, X., Asami, K. & Fujimoto, K. *Chem. Lett.* **31**, 836–837 (2002).

30. Gholap, R. V., Kut, O. M. & Bourne, J. R. *Ind. Eng. Chem. Res.* **31**, 2446–2450 (1992).

31. Gholap, R. V., Kut, O. M. & Bourne, J. R. *Ind. Eng. Chem. Res.* **31**, 1597–

1601 (1992).

32. Vilhanová, B., Ranocchiari, M. & Van Bokhoven, J. A. *ChemCatChem* **8**, 308–312 (2016).

33. Gilmont, P., Blanchard, A. A., Mason, C. M. & Barnard, R. L. *in Inorganic syntheses*; ed. Fernelius, W. C. Wiley, Hoboken, 2007.

34. Tucci, E. R. *Ind. Eng. Chem. Prod. Res. Dev.* **24**, 38–42 (1985).

35. Sakthivel, A., Mahato, N. R., Baskaran, T. & Christopher, J. *Catal. Commun.* **65**, 55–61 (2015).

36. Morel, F. L., Ranocchiari, M. & Van Bokhoven, J. A. *Ind. Eng. Chem. Res.* **53**, 9120–9127 (2014).

37. Morel, F. L., Pin, S., Huthwelker, T., Ranocchiari, M. & Van Bokhoven, J. A. *Phys. Chem. Chem. Phys.* **17**, 3326–3331 (2015).

38. Xu, X., Rummelt, S. M., Morel, F. L., Ranocchiari, M. & Van Bokhoven, J. A. *Chem. - A Eur. J.* **20**, 15467–15472 (2014).

39. Hebrard, F. & Kalck, P. *Chem. Rev.* **109**, 4272–4282 (2009).

40. Dubois, R. A., Garrou, P. E., Lavin, K. D. & Allcock, H. R. *Organometallics* **5**, 460–466 (1986).

41. Yu, J., Xie, L. H., Li, J. R., Ma, Y., Seminario, J. M. & Balbuena, P. B. *Chem. Rev.* **117**, 9674–9754 (2017).

42. Xiao, D. J., Oktawiec, J., Milner, P. J. & Long, J. R. *J. Am. Chem. Soc.* **138**, 14371–14379 (2016).

43. Haag, W. O. in *10th International Zeolite Conference, Garmisch-Partenkirchen, Germany, 17-22 July 1994* vol. 84 1375–1394 Elsevier, 1994.

44. Van Bokhoven, J. A., Williams, B. A., Ji, W., Koningsberger, D. C., Kung, H. H. & Miller, J. T. *J. Catal.* **224**, 50–59 (2004).

45. Mayo, S. L., Olafson, B. D. & Goddard, W. A. *J. Phys. Chem.* **94**, 8897–8909 (1990).

46. Marx, D. & Nielaba, P. *Phys. Rev. A* **45**, 8968–8971 (1992).

47. Rappé, A. K., Casewit, C. J., Colwell, K. S., Goddard, W. A. & Skiff, W. M. *J. Am. Chem. Soc.* **114**, 10024–10035 (1992).

48. Wick, C. D., Martin, M. G. & Siepmann, J. I. *J. Phys. Chem. B* **104**, 8008–8016 (2000).

49. Stubbs, J. M., Potoff, J. J. & Siepmann, J. I. *J. Phys. Chem. B* **108**, 17596–17605 (2004).

50. Martín-Calvo, A., Lahoz-Martín, F. D. & Calero, S. *J. Phys. Chem. C* **116**, 6655–6663 (2012).

51. Frenkel, D. & Smit, B. *Understanding molecular simulation*; Elsevier, 2001.

52. Ongari, D., Boyd, P. G., Barthel, S., Witman, M., Haranczyk, M. & Smit, B. *Langmuir* **33**, 14529–14538 (2017).

53. Smit, B. & Maesen, T. L. M. *Nature* **451**, 671–678 (2008).

54. Wender, I., Metlin, S., Ergun, S., Sternberg, H. W. & Greenfield, H. *J. Am. Chem. Soc.* **78**, 5401–5405 (1956).

55. Mathias, P. M. & Copeman, T. W. *Fluid Phase Equilib.* **13**, 91–108 (1983).

56. Hutter, J., Iannuzzi, M., Schiffmann, F. & Vandevondele, J. *Wiley Interdiscip. Rev. Comput. Mol. Sci.* **4**, 15–25 (2014).

57. Perdew, J. P., Ruzsinszky, A., Csonka, G. I., Vydrov, O. A., Scuseria, G. E., Constantin, L. A., Zhou, X. & Burke, K. *Phys. Rev. Lett.* **100**, 136406 (2008).

58. Campañá, C., Mussard, B. & Woo, T. K. *J. Chem. Theory Comput.* **5**, 2866–2878 (2009).

59. Dubbeldam, D., Calero, S., Ellis, D. E. & Snurr, R. Q. *Mol. Simul.* **42**, 81–101 (2016).

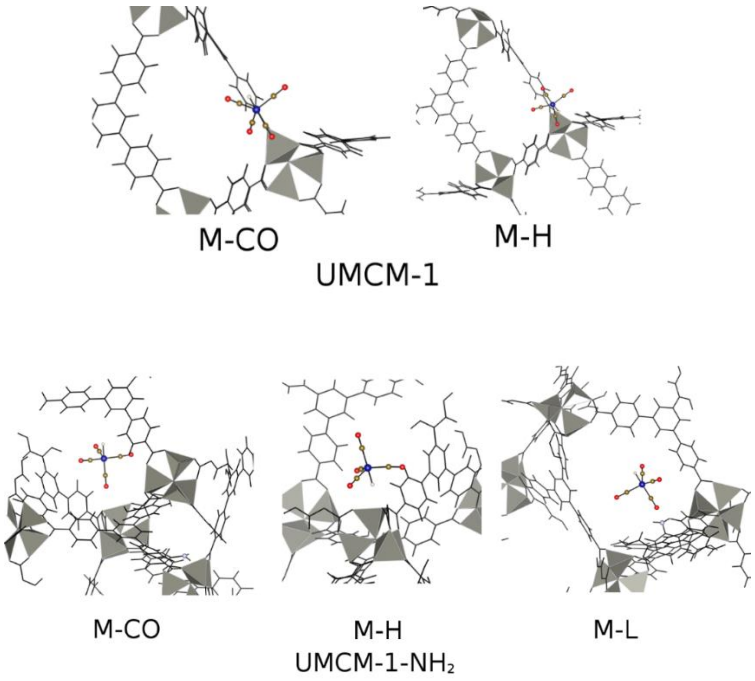
60. Willems, T. F., Rycroft, C. H., Kazi, M., Meza, J. C. & Haranczyk, M. *Microporous Mesoporous Mater.* **149**, 134–141 (2012).

Annex: author's contribution and unpublished data

Since the work depicted in the previous chapter gathers data from three different research groups, in the following annex section there will be described all the data contributed by the author as well as extra work that was omitted on the final publication of the article.

The data obtained by the author is depicted in the section "Electronic interactions are unlikely" in the final manuscript. In order to avoid redundancy, only a summary of the data obtained by the author will be represented below.

Initially, it was proposed that the Co catalyst would be directly coordinated to the MOF structure, concretely coordinated to the organic linker through a P-Co bond. In order to confirm that nature of the system under study and that indeed the Co catalyst was coordinated to the framework it was performed DFT calculations to modulate interaction energies for $HCo(CO)_4$ and $HCo(CO)_3$ complexes within MOFs UMCM-1 and MOF-74(Zn) (see Figure 5.4).



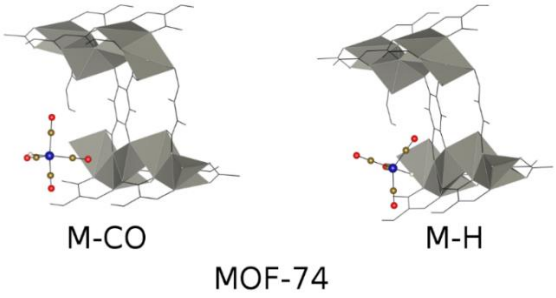


Figure 5.4 From top to bottom: Optimised adsorption geometry of $HCoCO_4$ with UMCM-1. Optimised adsorption geometry of HCoCO4 and UMCM-1-NH_2. Optimised adsorption geometry of $HCoCO_4$ and MOF-74(Zn). Colour scheme: Co = blue, O = red, C = brown, H = beige, N = pale blue. The organic ligand and inorganic node of the MOF are represented as black line and grey polyhedral for clarity

The calculated interaction energy between the catalysts and both frameworks reveal that those energies are indeed in the range of van der Waals interactions and not of a coordination bond (see Table 5.4).

Table 5.4 DFT interaction energy of $HCo(CO)_4$. M-Co (MOF–$COCo(H)(CO)_3$ in the main text) is the adsorption of $HCoCO_4$ to the metal node via its axial carbonyl. M-H (MOF–H-$Co(CO)_4$ in the main text) is the adsorption of $HCoCO_4$ to the metal node via its hydride. L-CO = adsorption of $HCoCO_4$ to the function via its axial carbonyl.

	M-CO (kcal/mol)	M-H (kcal/mol)	L-CO (kcal/mol)
UMCM-1	1.20	0.19	/
UMCM-1-NH_2	0.69	0.01	-0.27
UMCM-1-PPh_2	-0.03	-0.09	-0.09
MOF-74(Zn)	-1.68	-2.53	/

Further calculations considering the MOF–$Co(H)(CO)_3$ specie were also carried out to study the interaction between MOF and catalyst. In order to promote the coordination between MOF and Co catalyst, it has been also studied the interaction between $Co(H)(CO)_3$ and P-MOFs which show strong coordinatively bonds with Co (in Figure 5.5 and Figure 5.6 are represented all the interactions mentioned above).

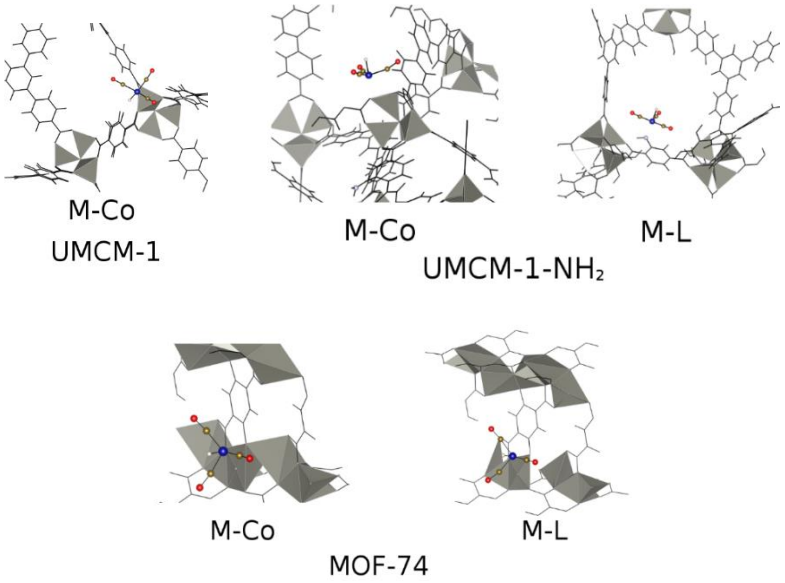


Figure 5.5 Top left: optimised binding geometry of $HCoCO_3$ and UMCM-1. Top right: optimised binding geometry of $HCoCO_3$ and UMCM-1-NH_2. Bottom: optimised binding geometry of $HCoCO_3$ and MOF-74(Zn). Colour scheme: Co = blue, O = red, C = brown, H = beige, N = pale blue. The organic ligand and inorganic node of the MOF are represented as black line and grey polyhedral for clarity reason.

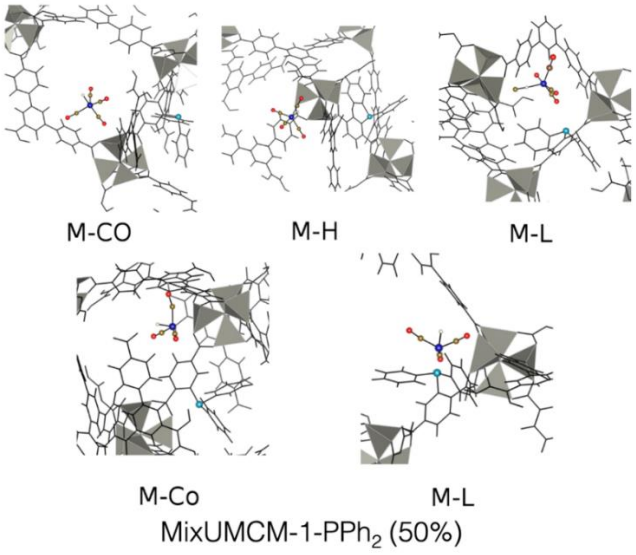


Figure 5.6 On the top, optimized geometry of $HCoCO_4$ and MixUMCM-1- PPh_2 (50%). On the bottom, optimized binding geometry of $HCoCO_3$ and MixUMCM-1-PPh_2 (50%). Colour scheme: Co = blue, O = red, C = brown, H = beige, P = bright blue. The organic ligand and inorganic node of the MOF are represented as black line and grey polyhedral for clarity reason.

All the binding energies obtained for the geometries depicted above (see Table 5.5) show to be lower in energy than the CO-Co(H)$(CO)_3$ (−62.7 and −61.6 kcal/mol for the axial and equatorial CO, respectively) and 1-hexene–Co(H)CO3 (−52.8 kcal/mol) binding energies.

Table 5.5 DFT binding energies. M-Co (MOF–Co(H)$(CO)_3$ in the main text) is the binding energy between the metal of the MOF and the Co of $HCoCO_3$. L-Co (MOFFunc–Co(H)$(CO)_3$ in the main text) is the binding energy between the functional group of the MOF and the Co of $HCoCO_3$.

	M-Co	L-Co
UMCM-1	-3.49	/
UMCM-1-NH_2	-20.22	-34.02
UMCM-1-PPh_2	-54.95	-53.39
MOF-74(Zn)	-28.74	-33.84

DFT calculations performed by the author helped in to corroborate that the Co catalyst is indeed not attached to the MOF framework. Matter of fact, it suggests that the branched selectivity is not coming from an electronic interaction between the Co catalyst and the MOF material moreover, the formation of the linear aldehyde is kinetically driven and any coordination with the MOF structure would increase the steric hindrance promoting the formation of the linear aldehyde.

The data depicted above is the author's contribution to the final published article represented in this chapter, however, it was performed extra work which was omitted on the final publication.

Mechanistic studies following the catalytic cycle depicted in Figure 5.7, were performed in order to understand how electronically could affect the use of a Co-MOF coordinated catalyst to the branch selectivity.

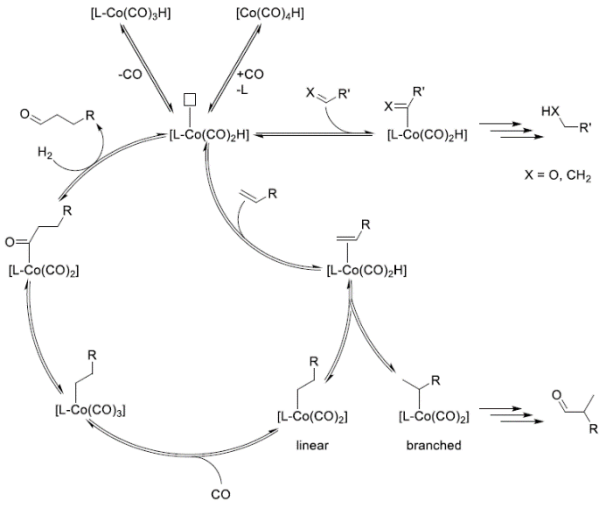


Figure 5.7 Accepted catalytic cycle for the Co-catalysed hydroformylation of olefines.

First calculations were performed only considering the $Co(CO)_4H$ catalyst in order to obtain a full knowledge of the reaction mechanism proposed in Figure 5.7.

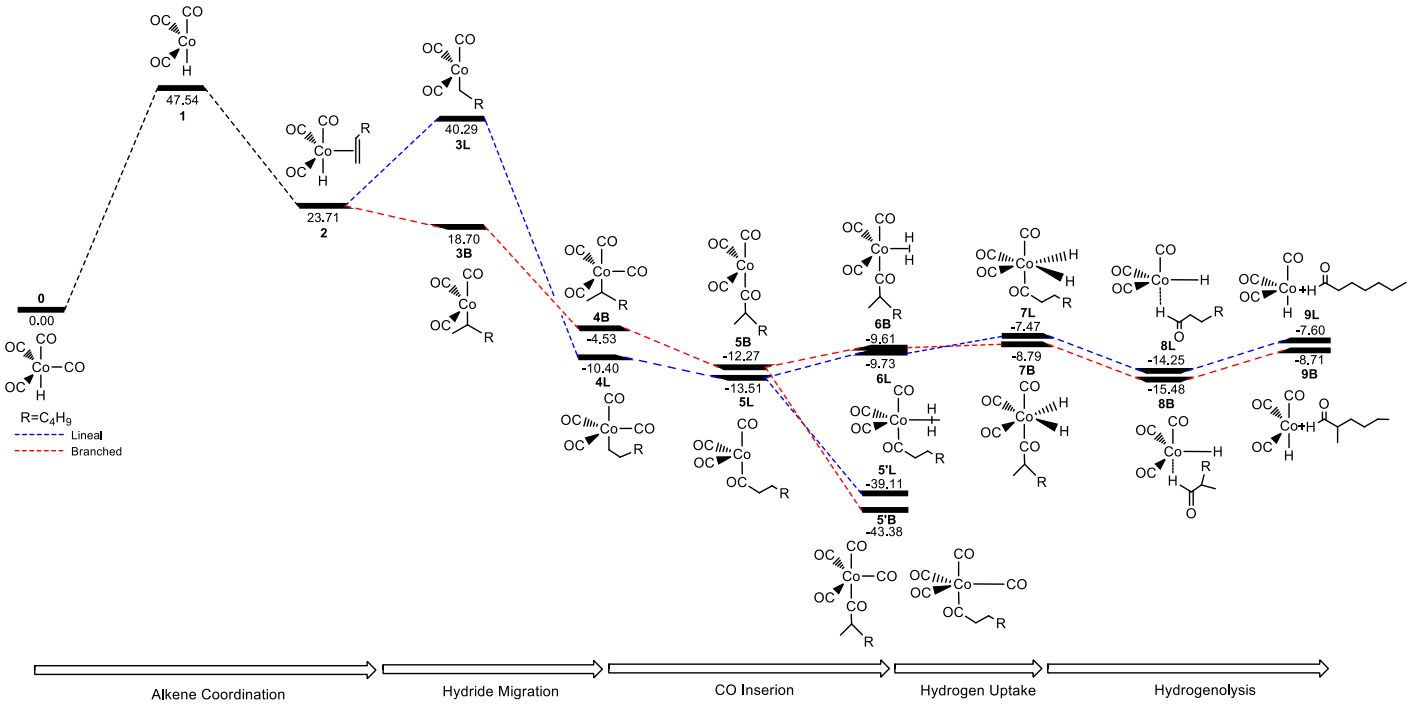


Figure 5.8 Relative energy profile in kcal/mol for the Co-catalysed hydroformylation of olefines, considering as zero the 18e specie ($Co(CO)_4H$). Represented in blue colour the reaction pathway of the linear product and in red colour the branched product.

The reaction mechanism proposed in Figure 5.8 begins with the activation of the catalyst, where ($Co(CO)_4H$) (**0**) losses a CO molecule to become the 16-electron compound **1** which is then coordinates with the alkene 1,2-hexane (C_6H_{12}) leading to the formation of the local minima **2**.

Next step in the reaction pathways is the hydride migration, the H previously coordinated to the Co catalyst migrates to one of the sp2 carbons coordinated to the metal **3**. In this step is observed the first differentiation between linear and branched, if one considers the migration of the H to the first sp2 carbon it is obtained the linear compound **3L** on the other hand, if this migrates to the second sp2 carbon it is formed the branched compound **3B**. Branched intermediate is stabilized by 18.70 kcal/mol while the linear one is indeed less stable than the predecessor, it shows a relative energy of 40.29 kcal/mol, being the branched system 21.59 kcal/mol more stable. At this point the formation of the branched product shows to be thermodynamically more stable. Following with the reaction mechanism, both species incorporate a carbon monoxide to form the corresponding tetracarbonyl species **4**. In this last step the energetic difference between both branched and linear systems becomes minimal and this trend is maintained during all the rest of the reaction process.

Systems in step **4** can undergo CO insertion into the cobalt-alkyl bond to yield an unsaturated acyl species **5**, where the difference between linear and branched is again very small (around 1.24 kcal/mol). Again, the 16e system can incorporate a carbon monoxide molecule to yield the saturated acylcobalt tetracarbonyl species **5'**, even though this reaction step is not considered within the reaction process it is relevant to consider that the 16e intermediates can incorporate a CO ligand.

Following with the cycle the next step is the hydrogen uptake, where an addition of a hydrogen molecule leads to the dihydrogen complex **6**. Again, the difference between linear and branched is insignificant (about 0.13 kcal/mol). Dihydrogen activation can then occur yielding to the dihydride complex **7** where the difference between intermediates is still very small (about 1.32 kcal/mol).

Finally, the last step is hydrogenolysis consisting in a reductive elimination to form a weakly bonded complex **8** between the product (linear or branched) and

the Co complex. Completing the formal catalytic cycle this specie can release the corresponding product obtaining again the specie **1** or adding a carbon monoxide obtaining **0**. Following the trend of the last species, the difference between linear and branched is very small, about 1.23 kcal/mol between **8L** and **8B** and 1.11 kcal/mol between **9L** and **9B**.

In general terms, it is not observed a relevant difference between branched and linear compounds on the thermodynamic profile of the reaction process, only intermediates **3L** and **3B** presents a significant difference being the **3B** compound 21.59 kcal/mol more stable than **3L**. Since it has been only studied the thermodynamics of the reaction mechanism is not possible to determinate the kinetics of the reaction mechanism (transition states are needed to perform such analysis), however it is possible to affirm that the branched process is thermodynamically favorable.

Following the analysis of the reaction mechanism, it has been proposed to study the reaction pathway however under the influence of a cluster of the MOF UMCM-1. Here the Co catalyst is coordinated to the framework through a MOF-P-Co bond. The purpose of studying the system only with a cluster of the MOF is to understand how the coordination of the Co catalyst to the framework can electronically affect to the reaction pathway and if this indeed changes the reaction behavior increasing the formation of branched product.

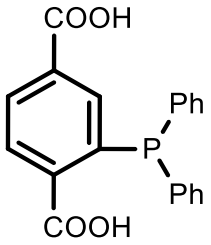


Figure 5.9 The 2-(diphenylphosphino) terephthalic acid is the specie used as a rough approximation of the organic linker of UMCM-1.

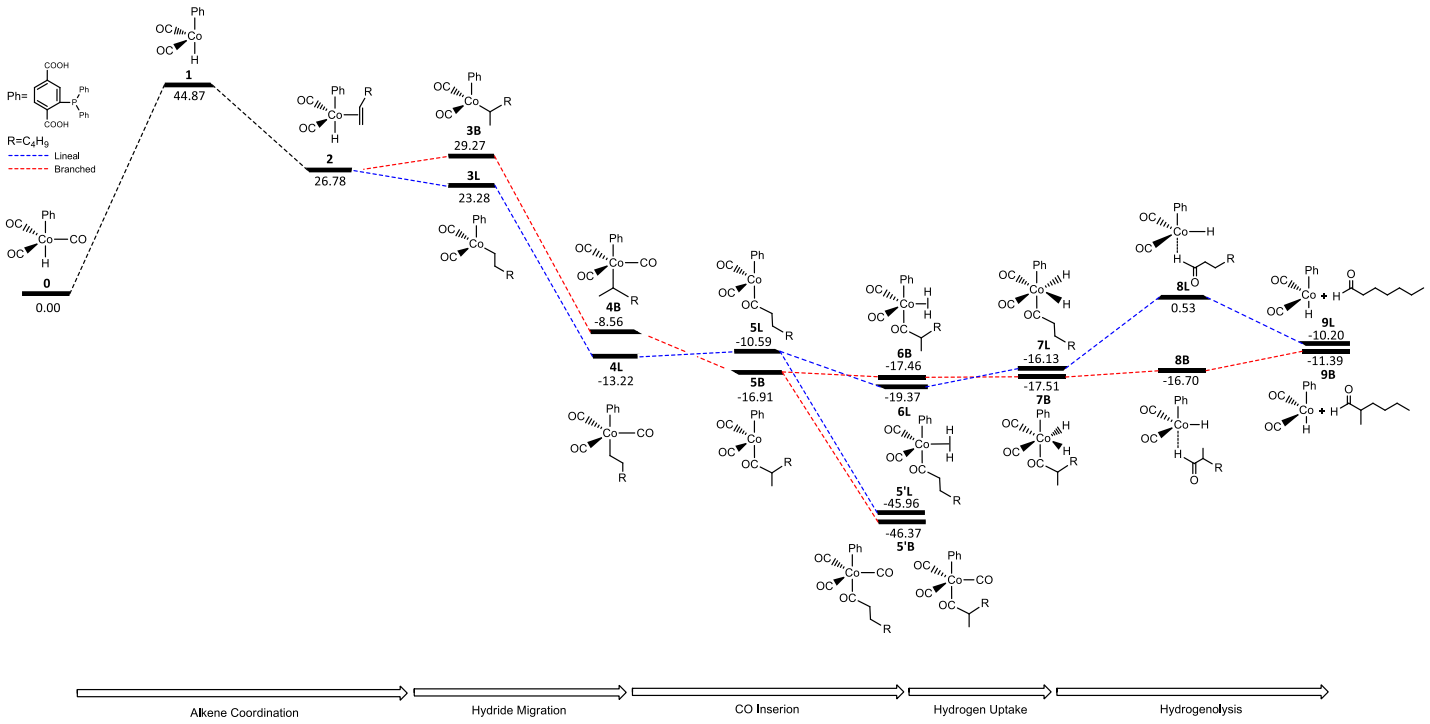


Figure 5.10 Relative energy profile in kcal/mol for the Co-catalysed hydroformylation of olefines, considering as zero the activated 16e specie (PPh_2-$Co(CO)_2H$). Represented in blue colour the reaction pathway of the linear product and in red colour the branched product.

Energy profile represented in Figure 5.10 follows the same reaction mechanism proposed above, however here the Co catalyst is coordinated to the terephthalic acid organic linker of UMCM-1 through a MOF-P-Co bond (see Figure 5.9 and also Ph abbreviation in Figure 5.10). In general terms the reaction mechanism does not change much compared with the previous one, only two steps show considerable differences.

Intermediate **3L** presents an overstabilization being now 6 kcal/mol more stable than the branched equivalent **3B**. Subsequent steps show to be similar, there are not observed major differences between linear and branched compounds. Until step **8** where it is observed a destabilization of the intermediate **8L**, **8B** shows no variations. The reaction profile for the branched product does not change when adding the cluster of the MOF with the phosphine anchor, indeed this would be expected. Once the Co catalyst is coordinated to the framework of the MOF the steric hindrance around the active center increases which directly affects to the kinetic driven product, the linear compound. Again, it is difficult to extract

definitive conclusions as the transition state analysis is missing, however, increasing the steric hindrance around the metal not only does not directly affect to the branched production but also promotes the formation of the linear product. One can consider that the linear production is enhanced, due to first a stabilization of the first intermediate **3L** and second a destabilization of the intermediate **8L** being closer to the following transition state, thus promoting a faster production of **9L**.

Finally, it was planned that the analysis of the reaction mechanism would conclude with the study of the same reaction pathway now considering the full MOF and performing such calculations under Periodic Boundary Condition (PBC) and using the primitive cell of UMCM-1 where the Co catalyst is anchored to the organic linker through a MOF-P-Co bond (see Figure 5.11). However, prior the study of the reaction mechanism there were performed calculations in order to understand the type of bonding between the MOF structure and the Co catalyst. The output of this calculations revealed that the catalyst was indeed not attached to the framework, being the final data reproduced on the article. Due to the fact of the Co catalyst was not bonded to the material further calculations on the reaction mechanism were not considered. Nevertheless, the author considers that even though these data it was not included in the final article it is relevant on the context of the thesis and opens a new line of study.

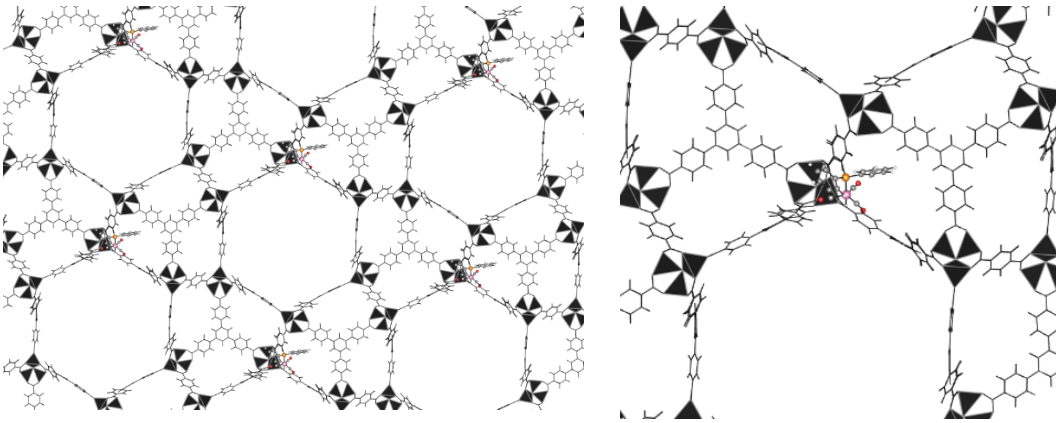


Figure 5.11 Left: zoom out of the optimised MOF-P-Co$(CO)_3$H structure, it is observable the different active sites spread along the framework. Right: zoom in on the active site MOF-P-Co$(CO)_3$H optimised geometry. Colour scheme: Co = pink, O = red, C = grey, H = white, P = orange. The organic ligand and inorganic node of the MOF are represented as black line and black polyhedral for clarity reason.

Chapter 6. MOF encapsulation of Ru olefin metathesis catalysts to block catalyst decomposition

Data reproduced from the article published in *Catalysts* **10**, 687 (2020).

Abstract

In the present work, a catalyst variation of the second-generation Hoveyda–Grubbs catalyst, particularly the ammonium-tagged Ru-alkylidene metathesis catalyst AquaMet^{TM}, is under study, not simply to increase the efficiency in olefin metathesis but also the solubility in polar solvents. Moreover, this ionic catalyst was combined with the metal organic framework (MOF) (Cr)MIL-101-SO_3^-(Na·15-crown-5)$^+$. We started from the experimental results by Grela et al., who increased the performance when the ruthenium catalyst was confined inside the cavities of the MOF, achieving non-covalent interactions between both moieties. Here, using density functional theory (DFT) calculations, the role of the ammonium N-heterocyclic carbene (NHC) tagged and the confinement effects are checked. The kinetics are used to compare reaction profiles, whereas SambVca steric maps and NCI plots are used to characterize the role of the MOF structurally and electronically.

Reproduced with permission from:

Pareras, G., Tiana, D. & Poater, A. *Catalysts* **10**, 687 (2020).

Introduction

Olefin metathesis by Ru-based catalysts certainly has a promising position for finding new applications for industry.[1–3] The basic transformations of raw materials in the oil refinery, polymer chemistry, as well as the fine chemical synthesis in the pharmaceutical industry, are the main examples of the industrial-level potential of this transition metal-catalysed reaction.[4–7] Basically, the goal is to obtain double C-C bonds from other existing ones. Although it may seems like an easy redistribution of C-C double bonds,[8,9] a thorough understanding of its mechanism, as well as any unwanted parallel processes that could decrease its efficiency are necessary.[10–13] If that were not enough, apart from the activity, then an additional effort is needed to control the chemo-, regio- and stereoselectivity of the metathesis.[14–16]

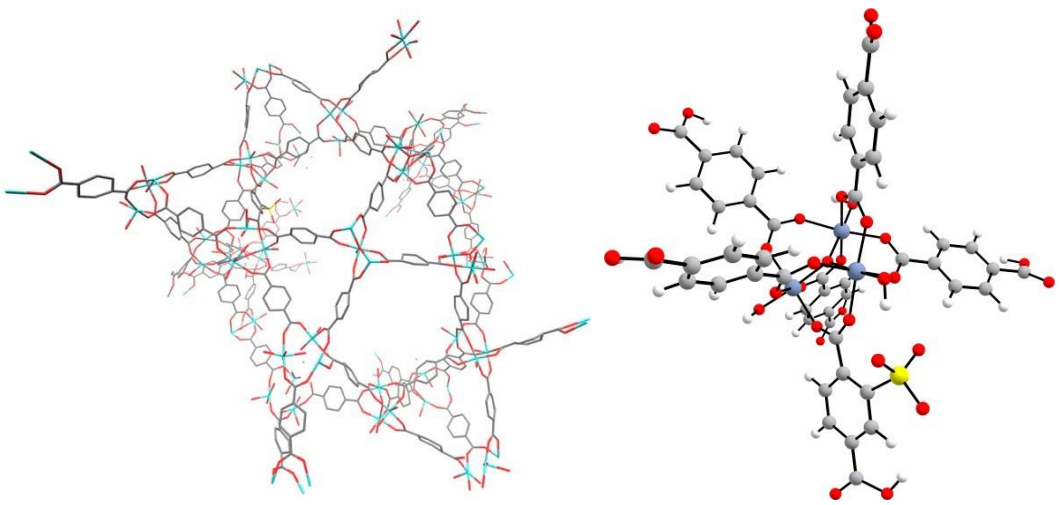
To improve the performance of olefin metathesis catalysts, attempts to anchor them by means of their ionization led to ammonium-tagged Ru-alkylidene metathesis catalysts.[17–19] This represents the addition of the Brönsted acid nature in the framework of olefin metathesis.[20–22] Actually, depending on the generation of olefin metathesis catalysts, results were significantly different. The first generation of catalysts has the ammonium group installed in the benzylidene ligand, giving relatively pure metathesis products. Moreover, they are used in polar solvents including water[23] or immobilised on various supports. On the other hand, for the second generation, catalysts tagged in the N-heterocyclic carbene (NHC) ligand became more stable, and consequently the metal contamination levels decreased. Promising for future industrial purposes, the non-dissociating ligand tagged systems were successfully immobilised on zeolites and metal organic frameworks (MOFs). This allows their use in batch and in continuous flow conditions.

Furthermore, to increase selectivity, a combination of olefin metathesis catalysts with MOFs by Grela and co-workers[24] imposed a special confinement.[25] Particularly, the MOF (Cr)MIL-101-SO_3^-(Na·15-crown-5)$^+$ with the catalyst AquaMet^{TM} created a non-covalent immobilization in the MOF.[26–28]

Although we should have a good knowledge of the mechanism of olefin metathesis by Ru-based catalysts, both experimentally[29–43] and theoretically,[44–58] as well as the potential decomposition reactions[59–65] or non-productive (or degenerate)

metathesis,[66,67] we have not mastered them all, despite attempts to improve them.[68,69] In this study, confining the catalyst inside the cavities of a MOF can improve the performance (see Figure 6.1), simply by reducing any undesired reaction due to the interaction between two catalytic moieties, leading to the formation of Ru-H hydrides via bimolecular decomposition.[70]

This study, using density functional theory (DFT) calculations, aims to unveil the role of the NHC-tagged catalyst AquaMet, and type of the confinement of the ruthenium catalyst inside a cavity of the MOF (Cr)MIL-101-SO_3^-(Na·15-crown-5)$^+$. The X-ray structure of the MOF included in Figure 6.1a was obtained from Grela and Chmielewski,[26] and the model of the MOF (Figure 6.1b) consists of a Cr-trimer linked to a six 1,4-benzenedicarboxylic acid (bdc) ligand.



(a) (b)

Figure 6.1 (a) Snapshot of the X-ray for the metal organic framework (MOF) (Cr)MIL-101-SO_3^-(Na·15-crown-5)$^+$,[26] and (b) with the addition of the catalyst AquaMet^{TM} as part of the MOF.

Results and Discussion

The study started with the reaction profile with ethylene of the initiation for the neutral Hoveyda-type catalyst (HOV) displayed in Figure 6.2a, for the sake of comparison with the ammonium-tagged ones (Figure 6.2b,c). The first step of the reaction profile can be dissociative or concerted,[71] especially considering the small nature of the olefin chosen. Figure 6.3 confirms that the 18e species is too sterically

demanding and the system kinetically prefers 2.1 kcal/mol to go first via the 14e species. We applied the method of Martin and co-workers[72] to delicately deal with the overestimation of the entropy when joining several chemical moieties, and proved olefin metathesis for the activation of Ru-based olefin metathesis catalysts.[73] Otherwise, this energy difference would enlarge up to 5.5 kcal/mol without this correction, confirming the dissociative nature of the first step for HOV. Next, from the latter 14e species, the entering olefin bonds to ruthenium overcoming an energy barrier of 3.4 kcal/mol. The corresponding coordination intermediate Ci1 is rather unstable and by overcoming an energy barrier of just only 2.5 kcal/mol the Mcy is reached. This latter metallacycle is interestingly rather unstable, placed 16.7 kcal/mol above the initial catalyst. The opening of the metallacycle is 4.3 kcal/mol more expensive than the previous closure, and leads to a second coordination intermediate Ci2, also less stable, by 7.3 kcal/mol than the first. Finally, via a barrierless process the olefin is released. However, there is probably a more energetic step in-between that consists of a nearly 90º rotation of the product olefin. Even though the rate determining step (rds) were supposed to be the olefin release according to Solans-Monfort and co-workers,[74] the opening of the metallacycle would be here.

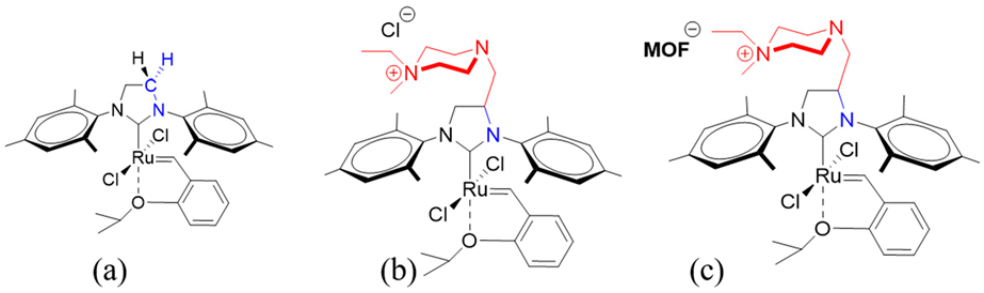


Figure 6.2 Three-dimensional (3D) Lewis structure of the olefin metathesis catalysts studied: (a) Hoveyda-type catalyst (HOV); (b) AquaMet™; (c) MOF-AquaMet™

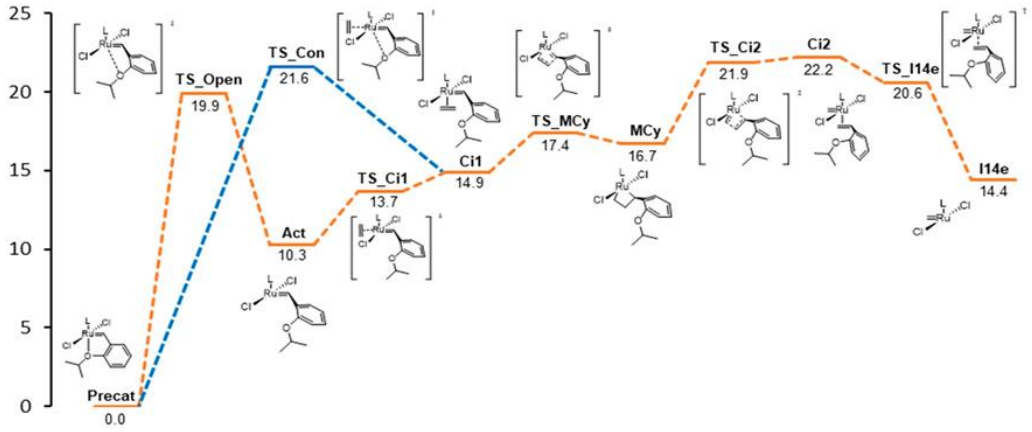


Figure 6.3 Calculated reaction profile for the initiation of the neutral HOV catalyst (free energies in kcal/mol). Blue lines correspond the concerted bonding of ethylene together with the Ru–O bond cleavage (free energies in solvent given in kcal/mol).

As shown in Figure 6.2b, the HOV was combined with a chloride counteranion, since the substitution of one hydrogen of the backbone of the NHC ligand by a cationic chain led to the neutral ammonium-tagged AquaMet^{TM}. For the sake of consistency, the cationic AquaMet^{TM+} was also studied (i.e., an ammonium NHC-tagged olefin metathesis catalyst). Moreover, it is its cationic part that deals with the MOF. The comparison of the results displayed in Figure 6.3, with respect to the homologous ammonium NHC-tagged olefin metathesis catalyst, unveil minimal energy differences.[75] Table 6.1 confirms that there are insignificant differences not only between the neutral HOV and AquaMet^{TM}, but also with respect to the charged AquaMet^{TM+}. To point out, the rds goes down by 2.0 and 1.5 kcal/mol for AquaMet^{TM+} and AquaMet^{TM}, respectively (see Figure 6.4). Thus, kinetically speaking, the ammonium-tagged catalysts should perform slightly better, whereas the thermodynamics are quite similar. On the other hand, the concerted transition state is located even further, and the energy difference with respect to the initial Ru-O bond cleavage rises from 1.7 kcal/mol for HOV to 8.3 and 9.0 kcal/mol for AquaMet^{TM+} and AquaMet^{TM}, respectively.

Table 6.1 Relative energies of the reaction profile of the initiation in olefin metathesis with ethylene as a substrate for the Hoveyda catalysts (HOV), with the tagged N-heterocyclic carbene (NHC) ligand, including the chloride counteranion (AquaMet^{TM}) or not (AquaMet^{TM+}). Energy values in kcal/mol.

Catalyst	Precat	TS_open	Act	TS_Ci1	Ci1	TS_MCy	MCy	TS_Ci2	Ci2	TS_I14e	I14e
HOV	0.0	19.9	10.3	13.7	14.9	17.4	16.7	21.9	22.2	20.6	14.4
AquaMet^{TM+}	0.0	15.8	9.0	12.5	15.0	16.6	16.1	19.9	19.0	19.4	13.4
AquaMet^{TM}	0.0	15.4	10.9	13.7	14.2	17.8	16.4	20.4	21.7	19.9	14.0

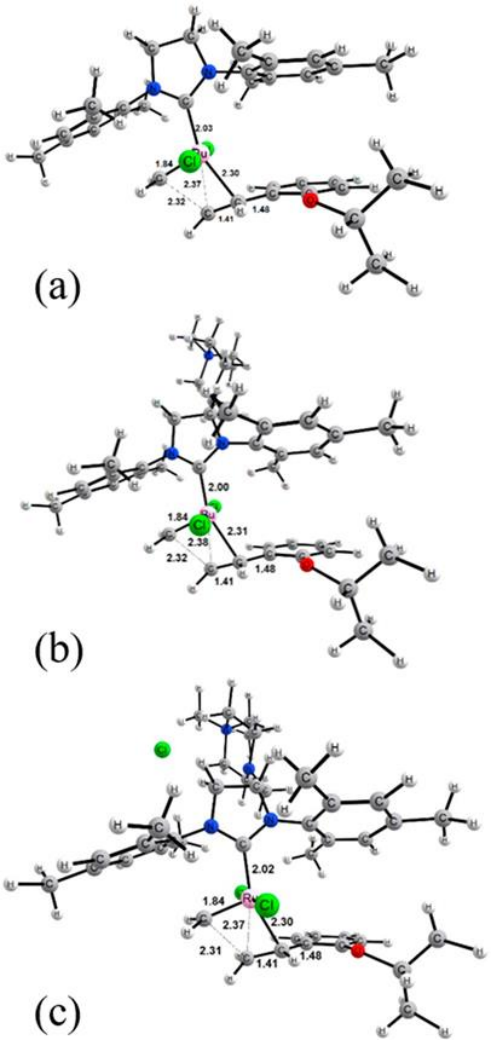


Figure 6.4 Transition state TS_Ci2 of the opening of the metallacycle for (a) HOV, (b) AquaMet^{TM+} and (c) AquaMet^{TM} (selected distances in Å).

Table 6.2 demonstrates that the key bonds are not that different holding the ammonium-tagged ligand or not. The ruthenium with the ylidene group bonds similarly. In addition, the Ru–O bond is slightly weaker (elongated by 0.007 Å) and translates into a decrease of the energy barrier of the Ru–O bond cleavage by 4.1

and 4.5 kcal/mol for AquaMet^{TM+} and AquaMet^{TM}, respectively. Thus, the presence of the ammonium-tagged ligand facilitates this bond cleavage.

Table 6.2 Main distances for catalysts HOV, AquaMet^{TM} and MOF-AquaMet^{TM} (in Å).

Catalyst	Bond	Precat	Act	Ci1	MCy	Ci2	I14e
HOV	Ru=C$_{ylidene(1)}$	1.848	1.846	1.873	2.035	2.241	-
	Ru=C$_{ylidene(2)}$	-	-	2.276	1.980	1.814	1.809
	Ru–C$_{NHC}$	1.965	1.927	2.033	2.016	2.076	1.933
	Ru–O	2.304	-	-	-	-	-
AquaMet^{TM+}	Ru=C$_{ylidene(1)}$	1.850	1.851	1.877	2.042	2.283	-
	Ru=C$_{ylidene(2)}$	-	-	2.291	1.981	1.824	1.809
	Ru–C$_{NHC}$	1.953	1.916	2.014	2.007	1.981	1.917
	Ru–O	2.296	-	-	-	-	-
AquaMet^{TM}	Ru=C$_{ylidene(1)}$	1.848	1.845	1.871	2.033	2.240	-
	Ru=C$_{ylidene(2)}$	-	-	2.275	1.979	1.814	1.809
	Ru–C$_{NHC}$	1.966	1.935	2.034	2.015	2.079	1.939
	Ru–O	2.311	-	-	-	-	-

Moving to electronics, conceptual DFT was considered to find out if the nature of the studied olefin metathesis catalysts allows any differentiation. Among definitions, electrophilicity and chemical hardness are the parameters that could fit here. The electrophilicity of the catalysts was evaluated by means of the Parr electrophilicity index, using Equation (1),[76] where μ and η are the chemical potential and the molecular hardness, respectively. Using DFT,[77] μ and η for an N-electron system with total electronic energy E and subject to an external potential are defined as the first and second derivatives of the energy with respect to N at a fixed external potential. By Koopmans' theorem,[78] μ and η can be approximated with the finite difference formulas of Equation (2), where εH and εL are the energies of the highest occupied molecular orbital (HOMO) and the lowest unoccupied molecular orbital (LUMO), respectively.

$$\omega = \frac{\mu^2}{2\eta} \qquad (1)$$

$$\mu \div \frac{1}{2}(\varepsilon L + \varepsilon H) and\ \eta \div \frac{1}{2}(\varepsilon L - \varepsilon H) \qquad (2)$$

Regarding the results in Table 6.3, and focusing on chemical hardness, the addition of the ammonium moiety is demonstrated as sterile, whereas

electrophilicity shows subtle differentiating effects. Although electrophilicity is similar for AquaMet^{TM}, it is worth noting the almost doubly positive value for the cationic part of it. Since with the MOF the interaction occurs from this fragment, although it is partially stabilized with the negative charge of a sulfonated group, here the electrophilicity is more incipient for this cationic fragment. This trend is maintained for both 14e species, Act and I14e.

Table 6.3 Conceptual density functional theory (DFT) analysis (μ = chemical potential, η = chemical hardness, ε = Parr electrophicity; in a.u.) for Precat, Act and I14e.

Catalyst		Precat			Act			I14e		
		μ	η	ε	μ	η	ε	μ	η	ε
HOV	Gas	−0.125	0.059	0.134	−0.129	0.069	0.120	−0.133	0.079	0.111
	Solvent	−0.139	0.117	0.082	−0.141	0.124	0.080	−0.142	0.142	0.071
AquaMet^{TM+}	Gas	−0.184	0.064	0.265	−0.187	0.072	0.243	−0.197	0.084	0.232
	Solvent	−0.157	0.119	0.103	−0.158	0.124	0.101	−0.161	0.145	0.090
AquaMet^{TM}	Gas	−0.115	0.057	0.116	−0.115	0.066	0.099	−0.118	0.076	0.091
	Solvent	−0.135	0.116	0.078	−0.134	0.123	0.073	−0.136	0.141	0.065

The positive charge of the cationic ammonium species remains on the ammonium-tagged ending group, whereas the first sphere containing the atoms around the metal centre is not significantly affected. Table 6.4 gathers all the information related to natural bond orbital (NBO) charges. The charge on the ruthenium is the same for the first 14e species Act, but interestingly for the initial precatalytic structure Precat, HOV presents a less positive charge; thus, it is less prone to react with potential olefins, but the difference is just 0.003 e^{-}.

Table 6.4 Natural bond orbital (NBO) charge analysis on the metal, oxygen, two Cylidene, CNHC and two chlorides (in e^-).

Catalyst	Atom	Precat	Act	Ci1	MCy	Ci2	I14e
HOV	Ru	−0.253	−0.157	−0.337	−0.269	−0.283	−0.178
	$Ru=C_{ylidene(1)}$	−0.001	−0.024	0.051	−0.164	−0.443	-
	$Ru=C_{ylidene(2)}$	-	-	−0.426	−0.333	−0.147	−0.205
	C_{NHC}	0.487	0.505	0.458	0.481	0.462	-
	O	−0.475	−0.531	−0.529	−0.541	−0.544	-
	Cl_1	−0.268	−0.253	−0.296	−0.308	−0.303	-
	Cl_2	−0.269	−0.264	−0.288	−0.306	−0.298	-
$AquaMet^{TM+}$	Ru	−0.253	−0.156	−0.342	−0.274	−0.342	−0.174
	$Ru=C_{ylidene(1)}$	0.002	−0.020	0.050	−0.161	−0.465	-
	$Ru=C_{ylidene(2)}$	-	-	−0.424	−0.328	−0.133	−0.197
	C_{NHC}	0.485	0.502	0.464	0.482	0.473	-
	O	−0.476	−0.533	−0.531	−0.545	−0.537	-
	Cl_1	−0.253	−0.240	−0.291	−0.308	−0.294	-
	Cl_2	−0.264	−0.263	−0.286	−0.295	−0.327	-
$AquaMet^{TM}$	Ru	−0.250	−0.157	−0.336	−0.263	−0.282	−0.179
	$Ru=C_{ylidene(1)}$	−0.009	−0.034	0.046	−0.171	−0.445	-
	$Ru=C_{ylidene(2)}$	-	-	−0.427	−0.333	−0.148	−0.210
	C_{NHC}	0.489	0.508	0.463	0.486	0.464	-
	O	−0.475	−0.531	−0.530	−0.546	−0.546	-
	Cl_1	−0.261	−0.245	−0.294	−0.305	−0.294	-
	Cl_2	−0.273	−0.269	−0.291	−0.312	−0.309	-

To check if the MOF has any role in terms of energetics or nature of the reaction intermediates (see Figure 6.5 to see how the olefin metathesis catalyst interacts with the MOF), CP2K calculations were performed. To point out that the MOF was truncated (see Figure 6.1b), and the anionic MOF moiety was coupled with the ammonium NHC-tagged olefin metathesis catalyst MOF-$AquaMet^{TM}$ (displayed in Figure 6.2c) without the chloride. The binding energy for the Precat was 63.8 kcal/mol between both ionic moieties. In particular, the sulfonate of the MOF and the ammonium group are linked by a series of H-bonds. Table 6.5 collects the relative energies, collected in gas phase since calculations by CP2K were performed without explicit solvent molecules. The different nature of the calculations with both computational packages (CP2K and Gaussian), despite significant absolute energies, shows results that qualitatively agree, and are very close in terms of electronic energies. Particularly, among the results with CP2K, the introduction of the MOF model, instead of the chloride counteranion, involves a flattening of the potential energy surface. Interestingly, both coordination

intermediates (Ci1 and Ci2) are especially stabilized, while the metallacycle is relatively less stable, which would favour olefin metathesis.[79]

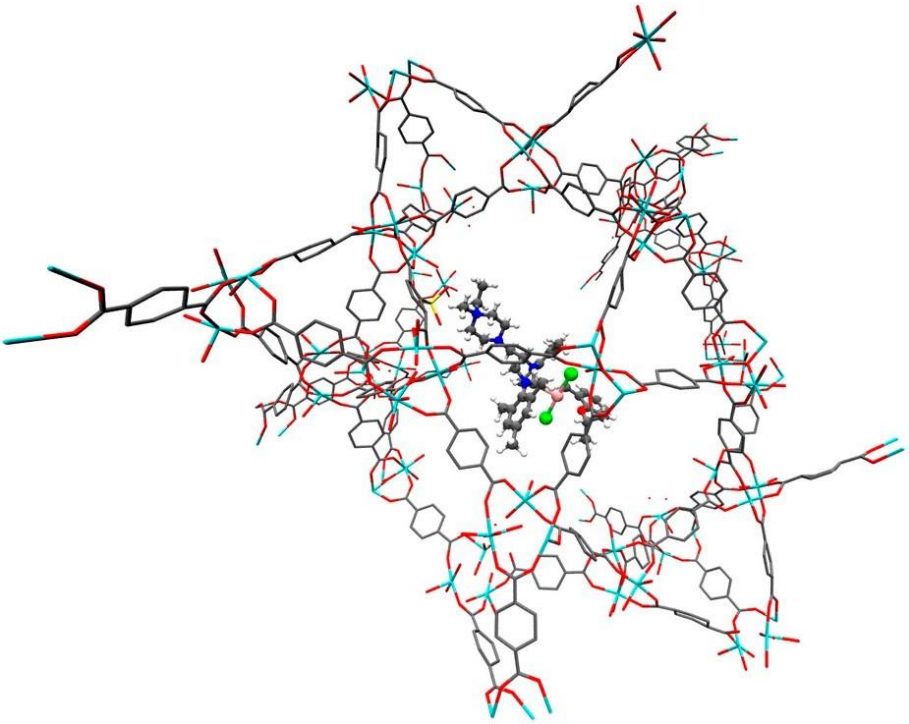


Figure 6.5 Snapshot of the MOF from the X-Ray with an inserted ammonium NHC-tagged olefin metathesis catalyst AquaMet^{TM} in a cavity.

Table 6.5 Relative energies in gas phase (in kcal/mol) of the intermediates for catalysts HOV, AquaMet^{TM} and MOF-AquaMet^{TM}, and including the model of MOF.

Model Catalyst	Precat	Act	Ci1	MCy	Ci2	I14e
AquaMet^{TM+} [(a)]	0.0	13.2	6.3	0.2	12.9	18.0
AquaMet^{TM} [(a)]	0.0	11.8	5.2	−2.4	13.1	13.2
MOF-AquaMet^{TM} [(a)]	0.0	2.1	−3.1	3.1	3.9	8.2
AquaMet^{TM+} [(b)]	0.0	13.6	6.0	1.0	7.0	14.4
AquaMet^{TM} [(b)]	0.0	14.7	5.8	−0.1	9.9	10.8
HOV[(b)]	0.0	12.9	5.6	0.5	10.4	13.0
HOV[(b,c)]	0.0	10.5	15.0 (18.7)	11.6 (15.4)	20.0 (23.8)	9.8 (9.0)

[(a)]calculated by CP2K; [(b)]calculated by Gaussian (in parentheses values calculated without the correction of Martin, at 1 atm); [(c)]Gibbs free energies in gas phase.

To see if the ammonium-tagged catalysts change their catalytic properties for structural reasons in presence of the MOF around, or if the entry of a substrate is prevented, especially when the metal catalyst is confined inside the MOF, steric

maps were made around the metal.[80] In the first sphere, at 3.5 Å, this is where reactivity takes place.[81,82] If a ligand marks the reactivity by ruthenium complexes, this reaction is the effect caused by the NHC ligand. Consequently, the study was performed with all the catalysts studied here. To determine this steric hindrance around the metal,[83] topographical steric maps of NHC ligands were obtained by SambVca 2.1,[84] developed by Cavallo and co-workers. The radius of the sphere around the metal centre was set to 3.5 Å, whereas for the atoms we adopted the Bondi radii scaled by 1.17, and a mesh of 0.1 Å was used to scan the sphere for buried voxels.[85] As reported for the interaction of small molecules with carbo-benzenes,[86] the study was extended to higher ranks (i.e., 5.0, 8.0, 10.0, 12.0 and 15.0 Å). The elucidation of the steric maps, together with the total and quadrant %VBur values, give quantitative and qualitative data to predict the reactivity of the metal catalysts. These two-dimensional isocontours represent the interaction surface as topographic maps. Even though the NHC ligand affects up to 12–13 Å, its interaction is basically in the first 3.5 Å length around the metal (see Figure 5b).[87] However, here we had to check how the MOF could sterically take part in the region around the metal where the olefin enters. From Table 6 it is clear that the MOF alone has no significant participation till a range of 12.0–15.0 Å (see Figure 5c,d), which confirms that the catalysis inside the MOF is the same as outside the MOF for the Ru-based olefin metathesis catalyst. The %VBur and steric maps including all the atoms, with or without the MOF, are quite similar around the metal (see Supplementary Information for further details). On the other hand, the ammonium-tagged catalyst AquaMet^{TM} is as sterically demanding as HOV, with almost null differences.

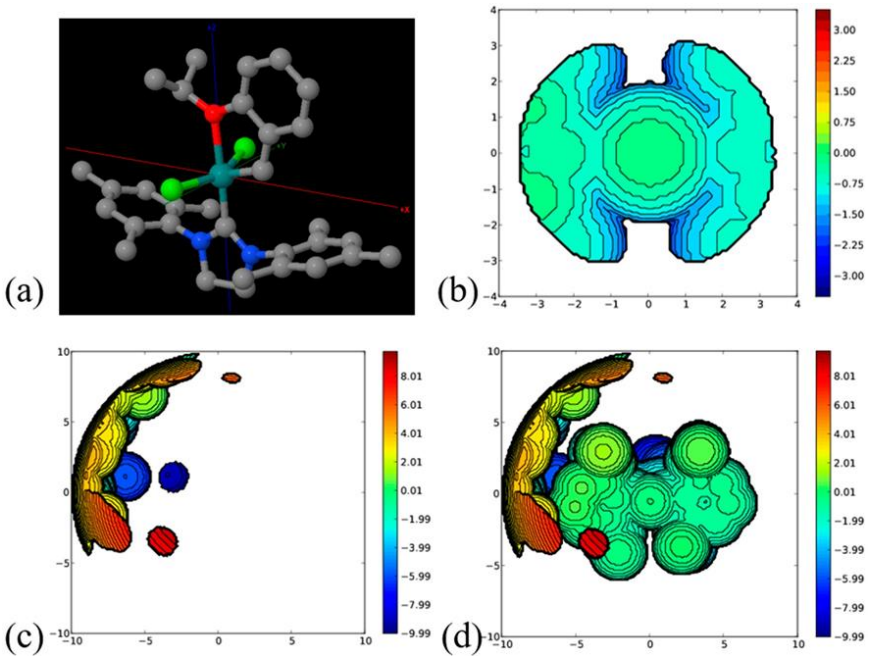


Figure 6.6 Topographic steric maps of the section of the MOF (plane xy) from the X-ray: (a) orientation of the axis; (b) HOV with a radius of 3.5 Å; (c) MOF with a radius of 10 Å and (d) MOF-AquaMet^{TM} with a radius of 10 Å. The linking C atom of the NHC is on the z axis, and the metal atom is 2 Å below the plane described by the metal and both chloride atoms. The isocontour curves of the steric maps are given in Å.

Due to the low covalent character presented by the interactions between the metal catalyst and the MOF, we computed the NCI plots using the NCIPLOT package of Contreras-Garcia and co-workers.[88,89] The NCI plots allow to observe and qualitatively evaluate the strength of the non-covalent interactions between different moieties, pointing out that they are not available for pseudopotential. This did not represent an issue since the nature of the metal, ruthenium, is not that affected by relativistic effects.[90,91] Figure 6.7 shows the NCI plot obtained for Precat. Qualitatively we did not notice any significant difference with respect to the other NCI plots (see Figure S1).

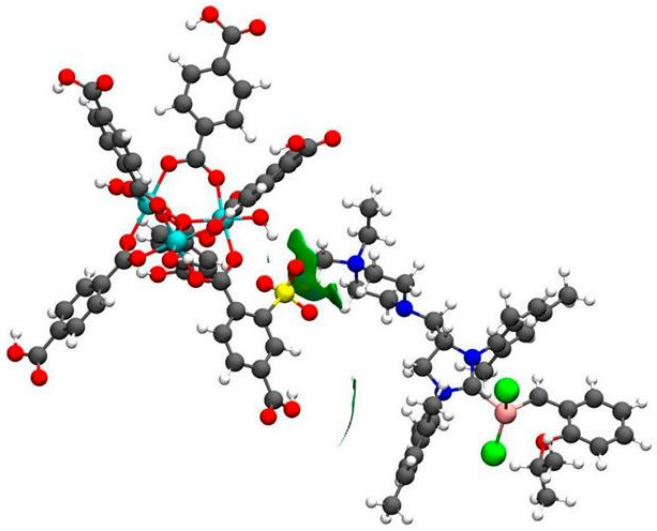


Figure 6.7 NCI plot of the truncated MOF in combination with Precat.

In the representations, we plotted the isocontour obtained for a value of 0.5 on the reduced density gradient; and for the colour scale, we used the interval from −0.5 to 0.5 of the second density Hessian eigenvalue, going from blue (attractive) to red (repulsive). From a qualitative point of view, we only observed a rather strong interaction between the model of the MOF and the cationic moiety on the backbone of the NHC ligand, defined by a clear H-bond between an oxygen of the anionic sulfonate and the ending H atom of the cationic chain on the backbone of the NHC ligand (O···H = 2.178 Å). Other relevant interactions came from the hydroxyl of a carboxylic chemical group and the closest isopropyl of the NHC ligand. However, the intensity is rather low in agreement with the weak H-bond among them (O···H = 4.389 Å).

Conclusions

When starting a computational project, the aim is always to achieve challenging objectives, that at an experimental level were not possible with the second-generation Hoveyda–Grubbs catalyst studied here, or that could not be explained as a whole or part. The research group of Grela studied catalytic activity on olefin metathesis[26] confined within a MOF and managed to find an explanation that is both humble and simple, and in line with the results on capsules by Reek and collaborators.[92] Anchoring the catalyst within the MOF is intended to be almost like a heterogeneous catalyst, and to prevent undesired decomposition reactions. Computationally, the results are somewhat similar, with a slight destabilization of

the metallacycle that helps to get better catalytic performance.[79] The cationic moiety on the backbone of the NHC is unveiled to positively affect the kinetics, with roughly 2 kcal/mol of stabilization. Despite not finding big differences, we observed that the confinement of the catalysts enhances their catalytic capacity;[26] this could be a result of avoiding the decomposition of olefin metathesis by means of the interaction of two metal moieties.[71] Thus, either we find a vaccine (i.e., a modification of the catalysts to minimize or remove the decomposition reactions) or the MOFs here are a perfect vaccine for this issue. Overall, this study confirms that the NHC-tagged catalysts perform better for the Brönsted acid nature, but the enhancement of the reactivity is also due to the confinement of the ruthenium catalyst inside a cavity of the MOF, blocking the potential decomposition of the metal catalyst.

Computational details

All DFT calculations were performed using the Gaussian09 set of programs.[93] In these calculations, the BP86 of Becke and Perdew was employed.[94,95] The electronic configuration of the studied molecules was described with the standard split valence basis set with a polarization function for H, C, Cl, N and O (Def2SVP keyword in Gaussian) of Ahlrichs and co-workers.[96] The quasi relativistic, small-core, effective core potential of Stuttgart/Dresden, with an associated valence basis set (SDD keyword in Gaussian) was used for Ru atom.[97]

Solvent effects on the potential energy surfaces of the oligomerization cycle were estimated based on the polarizable continuum solvation model (PCM) using dimethyl carbonate (DMC) as solvent,[98,99] the B3LYP, hybrid GGA functional of Becke-Lee, Parr, and Yang[100] and triple-ζ basis set (cc-pVTZ keyword in Gaussian),[101] together with the Grimme D3 correction term for the electronic energy.[102] Thus, the free energies discussed throughout the manuscript include the electronic energies in solvent that are corrected by the thermal corrections calculated in the gas phase at T = 323.15 K and P = 1354 atm.[72]

The unit cell of Mil-101 is excessively large for periodic DFT calculations, therefore, we performed the calculations on a fragmented cluster of the MOF (Figure 1). All the simulations of the cluster were performed with CP2K[103] at density functional level of theory, considering gas phase. The semi-local PBE

functional of Perdew, Burke and Ernzerhof was adopted[104] using the DZVP-MOLOPT-SR-GTH Gaussian basis set for all the atom types,[105] and a cutoff of 450 Ry for the plane wave auxiliary basis set. Atom positions were optimised converging the force up to 5×10^{-3} a.u. and the electronic structure up to 1×10^{-3} a.u. The cubic simulation box size was set to $25 \times 25 \times 25$ Å^3 ensuring isolated molecule simulation.

References

1. Sytniczuk, A., Forcher, G., Grotjahn, D. B. & Grela, K. *Chem. - A Eur. J.* **24**, 10403–10408 (2018).
2. Rouen, M., Queval, P., Borré, E., Falivene, L., Poater, A., Berthod, M., Hugues, F., *et al. ACS Catal.* **6**, 7970–7976 (2016).
3. Sytniczuk, A., Dabrowski, M., Banach, Ł., Urban, M., Czarnocka-Śniadała, S., Milewski, M., Kajetanowicz, A. & Grela, K. *J. Am. Chem. Soc.* **140**, 8895–8901 (2018).
4. Grubbs, R. H. & O'Leary, D. J. *Handbook of Metathesis. Volume 2: Applications in Organic Synthesis*; Wiley-VCH: Weinheim, Germany, 2003.
5. Samojłowicz, C., Bieniek, M. & Grela, K. *Chem. Rev.* **109**, 3708–3742 (2009).
6. Vougioukalakis, G. C. & Grubbs, R. H. *Chem. Rev.* **110**, 1746–1787 (2010).
7. Ogba, O. M., Warner, N. C., O'Leary, D. J. & Grubbs, R. H. *Chem. Soc. Rev.* **47**, 4510–4544 (2018).
8. Poater, A. & Cavallo, L. *Beilstein J. Org. Chem.* **11**, 1767–1780 (2015).
9. Grela, K. & Kajetanowicz, A. *Beilstein J. Org. Chem.* **15**, 2765–2766 (2019).
10. Bailey, G. A., Foscato, M., Higman, C. S., Day, C. S., Jensen, V. R. & Fogg, D. E. *J. Am. Chem. Soc.* **140**, 6931–6944 (2018).
11. Van Rensburg, W. J., Steynberg, P. J., Meyer, W. H., Kirk, M. M. & Forman, G. S. *J. Am. Chem. Soc.* **126**, 14332–14333 (2004).
12. Poater, A., Bahri-Laleh, N. & Cavallo, L. *Chem. Commun.* **47**, 6674–6676

(2011).

13. Manzini, S., Poater, A., Nelson, D. J., Cavallo, L., Slawin, A. M. Z. & Nolan, S. P. *Angew. Chemie - Int. Ed.* **53**, 8995–8999 (2014).

14. Pump, E., Poater, A., Bahri-Laleh, N., Credendino, R., Serra, L., Scarano, V. & Cavallo, L. *Catal. Today*. (2020), in press.

15. Ahmed, T. S., Montgomery, T. P. & Grubbs, R. H. *Chem. Sci.* **9**, 3580–3583 (2018).

16. Nechmad, N. B., Phatake, R., Ivry, E., Poater, A. & Lemcoff, N. G. *Angew. Chemie - Int. Ed.* **59**, 3539–3543 (2020).

17. Jana, A. & Grela, K. *Chem. Commun.* **54**, 122–139 (2017).

18. Schmid, T. E., Dumas, A., Colombel-Rouen, S., Crévisy, C., Baslé, O. & Mauduit, M. *Synlett* **28**, 773–798 (2017).

19. Patrzałek, M., Piaotkowski, J., Kajetanowicz, A. & Grela, K. *Synlett* **30**, 1981–1987 (2019).

20. Klučiar, M., Grela, K. & Mauduit, M. *Dalt. Trans.* **42**, 7354–7358 (2013).

21. Szczepaniak, G., Kosiński, K. & Grela, K. *Green Chem.* **16**, 4474–4492 (2014).

22. Skowerski, K., Biatecki, J., Czarnocki, S. J., Zukowska, K. & Grela, K. *Beilstein J. Org. Chem.* **12**, 5–15 (2016).

23. Skowerski, K., Szczepaniak, G., Wierzbicka, C., Gułajski, Ł., Bieniek, M. & Grela, K. *Catal. Sci. Technol.* **2**, 2424–2427 (2012).

24. Chołuj, A., Zieliński, A., Grela, K. & Chmielewski, M. J. *ACS Catal.* **6**, 6343–6349 (2016).

25. Mínguez Espallargas, G. & Coronado, E. *Chem. Soc. Rev.* **47**, 533–557 (2018).

26. Chołuj, A., Karczykowski, R. & Chmielewski, M. J. *Organometallics* **38**, 3392–3396 (2019).

27. Chołuj, A., Krzesiński, P., Ruszczyńska, A., Bulska, E., Kajetanowicz, A. &

Grela, K. *Organometallics* **38**, 3397–3405 (2019).

28. Chołuj, A., Nogaś, W., Patrzałek, M., Krzesiński, P., Chmielewski, M. J., Kajetanowicz, A. & Grela, K. *Catalysts* **10**, 438 (2020).

29. Slugovc, C., Perner, B., Stelzer, F. & Mereiter, K. *Organometallics* **23**, 3622–3626 (2004).

30. Ung, T., Hejl, A., Grubbs, R. H. & Schrodi, Y. *Organometallics* **23**, 5399–5401 (2004).

31. Grubbs, R. H., Burk, P. L. & Carr, D. D. *J. Am. Chem. Soc.* **97**, 3265–3267 (1975).

32. Sandford, M. S., Love, J. A. & Grubbs, R. H. *J. Am. Chem. Soc.* **123**, 6543–6554 (2001).

33. Conrad, J. C., Parnas, H. H., Snelgrove, J. L. & Fogg, D. E. *J. Am. Chem. Soc.* **127**, 11882–11883 (2005).

34. Manzini, S., Urbina Blanco, C. A., Nelson, D. J., Poater, A., Lebl, T., Meiries, S., Slawin, A. M. Z., Falivene, L., Cavallo, L. & Nolan, S. P. *J. Organomet. Chem.* **780**, 43–48 (2015).

35. Małecki, P., Gajda, K., Gajda, R., Woźniak, K., Trzaskowski, B., Kajetanowicz, A. & Grela, K. *ACS Catal.* **9**, 587–598 (2019).

36. Vehlow, K., Gessler, S. & Blechert, S. *Angew. Chemie - Int. Ed.* **46**, 8082–8085 (2007).

37. Romero, P. E., Piers, W. E. & McDonald, R. *Angew. Chemie - Int. Ed.* **43**, 6161–6165 (2004).

38. Romero, P. E. & Piers, W. E. *J. Am. Chem. Soc.* **127**, 5032–5033 (2005).

39. Wenzel, A. G. & Grubbs, R. H. *J. Am. Chem. Soc.* **128**, 16048–16049 (2006).

40. Van Der Eide, E. F., Romero, P. E. & Piers, W. E. *J. Am. Chem. Soc.* **130**, 4485–4491 (2008).

41. Vorfait, T., Leuthäußer, S. & Plenio, H. *Angew. Chemie - Int. Ed.* **48**, 5191–5194 (2009).

42. Huang, J., Stevens, E. D., Nolan, S. P. & Petersen, J. L. *J. Am. Chem. Soc.* **121**, 2674–2678 (1999).

43. Weskamp, T., Kohl, F. J., Hieringer, W., Gleich, D. & Herrmann, W. A. *Angew. Chemie - Int. Ed.* **38**, 2416–2419 (1999).

44. Vyboishchikov, S. F., Bühl, M. & Thiel, W. *Chem. - A Eur. J.* **8**, 3962–3975 (2002).

45. Occhipinti, G., Bjørsvik, H. R. & Jensen, V. R. *J. Am. Chem. Soc.* **128**, 6952–6964 (2006).

46. Stewart, I. C., Benitez, D., O'Leary, D. J., Tkatchouk, E., Day, M. W., Goddard, W. A. & Grubbs, R. H. *J. Am. Chem. Soc.* **131**, 1931–1938 (2009).

47. Voccia, M., Nolan, S. P., Cavallo, L. & Poater, A. *Beilstein J. Org. Chem.* **14**, 2956–2963 (2018).

48. Yang, H. C., Huang, Y. C., Lan, Y. K., Luh, T. Y., Zhao, Y. & Truhlar, D. G. *Organometallics* **30**, 4196–4200 (2011).

49. Zhao, V. & Truhlar, D. G. *Org. Lett.* **9**, 1967–1970 (2007).

50. Poater, A., Ragone, F., Correa, A. & Cavallo, L. *Dalt. Trans.* **40**, 11066–11069 (2011).

51. Ben-Asuly, A., Aharoni, A., Diesendruck, C. E., Vidavsky, Y., Goldberg, I., Straub, B. F. & Lemcoff, N. G. *Organometallics* **28**, 4652–4655 (2009).

52. Benitez, D., Tkatchouk, E. & Goddard, W. A. *Chem. Commun.* **41**, 6194–6196 (2008).

53. Correa, A. & Cavallo, L. *J. Am. Chem. Soc.* **128**, 13352–13353 (2006).

54. Barbasiewicz, M., Szadkowska, A., Bujok, R. & Grela, K. *Organometallics* **25**, 3599–3604 (2006).

55. Benitez, D. & Goddard, W. A. *J. Am. Chem. Soc.* **127**, 12218–12219 (2005).

56. Cavallo, L. *J. Am. Chem. Soc.* **124**, 8965–8973 (2002).

57. Adlhart, C. & Chen, P. *Angew. Chemie - Int. Ed.* **41**, 4484–4487 (2002).

58. Adlhart, C. & Chen, P. *J. Am. Chem. Soc.* **126**, 3496–3510 (2004).

59. Mathew, J., Koga, N. & Suresh, C. H. *Organometallics* **27**, 4666–4670 (2008).

60. Fogg, D. E. *Organometallics* **36**, 1881–1883 (2017).

61. Manzini, S., Nelson, D. J., Lebl, T., Poater, A., Cavallo, L., Slawin, A. M. Z. & Nolan, S. P. *Chem. Commun.* **50**, 2205–2207 (2014).

62. Hong, S. H., Chlenov, A., Day, M. W. & Grubbs, R. H. *Angew. Chemie - Int. Ed.* **46**, 5148–5151 (2007).

63. Manzini, S., Urbina-Blanco, C. A., Poater, A., Slawin, A. M. Z., Cavallo, L. & Nolan, S. P. *Angew. Chemie - Int. Ed.* **51**, 1042–1045 (2012).

64. Poater, A. & Cavallo, L. *J. Mol. Catal. A Chem.* **324**, 75–79 (2010).

65. Jawiczuk, M., Młodzikowska-Pieńko, K., Osella, S. & Trzaskowski, B. *Organometallics* **39**, 239–246 (2020).

66. Webster, C. E. *J. Am. Chem. Soc.* **129**, 7490–7491 (2007).

67. Stewart, I. C., Keitz, B. K., Kuhn, K. M., Thomas, R. M. & Grubbs, R. H. *J. Am. Chem. Soc.* **132**, 8534–8535 (2010).

68. Poater, A., Chaitanya Vummaleti, S. V., Pump, E. & Cavallo, L. *Dalt. Trans.* **43**, 11216–11220 (2014).

69. Bantreil, X., Poater, A., Urbina-Blanco, C. A., Bidal, Y. D., Falivene, L., Randall, R. A. M., Cavallo, L., Slawin, A. M. Z. & Cazin, C. S. J. *Organometallics* **31**, 7415–7426 (2012).

70. Soon, H. H., Wenzel, A. G., Salguero, T. T., Day, M. W. & Grubbs, R. H. *J. Am. Chem. Soc.* **129**, 7961–7968 (2007).

71. Urbina-Blanco, C. A., Poater, A., Lebl, T., Manzini, S., Slawin, A. M. Z., Cavallo, L. & Nolan, S. P. *J. Am. Chem. Soc.* **135**, 7073–7079 (2013).

72. Martin, R. L., Hay, P. J. & Pratt, L. R. *J. Phys. Chem. A* **102**, 3565–3573 (1998).

73. Poater, A., Pump, E., Vummaleti, S. V. C. & Cavallo, L. *J. Chem. Theory*

Comput. **10**, 4442–4448 (2014).

74. Núñez-Zarur, F., Solans-Monfort, X., Pleixats, R., Rodríguez-Santiago, L. & Sodupe, M. *Chem. - A Eur. J.* **19**, 14553–14565 (2013).

75. Tracz, A., Gawin, A., Bieniek, M., Olszewski, T. K. & Skowerski, K. *New J. Chem.* **42**, 8609–8614 (2018).

76. Parr, R. G., Szentpály, L. V. & Liu, S. *J. Am. Chem. Soc.* **121**, 1922–1924 (1999).

77. Geerlings, P., De Proft, F. & Langenaeker, W. *Chem. Rev.* **103**, 1793–1873 (2003).

78. Koopmans, T. *Physica* **1**, 104–113 (1934).

79. Poater, A., Solans-Monfort, X., Clot, E., Copéret, C. & Eisenstein, O. *Dalt. Trans.* 2006, 3077–3087 (2006).

80. Falivene, L., Cao, Z., Petta, A., Serra, L., Poater, A., Oliva, R., Scarano, V. & Cavallo, L. *Nat. Chem.* **11**, 872–879 (2019).

81. Poater, A. & Cavallo, L. *Dalt. Trans.* 8885–8890 (2009).

82. Mariz, R., Poater, A., Gatti, M., Drinkel, E., Bürgi, J. J., Luan, X., Blumentritt, S., Linden, A., Cavallo, L. & Dorta, R. *Chem. - A Eur. J.* **16**, 14335–14347 (2010).

83. Jacobsen, H., Correa, A., Poater, A., Costabile, C. & Cavallo, L. *Coord. Chem. Rev.* **253**, 687–703 (2009).

84. Falivene, L., Credendino, R., Poater, A., Petta, A., Serra, L., Oliva, R., Scarano, V. & Cavallo, L. *Organometallics* **35**, 2286–2293 (2016).

85. Poater, A., Cosenza, B., Correa, A., Giudice, S., Ragone, F., Scarano, V. & Cavallo, L. *Eur. J. Inorg. Chem.* **2009**, 1759–1766 (2009).

86. Turias, F., Poater, J., Chauvin, R. & Poater, A. *Struct. Chem.* **27**, 249–259 (2016).

87. Poater, A., Falivene, L., Urbina-Blanco, C. A., Manzini, S., Nolan, S. P. & Cavallo, L. *Dalt. Trans.* **42**, 7433–7439 (2013).

88. Johnson, E. R., Keinan, S., Mori-Sánchez, P., Contreras-García, J., Cohen, A. J. & Yang, W. *J. Am. Chem. Soc.* **132**, 6498–6506 (2010).

89. Contreras-García, J., Johnson, E. R., Keinan, S., Chaudret, R., Piquemal, J. P., Beratan, D. N. & Yang, W. *J. Chem. Theory Comput.* **7**, 625–632 (2011).

90. Poater, J., Gimferrer, M. & Poater, A. *Inorg. Chem.* **57**, 6981–6990 (2018).

91. Masdemont, J., Luque-Urrutia, J. A., Gimferrer, M., Milstein, D. & Poater, A. *ACS Catal.* **9**, 1662–1669 (2019).

92. Jans, A. C. H., Gómez-Suárez, A., Nolan, S. P. & Reek, J. N. H. *Chem. - A Eur. J.* **22**, 14836–14839 (2016).

93. Frisch, M.J.; Trucks, G.W.; Schlegel, H.B.; Scuseria, G.E.; Robb, M.A.; Cheeseman, J.R.; Scalmani, G.; Barone, V.; Mennucci, B.; Petersson, G.A.; et al. Gaussian 09, Revision E.01; Gaussian, Inc.: Wallingford, CT, USA, 2009.

94. Becke, A. D. *Phys. Rev. A* **38**, 3098–3100 (1988).

95. Perdew, J. P. *Phys. Rev. B* **33**, 8822–8824 (1986).

96. Schäfer, A., Horn, H. & Ahlrichs, R. *J. Chem. Phys.* **97**, 2571–2577 (1992).

97. Küchle, W., Dolg, M., Stoll, H. & Preuss, H. *J. Chem. Phys.* **100**, 7535–7542 (1994).

98. Barone, V. & Cossi, M. *J. Phys. Chem. A* **102**, 1995–2001 (1998).

99. Tomasi, J. & Persico, M. *Chem. Rev.* **94**, 2027–2094 (1994).

100. Perdew, J. P., Burke, K. & Ernzerhof, M. *Phys. Rev. Lett.* **77**, 3865–3868 (1996).

101. Kendall, R. A., Dunning, T. H. & Harrison, R. J. *J. Chem. Phys.* **96**, 6796–6806 (1992).

102. Grimme, S., Antony, J., Ehrlich, S. & Krieg, H. *J. Chem. Phys.* **132**, 154104 (2010).

103. Hutter, J., Iannuzzi, M., Schiffmann, F. & Vandevondele, J. *Wiley Interdiscip. Rev. Comput. Mol. Sci.* **4**, 15–25 (2014).

104. Perdew, J. P., Ruzsinszky, A., Csonka, G. I., Vydrov, O. A., Scuseria, G. E., Constantin, L. A., Zhou, X. & Burke, K. *Phys. Rev. Lett.* **100**, 136406 (2008).

105. VandeVondele, J. & Hutter, J. *J. Chem. Phys.* **127**, 114105 (2007).

Chapter 7. Conclusions and Future Work

Conclusions

In the following chapter it will be depicted the general conclusions of the thesis manuscript, it is not an intention of rewriting conclusions gathered in chapters 3 to 6, however some information will be repeated. This chapter is an intention of giving a general view in context with the thesis as a whole.

Metal-Organic Frameworks (MOFs) have been positioned as very versatile and controversial materials, not only for their vast applicability in different fields but also for their almost infinite spectrum of configurations. However, the characteristics that makes MOFs as unprecedent materials, at the same time makes an impossible task to experimentally study the applications of them all as well as testing all the possible candidates for an application in particular. Computational chemistry has been proposed as the solution for this bottle neck situation, as predicting possible candidates for given applications as well as exploring the applicability of new MOF configurations would reduce the number of experiments needed to perform to find the suitable candidates. Thus, a computationally aided strategy would be the right one in order to overcome the bottle-neck situation.

The four different works presented on this thesis helped in to predict and rationalize a different set of MOFs in the field of catalysis. It has been also studied different ways to use the MOF in this matter, from being simple catalyst supports to being functionalized and acting as catalysts themselves. Finally, in order to understand how computational chemistry is dealing with the study of these materials there have been used two different approaches, studying the MOF as a periodic repetitive unit under periodic boundary conditions or selecting a molecular cluster of the material.

In general terms it has been possible to in all the studies predict the behaviour of the material under study when performing the relevant catalytic process. In three of the works showed here, it has been possible to aid experimental groups aiming the more suitable candidates.

In chapter 3, after performing an extensive computational study considering different candidates as well as different conditions it has been possible to predict that gamma-aminobutyric acid and 5-aminovaleric acid functionalized defective-UiO-66 can activate CO_2 and subsequently form carbamic acid. Moreover, it has

been observed that indeed only the 5-aminovaleric acid systems can adopt an extra H when working under water solvent conditions. The experimental data for this work is still under progress for this reason the data shown on this thesis will be then published in communications format.

In chapter 4, after the computational study it was observed that indeed performing the reaction process for obtaining methyl acrylate has a repercussion on the energetic pathway. Intermediates show to be more as well as the RDT and the β-hydride elimination transition states. The stabilization of the intermediates it has been observed in other works on this thesis (described below). More interestingly is the stabilization of the two beforementioned transition states. The active site shows to be more flexible when attached to the MOF framework, obtaining more degrees of freedom allowing positions that were restrained in the normal homogeneous catalyst. The elongation of the relevant bonds is not possible under homogeneous conditions as it would lead to the destruction of the catalyst. This work opens a new path for future research works, as it has been demonstrated homogeneous catalysts attached to the MOF can adopt impossible geometries in homogeneous conditions, one can say that the active site of the MOF is able to adopt more relaxed positions depending on the necessities without breaking it down. In this work it has been also performed calculations with a molecular cluster of UiO-66. It is not observed major differences with the TMEDA catalyst, confirming that PBC are required in order to obtain results that describe the true nature of the material under study.

In chapter 5, after performing the computational studies on the binding energies it was observed that indeed the catalyst was not attached to the framework UMCM-1, changing completely the initial idea of the project. Moreover, the unpublished data of Chapter 5 helps in to see the difference between studying the MOF as a cluster or as a periodic system. If calculations considering the whole cell of the MOF, thus considering the confinement of the catalyst within the pore of UMCM-1, would have not taken it would have never seen that indeed the catalyst is not attached to the structure, instead the true nature of the catalyst that is confined within the pore.

Finally, in chapter 6 instead of predicting any application for a relevant material it has been computationally studied an experimental work in order to

rationalize how the confinement of homogeneous catalyst within MOFs can directly affect to the reaction mechanism. Results obtained did not differ from experimental data, encapsulating the homogeneous catalyst is a good strategy for avoiding decomposition reactions. More interestingly, reaction mechanism suggested that there is an enhancement of the reactivity when studying the molecular cluster system, as it is observed a stabilization of the different local minima. Same observations were made when studying the reaction mechanism of chapter 4.

Computational studies gathered in this thesis are an example of how computational chemistry is a valuable tool and that its strength goes beyond confirming reaction processes that are already studied. Computational results obtained on the different projects not only helped in future experimental works in aiming the best candidates, helping in avoiding the bottle-neck situation mentioned before, but also are our contribution to the preservation of the environment avoiding all the chemical waste that derivates from the experimental try-and-error methodologies.

Future Work

In the present manuscript has been demonstrated that computational chemistry is the perfect tool in order to study and understand catalytic applications using MOF as either supporter or catalysts themselves. The four different works presented here demonstrate that MOF can be not only functionalised with a different variety of species from amino acids to adapted homogeneous catalyst but also can work as a support for already existing homogeneous catalysts.

The following steps in the study of MOF as catalysts in the branch of computational chemistry, relay on going one step forward on the understanding the systems and deepen on the computational analysis. In the works present here we study systems on has phase and we provide enthalpic energies. Due to the expensive computational cost of the calculations, it is difficult to perform calculations where entropic effects are considered. In order to go one step forward and be closer to the reality of the systems under study, obtaining Gibbs energy values would be one of the first things to carry out. Going chapter by chapter, chapter 1 represented a very interesting approach of how defective MOF can be functionalised. Since they are a very novel structures, further studies of how these systems can be functionalized

and with which different systems, would be the initial approach. Following to study in more detail the cooperative effect between the amino acids mentioned on the study, they are able to activate CO_2, but they can be used in many different reaction processes. In chapter 2, it is used a direct heterogenization of a homogeneous catalyst. This approach is one of the initial applications of MOFs, it would solve all the problems related to the post reaction treatments. However, we saw that not only this, by functionalizing the MOF with a homogeneous catalyst we unlock unexplored reaction pathways. Future work on this matter, would be in deepen in the capacities of MOF to tailor made rection mechanism, reactions that are impossible under homogenous conditions could be carried out considering the MOF environment. Chapter 3 demonstrates that the reactions are not only enhanced within the framework but also are able to increase selectivity towards an isomer. This approach is very interesting and opens a new branch of study, first in order to understand how MOFs are able to change the reactivity and second, studying which kind of reactions that have isomerization can indeed be affected by the confinement of the MOF. Finally, chapter 4 demonstrates that catalyst encapsulation within the MOF is feasible and that slightly enhance reactivity. It would be interesting in future works to study the different types of confinement and howe behave different catalyst within the framework. If all of them follow a similar trend or exists different types of confinements.

Finally, in this work it has been studied basic reactivity, however MOFs have demonstrated to have applicability in many different branches, it would be interesting to keep studying how MOFs can affect in trickier and state of the art reactivity such as the fields of electrochemistry, or processes that involve the movement of electrons.

Supplementary material for chapter 3

Computational details

All calculations were performed using the code CP2K[1] at density functional level of theory. The semi-local PBEsol functional was adopted[2] using the DZVP-MOLOPT-SR-GTH gaussian basis set for all the atom types,[3] a cutoff of 500 Ry for the plane wave auxiliary basis set and SCF convergence set at $1.0E^{-5}$, considering gas phase on the optimization and further energy corrections considering solvation effects with water and using the Polarizable Continuum Model (PCM). MOF structure was obtained from IR data base. In order to relieve the computational cost of the calculations, all the systems were studied using the primitive cell. Full geometry optimization i.e., both atomic positions and cell parameters were performed to optimize the MOF system considering periodic conditions. After MOF optimization it has been performed geometry optimizations including the CO_2 molecule within the pore of the MOF, such optimization was performed under the same conditions mentioned before.

Single point calculations were then performed to calculate binding energies (BE) between the MOF and the molecular gas including the basis-set superimposition error. It has been also considered the self-consistent continuum solvation (SCCS) model as implemented in CP2K[4] using water as a solvent. In CP2K the interaction energy can be calculated defining 2 fragments A and B. Two fragments corresponding to the MOF (EA) and the catalyst (EB) were defined in each case.

$$E_{int} = E_{AB} - (E_A + E_B) \quad (1)$$

Defective MOFs optimization.

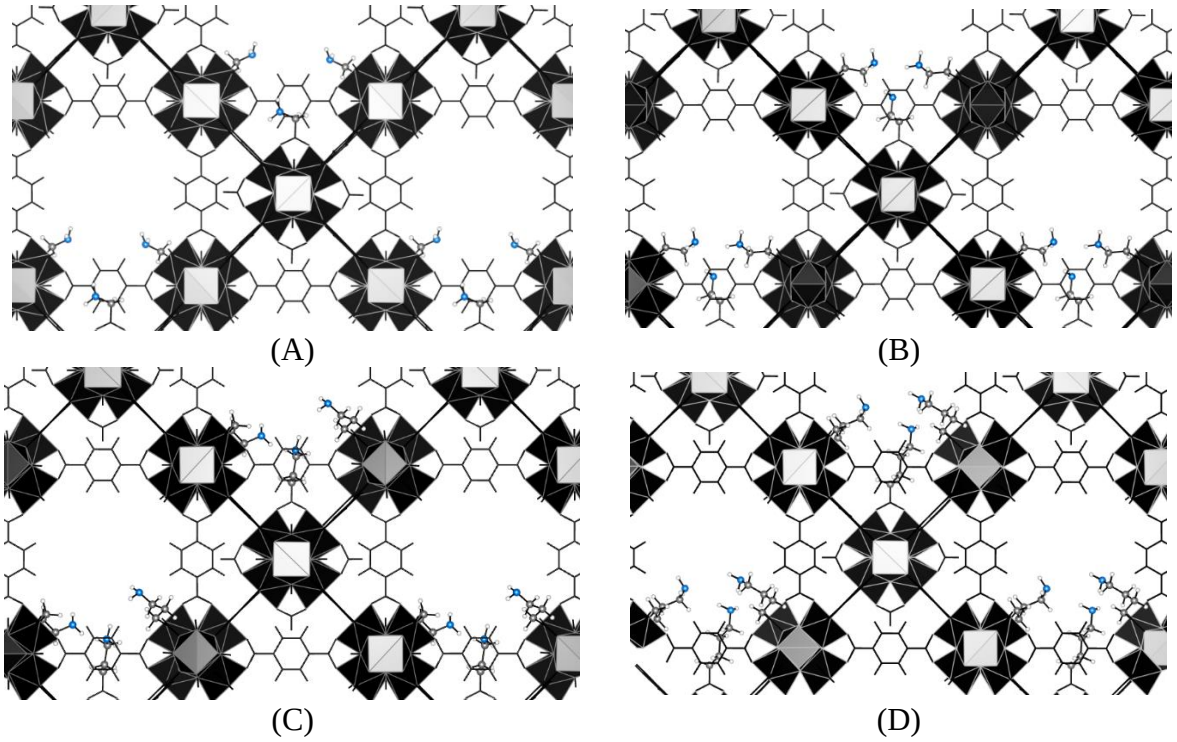


Figure S1 Optimized geometries for systems; (A) UiO-66_gly, (B) UiO-66_ala and (C), UiO-66_gaba and (D) UiO-66_ava. Colour scheme: C = grey, H = white, N = Blue. The organic ligand and inorganic node of the MOF are represented as black line and black polyhedral for clarity reason.

Table S1 Protonation of the 1st amine group. Only configurations in which a H bond can be formed between the protonated and the unprotonated amines are favourable. Values are in kcal·mol^{-1}.

System-1	Vacuum	Solution	System-2	Vacuum	Solution
UiO-66_gly	0.00	0.00	UiO-66_gaba	0.00	0.00
UiO-66_gly_HIN	19.61	14.16	UiO-66_gaba_HIN	25.02	21.55
UiO-66_gly_HIN_2	6.23	3.07	UiO-66_gaba_HIN_2	30.18	11.31
UiO-66_gly_HIN_3	21.77	18.51	UiO-66_gaba_HIN_3	10.51	4.54
UiO-66_gly_HOUT	35.33	22.42	UiO-66_gaba_HOUT	21.90	15.74
UiO-66_gly_HOUT_2	20.29	7.95	UiO-66_gaba_HOUT_2	50.11	27.23
UiO-66_gly_HOUT_3	19.86	8.16	UiO-66_gaba_HOUT_3	3.44	-4.53
Average	20.52	12.38	Average	23.53	12.64
System-3	**Vacuum**	**Solution**	**System-4**	**Vacuum**	**Solution**
UiO-66_ala	0.00	0.00	UiO-66_ava	0.00	0.00
UiO-66_ala_HIN	12.15	6.50	UiO-66_ava_HIN	7.98	-6.98
UiO-66_ala_HIN_2	27.53	9.06	UiO-66_ava_HIN_2	16.38	9.69
UiO-66_ala_HIN_3	15.95	9.06	UiO-66_ava_HIN_3	6.63	-6.88
UiO-66_ala_HOUT	15.29	0.98	UiO-66_ava_HOUT	7.61	-7.60
UiO-66_ala_HOUT_2	49.31	26.50	UiO-66_ava_HOUT_2	7.61	-6.93

UiO-66_ala_HOUT_3	9.84	0.76	UiO-66_ava_HOUT_3	7.01	-19.69
Average	21.68	8.81	Average	8.87	-6.40

Table S2 Protonation of the 2nd and 3rd ammine. Values are in kcal·mol^{-1}. The 3rd protonation was not calculated if the 2nd was already energetically unfavourable.

Multiple proton transfer	Solution
UiO-66_ava	0.00
UiO-66_ava_HIN	-6.98
UiO-66_ava_HIN_2H	24.56
UiO-66_ava_HIN_3H	-
UiO-66_ava_HIN_3	-6.88
UiO-66_ava_HIN_3_2H	3.92
UiO-66_ava_HIN_3_3H	33.88
UiO-66_ava_HOUT	-7.60
UiO-66_ava_HOUT_2H	-0.86
UiO-66_ava_HOUT_3H	21.27
UiO-66_ava_HOUT_2	-6.93
UiO-66_ava_HOUT_2_2H	20.66
UiO-66_ava_HOUT_2_2H	-
UiO-66_ava_HOUT_3	-19.69
UiO-66_ava_HOUT_3_2H	13.32
UiO-66_ava_HOUT_3_3H	35.31

CO_2 adsorption and activation.

Table S3 Binding energy (BE) and geometrical parameters for the adsorption of CO_2 at the inorganic node of UiO-66. Energies in kcal·mol^{-1}; Bond distances in Angstrom; Angle in degree. CO_2 is considered activated when there is an elongation of the CO bond compared to 1.18 Ang, the calculated value for isolated CO_2.

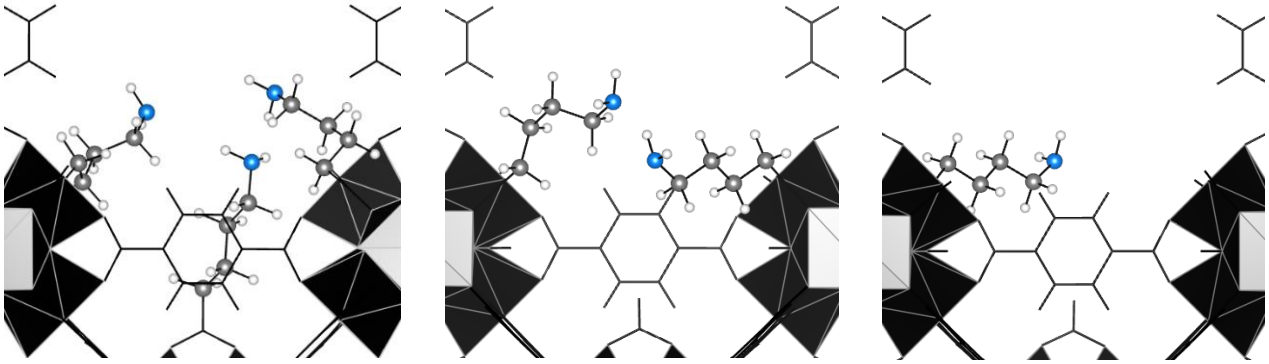
System	BE	CO	CO	OCO
UiO-66_ava_CO2_NODE	-1.95	1.18	1.18	179.53
UiO-66_ava_CO2_NODE_2	-1.01	1.18	1.18	179.83
UiO-66_ava_CO2_NODE_3	-0.87	1.18	1.18	179.66
UiO-66_ava_CO2_NODE_4	-0.84	1.18	1.18	179.63
UiO-66_ava_CO2_NODE_5	-0.12	1.18	1.18	179.02
UiO-66_ava_CO2_NODE_6	-0.93	1.18	1.18	178.98
UiO-66_ava_CO2_HOUT_NODE	-2.8	1.18	1.18	179.71
UiO-66_ava_CO2_HOUT_NODE_IN	-2.82	1.18	1.18	179.81
UiO-66_ava_CO2_HOUT_NODE_2	-2.75	1.18	1.18	179.88

Table S4 Binding energy (BE) and geometrical parameters for the adsorption of CO_2. Energies in kcal·mol^{-1}; Bond distances in Angstrom; Angle in degree. CO_2 is considered activated when there is an elongation of the CO bond compared the calculated value for isolated CO_2 = 1.18 Ang. Calculated CN distance in carbamic acid = 1.37 Ang.

System	BE	N1C	N2C	N3C	CO1	CO2	OCO	CO_2 act
UiO-66_gly	-3.85	4.24	2.71	6.29	1.18	1.18	176	N
UiO-66_gly_2	-0.52	4.57	4.23	6.02	1.18	1.18	180	N
UiO-66_gly_3	-3.9	3.97	2.76	6.76	1.18	1.18	176	N
UiO-66_gly_4	-3.75	3.82	3.32	5.27	1.18	1.18	178	N
UiO-66_gly_5	0.15	5.14	4.76	5.35	1.18	1.18	180	N
UiO-66_gly_6	-4.07	5.00	2.85	6.67	1.18	1.18	176	N
AVERAGE	-2.6567						178	0%
UiO-66_ala	-3.33	4.80	2.96	5.15	1.18	1.18	177	N
UiO-66_ala_2	-3.91	4.39	2.83	7.38	1.18	1.18	175	N
UiO-66_ala_3	-6.21	4.20	2.64	3.66	1.18	1.18	173	N
UiO-66_ala_4	-4.69	4.75	2.64	7.81	1.18	1.18	172	N
UiO-66_ala_5	-0.22	4.62	4.62	6.61	1.18	1.18	179	N
UiO-66_ala_6	-7.23	3.56	2.54	4.09	1.18	1.18	170	N
UiO-66_ala_7	-6.8	4.00	2.56	4.06	1.18	1.18	170	N
UiO-66_ala_8	-3.06	4.10	3.06	3.75	1.18	1.18	178	N
AVERAGE	-4.4313						174	0%
UiO-66_gaba	-5.07	3.50	2.77	3.78	1.18	1.18	174	N
UiO-66_gaba_2	-4.08	3.73	2.78	7.13	1.18	1.18	175	N
UiO-66_gaba_3	-4.66	3.84	2.74	7.24	1.18	1.18	175	N
UiO-66_gaba_4	-38.06	3.13	1.71	5.44	1.22	1.23	142	Y
UiO-66_gaba_5	-39.81	3.15	1.71	5.20	1.22	1.23	142	Y
UiO-66_gaba_6	-43.14	3.08	1.68	4.02	1.22	1.24	141	Y
UiO-66_gaba_7	-40.9	3.29	1.71	3.53	1.23	1.22	142	Y
AVERAGE	-25.103						156	57%
UiO-66_ava	-6.76	2.89	2.88	4.72	1.18	1.18	174	N
UiO-66_ava_2	-49.19	3.05	1.66	3.39	1.23	1.24	139	Y
UiO-66_ava_3	-6.08	4.30	2.58	5.20	1.18	1.18	171	N
UiO-66_ava_4	-35.95	3.26	1.75	5.12	1.23	1.22	144	Y
UiO-66_ava_5	-5.88	4.11	2.62	5.06	1.18	1.18	172	N
UiO-66_ava_6	-8.24	2.87	2.63	3.39	1.18	1.18	172	N
AVERAGE	-18.683						162	33%

Table S5 Binding energy (BE) and geometrical parameters for the adsorption of CO_2 in protonated UiO-66_ala. HIN indicates that the transfer is from an OH group of the same inorganic node of the amine, HOUT the H is from another OH. Energies in kcal·mol^{-1}; Bond distances in Angstrom; Angle in degree. CO_2 is considered activated when there is an elongation of the CO bond compared the calculated value for isolated CO_2 = 1.18 Ang. Calculated CN distance in carbamic acid = 1.37 Ang.

Structure	BE	N1C	N2C	N3C	CO1	CO2	OCO	CO_2 act
UiO-66_ava_HIN	-98.23	3.12	1.53	3.3	1.27	1.23	131.67	Y
UiO-66_ava_HIN_2	-0.87	3.51	3.48	4.66	1.18	1.18	178.26	N
UiO-66_ava_HIN_3	-0.19	7.12	5.38	5.1	1.18	1.18	179.12	N
UiO-66_ava_HIN_4	-0.33	3.17	3.26	4.6	1.18	1.18	175.96	N
UiO-66_ava_HIN_5	-65.08	3.31	1.63	6.05	1.22	1.25	136.78	Y
UiO-66_ava_HIN_6	-105.27	3.16	1.5	3.39	1.27	1.23	131.27	Y
UiO-66_ava_HOUT	-156.97	3.13	1.43	3.06	1.28	1.26	126.73	Y
UiO-66_ava_HOUT_2	-2.16	3.67	4.86	4.17	1.18	1.17	178.43	N
UiO-66_ava_HOUT_3	-74.18	3.42	1.58	6.21	1.27	1.22	135.89	Y
UiO-66_ava_HOUT_4	-1.08	3.42	3.26	4.73	1.18	1.18	176.75	N
UiO-66_ava_HOUT_5	-67.04	3.24	1.62	5.76	1.22	1.26	136.56	Y
UiO-66_ava_HOUT_6	-108.7	3.14	1.51	3.46	1.23	1.27	131.06	Y
Average	-56.675							50%



(A) (B) (C)

Figure S2 Optimized geometries for; (A) UiO-66_ava, (B) UiO-66_ava_NonFun_1 and (C) UiO-66_ava_NonFun_2. Colour scheme: C = grey, H = white, N = Blue. The organic ligand and inorganic node of the MOF are represented as black line and black polyhedral for clarity reason.

Table S6 Binding energies in kcal·mol^{-1} for the CO_2 activated system with different amount of defect functionalisation for the active configurations of unprotonated UiO-66_gaba and UiO-66_ava.

Number of amino acids in the pore	3	2	1
UiO-66_gaba_4	-38.06	-33.86	-3.11
UiO-66_gaba_5	-39.81	-36.75	-3.38
UiO-66_gaba_6	-43.14	-35.26	-3.41
UiO-66_gaba_7	-40.90	-32.85	-4.70
UiO-66_ava_2	-49.19	-31.72	-4.54
UiO-66_ava_4	-35.95	-31.16	-4.90

Table S7 Binding energies in kcal·mol^{-1} for the CO_2 activated system with different amount of defect functionalisation for the active configurations of protonated UiO-66_ava.

Number of amino acids in the pore	3	2	1
UiO-66_ava_HIN	-98.23	-61.85	-5.91
UiO-66_ava_HIN_5	-65.08	-65.09	-6.93
UiO-66_ava_HIN_6	-105.27	-64.61	-5.67
UiO-66_ava_HOUT	-156.97	-55.57	-6.38
UiO-66_ava_HOUT_3	-74.18	-74.17	-6.82
UiO-66_ava_HOUT_5	-67.04	-67.24	-7.22
UiO-66_ava_HOUT_6	-108.70	-70.38	-5.28

Hydrogen transfer and subsequent carbamate formation

Table S8 Hydrogen transfer relative energies for the active unprotonated UiO-66_gaba and UiO-66_ava. Values in kcal·mol^{-1}.

UiO-66_gaba configurations	Relative Energy
UiO-66_gaba_4	0.00
UiO-66_gaba_4_H-tran	-7.69
UiO-66_gaba_5	0.00
UiO-66_gaba_5_H-tran	-8.20
UiO-66_gaba_6	0.00
UiO-66_gaba_6_H-tran	-7.10
UiO-66_gaba_7	0.00
UiO-66_gaba_7_H-tran	-8.72
UiO-66_ava configurations	**Relative Energy**
UiO-66_ava_2	0.00
UiO-66_ava_2_H-tran	-1.22
UiO-66_ava_b	0.00
UiO-66_ava_b_H-tran	-3.89

Table S9 Hydrogen transfer relative energies for the active protonated UiO-66_ava. Values in kcal·mol^{-1}.

Configuration	Relative Energy
UiO-66_ava_2	0.00
UiO-66_ava_2_H-tran	-2.39
UiO-66_ava_HIN_6	0.00
UiO-66_ava_HIN_6_H-tran	-8.08
UiO-66_ava_6	0.00
UiO-66_ava_6_H-tran	-8.24

Table S10 Relative energies for the active unprotonated UiO-66_gaba and UiO-66_ava with only two amines for the hydrogen transfer. Values in kcal·mol^{-1}.

UiO-66_gaba configurations	Relative Energy
UiO-66_gaba_4_NonFun	0.00
UiO-66_gaba_4_NonFun_H-tran	-8.69
UiO-66_gaba_5_NonFun	0.00
UiO-66_gaba_5_NonFun_H-tran	-8.31
UiO-66_gaba_6_NonFun	0.00
UiO-66_gaba_6_NonFun_H-tran	-8.45
UiO-66_gaba_7_NonFun	0.00
UiO-66_gaba_7_NonFun_H-tran	-8.17
UiO-66_ava configurations	**Relative Energy**
UiO-66_ava_2_NonFun	0.00
UiO-66_ava_2_NonFun_H-tran	-4.80
UiO-66_ava_4_NonFun	0.00
UiO-66_ava_4_NonFun_H-tran	-6.48

Table S11 Relative energies for the active protonated UiO-66_ava for the hydrogen transfer to the hydroxyl group. Values in kcal·mol^{-1}.

System	Relative Energy
UiO-66_gly_HIN_3	0.00
UiO-66_gly_HIN_3_H-back	-22.18
UiO-66_gly_HOUT_2	0.00
UiO-66_gly_HOUT_2_H-back	-19.34
UiO-66_ava_HIN	0.00
UiO-66_ava_HIN_1_H-back	-20.15
UiO-66_ava_HIN_5	0.00
UiO-66_ava_HIN_5_H-back	-43.70
UiO-66_ava_HIN_6	0.00
UiO-66_ava_HIN_6_H-back	-23.13
UiO-66_ava_HOUT	0.00
UiO-66_ava_HOUT_H-back	-30.60
UiO-66_ava_HOUT_5	0.00
UiO-66_ava_HOUT_5_H-back	-34.16
UiO-66_ava_HOUT_6	0.00
UiO-66_ava_HOUT_6_H-back	-29.25

Table S12 Relative energies for the active protonated UiO-66_ava with only two amines for the hydrogen transfer to the hydroxyl group. Values in kcal·mol^{-1}.

System	Relative Energy
UiO-66_ava_HIN_NonFun	0.00
UiO-66_ava_HIN_NonFun_H-back	-30.60
UiO-66_ava_HIN_5_NonFun	0.00
UiO-66_ava_HIN_5_NonFun_H-back	-42.96
UiO-66_ava_HIN_6_NonFun	0.00
UiO-66_ava_HIN_6_NonFun_H-back	-43.12
UiO-66_ava_HOUT_3_NonFun	0.00
UiO-66_ava_HOUT_3_NonFun_H-back	-42.24
UiO-66_ava_HOUT_5_NonFun	0.00
UiO-66_ava_HOUT_5_NonFun_H-back	-32.57
UiO-66_ava_HOUT_6_NonFun	0.00
UiO-66_ava_HOUT_6_NonFun_H-back	-43.21

References

1. Hutter, J., Iannuzzi, M., Schiffmann, F. & Vandevondele, J. *Wiley Interdiscip. Rev. Comput. Mol. Sci.* **4**, 15–25 (2014).

2. Perdew, J. P., Ruzsinszky, A., Csonka, G. I., Vydrov, O. A., Scuseria, G. E., Constantin, L. A., Zhou, X. & Burke, K. *Phys. Rev. Lett.* **100**, 136406 (2008).

3. VandeVondele, J. & Hutter, J. *J. Chem. Phys.* **127**, 114105 (2007).

4. Andreussi, O., Dabo, I. & Marzari, N. *J. Chem. Phys.* **136**, 064102 (2012).

Supplementary material for chapter 4

Table S1 Relevant distances in Angstroms (Å) for step A of the three different systems under study.

A	TMEDA_A	UiO-67-DMAP	TFA-DMAP
N1··Ni	1.94	1.95	1.96
N2··Ni	2.02	2.03	2.05
Ni··αC	1.90	1.90	1.90
Ni··βC	-	2.80	2.78
Ni··ORing	1.82	1.81	1.81
αC··βC	1.53	1.53	1.53
P··CTPA	-	1.86	1.89
P··N1	-	1.80	1.79
P··N2	-	1.76	1.76

Table S2 Relevant distances in Angstroms (Å) for step TS_AB of the three different systems under study.

TS_AB	TMEDA_A	UiO-67-DMAP	TFA-DMAP
N1··Ni	1.96	1.95	1.98
N2··Ni	2.04	2.06	2.13
Ni··αC	1.91	1.91	1.90
Ni··βC	-	2.81	2.74
Ni··ORing	1.86	1.85	1.85
αC··βC	1.52	1.52	1.52
ORing··CMeI	2.25	2.22	2.22
CMeI··I	3.07	3.11	3.01
Ni··I	3.22	3.20	3.05
P··CTPA	-	1.85	1.90
P··N1	-	1.80	1.79
P··N2	-	1.78	1.77

Table S3 Relevant distances in Angstroms (Å) for step B of the three different systems under study.

B	TMEDA_A	UiO-67-DMAP	TFA-DMAP
N1··Ni	1.97	1.98	1.97
N2··Ni	2.06	2.06	2.08
Ni··αC	1.93	1.91	1.92
Ni··βC	-	2.82	3.01
αC··βC	1.54	1.54	1.53
ORing··CMeI	1.44	1.44	-
Ni··I	2.50	2.49	2.48
Ni··βH	2.99	2.88	3.21
βC··βH	1.10	1.10	1.10
P··CTPA	-	1.85	1.89
P··N1	-	1.80	1.80
P··N2	-	1.77	1.76
βC-γC-O	112.86	111.95	111.22

Table S4 Relevant distances in Angstroms (Å) for step TS_BC of the three different systems under study.

TS_BC	TMEDA_A	UiO-67-DMAP	TFA-DMAP
N1··Ni	2.35	2.95	2.37
N2··Ni	2.08	2.03	2.08
Ni··αC	1.94	1.96	1.95
Ni··βC	2.00	1.98	1.98
αC··βC	1.44	1.42	1.43
ORing··CMeI	1.44	1.44	-
Ni··I	2.56	2.54	2.54
Ni··βH	1.45	1.46	1.47
βC··βH	1.65	1.90	1.69
P··CTPA	-	1.86	1.86
P··N1	-	1.68	1.73
P··N2	-	1.85	1.78
βH-βH-γC-O	15.87	13.54	15.87

Table S5 Relevant distances in Angstroms (Å) for step C of the three different systems under study.

C	TMEDA_A	UiO-67-DMAP	TFA-DMAP
N1··Ni	2.06	2.09	2.12
N2··Ni	2.10	2.12	2.15
Ni··αC	1.95	1.95	1.96
Ni··βC	1.98	1.98	1.97
αC··βC	1.43	1.43	1.43
ORing··CMeI	1.44	1.44	-
Ni··I	2.66	2.64	2.60
Ni··βH	1.43	1.45	1.46
βC··βH	-	-	2.39
P··CTPA	-	1.85	1.88
P··N1	-	1.79	1.78
P··N2	-	1.78	1.76

Table S6 Relevant distances in Angstroms (Å) for step TS_CD of the three different systems under study.

TS_CD	TMEDA_A	UiO-67-DMAP	TFA-DMAP
N1··Ni	2.04	2.36	2.16
N2··Ni	2.00	1.91	2.06
Ni··αC	3.51	3.49	3.08
Ni··βC	3.45	3.30	3.28
αC··βC	1.35	1.34	1.35
ORing··CMeI	1.44	1.44	-
Ni··I	2.51	2.49	2.46
Ni··βH	1.44	1.44	1.44
P··CTPA	-	1.86	1.85
P··N1	-	1.76	1.77
P··N2	-	1.86	1.78

Table S7 Relevant distances in Angstroms (Å) for step D of the three different systems under study.

D	TMEDA_A	UiO-67-DMAP	TFA-DMAP
N1··Ni	2.03	2.04	2.07
N2··Ni	1.92	1.93	1.94
Ni··I	2.45	2.45	2.43
Ni··βH	1.44	1.44	1.44
P··CTPA	-	1.85	1.87
P··N1	-	1.77	1.76
P··N2	-	1.80	1.79

Table S8 Negative frequency values for the three different transition states and systems.

System	Neg. Freq.
TMEDA_TS_AB	-317.62
TMEDA_TS_BC	-387.98
TMEDA_TS_CD	-609.87
UiO-67_TS_AB	-471.85
UiO-67_TS_BC	-821.42
UiO-67_TS_CD	-403.41
DPTPA_TS_AB	-333.50
DPTPA_TS_BC	-314.10
DPTPA_TS_CD	-144.21

Table S9 HOMO-LUMO gap values in electronolts (eV) for the different reaction steps and the three systems under study.

Reaction step	TMEDA	UiO-67-DMAP	TFA-DMAP
A	2.40	0.54	0.33
TS_AB	0.50	0.48	0.19
B	1.87	0.57	0.25
TS_BC	1.70	1.35	1.03
C	2.29	1.56	1.47
TS_CD	0.08	0.43	0.10
D	2.20	0.57	0.61

Supplementary material for chapter 5

Chemical and reagents

If not noted differently, all manipulations were carried out under inert atmosphere using standard Schlenk and glove box techniques. The solvents were purified and dried using standard techniques[1] and stored over activated molecular sieves (3 Å). Deuterated solvents were purchased from Armar Chemicals. All other chemicals were purchased from commercial sources. The following chemicals were synthesized according to published procedures: 1,3,5-tri(4-carboxyphenyl)benzene (H_3BTB),[2] 2-diphenylphosphinobenzenedicarboxylic acid (diphenylphosphino-terephthalic acid; Ph_2P-BDC),[3] UMCM-1 $[Zn_4O(BDC)(BTB)_{4/3}]_n$,[4] MixUMCM-1-$NH_2$ (28 mol% NH_2; $[Zn_4O(BDC)_{0.72}(NH_2\text{-}BDC)_{0.28}(BTB)_{4/3}]_n$),[4] UMCM-1-$NH_2$ ($[Zn_4O(NH_2\text{-}BDC)_1(BTB)_{4/3}]_n$),[4] MIL-101(Al),[5] MIL-101(Cr).[6]

Physical methods

NMR spectra were recorded on a Bruker Avance 500 ^1H NMR chemical shifts were referenced to residual solvent peak as determined relative to TMS (δ = 0 ppm). ^{31}P spectra were referenced to $NH_4H_2PO_4$ (solid state; δ = 1.0 ppm) and 85% H_3PO_4 in D_2O (solution NMR; δ = 0.0 ppm). GC measurements were conducted on an Agilent 6890 GC equipped with an HP-5 column and FI-detector. GC-MS measurements were conducted on an Agilent 7890A GC equipped with HP-5 column and an Agilent 5975C XL MSD. Powder-XRD measurements were performed at room temperature on a Bruker AXS D8 Advance Bragg-Brentano Diffractometer equipped with a Braun detector at 40 kV, 40 mA with CuKα (λ = 1.54 Å) radiation, step size 0.02 s and a 2θ range of 4-40°. The nitrogen adsorption isotherms are calculated by the BET (Brunauer-Emmet-Teller) method and the measurements were performed by the Micromeritics Tristar II 3020 equipped with a VacPrep 061 degassing station. The pore size distribution was calculated using the Horvath-Kawazoe model modified by Saito and Foley for cylindiral pores. UPLC experiments were performed on a Waters Acquity UPLC H-Class system equipped with a UV/Vis detector, a Waters BEH C18 (1.7 µm) column and Acquity QDa mass detector. For SEM images, thin layers of MOF-74(Zn) were spread on a flat surface of carbon tape on top of an aluminium stump. The sample was coated with a 5 nm thick carbon layer using a CCU-010 Carbon Coater Safematic. The

images were collected using a SEM JSM-7100F JEOL scanning electron microscope at 15.0 keV with a working distance of 11 mm. Optical microscope images were acquired using a Leica M165 C microscope equipped with a Leica DFC425 C camera. The images were processed with Leica Application Suite 4.12.0. FT-IR spectra were measured on a ThermoFischer Nicolet iS50 FT-IR using its ATR cell.

Experimental section

Synthesis

MixUMCM-1-PPh$_2$ (29%; [Zn$_4$O(BTB)$_{4/3}$(PPh$_2$-BDC)$_{0.29}$(BDC)$_{0.71}$]$_n$)

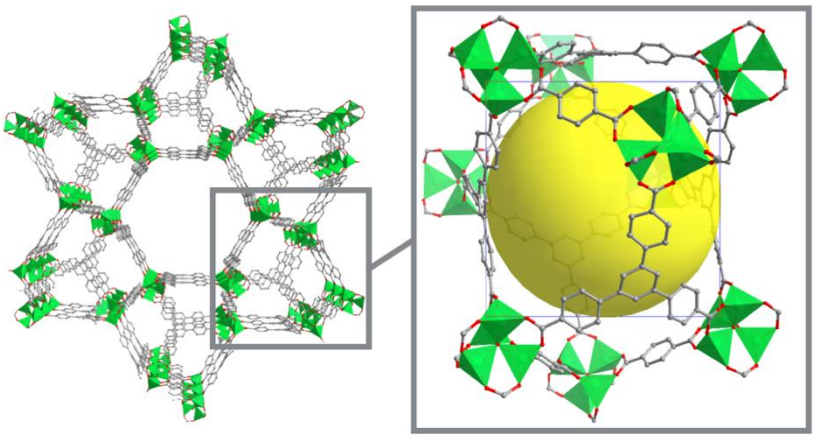


Figure S1 Structure of MixUMCM-1-PPh2 (29%).

Based on literature procedure:[4]

$Zn(NO_3)_2$•$6H_2O$ (1.61 g, 5.41 mmol), terephthalic acid (BDC; 150 mg, 0.90 mmol), diphenylphosphino-terephthalic acid (PPh_2-BDC; 178 mg, 0.51 mmol) and H_3BTB (212 mg, 0.48 mmol) were dissolved in DMF (50 mL). The solution was divided into 10 mL portions and transferred into 20 mL glass vials. The vials were placed in a sand bath and transferred into an isothermal oven heated at 85 °C for 72 h while continuously flushing with N_2.

After cooling down the oven to room temperature, the vials were removed from the oven and the mother liquor was decanted. The crystals were collected and washed with fresh DMF (3 × 15 mL) and soaked in $CHCl_3$ (15 mL) for 3 days with the replacement of the fresh $CHCl_3$ each 24 h. The obtained crystals were stored in toluene until use.

PPh_2-BDC loading

The MOF sample (3 mg dry mass) was placed in an NMR tube and suspended in DCl solution (0.1 mL; 20% in D_2O) using an ultrasonification bath. The solids were then dissolved by adding DMSO-d_6 (0.5 mL) and analyzed by NMR.

MOF-74(Zn)

In a 20 ml microwave tube, 2,5-dihydroxyterephthalic acid (200 mg; 1.01 mmol) and $Zn(acac)_2$•H_2O (568 mg; 2.02 mmol) were dissolved in DMF (19 ml) and H_2O (1 ml) to give a yellow solution. The reaction mixture was stirred at 130°C for 60 min in a microwave oven. The solid of the reaction mixture was filtered by membrane filter, washed with DMF, H_2O and EtOH and dried in the vacuum oven. Yield: 388 mg (81% calculated on dry MOF).

MOF-74(Co)

In a 20 ml microwave tube, 2,5-dihydroxyterephthalic acid (400 mg, 2.02 mmol) and $Co(NO_3)_2$•$6H_2O$ (1.82g, 6.26 mmol) were dissolved in DMF/EtOH/H_2O (20 mL, Ratio = 1/1/1) to give a yellow solution. The reaction mixture was stirred at 130°C for 1.5 h in a microwave oven. Yield: 850 mg (40% calculated on dry MOF). The resulting solid was filtered by membrane filter, washed with DMF, EtOH and *tert*-butylmethylether and dried *in vacuo*.

MOF-74(Ni)

Based on a literature procedure:[7]

In a 250 ml round-bottomed flask, 2,5-dihydroxyterephthalic acid (2.0 g, 10.09 mmol) and $Ni(NO_3)_2$•$6H_2O$ (3.1 g, 31.29 mmol) were dissolved in DMF/EtOH/H_2O (100 mL, Ratio = 1/1/1) to give a brown solution. The solution was equally distributed into five 20 mL microwave tubes. The reaction mixture was

stirred at 130°C for 1.5 h in a microwave oven giving a brown suspension. The resulting solid was filtered by membrane filter, washed with DMF, EtOH and *tert*-butylmethylether and dried *in vacuo*. Yield: 3.75 g (53% calculated on dry MOF).

MOF-74(Mg)

In a 2000 mL round bottom flask, 2,5-dihydroxyterephthalic acid (2.58 g, 13.00 mmol) and $Mg(NO_3)_2 \cdot 6H_2O$ (6.67g, 26.00 mmol) were dissolved in DMF (1240 ml) and H_2O (60 ml) to give a yellow solution. The reaction mixture was stirred at reflux (bath 140°C) for 22 h. The resulting solid was filtered by membrane filter, washed with DMF, EtOH and *tert*-butylmethylether and dried *in vacuo*. Yield: 3.15 g (57% calculated on wet MOF).

Characterization of Metal-Organic Frameworks

Powder X-Ray Diffractograms

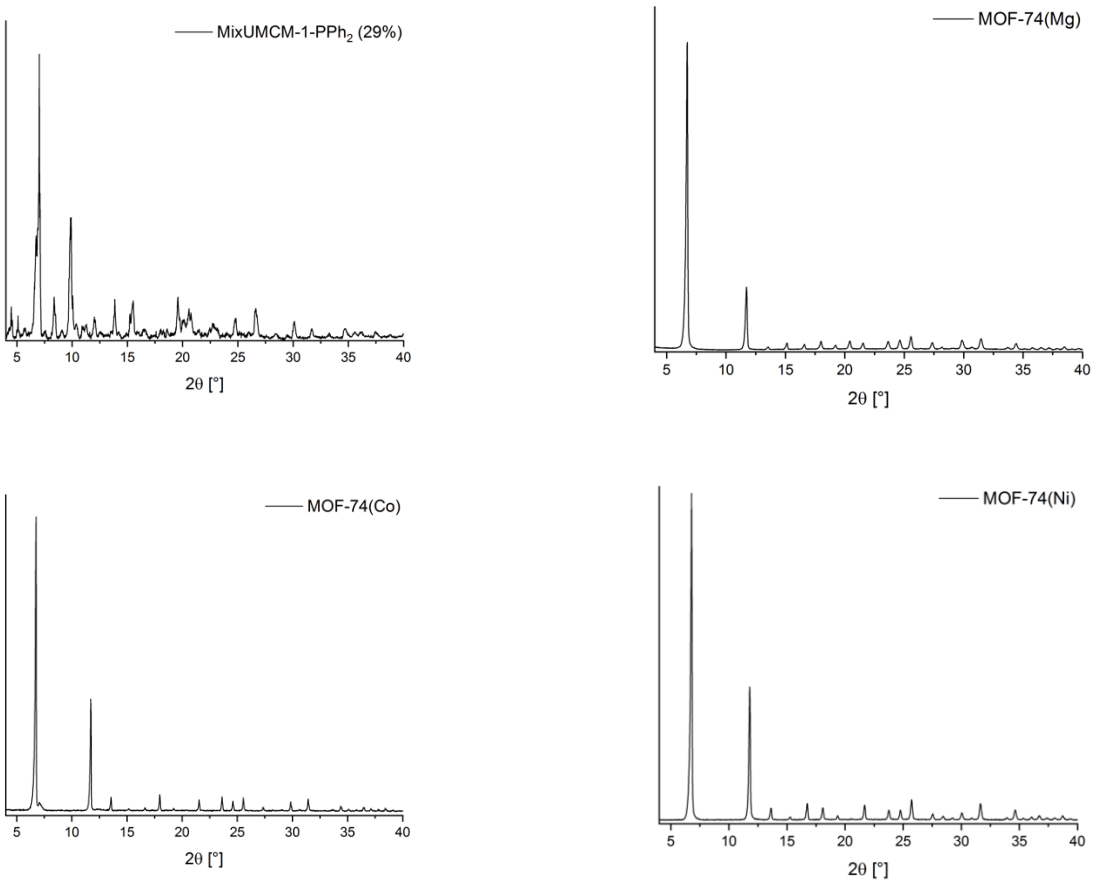


Figure S2 Powder X-Ray pattern of the MOFs used in this work. MixUMCM-1-PPh2 (29%), MOF-74(Mg), MOF-74(Ni) and MOF-74(Co) when starting from top left and going clockwise.

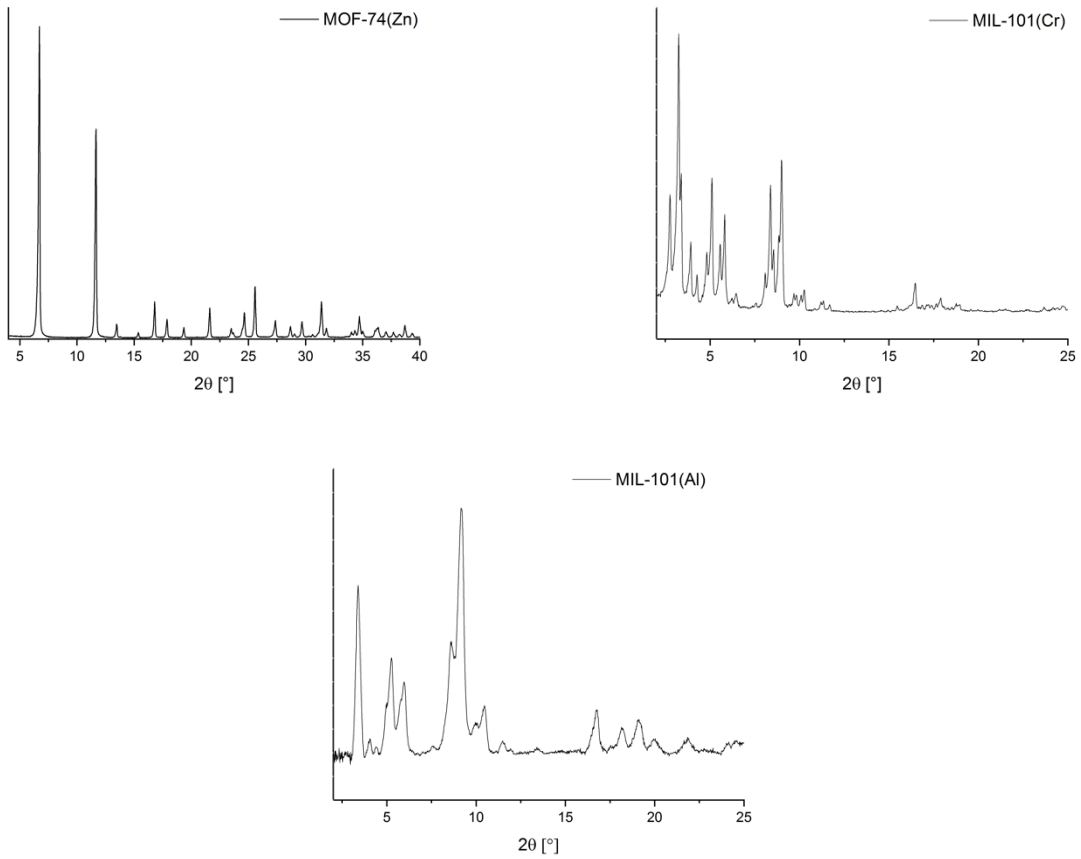


Figure S3 Powder X-Ray pattern of the MOFs used in this work. MixUMCM-1-PPh2 (29%), MOF-74(Mg), MOF-74(Ni) and MOF-74(Co) when starting from top left and going clockwise.

Powder X-Ray Diffractograms before and after catalysis

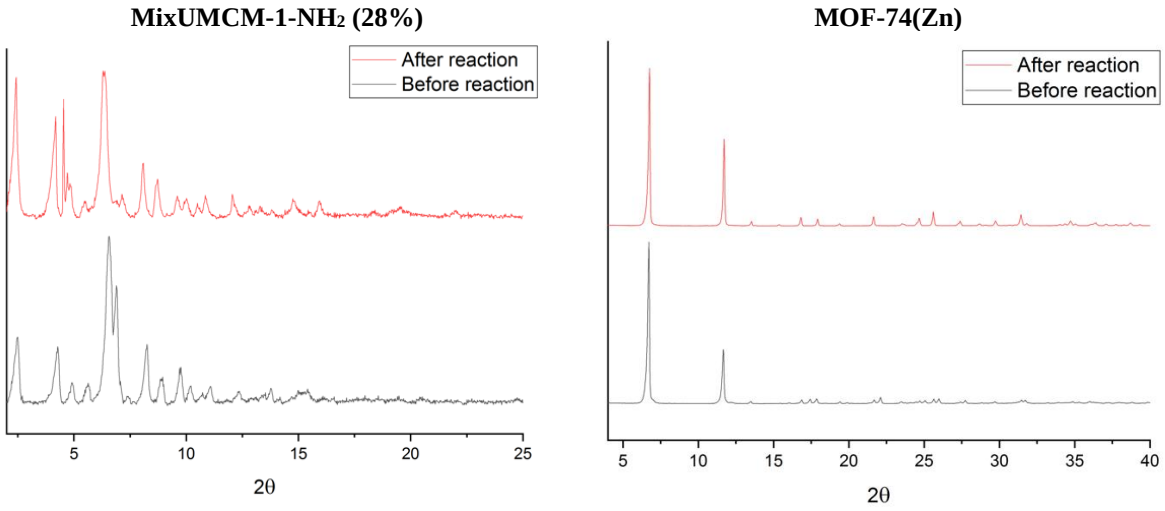


Figure S4 Powder X-Ray pattern of MixUMCM-1-NH2 (28%) (left) and MOF74(Zn) (right) after (red) and before (black) catalysis respectively.

N_2 Adsorption Isotherms (at 77K)

UMCM-1 samples preparation:

Materials with UMCM-1 topology were measured after work up. The supernatant solution was decanted off and the MOF was dried under a stream of Ar. The sample was then transferred to a BET sample vial and activated at 120 mTorr and 120°C. The weight was determined after activation. For BET measurements after catalysis, the reaction mixture was filtered and the solid was washed with $CHCl_3$ (3 x 10 ml) before it was activated and measured as stated above.

MOF-74(M) samples preparation:

The MOF-74(M) materials were transferred to a BET sample vial and activated at 120 mTorr and 250°C. The weight was determined after activation. For BET measurements after catalysis, the reaction mixture was filtered and the solid was washed with THF and EtOH (both 3 x 10 ml) followed by Soxhlet extraction (THF, 3 d). The obtained solid was activated and measured as stated above.

BET Numbers:

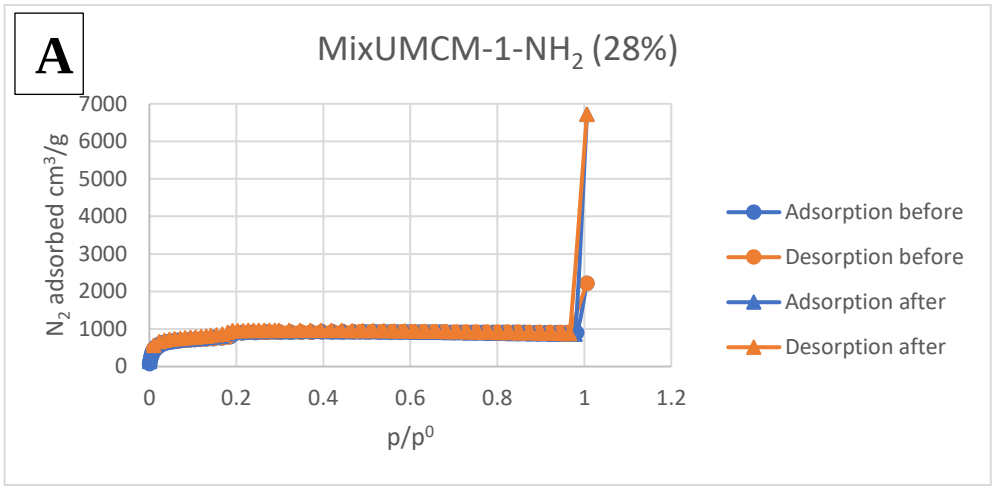
Table S1 BET numbers of the MOFs used in this work.

Entry	MOF	BET Number ($m^2 \cdot g^{-1}$)	BET Number after catalysis ($m^2 \cdot g^{-1}$)
1	MixUMCM-1-PPh_2 (29%)	1470	n/a
2	MixUMCM-1-NH_2 (28%)[a]	1760	600 (After Table 5.3 Entry 1)
3	MixUMCM-1-NH_2 (28%)[b]	2870	2980 (After Table 5.1 Entry 4)
4	MOF-74(Mg)	1370	n/a
5	MOF-74(Co)	1260	n/a
6	MOF-74(Ni)	1360	n/a
7	MOF-74(Zn)	990	20 (After Table 5.3 Entry 1)
8	MOF-74(Zn)	1000	150 (After Table 5.1 Entry 6)
9	MIL-101(Al)	2790	n/a
10	MIL-101(Cr)	2810	n/a

a. Sample used in the experiments of Table 5.1 Entries 3 and 5 in the manuscript.

b. Sample used in Table 5.1 entry 5, Table S7 to Table S9, for pore size analysis, for SEM analysis, and for impregnation experiments (Table S2).

Nitrogen Physisorption before and after catalysis (Table 5.1 Entry 3 (A), Table 5.1 Entry 8 (B))



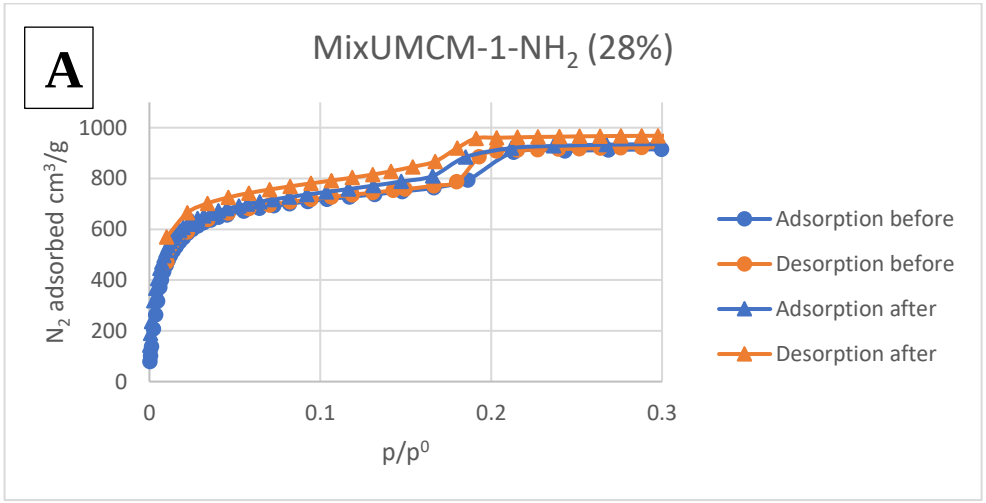


Figure S5 Nitrogen Physisorption curves of MixUMCM-1-NH2 (28%). Blue and red symbols representing the adsorption and desorption branch respectively. Circles show the values before and triangles the ones after catalysis.

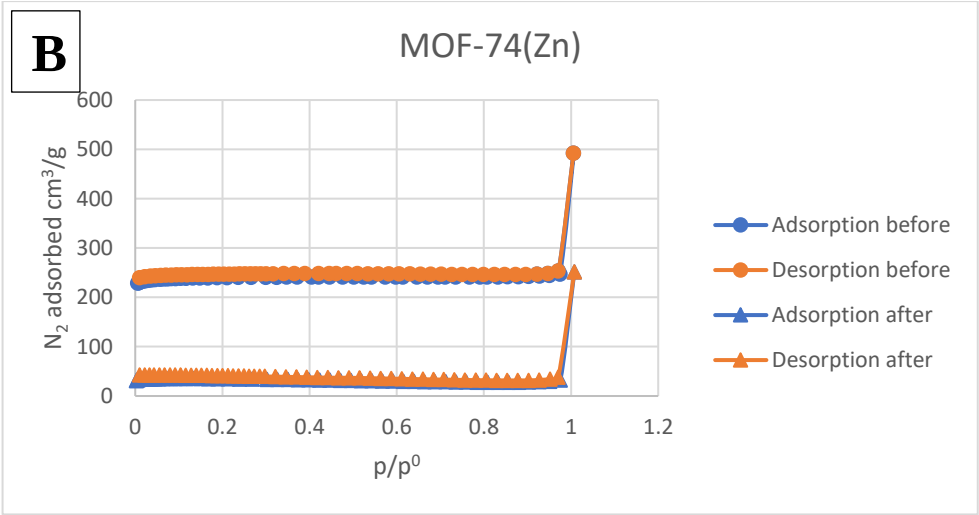


Figure S6 Nitrogen Physisorption curves of MOF-74(Zn). Blue and red symbols representing the adsorption and desorption branch respectively. Circles show the values before and triangles the ones after catalysis.

Pore Size Distribution

Below are the Horvath-Kawazoe differential pore volume plots of the samples before and after catalysis under conditions of Table 5.1. The mesopores in MixUMCM-1-NH_2 (28%) are not detected because the model is optimized for micropores.

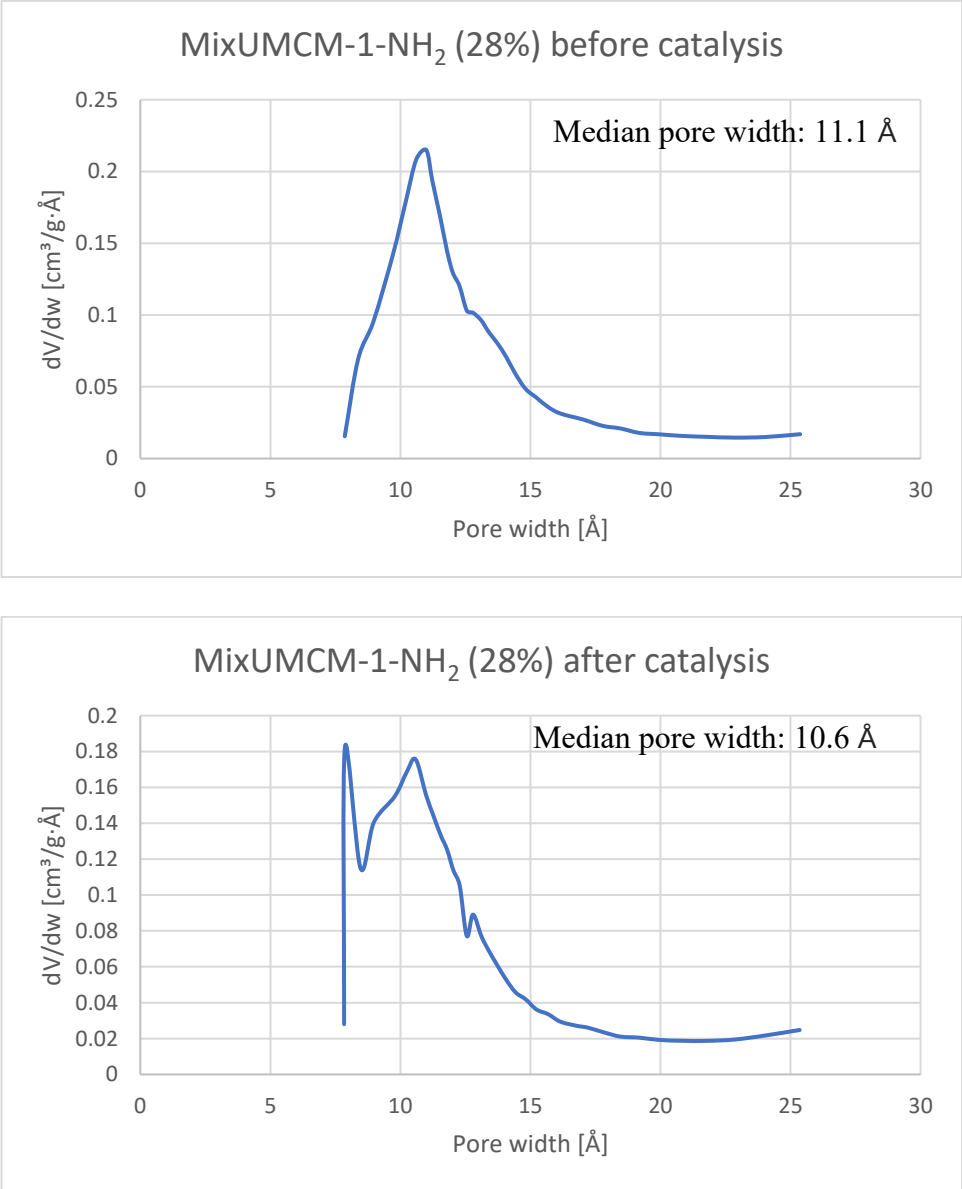


Figure S7 Calculated by Horvath-Kawwazoe model for MixUMCM-1-NH2 (28%) before (top) and after (bottom) catalysis.

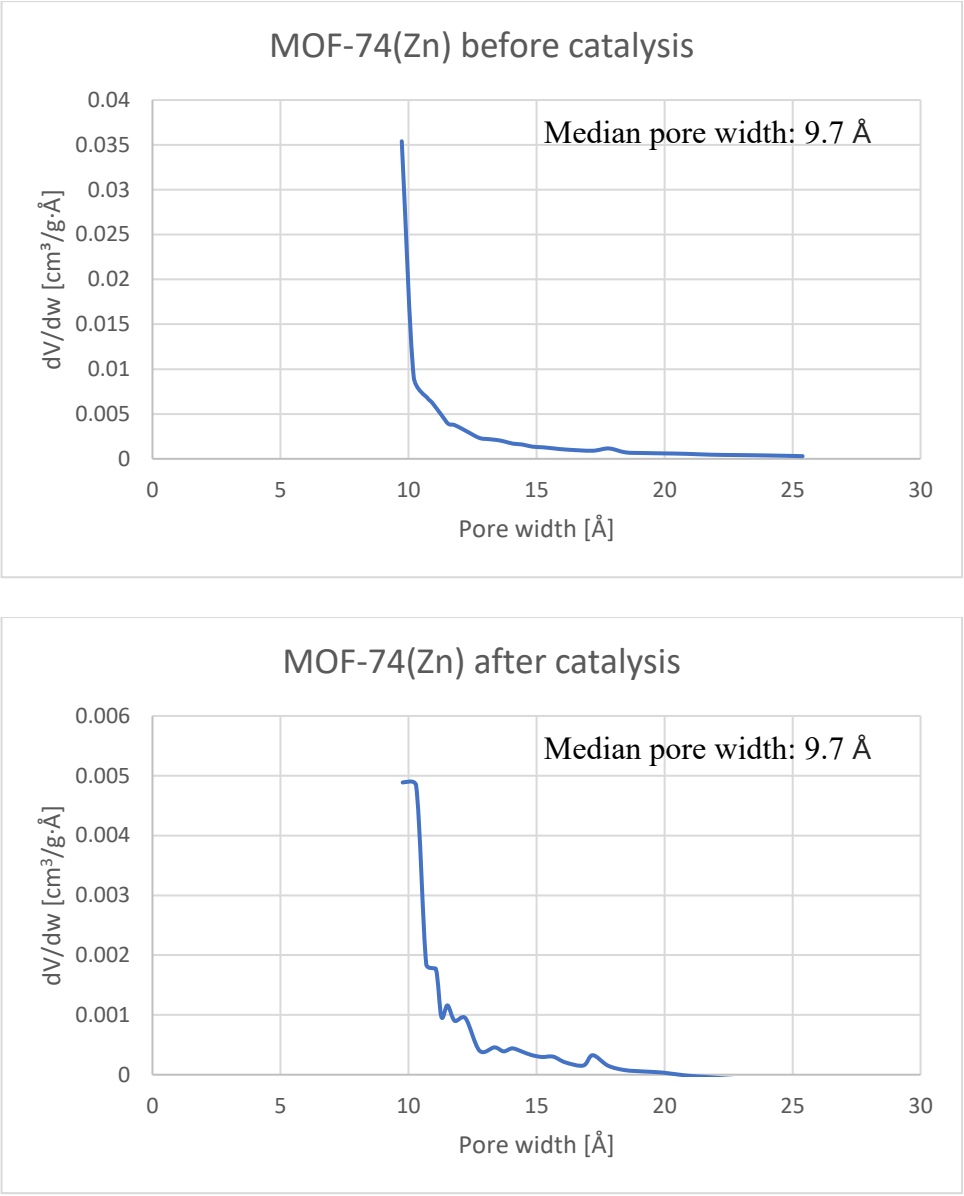


Figure S8 Calculated by Horvath-Kawwazoe model for MOF-74(Zn) before (top) and after (bottom) catalysis.

Hydroformylation

General procedure for hydroformylation of 1-hexene (Table 5.1 in the main text and Table S5 to Table S9)

A stock solution of $Co_2(CO)_8$ in 1-hexene was prepared inside the glove box. In a 1.5 mL GC crimp vial the MOF was weight in and activated at 150 °C overnight. The MOF was then suspended in 250 µL Co/hexene stock solution and the vial was closed. The vial put in a 50 mL Premex® autoclave and purged with Ar. The autoclave was then briefly opened (under a flow of Ar) and the septum was pierced with a needle. The autoclave was closed, then syngas ($CO:H_2$ = 1) was introduced and the reaction mixture was heated to 100°C for 18 hours.

The reaction mixture was cooled to room temperature and the pressure was slowly released. The samples were topped up with 1 mL acetonitrile and 50 µL were transferred in a GC vial filled with acetonitrile and *p*-cymene. The conversion and branched:linear ratios were obtained by GC-FID with *p*-cymene as external standard using the same response factor (R_f) for all aldehyde products. In addition to the hydroformylation products, the chromatograms showed traces of unknown compounds, which never exceeded 5% of the total area of 1-hexene and hydroformylation products.

General procedure for the substrate scope (Table 5.3 in the main text)

The MOF (10 mol% to the olefin for MOF-74(Zn), 1 mol% to the olefin for UMCM-1 derivatives) was placed in a crimp vial, which was closed with a crimp cap and pierced with a needle. In the case of MOF-74(Zn), the vial was placed into a round-bottom flask and activated at 150 °C in vacuum for 24 h. The round-bottom flask was allowed to cool to room temperature but remained under vacuum until it was introduced into a nitrogen-filled glovebox. UMCM-1 derivatives were stored in the glovebox and weighed in without pervious activation. $Co_2(CO)_8$ 1.5 mol%) was dissolved in the olefin (500 µL), and the whole solution was added to the MOF. The vials were placed into a 50 mL Premex® autoclave and purged with Ar several times. The valves to and from the autoclave were closed and the syngas line flushed once. Syngas pressure ($CO:H_2$ 1:1, 30 bar) was applied and the autoclaves heated at 100 °C for 17 h. The autoclave was allowed to cool down to room temperature

before the pressure was released slowly over 15 min. The autoclave was flushed with nitrogen before it was opened to remove additional syngas.

Analysis of the conversion and branched to linear ratio

The content of the reaction vials was transferred into a 5 ml volumetric flask and filled with THF. The MOF was extracted for 30 min before 200 µl of the suspension was added to 800 µl of a solution of the internal standard (p-cymene 0.048 M in THF). This suspension was filtered and analyzed by GC-FID. The branched to linear ratio was calculated from the ratio between the integrals of the isomers assuming the same R_f. Conversion and aldehyde yield in Table 5.3 and Table S10 were calculated with GC-FID upon calibration of the olefins and the linear aldehydes with p-cymene. The R_f of all olefin isomers were assumed the same. The R_f of all aldehydes were assumed the same. The total oxo products yield was determined as described below.

Quantification of the oxo-products in Table 5.3 of the main text

The total yield of oxo products (aldehydes + aldol products), which is an indication of the performance of hydroformylation, was calculated since we always observed aldol products at the high conversion in Table 5.3 (See GC-MS data above). Desorbing the aldehydes from the pores of the MOFs without decomposing them after catalysis was a challenge.

The method to yield determination of the oxo products was:

1. measure the mass of the raw product after catalysis;
2. calculate the mass of the pure oxo products by removing the mass of non converted olefin and of impurities detected by GC;
3. calculate mol of oxo products with the corrected mass and the molar mass of the corresponding aldehydes. This is a safe assumption since aldol products have molar mass multiple to that of the aldehyde.

Synthesis of $HCo(CO)_3$(MixUMCM-1-PPh_2)

Inside the glove box, $Co_2(CO)_8$ (18 mg, 108 µmol) and MixUMCM-1-PPh_2 (29 mol%) (92 mg, 25.2 µmol PPh_2) were weight into a 10 mL crimp vial and toluene (5.0 mL) was added. The vial was placed in a 50 mL Premex® autoclave

and purged with Ar. The autoclave was then briefly opened (under a flow of Ar) and the septum was pierced with a needle. The autoclave was closed, then syngas (10 bar, $CO:H_2$ = 1) was introduced and the reaction mixture was kept at room temperature for 72 hours. After pressure release the sample was immediately placed inside the glove box and the supernatant reaction solution was decanted off. The residual MOF was quickly washed with 2 x 0.5 mL toluene and left open to the atmosphere to evaporate the excess solvent and submerged in toluene (5 mL) for 24 hours in order to leach the excess Co-species. This procedure was repeated twice.

Hydroformylation with $HCo(CO)_3$(MixUMCM-1-PPh_2)

Inside the glove box, a 1.5 mL GC crimp vial was charged with pre-treated MOF (4.5 mg dry mass). The MOF was then suspended in 250 µL neat 1-hexene. The vial was then closed and put in a 50 mL Premex® autoclave and purged with Ar. The autoclave was then briefly opened (under a flow of Ar) and the septum was pierced with a needle. The autoclave was closed again, the syngas ($CO:H_2$ = 1/1) was introduced and the reaction mixture was heated to 100°C for 17 hours.

Co@MOFs

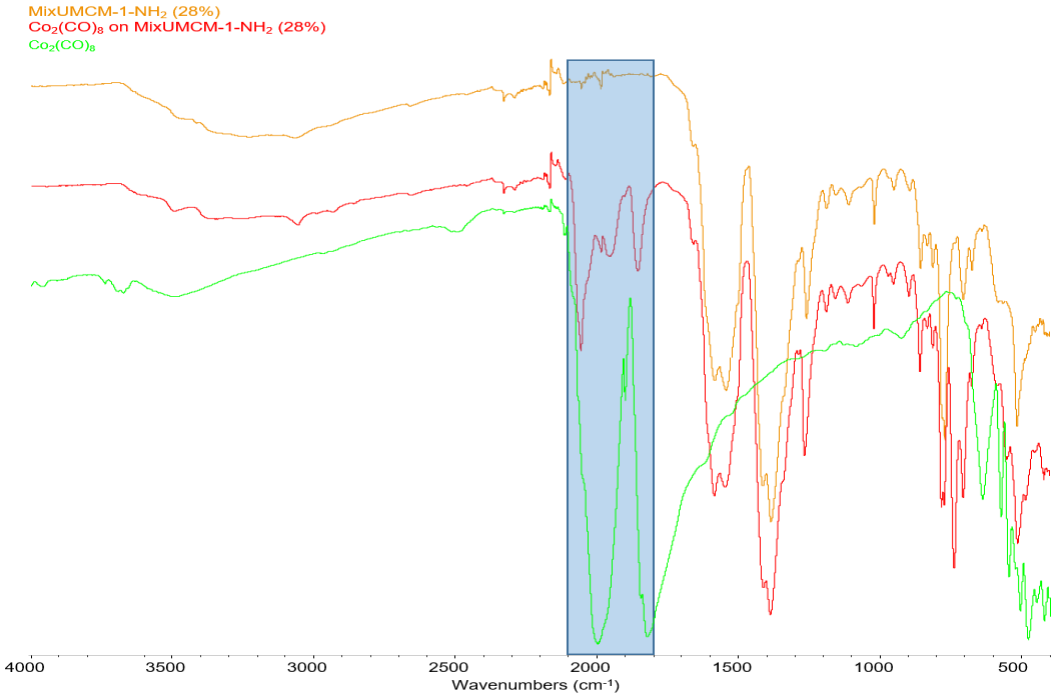
MixUMCM-1-NH_2 (28 %) was activated at 100 °C under vacuum for 24 h. MOF-74(Zn) was activated in a round-bottom flask at 200 °C under vacuum for 8 h. The MOF was transferred to a nitrogen-filled glove box. A solution of $Co_2(CO)_8$ (99.2 mg) in DCM (1 ml) was prepared, diluted with DCM (1.0 x, 2.0 x and 3.0 x, See Table S2). The resulting solutions were slowly added to the MOFs via a syringe. To make the mixture as homogeneous as possible, MOFs were stirred carefully with a spatula. The samples were allowed to dry for at least 8 h at room temperature in the glovebox before they were used for catalysis.

Table S2 Overview incipient-wetness impregnated samples.

Entry	Sample	Conc. Solution [M]	Amount Solution [µl]	Amount MOF [mg]	Co loading Wt% $Co_2(CO)_8$
1	Co@MixUMCM-1-NH_2-13	0.293	300	196.5	13
2	Co@MOF-74(Zn)-9.3	0.290	200	191.8	9.3
3	Co@MOF-74(Zn)-4.3	0.145	200	220.5	4.3
4	Co@MOF-74(Zn)-3.8	0.097	200	164.1	3.8

FT-IR of Co@MOFs

Fourier transform infrared spectroscopy (FT-IR) of MixUMCM-1-NH_2 (28%) impregnated with $Co_2(CO)_8$ showed CO stretches between 1800 cm^{-1} and 2000 cm^{-1} indicating little – if any – electronic interaction between the pre-catalyst and the MOF. FT-IR of MOF-74 impregnated with $Co_2(CO)_8$ showed no CO stretches between 1800 cm^{-1} and 2000 cm^{-1} with contomitant colour change from dark black to light grey indicating fast decomposition of $Co_2(CO)_8$ under O_2 and/or moisture. The IR spectra and comparison with the $Co_2(CO)_8$ and the MOFs are shown below.



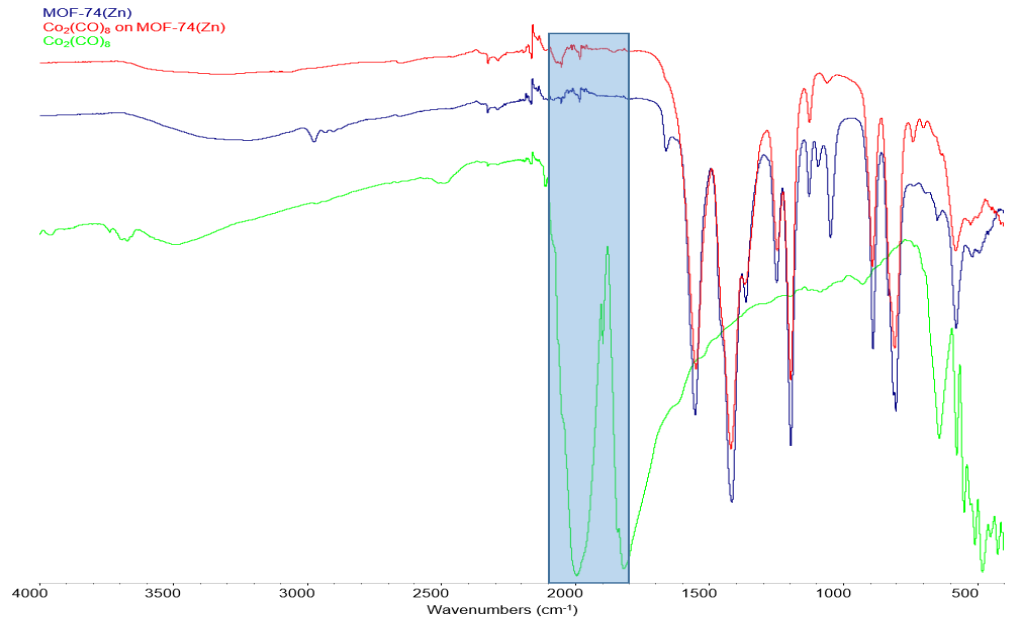


Figure S9 FT-IR spectra. Pristine MOF (top), catalyst-loaded MOF (middle) and catalyst (bottom) for MixUMCM-1-NH2 (28%) (top spectrum) and MOF-74(Zn) (bottom spectrum).

Hydroformylation with Co@MOF

Co@MOF (amount in Table S11) was added to a 2 ml crimp vial in a nitrogen-filled glove box. 1-Hexene (500 µl, 4.0 mmol, 1.0 eq.) was added to all vials before they were closed with a crimp cap and taken out of the glove box. The vials were placed in the autoclave which was flushed several times before syngas pressure was set to 30 bar at room temperature. The reactor was heated to 100°C leading to a pressure of 35 bar and the substrates were allowed to react for 16 h. The autoclave was cooled down to room temperature and the remaining syngas pressure was slowly released to avoid spilling.

Recycling of Co@MOF

After the first catalytic run, the reaction mixture was removed with a syringe. The MOF was washed once by 1-hexene (1 mL) and then the solvent extracted with a syringe. Fresh 1-hexene (500 µl, 4.0 mmol) was added again, the vials were closed and the reaction was carried out as stated above.

Recycling MOF

After the first catalytic run, the MOF was filtered off and washed with $CHCl_3$ (3 x 10 ml) in the case of MixUMCM-1-NH_2 (28%). MOF-74(Zn) samples

were washed with THF (3 x 10 ml) and EtOH (3 x 10 ml) before they were purified by Soxhlet extraction (5 d, THF). The purified MOFs were used for hydroformylation following the standard procedure of Table 5.1 in the main text.

ICP-MS Measurements

0.5 mL H_2O_2 (30%), 1 mL H_2SO_4 (96%) and 1 mL HCl (30%) were added to about 20 mg from each MOF samples (with and without Co) and then digested by using a high-pressure microwave unit (Anton Paar). Afterwards the digested samples were diluted with MilliQ H_2O to a total volume of 50 mL. Another two dilution steps were carried out with a 1% HCl solution resulting in total dilution factor of ~ 8.0 105.

The hexene liquid solutions were heated for several hours (at about 60°C) and then 1 mL HCl (30%) was added to each sample. The obtained solutions were then diluted in 2 steps by a factor of 2 104.

4 standard solutions of Co, P and Zn were prepared with concentration in the range of 0 to 100 ppb (ng/mL). The analysis was performed on an ICP-MS 7700x after optimizing the system for high sensitivity and low oxide rate. The isotopes ^{59}Co, ^{31}P and ^{66}Zn were measured and the corresponding three elements in all the samples were quantified by using external calibration procedure.

Table S3 Co-Loading in MixUMCM-1-NH2 (28%) after catalysis dependent on the pressure.

Entry	Syngas pressure (bar)	Co-uptake (%)
1	19	56
2	23	52
3	55	82
4	72	85
5	94	56

Table S4 Co-Loading in MOF-74(Zn) after catalysis dependent on the pressure.

Entry	Syngas pressure (bar)	Co-uptake (%)
1	30	60
2	61	36

GC-MS Chromatogram (Table 5.3 Entry 1 without MOF in Main Text)

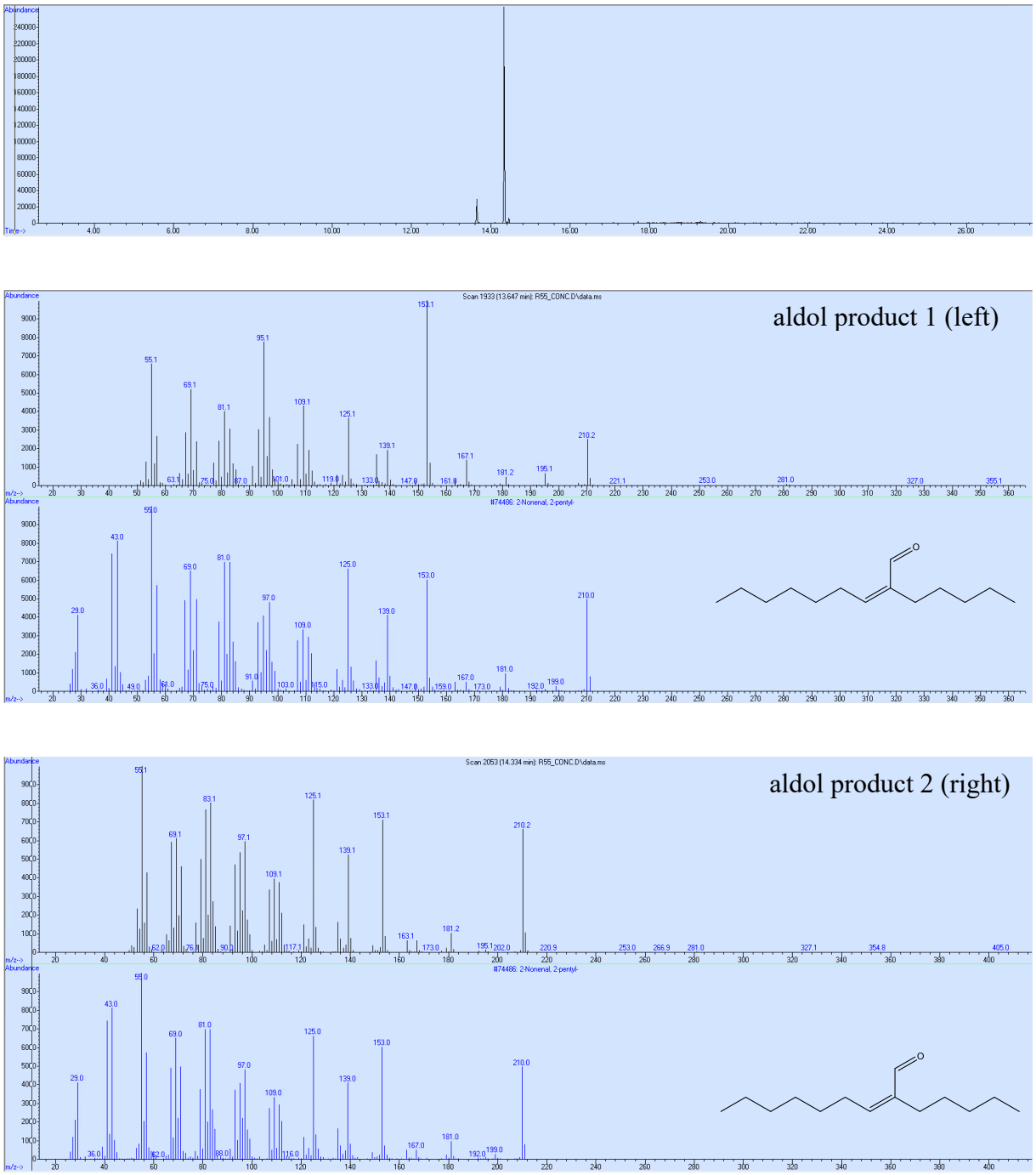
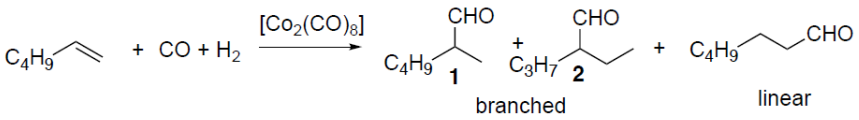


Figure S10 Extracted ion chromatogram for the mass of the aldol product (210 u) and mass spectra of the two found compounds compared to the best fitting substance in the database. The two products are likely isomers of the depicted aldol product.

Hydroformylation Catalysis Screening

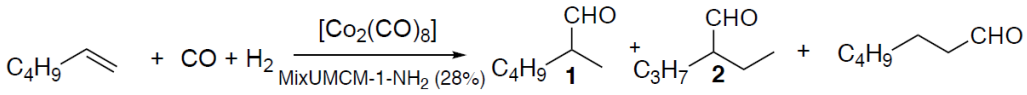
Table S5 Screening of reaction conditions in the homogeneous reaction.



Entry	Co amount (mol %)	Syngas pressure (bar)	Conversion (%)	*B/L*
1[a]	0.23	120	n/d	n/d
2[b]	0.23	120	<5%	n/a
3[c],[d]	0.23	19	15	66:34
4[c],[e]	0.23	23	24	45:55
5[c]	0.23	55	62	36:64
6[c]	0.23	94	66	32:68
7[c]	0.06	30	16	49:51
8[c]	0.12	30	35	46:54
9[c]	0.23	30	40	49:51
10[c]	0.47	30	61	54:46
11[c]	1.19	30	>99	54:46
12[c]	2.38	30	>99	51:49

[a] Reaction at 50°C; n/d = not detectable. [b] Reaction at 75°C. [c] Reaction at 100°C. [d].11 bar and [e] 7 bar of Ar were introduced additionally to minimize evaporation of the substrate during the reaction.

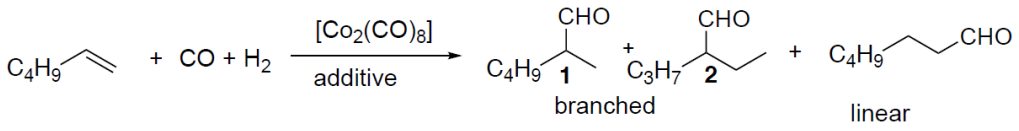
Table S6 Screening of reaction conditions with MixUMCM-1-NH2 (28%). Variation of MOF loading and pressure.[a]



Entry	mol_{MOF}/mol_{Co}	p [bar]	Conversion (%)	*B/L*
1	0.8	30	36	75:25
2	1.0	30	28	67:33
3	1.7	30	24	76:24
4	2.8	30	21	72:28
5	1.1	19	10	71:29
6	1.1	30	28	67:33
7	1.1	61	42	51:49
8	1.1	92	61	31:79

[a] $Co_2(CO)_8$ (0.8 mg) was dissolved in 1-hexene (250 µL) and MixUMCM-1-NH_2 (28%) was added; the mixture was brought to various syngas pressure (H_2:CO = 1) at 100°C for 17h

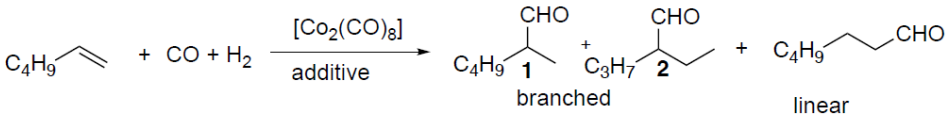
Table S7 Blank reaction with different Zn sources.[a]



Entry	Additive	mol_{Add}/mol_{Co}	Conversion (%)	*B*/*L*
1	ZnO	5.9	41	53:47
2	$Zn(OAc)_2$*2 H_2O	3.5	9	51:49
3	$Zn(acac)_2$*H_2O	1.8	5	64:36
4	$Zn(NO_3)_2$*6 H_2O	4.6	11	48:52
5	$ZnCl_2$	4.0	11	62:38
6	$ZnSO_4$*7 H_2O	3.0	21	47:53
7	H_3BTB	1.2	35	49:51
8	H_2BDC	2.8	37	54:47
9	H_2BDC-P(Ph)$_2$	1.4	35	49:51

[a] Co2(CO)8 (0.8 mg) was dissolved in 1-hexene (250 µL) and the additive was added; the mixture was brought to 30 bar syngas (H2:CO = 1) at 100°C for 17h.

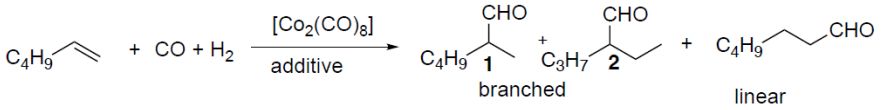
Table S8 Blank reaction with different MOFs.[a]



Entry	Additive	mol_{Add}/mol_{Co}	Conversion (%)	*B*/*L*
1	MOF-74(Zn)	41.3	26	85:15
2	UMCM-1	1.7	32	60:40
3	MixUMCM-1-NH_2 (28%)	1.7	24	76:24
4	UMCM-1-NH_2	1.7	20	76:24
5	MOF-74(Mg)	51.7	8	77:23
6	MOF-74(Co)	36.5	90	56:44
7	MOF-74(Ni)	41.3	45	55:45
8[b]	MIL-101(Al)	2.0	<5	n/a
9[b]	MIL-101(Cr)	1.8	<5	n/a
10[b]	Zeolite-Y	n/a	<5	n/a
11	MixUMCM-1-PPh_2 (29 %)	0.9	22	67:33
12	$HCo(CO)_3$(MixUMCM-1-PPh_2)[c]	n/a	9	50:50

[a] $Co_2(CO)_8$ (0.8 mg) was dissolved in 1-hexene (250 µL) and the additive was added; the mixture was brought to 30 bar syngas (H2:CO = 1) at 100°C for 17h.[b] The reaction was monitored after 17h, 24h, and 48h with no change in results. [c] The material was directly added as catalyst without the addition of $Co_2(CO)_8$

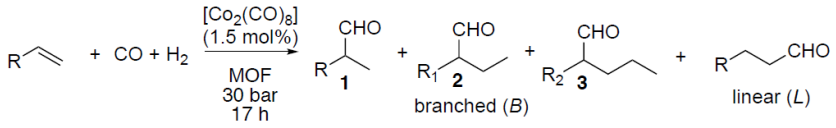
Table S9 Reactions at different pressures.[a]

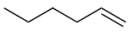
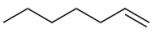
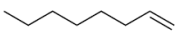
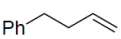


Entry	Additive	Pressure at 100 °C (bar)	Conversion (%)	*B*/*L*
1	/	19	15	66:34
2	/	30	40	49:51
3	/	61	79	34:66
4	/	92	84	27:73
5	MixUMCM-1-NH_2 (28%)[b]	19	10	71:29
6	MixUMCM-1-NH_2 (28%)[b]	30	28	67:33
7	MixUMCM-1-NH_2 (28%)[b]	61	42	51:49
8	MixUMCM-1-NH_2 (28%)[b]	92	61	31:79
9	MOF-74(Zn)	19	12	83:17
10	MOF-74(Zn)	30	25	85:15
11	MOF-74(Zn)	61	55	55:45
12	MOF-74(Zn)	92	62	41:59

[a] $Co_2(CO)_8$ (0.8 mg) was dissolved in 1-hexene (250 µL) and the additive was added; the mixture was brought to the pressure of syngas (H_2:CO = 1) and then heated at 100°C for 17h. [b] molMOF/molCo = 1.1. [c] molMOF/molCo = 20.

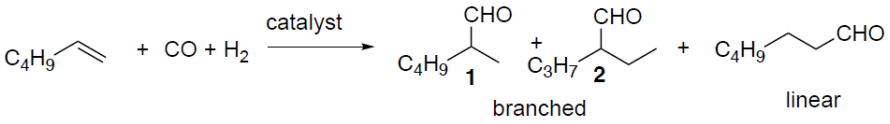
Table S10 Aldehyde yields in Table 5.3 of the main text determined by GCFID with p-cymene as external standard.[a]



Entry	Olefin	GC aldehydes yield [b]		
		MixUMCM-1-NH_2 (28%)[c]	MOF-74(Zn) [d]	No MOF
1		24	17	45
2		45	24	96
3		32	25	77
4		63	47	>99
5		n.a.	n.a.	n.a.

[a] Co2(CO)8 (1.5 mol%) were dissolved in olefin (500 µL) and the MOF was added. The mixture was brought to 30 bar and then heated to 100°C for 17 h. [b] Determined by GC-FID with calibrated linear aldehyde with p-cymene as internal standard. [c] molMOF/molCo = 0.4. [d] molMOF/molCo = 3.3.

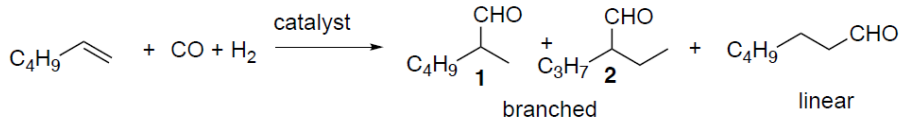
Table S11 Reactions with incipient-wetness impregnated MOFs.[a]



Entry	Catalyst	Co@MOF amount (mg)	Co mol%	Conversion (%)	*B/L*
1	Co@MixUMCM-1-NH_2-13	7	0.17	37	61:39
2	Co@MixUMCM-1-NH_2-13	15	0.33	40	65:35
3	Co@MixUMCM-1-NH_2-13	20	0.46	41	68:32
4	Co@MixUMCM-1-NH_2-13	23	0.50	47	68:32
5	Co@MOF-74(Zn)-9.3	20	0.30	50	60:40
6	Co@MOF-74(Zn)-9.3	40	0.60	63	68:32
7	Co@MOF-74(Zn)-4.3	19	0.13	16	51:49
8	Co@MOF-74(Zn)-4.3	41	0.27	20	54:46
9	Co@MOF-74(Zn)-3.8	19	0.11	7	52:48
10	Co@MOF-74(Zn)-3.8	41	0.24	11	53:47

[a] 1-Hexene (500 µL) was added to the catalyst; the mixture was brought to 30 bar pressure of syngas (H2:CO = 1) at room temperature and then heated at 100°C for 17h.

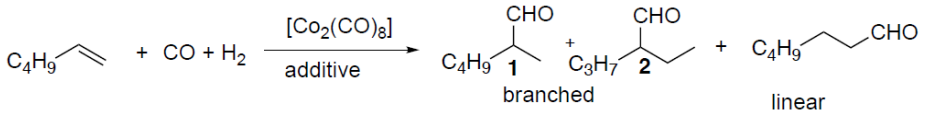
Table S12 Reactions with recycled incipient-wetness impregnated MOFs.[a]



Entry	Catalyst	Co mol% initial	Conversion (%)	*B/L*
1	Co@MixUMCM-1-NH_2-13	0.17	traces	~ 50:50
2	Co@MixUMCM-1-NH_2-13	0.33	traces	~ 50:50
3	Co@MixUMCM-1-NH_2-13	0.46	traces	~ 50:50
4	Co@MOF-74(Zn)-4.3	0.27	traces	~ 50:50
5	Co@MOF-74(Zn)-3.8	0.11	traces	~ 50:50
6	Co@MOF-74(Zn)-3.8	0.24	traces	~ 50:50

[a] After the first catalytic run, 1-Hexene (500 µL) was added to the catalyst; the mixture was brought to 30 bar pressure of syngas (H_2:CO = 1) at room temperature and then heated at 100°C for 17h.

Table S13 Reactions with recycled, washed MOFs.[a]



Entry	Additive	Conversion (%)	*B*/*L*
1	MixUMCM-1-NH_2-Recyc	5	64:36
2	MOF-74(Zn)-Recyc	35	68:32

[a] After the first catalytic run, $Co_2(CO)_8$ (0.25 mol%) was dissolved in 1-hexene (500 µL) and the MOF (20 mg) was added. The mixture was brought to 25 bar and then heated to 100°C for 17 h.

Computational Details

Interaction Energy Calculations:

All calculations were performed using the code CP2K[8] at density functional level of theory. The semi-local PBEsol functional was adopted[9] using the DZVP-MOLOPT-SR-GTH gaussian basis set for all the atom types,[10] and a cutoff of 500 Ry for the plane wave auxiliary basis set. The MOFs experimental structures were used as starting point and the catalyst was manually added close to the adsorption/binding site of the MOF. To relieve the computational cost of the calculations, all the systems were studied using the primitive cell. Due to its small size in the a direction, for MOF-74 a supercell 2 x 1 x 1 was adopted. Full geometry optimizations (i.e. both atomic positions and cell parameters) were performed to optimize the MOF-catalyst system. Single point calculations were then performed to calculate the interaction energies between the MOF and the catalyst including the basis-set superimposition error.

In CP2K the interaction energy can be calculated defining 2 fragments A and B. Two fragments corresponding to the MOF (E_A) and the catalyst (E_B) were defined in each case.

$$E_{int} = E_{AB} - (E_A + E_B) \qquad \textbf{(1)}$$

The adsorption/binding sites tested are shown Figure S11 to Figure S17.

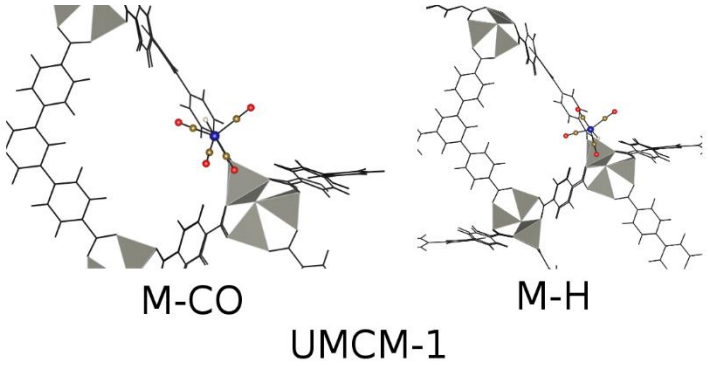


Figure S11 Optimised adsorption geometry of HCoCO4 with UMCM-1. Colour scheme: Co = blue, O = red, C = brown, H = white. The organic ligand and inorganic node of the MOF are represented as black line and grey polyhedral for clarity.

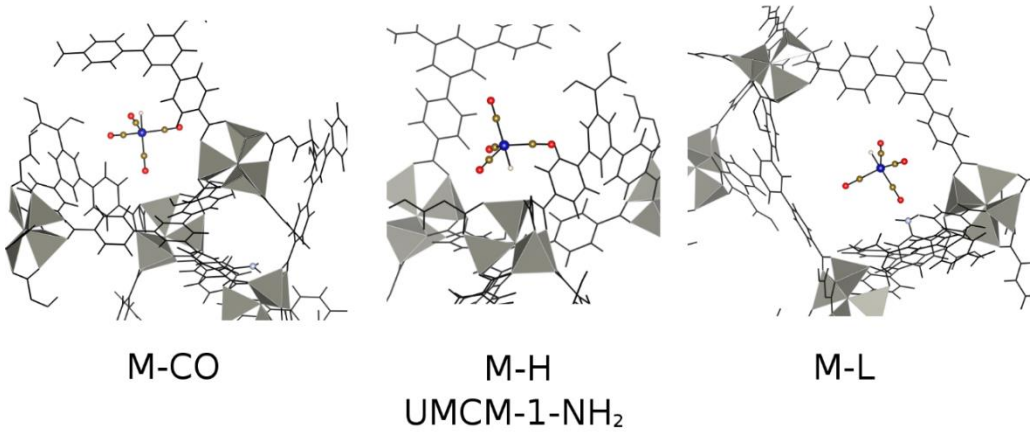


Figure S12 Optimised adsorption geometry of HCoCO4 and UMCM-1-NH2. Colour scheme: Co = blue, O = red, C = brown, H = white. The organic ligand and inorganic node of the MOF are represented as black line and grey polyhedral for clarity.

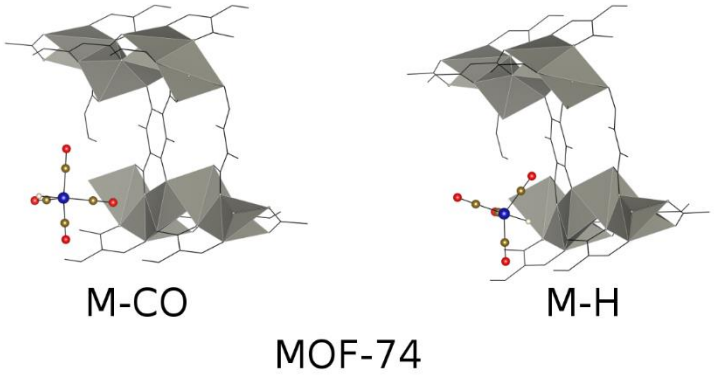


Figure S13 Optimised adsorption geometry of HCoCO4 and MOF-74(Zn). Colour scheme, Co = blue, O = red, C = brown, H = beige. The organic ligand and inorganic node of the MOF are represented as black line and grey polyhedral for clarity.

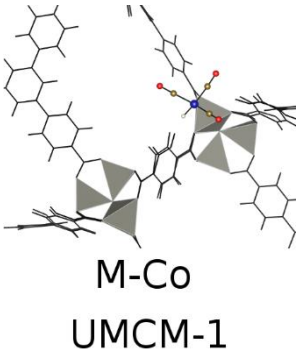


Figure S14 Optimised binding geometry of HCoCO3 and UMCM-1. Colour scheme: Co = blue, O = red, C = brown, H = beige. The organic ligand and inorganic node of the MOF are represented as black line and grey polyhedral for clarity.

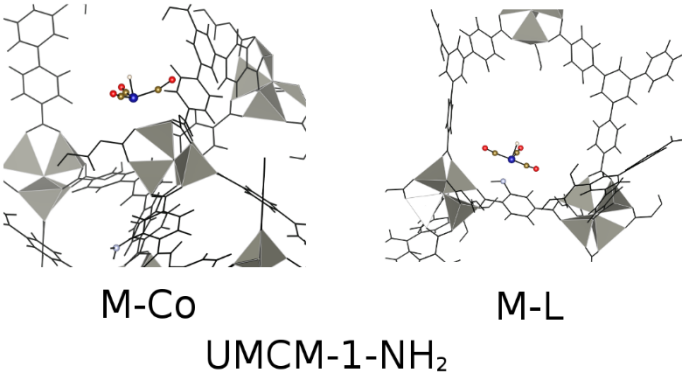


Figure S15 Optimised binding geometry of HCoCO3 and UMCM-1-NH2. Colour scheme: Co = blue, O = red, C = brown, H = beige, N = pale blue. The organic ligand and inorganic node of the MOF are represented as black line and grey polyhedral for clarity.

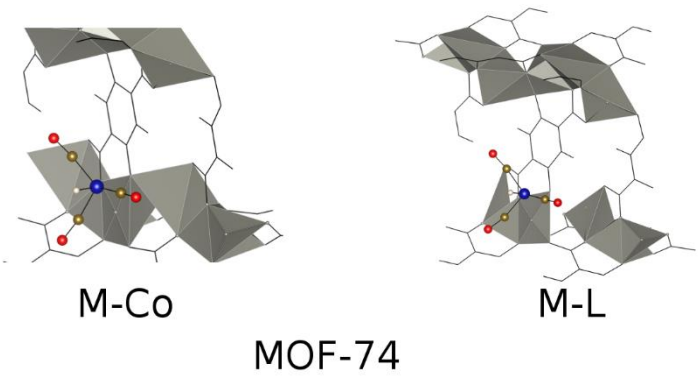


Figure S16 Optimized binding geometry of HCoCO3 and MOF-74(Zn). Colour scheme: Co = blue, O = red, C = brown, H = beige. The organic ligand and inorganic node of the MOF are represented as black line and grey polyhedral for clarity.

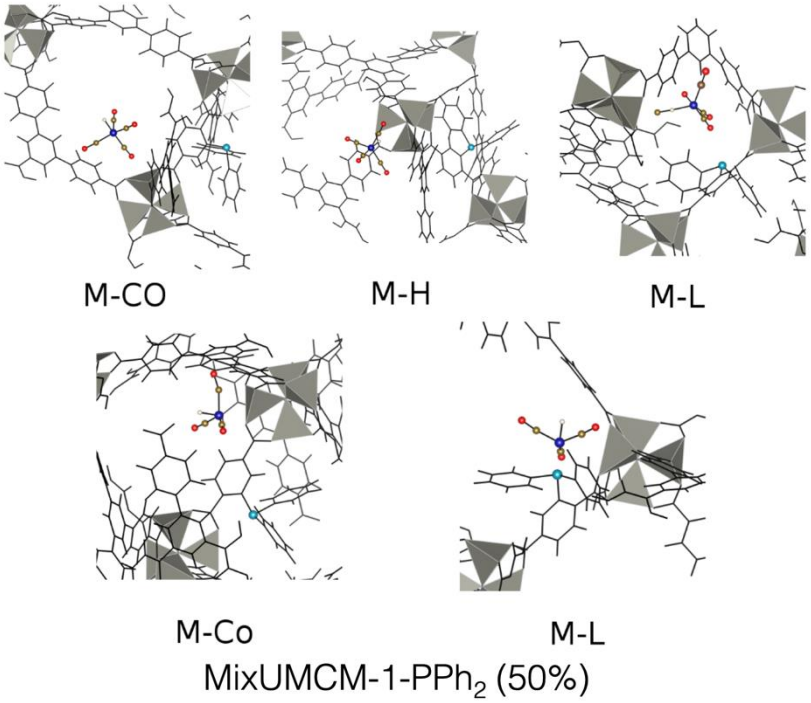


Figure S17 On the top, optimized geometry of HCoCO4 and MixUMCM-1-PPh2 (50%). On the bottom, optimized binding geometry of HCoCO3 and MixUMCM-1-PPh2 (50%). Colour scheme: Co = blue, O = red, C = brown, H = beige, P = bright blue. The organic ligand and inorganic node of the MOF are represented as black line and grey polyhedral for clarity reason.

Monte Carlo Simulations

Raspa 2.0 package was used for Monte Carlo simulations.[11] The interactions are computed using Lennard-Jones potential with a cutoff of 14.0 Angstroms for dispersions and a Coulombic potential for charges. As for framework's atom types, the parameters for dispersions are taken from DREIDING force field [12] integrated with UFF[13] for the missing atom types (Mg, Co, Ni and Zn). The choice of the force field is motivated by the good match with adsorption experiments of alkanes in MOF-type frameworks.[14] The point charges are computed using the REPEAT scheme[15] to fit the PBEsol electrostatic potential from geometry optimized structures. These periodic DFT calculations were run using CP2K software package, utilizing the DZVP-MOLOPT-SR-GTH gaussian basis set for all the atom types and a cutoff of 500 Ry for the plane wave auxiliary basis set. The position of the frameworks' atoms is kept fixed in all the calculation. 1-hexene and aldehydes are modelled using TraPPE force field,[16,17] where the only missing parameters are

for the O-CH-CH-CHx torsion potential of the carbonyl group of branched aldehydes. These parameters were computed from quantum mechanics using the MP2/6-31G* method in Gaussian09 (Figure S18) coherently with the TraPPE parametrization. Due to the similarity of the two species, only one of the two branched aldehydes is considered: **1** (2-methylhexanal) which is experimentally obtained with the highest ratio.

CO and H_2 molecules are treated as rigid particles. The CO interaction parameters adopted in this work were specifically designed for adsorption in MOF-type materials.[18] The parameters for H_2 are taken from the work of Marx et al.[19] and already validated for adsorption in MOFs.[20,21]

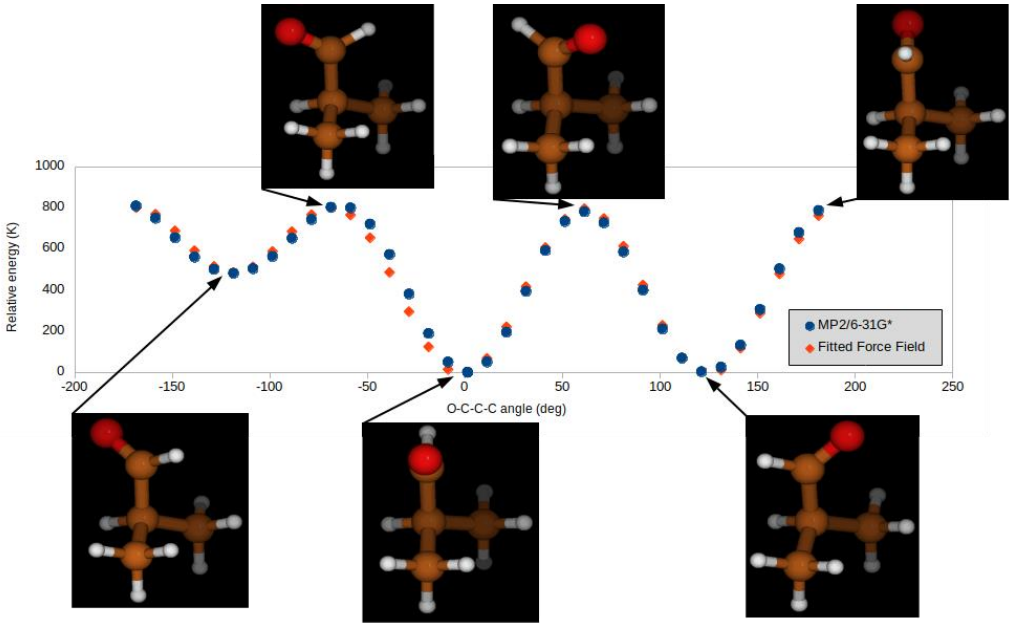


Figure S18 Torsional scan of the carbonyl group in a representative model for branched aldehydes. The torsional potential was computed using the MP2/6-31G* method and used to fit the parameters for the TraPPE force field. The plot shows the agreement of the fitting and the conformation of the molecule in the maximum and minimum points

In the following paragraph we describe the protocol used to compute the affinity of the reactive species with the frameworks. First, the amount of 1-hexene inside the bulk frameworks at 30 bar and 100°C was obtained for each considered MOF by performing a Grand Canonical Monte Carlo (GCMC) simulation,[22] where the fugacity of the solvent is derived using the Peng Robinson equation of state.[23] The results of GCMC simulation were averaged for 5,000 cycles, after other 5,000

cycles of initialization. Depending on the concentration of 1-hexene in the framework we computed the volume of the cubic box that simulates the homogenous phase, imposing the same number of molecules and the homogenous density of 1-hexene as computed from GCMC in the empty box (0.00395 molecules per cubic Angstrom). Note that this corresponds to a macroscopic density of 6.56 mol/L, which is slightly smaller than the reported experimental value of 7.11 mol/L. However, to be internally consistent with the simulations we keep the value of 6.56 mol/L as the reference density for the homogeneous phase.

To compute the affinity with the frameworks, one molecule for each reacting component (i.e., H_2. CO. linear heptanal and branched aldehyde **1**) was added to the mixture with saturated 1-hexane. The two simulation boxes, for the homogeneous and the crystal bulk phases, could exchange molecules according to the following rules: 1-hexene and aldehydes were allowed to swap identity between the two boxes and the gas molecules were allowed to be removed and reinserted in the other box. These two moves were possibly selected within the Monte Carlo cycle and attempted, similarly to the other standard molecular moves, i.e., translation, rotation, intramolecular displacement, and reinsertion. The choice for the swap rules follows from the consideration that 1-hexene and aldehydes have a similar size and therefore there is a higher probability that a change of identity between them will be accepted, while for the smaller H_2 and CO molecules, it is easier to find interstices between the solvent molecules to be inserted.

For each pair of systems (i.e., MOF + homogenous). ten independent simulations were run. executing 5.000 cycles of equilibration and 5.000 cycles of production. The final average and standard deviation for the reactant/product occupation is obtained by considering the output these ten runs for the block averaging. i.e., as the result of 50.000 production cycles. Since there are two molecules for each reactive species for each pair of systems (i.e., the framework and the homogenous box) we define as occupancy percentage (%occup.) the averaged probability to find the specie in the MOF's pore volume. divided by two. Therefore, one can observe %occup. =50% if the affinity is the same with both the system (i.e., on average there is one molecule of the specie per box). This is what we obtained when running the simulation for two equivalent boxes, that can be two homogenous boxes or two boxes modelling the bulk of the same MOF. One can

observe %occu. →100% when the species has a strong affinity with the MOF (i.e., there is a high probability of finding the two molecules of the species in the MOF's box). Finally, one can observe %occu. →0% when the species has a weak affinity with the MOF, relatively to the homogenous 1-hexane phase (i.e., there is a high probability of finding the two molecules of the species in the homogenous box).

To understand the reason of the higher affinity of the aldehydes with the MOFs. we performed extra calculations on MOF-74(Zn) and UMCM-1, by switching off the coulombic interactions in the simulation. The results reported in Table S18, compared with the ones computed from the charged model, show a significant reduction of the MOF affinity with the aldehydes when the carbonyl group is not interacting with the electrostatic potential in the pore volume of the frameworks. According to the TraPPE force field for aldehydes. the CH bead and the oxygen have a charge of 0.525 and -0.482, respectively. The Zn charge computed using the REPEAT method is 1.190 in MOF-74 and 1.27 in UMCM-1.

The MOF-aldehyde affinity is therefore enthalpic and apparently not dependent on the type of isomer (linear or branched), i.e., it is not due to a steric confinement as in the case of "shape selectivity" seen for hydrocarbons in zeolites. In the non-charged system, the affinity of the gas molecule that are only weakly polar, remains almost unvaried and suggests that there is a minor effect due to non-covalent interactions. We conclude that the higher affinity of the gas molecules with the liquid 1-hexene is due to an entropic motivation. The 1-hexene saturated in the pore volume has a higher density and the confinement effect is higher inside the MOF: this results in a lower probability of forming interstices where the small gas molecules can fit, i.e., the cavitation contribute to the solvation energy of H_2 and CO.

Pore Volume Calculations

The pore volume in the bulk frameworks, that was used to calculate the density of the saturated 1-hexene is computed with the "probe occupiable pore volume" (VOLPO) routine[24] as implemented in the Zeo++ v0.3 software package.[25,26] For the probing of the volume, 500.000 samples were used, together with the high accuracy (-ha) option in Zeo++. The radii of the atoms in the framework were taken as half of the Lennard-Jones sigma parameter of the force

field (DREIDING, integrated with UFF for the missing atom types). This choice is coherent with the potential used for the Monte Carlo simulations.

As for the probe size, a diameter of 3.703 Å was utilized. This value is the half average of the sigma parameters for the CH_3 (3.75 Å) and the CH_2 (3.675 Å) beads in TraPPE force field, that are, respectively, the head and the tail of the 1-hexene molecule.

DFT Calculations

Table S14 DFT interaction energy of $HCo(CO)_4$. M-Co (MOF–$COCo(H)(CO)_3$ in the main text) is the adsorption of $HCoCO_4$ to the metal node via its axial carbonyl. M-H (MOF–H-$Co(CO)_4$ in the main text) is the adsorption of $HCoCO_4$ to the metal node via its hydride. L-CO = adsorption of $HCoCO_4$ to the function via its axial carbonyl. Optimised geometries reported in supplementary notes (Figure S11 to Figure S17).

	M-CO (kcal/mol)	M-H (kcal/mol)	L-CO (kcal/mol)
UMCM-1	1.20	0.19	/
UMCM-1-NH_2	0.69	0.01	-0.27
UMCM-1-PPh_2	-0.03	-0.09	-0.09
MOF-74(Zn)	-1.68	-2.53	/

Table S15 DFT binding energies. M-Co (MOF–$Co(H)(CO)_3$ in the main text) is the binding energy between the metal of the MOF and the Co of $HCoCO_3$. L-Co (MOFFunc–$Co(H)(CO)_3$ in the main text) is the binding energy between the functional group of the MOF and the Co of $HCoCO_3$. Optimised geometries reported in supplementary notes (Figure S11 to Figure S17).

	M-Co	L-Co
UMCM-1	-3.49	/
UMCM-1-NH_2	-20.22	-34.02
UMCM-1-PPh_2	-54.95	-53.39
MOF-74(Zn)	-28.74	-33.84

Monte Carlo Simulations

Table S16 Grand Canonical Monte Carlo (GCMC) simulations. For each framework the first column lists the 1-hexene uptake measured from Grand Canonical Monte Carlo (GCMC) simulations (average and standard deviation over 5 blocks). The second column shows the rounded number of 1-hexene molecules that were used for the following simulations and to compute the size of the paired homogenous box that contains the same number of solvent molecules, reported in the third column.

Framework	1-hex. uptake (molec./UC)	1-hex. uptake (molec./box)	Homogeneous box volume ($Å^3$)
UMCM-1	176.0 ± 2.4	176	44.557
UMCM-1-NH_2	176.2 ± 2.4	176	44.557
UMCM-1-PPh_2	161.3 ± 3.5	161	40.759
MOF-74(Zn)	246.8 ± 3.0	247	62.532

Table S17 Affinity of the different species with the frameworks. This is reported as percentage occupancy (%occup.) which is related to the average number of molecules of that species in the MOF's simulation box. The error is computed as standard deviation over ten independent simulations. The last column reports the relative density of 1- hexene computed in the pore volume with respect to the density observed in the homogeneous simulation box (see also Table S16).

MOF	1-hexene Rel. density	H_2 %occup.	CO %occup.	n-Heptanal %occup.	**1** %occup.
UMCM-1	1.04 ± 0.01	40.0 ± 0.5%	41.3 ± 0.5%	66.7 ± 1.5%	64.0 ± 1.4%
UMCM-1-NH_2	1.04 ± 0.01	39.1 ± 0.1%	40.8 ± 0.5%	67.2 ± 0.7%	64.4 ± 2.2%
UMCM-1-PPh_2	1.04 ± 0.02	40.8 ± 0.5%	41.2 ± 0.6%	68.9 ± 2.2%	66.6 ± 1.9%
MOF-74 (Zn)	1.14 ± 0.01	22.4 ± 0.7%	21.9 ± 1.4%	80.9 ± 1.9%	81.5 ± 0.6%

Table S18 The affinity of the different species with UMCM-1 and MOF- 74(Zn). as setting to zero the Coulomb interactions. is reported with its standard deviation. The difference in the %occup. with the charged model shown in Supplementary Table S19 is also reported

Species	UMCM-1 (no charges) %occup.	difference	Zn-MOF-74 (no charges) %occup.	difference
Heptanal	55.1 ± 0.4%	-11.6%	66.3 ± 1.5%	-14.3%
2-metylhexanal (**1**)	55.5 ± 1.8%	-8.5%	66.0 ± 1.0%	-15.6%
H_2	40.6 ± 0.2%	+0.6%	20.1 ± 0.7%	-2.3%
CO	41.6 ± 0.7%	+0.3%	20.0 ± 1.3%	-1.9%

Kinetic Analysis

The kinetic analysis was based on the empirical rate of formations of the branched and the linear aldehydes reported in the paper.[27] The two equations are shown below and are also reported in the full text.

$$R_B = \frac{k_B \cdot [H_2]^{0.32} \cdot [CO] \cdot [Co_2(CO)_8]^{0.62} \cdot [alkene]}{(1+K_{BCO} \cdot [CO])^2} \quad (2)$$

$$R_L = \frac{k_L \cdot [H_2]^{0.55} \cdot [CO] \cdot [Co_2(CO)_8]^{0.75} \cdot [alkene]^{0.87}}{(1+K_{LCO} \cdot [CO])^2} \quad (3)$$

The kinetic and equilibrium constants at 110 °C were all taken from the publication:

$$k_B\ (110\ °C) = 2.12 \cdot 10^{-7} (m^3 \cdot mol^{-1}) \cdot 1.94 s^{-1}$$

$$K_{BCO}\ (110\ °C) = 1.35 \cdot 10^{-3} \cdot m^3 \cdot mol^{-1}$$

$$k_L\ (110\ °C) = 2\ .01 \cdot 10^{-7} (m^3 \cdot mol^{-1}) \cdot 2.17 s^{-1}$$

$$K_{LCO}\ (110\ °C) = 8.014 \cdot 10^{-3} \cdot m^3 \cdot mol^{-1}$$

The concentration of pure 1-hexene is $7.11 \cdot 10^3$ mol/m^3 at 30 bar and 100 °C (http://www.ddbst.com/en/EED/PCP/DEN_C100.php).

The concentration of H_2 and CO at different pressures in 1-hexene were calculated using the Soave modifications of the Redlich-Kwong equation (SRK)[28] and are reported in Table S19.

The concentrations of 1-hexene, CO and H_2 within the pores of the MOFs were calculated by multiplying the concentration in the homogeneous phase by a factor Z derived from the Monte Carlo simulations (Table S20). The Z factor for H_2 and CO were calculated by using equation (4). This is consistent with the fact that an %occup. of 50 would give a Z factor of 1 and therefore no preference of a molecule to be either in the homogeneous or the MOF phase, while with %occup. of 0 one would find null concentration inside the MOF as both CO and H_2 are found with %occup. < 50%.

$$Z = \%occup. / 50 \qquad (4)$$

The concentration of $Co_2(CO)_8$ was calculated from the catalyst loading relative to the 1-hexene concentration.

Table S19 Molar solubilities of H2 and CO in 1-hexene at 100 °C in function of pressure.

Pressure (bar)	Molar solubility of H_2 (mol/L)	Molar solubility of CO (mol/L)
10	0.0565855989	0.104422395
20	0.135717257	0.251731862
30	0.214408549	0.399737285
40	0.292661936	0.548459301
50	0.37048037	0.697919993
60	0.447866674	0.848143
70	0.524823672	0.999153594
80	0.60135418	1.15097877
90	0.677463539	1.30365115
100	0.753150085	1.45719046

Table S20 Correction factors Z used to calculate the modified concentration of the reactants within the pores of the MOFs.

MOF	Z[1-hexene]	Z[H_2]	Z[CO]
UMCM-1	1.04	0.80	0.82
UMCM-1-NH_2	1.04	0.78	0.82
MixUMCM-1-PPh_2 (50%)	1.04	0.82	0.82
MOF-74(Zn)	1.14	0.45	0.44

Rates of formation in homogeneous catalysis

[1-hexene] = $7.11 \cdot 10^3$ mol/m^3

[Co_2CO_8] = 8.53 mol/m^3

Table S21 Concentration of H_2 and CO at different syngas pressures. (H_2:CO = 1) Their effect on the rate of formations of the branched aldehyde RB and of the linear one RL for homogeneous catalysis is shown.

P Syngas (bar)	[H_2] (mol·m^{-3})	[CO] (mol·m^{-3})	R_B (mol·m^{-3}·s^{-1})	R_L (mol·m^{-3}·s^{-1})	R_B/R_L
10	20.5	24.7	0.208	0.204	1.019
15	39.8	62.3	0.340	0.473	0.719
20	59.2	99.9	0.380	0.654	0.581
25	78.5	137.4	0.387	0.772	0.502
30	97.9	175.0	0.382	0.849	0.450
35	117.2	212.6	0.371	0.899	0.413
40	136.6	250.1	0.358	0.932	0.385
45	155.9	287.7	0.345	0.952	0.363
50	175.3	325.3	0.333	0.964	0.345
55	194.6	362.9	0.320	0.971	0.330
60	214.0	400.4	0.309	0.973	0.318
65	233.3	438.0	0.298	0.972	0.307
70	252.7	475.6	0.289	0.969	0.298
75	272.0	513.1	0.279	0.964	0.290
80	291.4	550.7	0.271	0.958	0.282
85	310.7	588.3	0.263	0.952	0.276
90	330.1	625.9	0.255	0.945	0.270
95	349.4	663.4	0.248	0.937	0.265
100	368.8	701.0	0.241	0.929	0.260

Rates of formation within the pores of UMCM-1-NH_2

[1-hexene] = $7.39 \cdot 10^3$ mol/m^3

[Co_2CO_8] = 8.87 mol/m^3

Table S22 Concentration of H_2 and CO at different syngas pressures. (H_2:CO = 1) Their effect on the rate of formations of the branched aldehyde RB and of the linear one RL for catalysis within the pores of UMCM-1-NH2 is also shown.

P Syngas (bar)	[H_2] (mol·m^{-3})	[CO] (mol·m^{-3})	R_B (mol·m^{-3}·s^{-1})	R_L (mol·m^{-3}·s^{-1})	R_B/R_L	$\underline{R_B/R_L[MOF]}$ $R_B/R_L[Homogeneous]$
10	16.0	20.3	0.184	0.165	1.113	1.093
15	31.1	51.1	0.326	0.408	0.798	1.111
20	46.2	81.9	0.382	0.589	0.648	1.115
25	61.3	112.7	0.401	0.717	0.559	1.114
30	76.3	143.5	0.404	0.808	0.500	1.111
35	91.4	174.3	0.399	0.872	0.457	1.108
40	107.0	205.1	0.390	0.917	0.425	1.106
45	122.0	235.9	0.379	0.949	0.400	1.103
50	137.0	266.7	0.369	0.971	0.379	1.100
55	152.0	297.5	0.358	0.986	0.362	1.098
60	167.0	328.4	0.347	0.996	0.348	1.096
65	182.0	359.2	0.337	1.002	0.336	1.094
70	197.0	390.0	0.327	1.004	0.325	1.092
75	212.0	420.8	0.317	1.005	0.316	1.090
80	227.0	451.6	0.309	1.003	0.308	1.089
85	242.0	482.4	0.300	1.001	0.300	1.088
90	257.0	513.2	0.292	0.997	0.293	1.086
95	273.0	544.0	0.285	0.992	0.287	1.085
100	288.0	574.8	0.278	0.987	0.282	1.084

Rates of formation within the pores of MOF-74(Zn)

[1-hexene] = $8.10 \cdot 10^3$ mol/m^3

[Co_2CO_8] = 9.72 mol/m^3

Table S23 Concentration of H_2 and CO at different syngas pressures. (H_2:CO = 1) Their effect on the rate of formations of the branched aldehyde RB and of the linear one RL for catalysis within the pores of MOF-74(Zn) is also shown.

P Syngas (bar)	[H_2] (mol·m^{-3})	[CO] (mol·m^{-3})	R_B (mol·m^{-3}·s^{-1})	R_L (mol·m^{-3}·s^{-1})	R_B/R_L	$\underline{R_B/R_L[MOF]}$ $R_B/R_L[Homogeneous]$
10	9.2	10.9	0.118	0.087	1.363	1.338
15	17.9	27.4	0.259	0.251	1.032	1.436
20	26.6	43.9	0.348	0.407	0.856	1.472
25	35.3	60.5	0.403	0.542	0.744	1.482
30	44.0	77.0	0.437	0.657	0.666	1.480
35	52.8	93.5	0.457	0.753	0.607	1.472
40	61.5	110.1	0.468	0.833	0.562	1.462
45	70.2	126.6	0.473	0.899	0.526	1.451
50	78.9	143.1	0.474	0.954	0.496	1.439
55	87.6	159.7	0.472	1.000	0.472	1.429
60	96.3	176.2	0.468	1.039	0.451	1.418
65	105.0	192.7	0.463	1.071	0.433	1.409
70	114.0	209.3	0.458	1.097	0.417	1.400
75	122.0	225.8	0.451	1.120	0.403	1.392
80	131.0	242.3	0.445	1.138	0.391	1.384
85	140.0	258.8	0.438	1.153	0.380	1.377
90	149.0	275.4	0.431	1.166	0.370	1.370
95	157.0	291.9	0.424	1.176	0.361	1.364
100	166.0	308.4	0.418	1.184	0.353	1.358

Supplementary References

1. Ito, K., Kamiyama, N., Nakanishi, S. & Otsuji, Y. *Chem. Lett.* **12**, 657–660 (1983).

2. Servalli, M., Ranocchiari, M. & Van Bokhoven, J. A. *Chem. Commun.* **48**, 1904–1906 (2012).

3. Dubbeldam, D., Calero, S., Ellis, D. E. & Snurr, R. Q. *Mol. Simul.* **42**, 81–101 (2016).

4. Morel, F. L., Ranocchiari, M. & Van Bokhoven, J. A. *Ind. Eng. Chem. Res.* **53**, 9120–9127 (2014).

5. Bauer, G., Ongari, D., Xu, X., Tiana, D., Smit, B. & Ranocchiari, M. *J. Am. Chem. Soc.* **139**, 18166–18169 (2017).

6. Serra-Crespo, P., Ramos-Fernandez, E. V., Gascon, J. & Kapteijn, F. *Chem. Mater.* **23**, 2565–2572 (2011).

7. Sorribas, S., Gorgojo, P., Téllez, C., Coronas, J. & Livingston, A. G. *J. Am. Chem. Soc.* **135**, 15201–15208 (2013).

8. Wu, X., Bao, Z., Yuan, B., Wang, J., Sun, Y., Luo, H. & Deng, S. *Microporous Mesoporous Mater.* **180**, 114–122 (2013).

9. Hutter, J., Iannuzzi, M., Schiffmann, F. & Vandevondele, J. *Wiley Interdiscip. Rev. Comput. Mol. Sci.* **4**, 15–25 (2014).

10. Perdew, J. P., Ruzsinszky, A., Csonka, G. I., Vydrov, O. A., Scuseria, G. E., Constantin, L. A., Zhou, X. & Burke, K. *Phys. Rev. Lett.* **100**, (2008).

11. VandeVondele, J. & Hutter, J. *J. Chem. Phys.* **127**, 114105 (2007).

12. Mayo, S. L., Olafson, B. D. & Goddard, W. A. *J. Phys. Chem.* **94**, 8897–8909 (1990).

13. Rappé, A. K., Casewit, C. J., Colwell, K. S., Goddard, W. A. & Skiff, W. M. *J. Am. Chem. Soc.* **114**, 10024–10035 (1992).

14. Déroche, I., Rives, S., Trung, T., Yang, Q., Ghoufi, A., Ramsahye, N. A., Trens, P., *et al. J. Phys. Chem. C* **115**, 13868–13876 (2011).

15. Campañá, C., Mussard, B. & Woo, T. K. *J. Chem. Theory Comput.* **5**, 2866–2878 (2009).

16. Wick, C. D., Martin, M. G. & Siepmann, J. I. *J. Phys. Chem. B* **104**, 8008–8016 (2000).

17. Stubbs, J. M., Potoff, J. J. & Siepmann, J. I. *J. Phys. Chem. B* **108**, 17596–17605 (2004).

18. Martín-Calvo, A., Lahoz-Martín, F. D. & Calero, S. *J. Phys. Chem. C* **116**, 6655–6663 (2012).

19. Marx, D. & Nielaba, P. *Phys. Rev. A* **45**, 8968–8971 (1992).

20. Bobbitt, N. S., Chen, J. & Snurr, R. Q. *J. Phys. Chem. C* **120**, 27328–27341 (2016).

21. Bucior, B. J., Bobbitt, N. S., Islamoglu, T., Goswami, S., Gopalan, A., Yildirim, T., Farha, O. K., Bagheri, N. & Snurr, R. Q. *Mol. Syst. Des. Eng.* **4**, 162–174 (2019).

22. Frenkel, D. & Smit, B. *Understanding molecular simulation: From algorithms to applications (2nd ed., Vol. 1, Computational science)*; Academic Press, San Diego, 2002.

23. Peng, D. Y. & Robinson, D. B. *Ind. Eng. Chem. Fundam.* **15**, 59–64 (1976).

24. Ongari, D., Boyd, P. G., Barthel, S., Witman, M., Haranczyk, M. & Smit, B. *Langmuir* **33**, 14529–14538 (2017).

25. Willems, T. F., Rycroft, C. H., Kazi, M., Meza, J. C. & Haranczyk, M. *Microporous Mesoporous Mater.* **149**, 134–141 (2012).

26. http://www.zeoplusplus.org/ Last accessed at 13.11.2018.

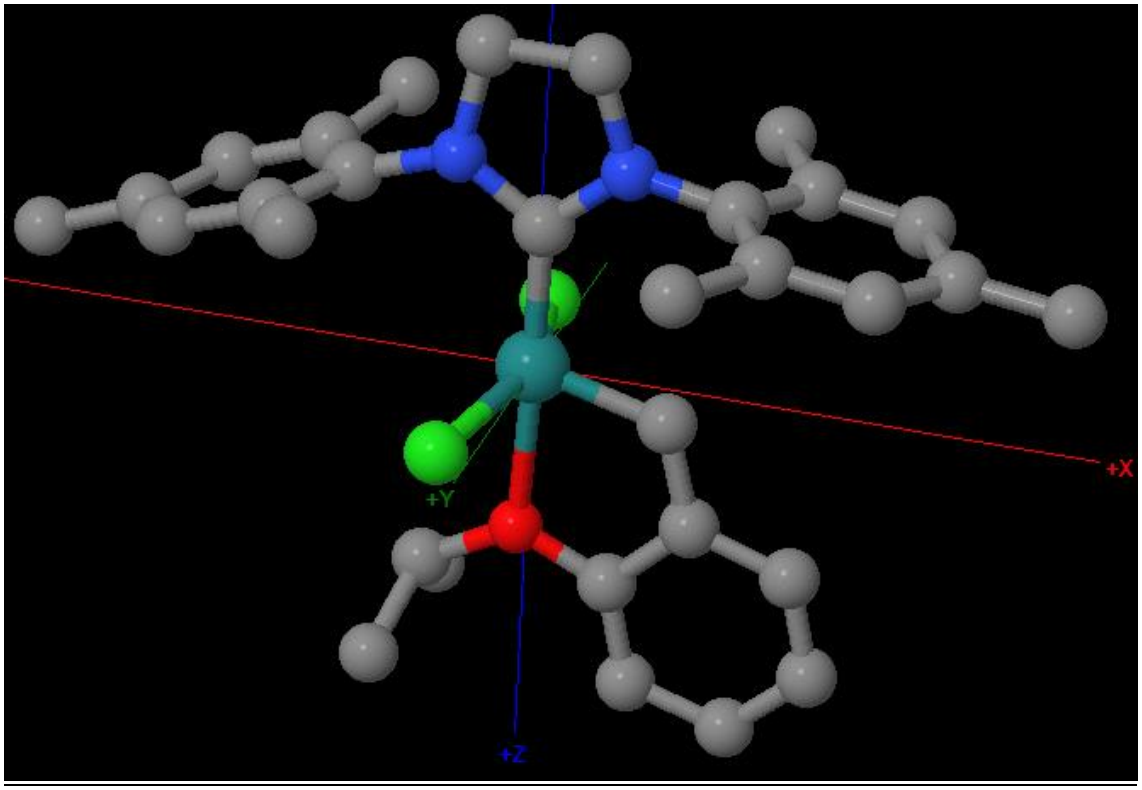
27. Gholap, R. V., Kut, O. M. & J. R. Bourne. *Ind. Eng. Chem. Res.* **31**, 2446–2450 (1992).

28. Mathias, P. M. & Copeman, T. W. *Fluid Phase Equilib.* **13**, 91–108 (1983).

Supplementary material for chapter 6

Steric maps

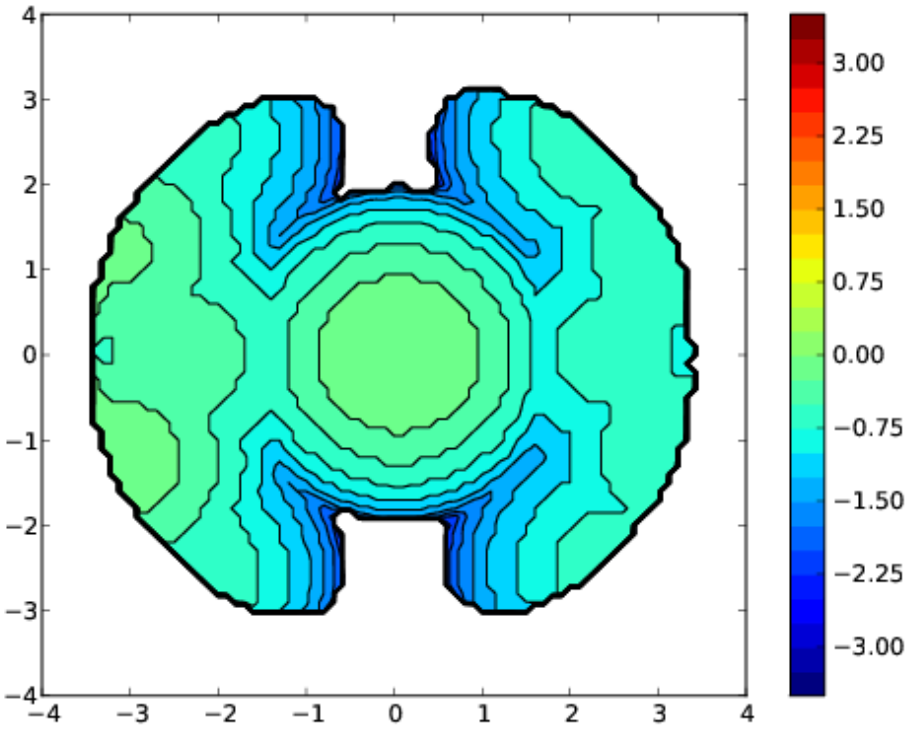
HOV



At 3.5 Å:

%V Free	%V Buried	% V Tot/V Ex
66.9	33.1	99.9

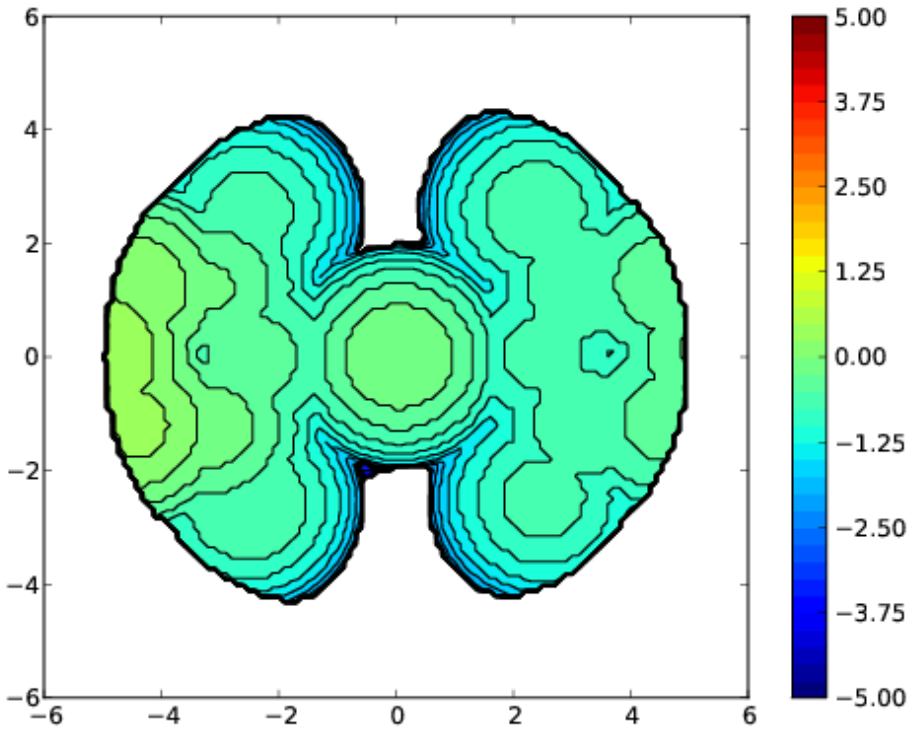
Quadrant	V f	V b	V t	%V f	%V b
SW	29.4	15.5	44.9	65.4	34.6
NW	29.7	15.2	44.9	66.2	33.8
NE	30.2	14.7	44.9	67.3	32.7
SE	30.8	14.0	44.9	68.7	31.3



At 5.0 Å:

%V Free	%V Buried	% V Tot/V Ex
64.6	35.4	99.9

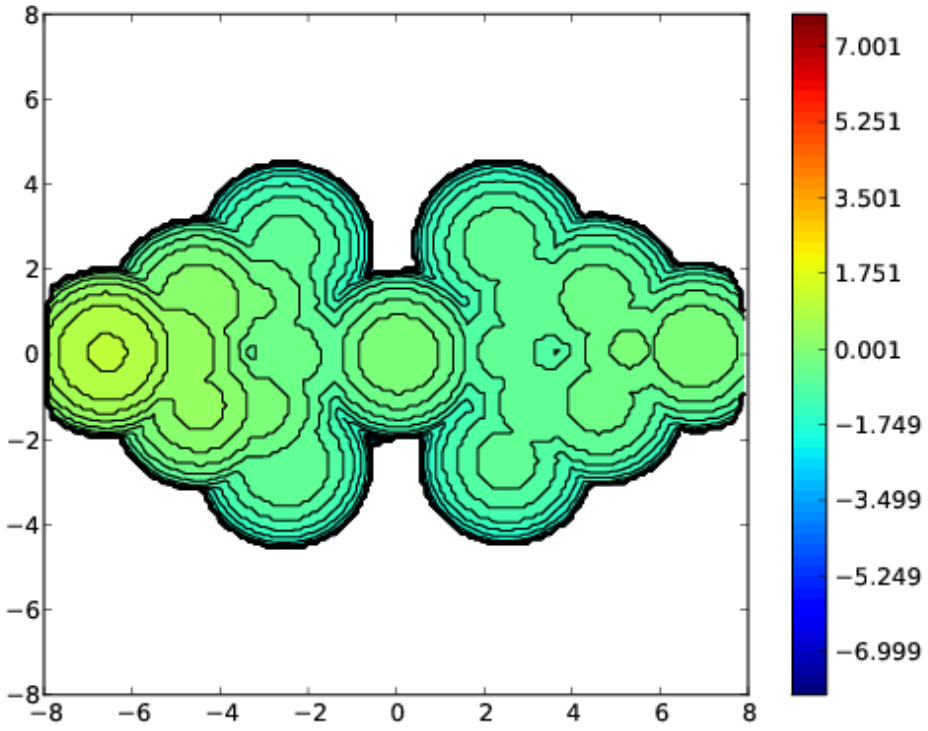
Quadrant	V f	V b	V t	%V f	%V b
SW	82.1	48.7	130.8	62.8	37.2
NW	83.6	47.2	130.8	63.9	36.1
NE	85.1	45.7	130.8	65.1	34.9
SE	87.4	43.5	130.8	66.8	33.2



At 8.0 Å:

%V Free	%V Buried	% V Tot/V Ex
83.4	**16.6**	100.0

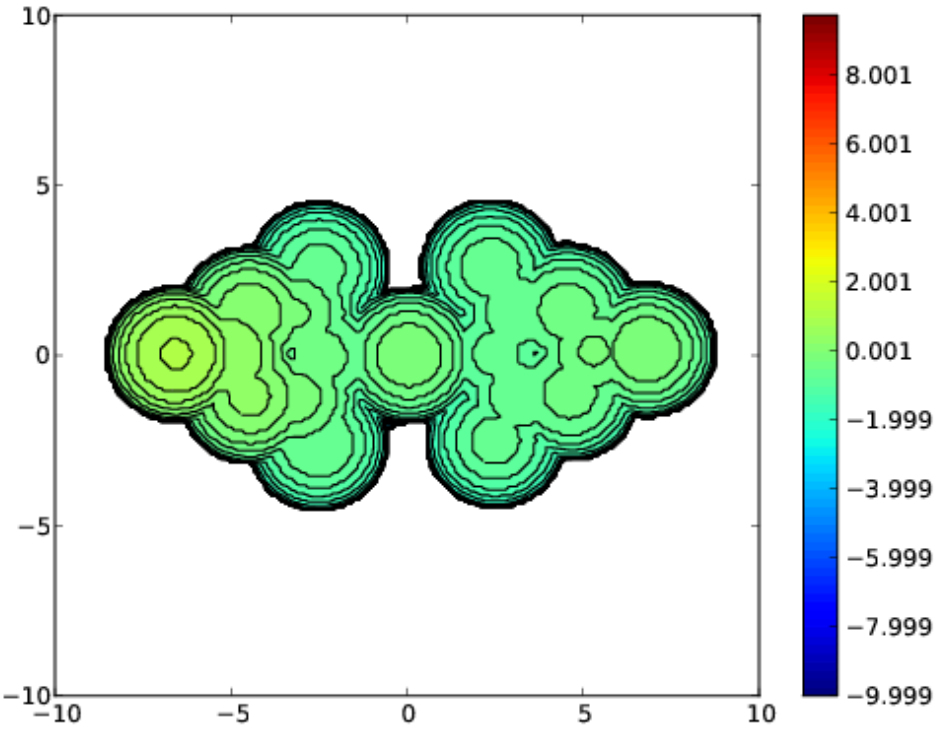
Quadrant	V f	V b	V t	%V f	%V b
SW	445.2	90.7	535.9	83.1	**16.9**
NW	446.4	89.5	535.9	83.3	**16.7**
NE	445.2	90.7	535.9	83.1	**16.9**
SE	451.3	84.7	535.9	84.2	**15.8**



At 10.0 Å:

%V Free	%V Buried	% V Tot/V Ex
91.3	8.7	100.0

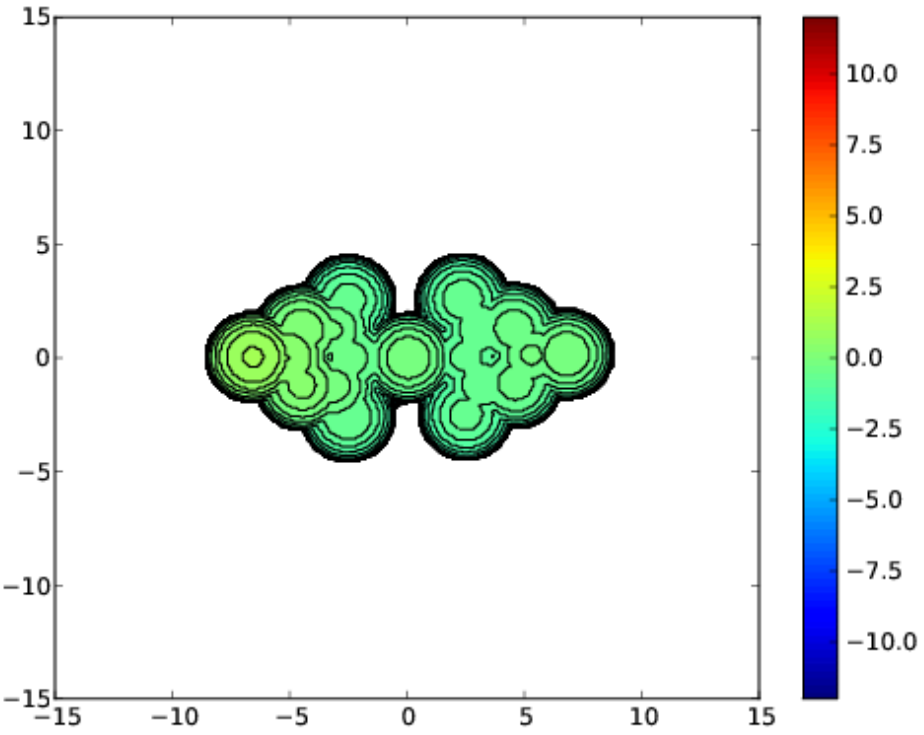
Quadrant	V f	V b	V t	%V f	%V b
SW	954.7	92.5	1047.2	91.2	8.8
NW	953.3	90.7	1044.0	91.3	8.7
NE	946.6	94.3	1040.9	90.9	9.1
SE	956.3	87.7	1044.0	91.6	8.4



At 12.0 Å:

%V Free	%V Buried	% V Tot/V Ex
95.0	5.0	100.0

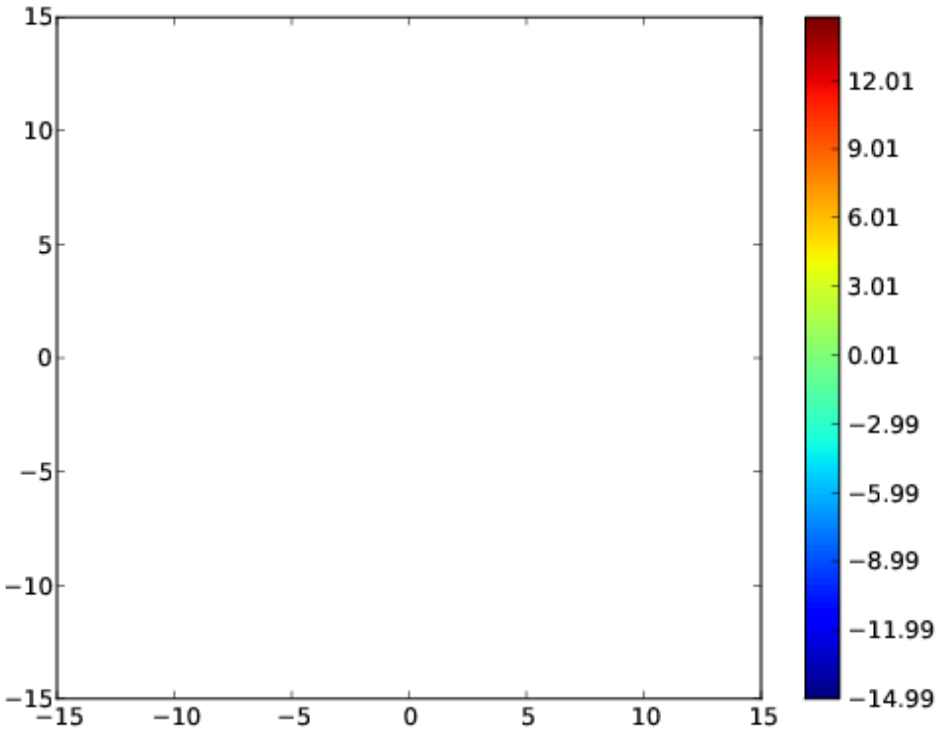
Quadrant	V f	V b	V t	%V f	%V b
SW	1717.1	92.0	1809.1	94.9	5.1
NW	1718.2	91.0	1809.1	95.0	5.0
NE	1714.4	94.7	1809.1	94.8	5.2
SE	1721.6	87.5	1809.1	95.2	4.8



At 15.0 Å:

%V Free	%V Buried	% V Tot/V Ex
100.0	0.0	100.0

Quadrant	V f	V b	V t	%V f	%V b
SW	3534.2	0.0	3534.2	100.0	0.0
NW	3527.1	0.0	3527.1	100.0	0.0
NE	3520.1	0.0	3520.1	100.0	0.0
SE	3527.1	0.0	3527.1	100.0	0.0

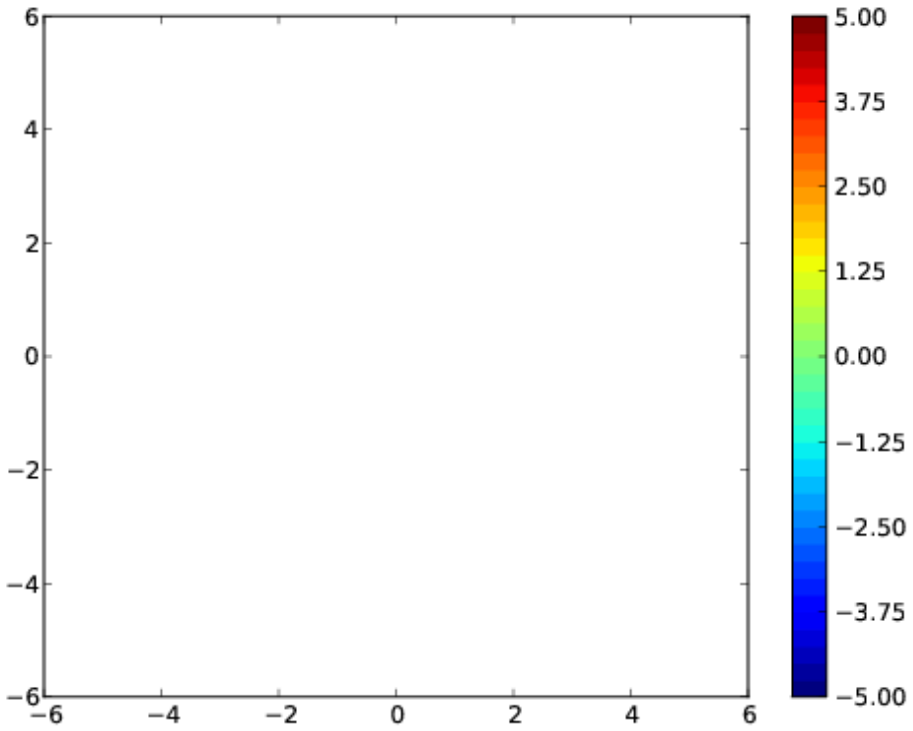


MOF, without the Ru catalyst:

At 3.5 and 5.0 Å:

%V Free	%V Buried	% V Tot/V Ex
100.0	0.0	99.9

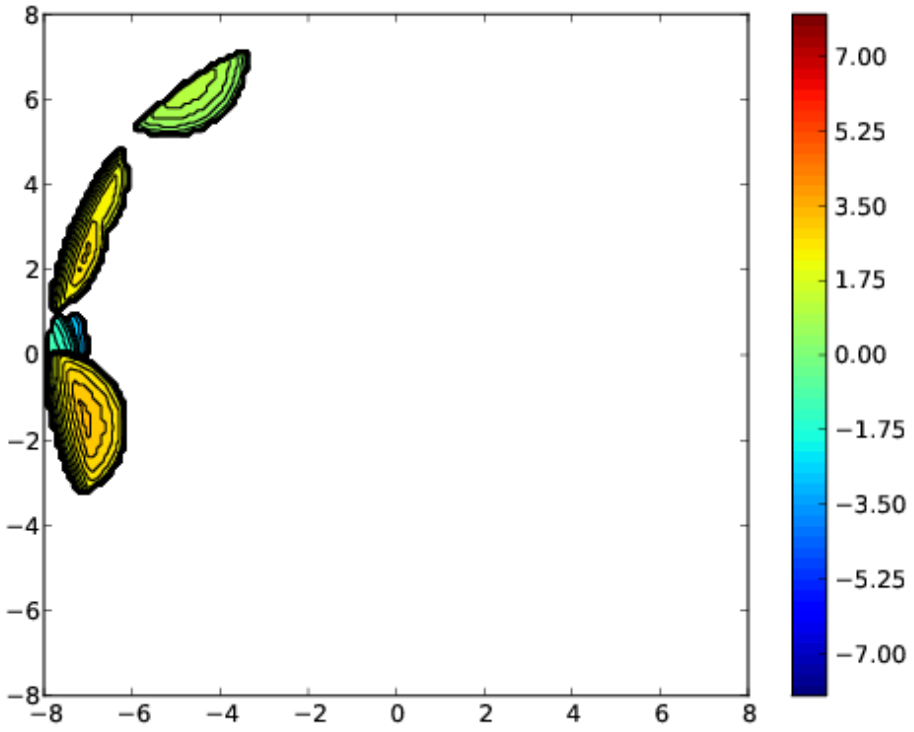
Quadrant	V f	V b	V t	%V f	%V b
SW	130.8	0.0	130.8	100.0	0.0
NW	130.8	0.0	130.8	100.0	0.0
NE	130.8	0.0	130.8	100.0	0.0
SE	130.8	0.0	130.8	100.0	0.0



At 8.0 Å:

%V Free	%V Buried	% V Tot/V Ex
99.1	0.9	100.0

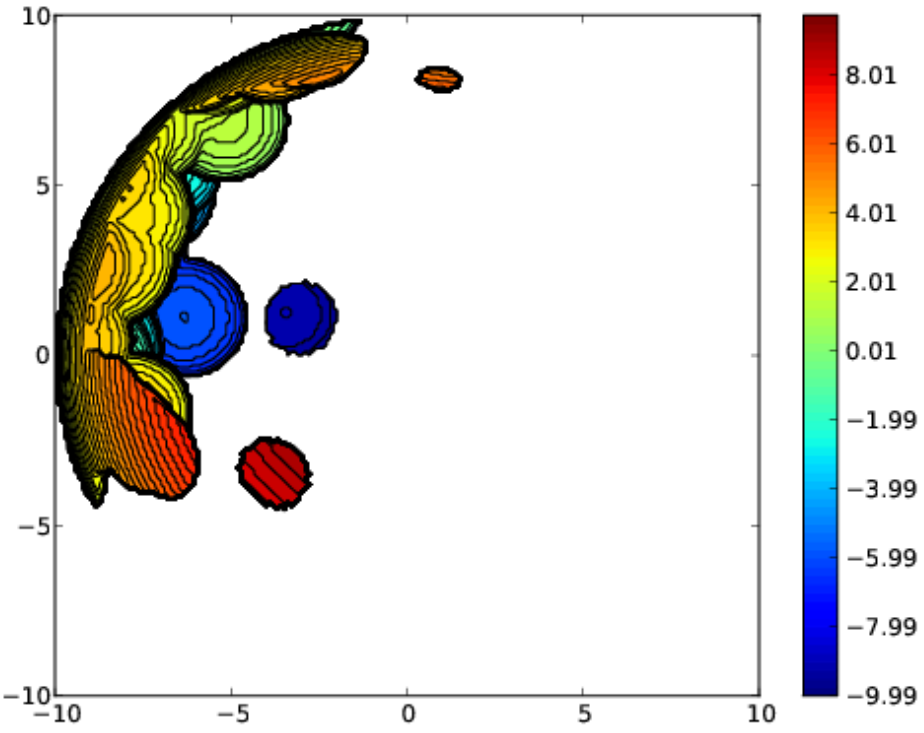
Quadrant	V f	V b	V t	%V f	%V b
SW	526.8	9.1	535.9	98.3	1.7
NW	525.2	10.7	535.9	98.0	2.0
NE	535.9	0.0	535.9	100.0	0.0
SE	535.9	0.0	535.9	100.0	0.0



At 10.0 Å:

%V Free	%V Buried	% V Tot/V Ex
95.0	5.0	100.0

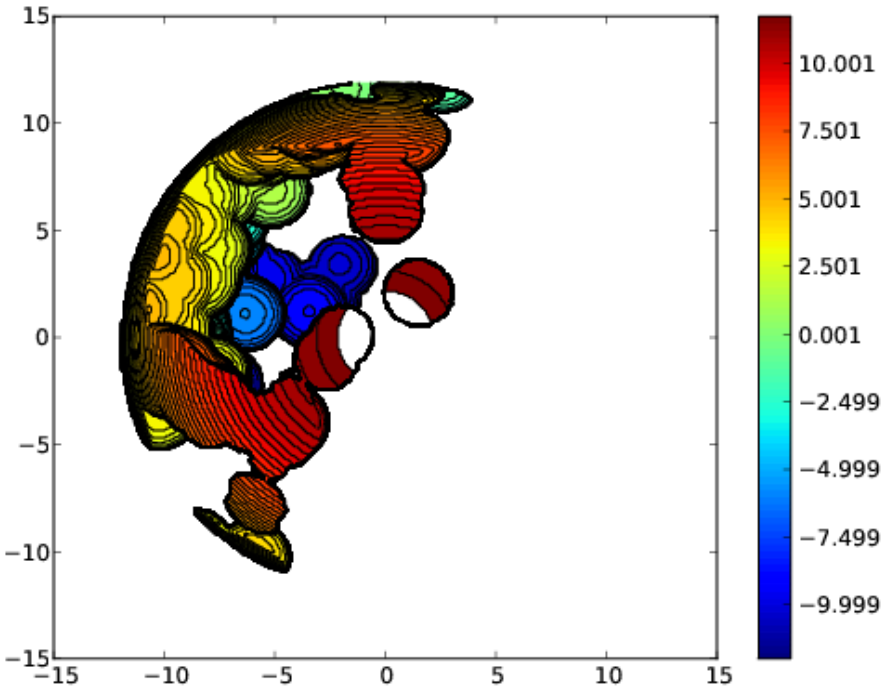
Quadrant	V f	V b	V t	%V f	%V b
SW	982.7	64.5	1047.2	93.8	6.2
NW	901.9	142.1	1044.0	86.4	13.6
NE	1040.8	0.1	1040.9	100.0	0.0
SE	1044.0	0.0	1044.0	100.0	0.0



At 12.0 Å:

%V Free	%V Buried	% V Tot/V Ex
89.8	10.2	100.0

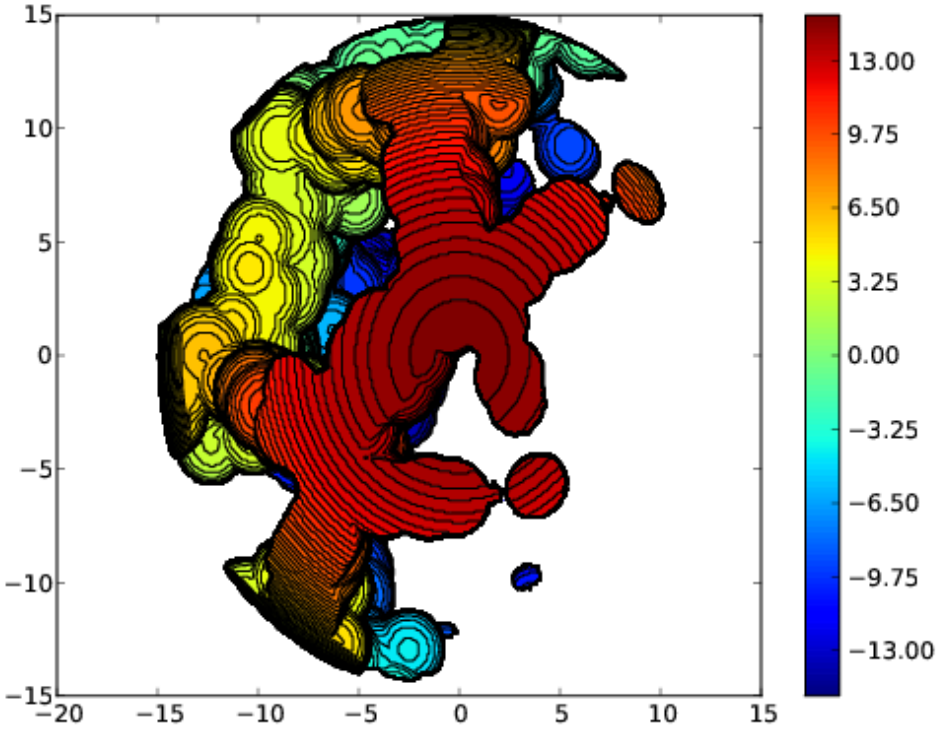
Quadrant	V f	V b	V t	%V f	%V b
SW	1578.4	230.8	1809.2	87.2	12.8
NW	1339.6	469.3	1808.9	74.1	25.9
NE	1774.2	34.4	1808.6	98.1	1.9
SE	1808.9	0.0	1808.9	100.0	0.0

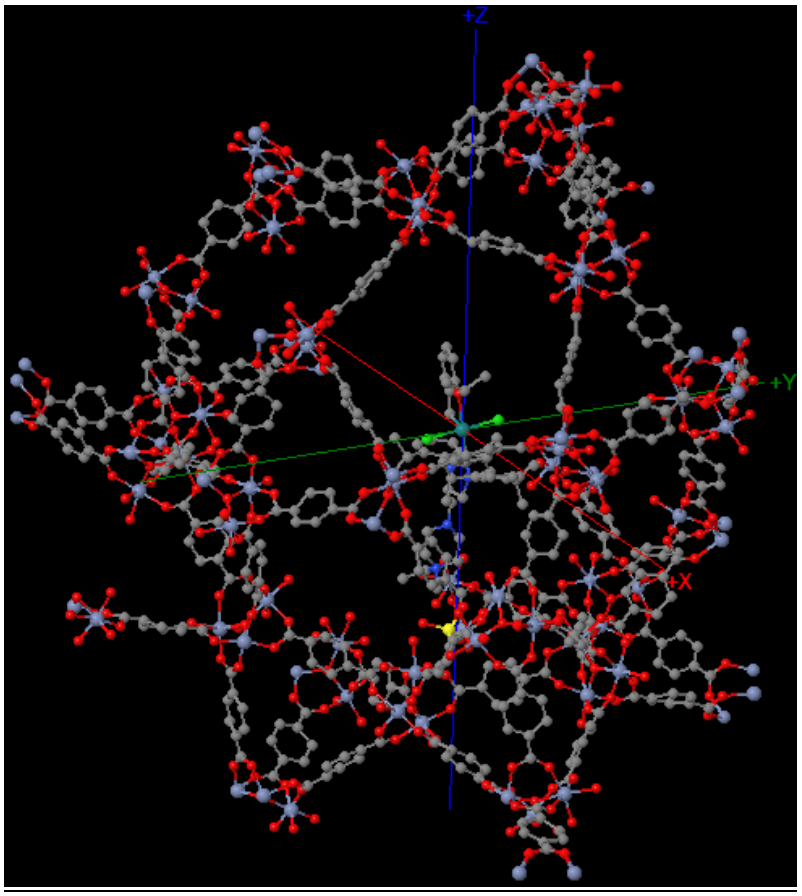


At 15.0 Å:

%V Free	%V Buried	% V Tot/V Ex
83.1	16.9	100.0

Quadrant	V f	V b	V t	%V f	%V b
SW	2638.6	895.7	3534.3	74.7	25.3
NW	2386.8	1147.5	3534.3	67.5	32.5
NE	3202.7	331.6	3534.3	90.6	9.4
SE	3519.3	15.0	3534.3	99.6	0.4

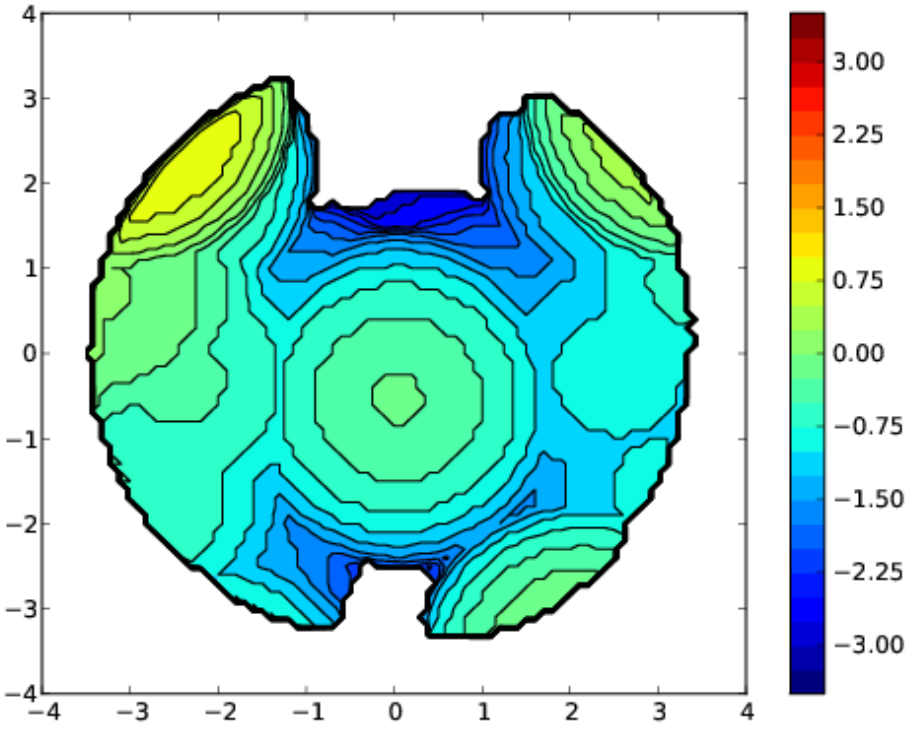



+Z
+Y
+X

At 3.5 Å:

%V Free	%V Buried	% V Tot/V Ex
67.1	32.9	99.9

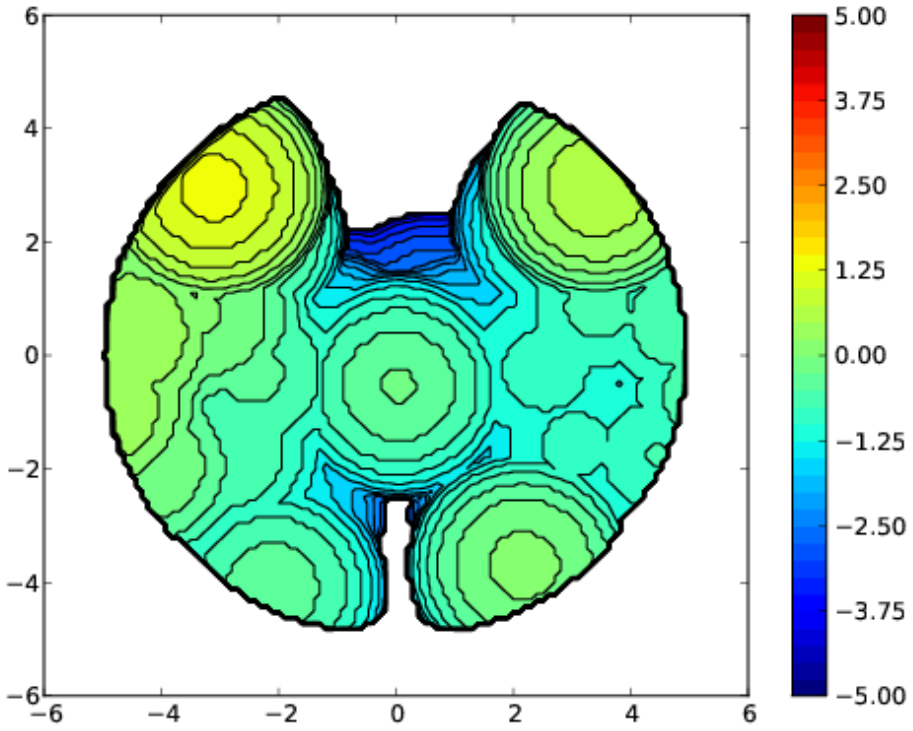
Quadrant	V f	V b	V t	%V f	%V b
SW	29.3	15.5	44.9	65.4	34.6
NW	28.3	16.6	44.9	63.1	36.9
NE	33.0	11.9	44.9	73.5	26.5
SE	29.8	15.1	44.9	66.4	33.6



At 5.0 Å:

%V Free	%V Buried	% V Tot/V Ex
60.4	39.6	99.9

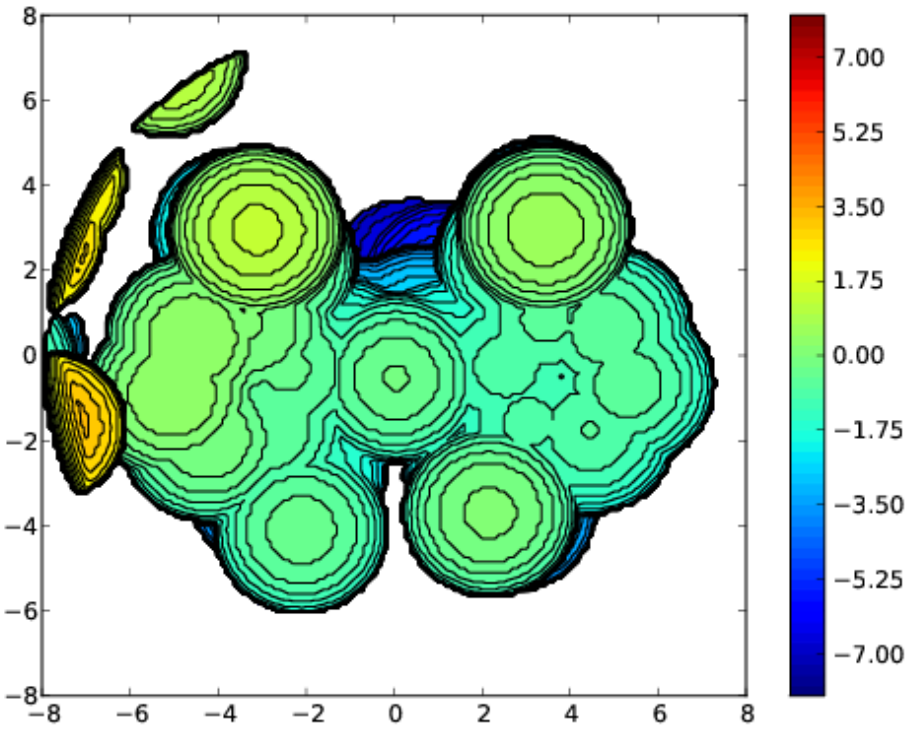
Quadrant	V f	V b	V t	%V f	%V b
SW	77.2	53.6	130.8	59.0	41.0
NW	74.6	56.2	130.8	57.0	43.0
NE	84.6	46.3	130.8	64.6	35.4
SE	79.9	50.9	130.8	61.1	38.9



At 8.0 Å:

%V Free	%V Buried	% V Tot/V Ex
75.2	24.8	100.0

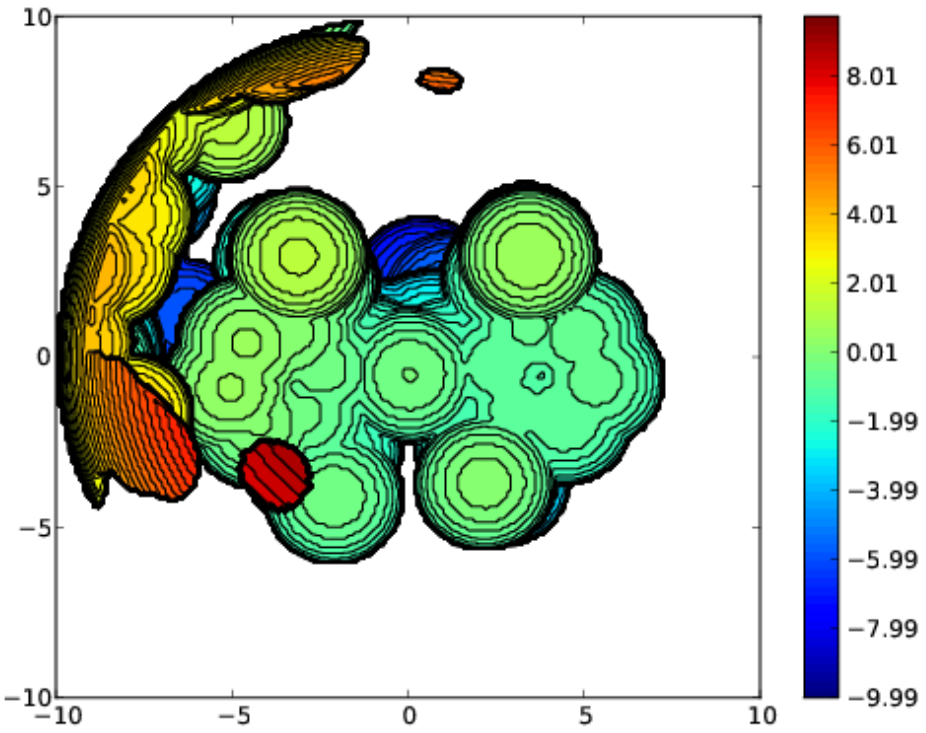
Quadrant	V f	V b	V t	%V f	%V b
SW	394.5	141.4	535.9	73.6	26.4
NW	414.1	121.8	535.9	77.3	22.7
NE	407.6	128.3	535.9	76.1	23.9
SE	395.8	140.1	535.9	73.9	26.1



At 10.0 Å:

%V Free	%V Buried	% V Tot/V Ex
81.6	18.4	100.0

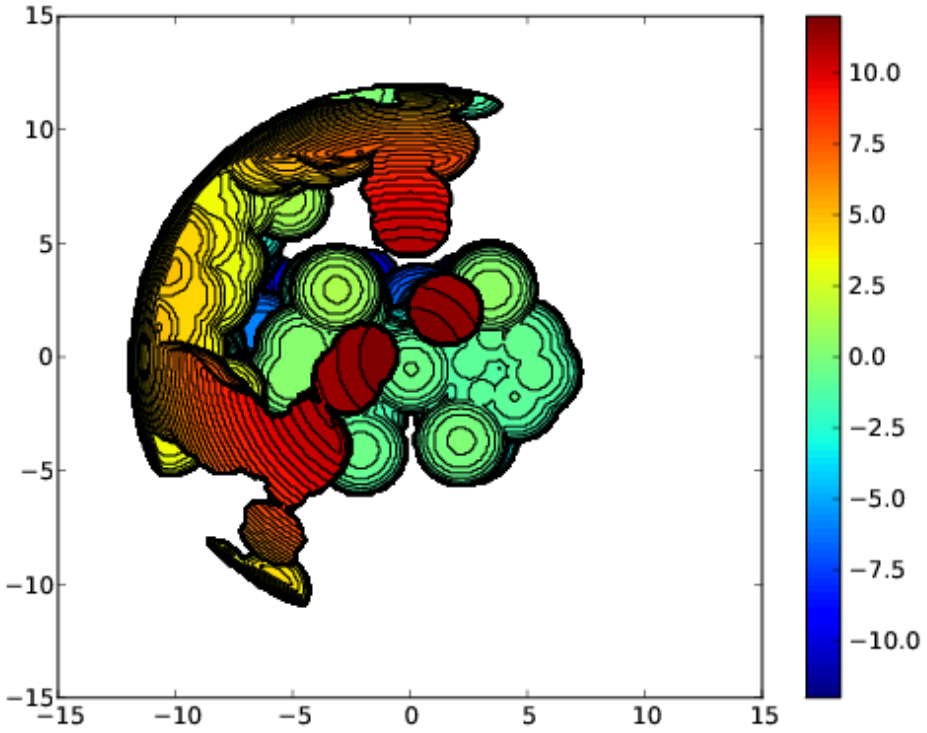
Quadrant	V f	V b	V t	%V f	%V b
SW	844.2	202.8	1046.9	80.6	19.4
NW	780.5	266.4	1046.9	74.6	25.4
NE	895.4	151.6	1046.9	85.5	14.5
SE	895.2	151.8	1046.9	85.5	14.5



At 12.0 Å:

%V Free	%V Buried	% V Tot/V Ex
81.4	18.6	100.0

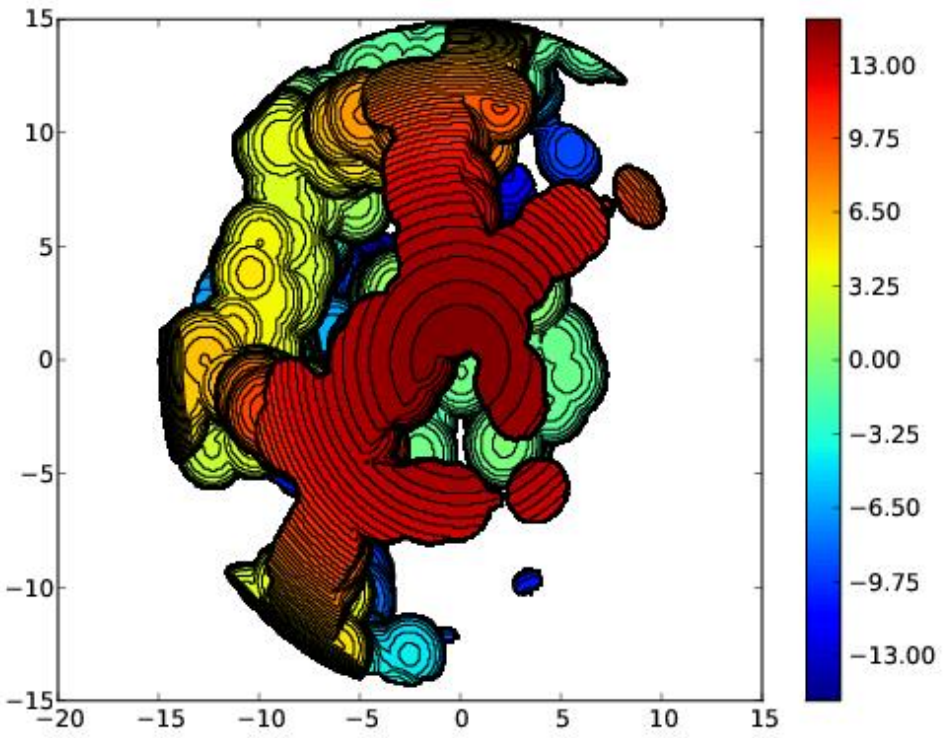
Quadrant	V f	V b	V t	%V f	%V b
SW	1439.1	370.3	1809.4	79.5	20.5
NW	1204.9	600.1	1805.0	66.8	33.2
NE	1583.8	216.7	1800.5	88.0	12.0
SE	1649.5	155.5	1805.0	91.4	8.6



At 15.0 Å:

%V Free	%V Buried	% V Tot/V Ex
78.7	21.3	100.0

Quadrant	V f	V b	V t	%V f	%V b
SW	2499.1	1035.3	3534.3	70.7	29.3
NW	2252.7	1281.6	3534.3	63.7	36.3
NE	3011.0	523.3	3534.3	85.2	14.8
SE	3364.1	170.2	3534.3	95.2	4.8

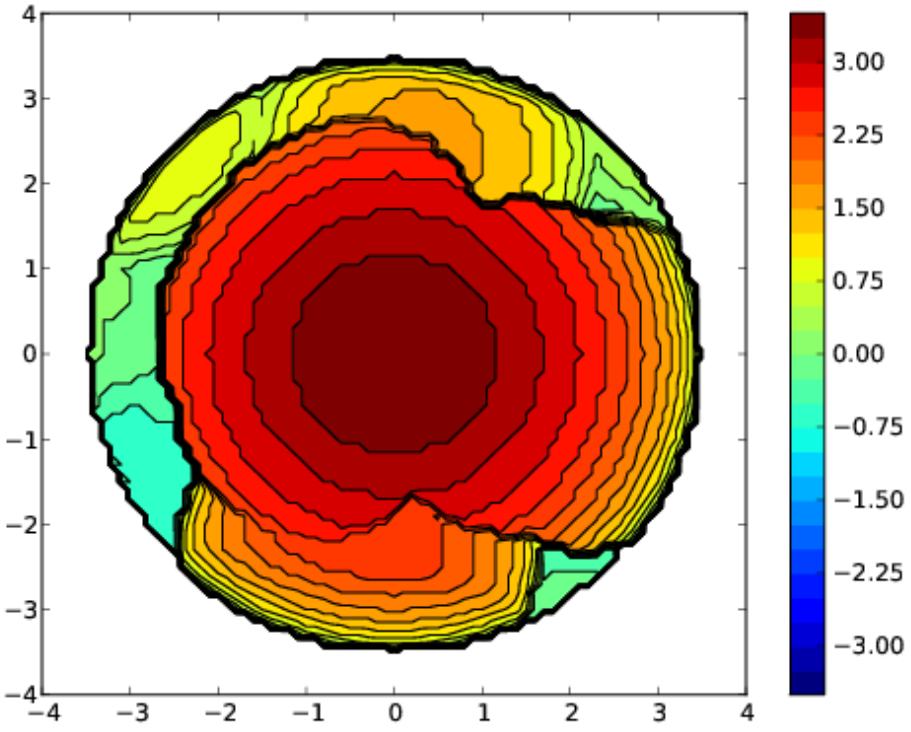


Including all the ruthenium catalyst and the MOF, as well:

At 3.5 Å:

%V Free	%V Buried	% V Tot/V Ex
8.9	**91.1**	99.9

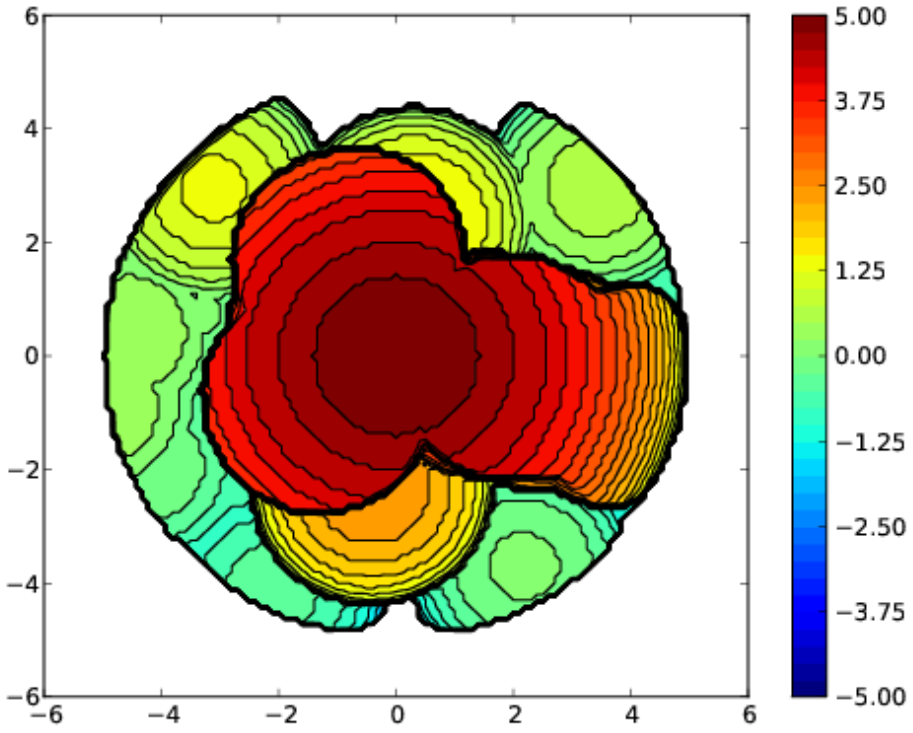
Quadrant	V f	V b	V t	%V f	%V b
SW	5.4	39.5	44.9	**11.9**	88.1
NW	5.7	39.2	44.9	**12.7**	87.3
NE	3.1	41.8	44.9	**6.9**	93.1
SE	1.9	43.0	44.9	**4.2**	95.8



At 5.0 Å:

%V Free	%V Buried	% V Tot/V Ex
25.4	74.6	99.9

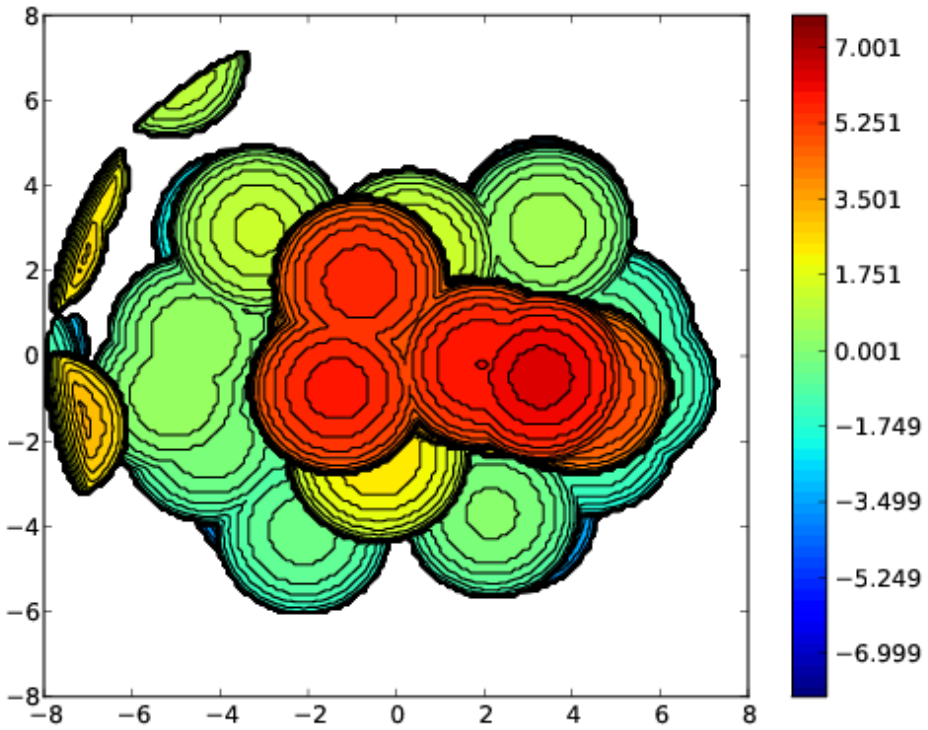
Quadrant	V f	V b	V t	%V f	%V b
SW	36.0	94.9	130.8	27.5	72.5
NW	35.1	95.7	130.8	26.8	73.2
NE	33.9	96.9	130.8	25.9	74.1
SE	28.1	102.8	130.8	21.4	78.6



At 8.0 Å:

%V Free	%V Buried	% V Tot/V Ex
63.7	36.3	100.0

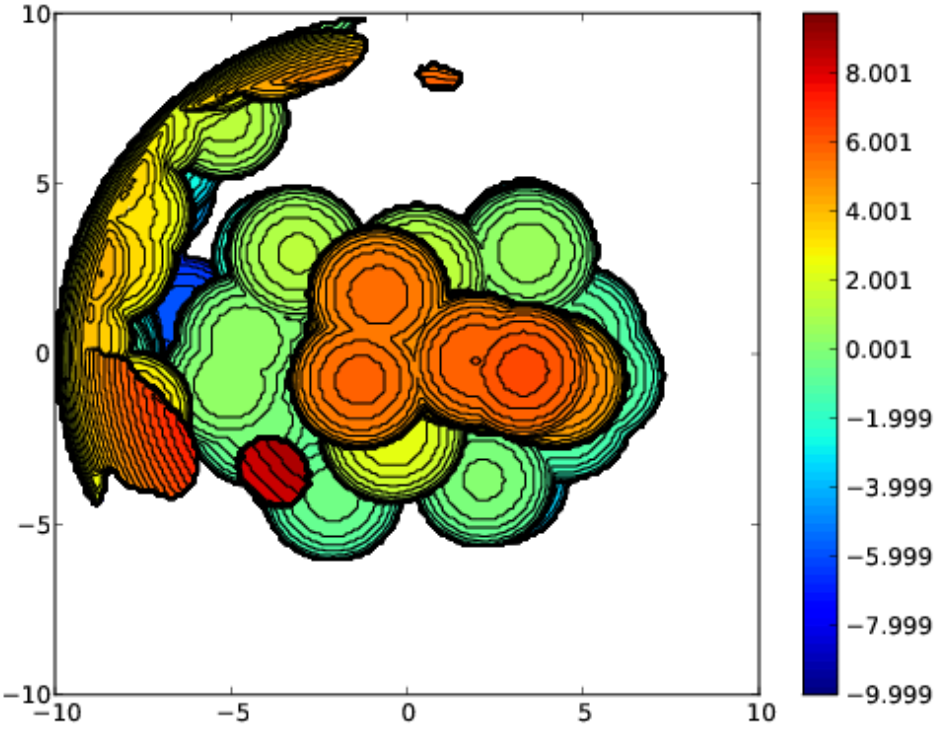
Quadrant	V f	V b	V t	%V f	%V b
SW	345.2	190.7	535.9	64.4	35.6
NW	365.3	170.5	535.8	68.2	31.8
NE	342.1	193.5	535.6	63.9	36.1
SE	312.1	223.7	535.8	58.3	41.7



At 10.0 Å:

%V Free	%V Buried	% V Tot/V Ex
75.7	24.3	100.0

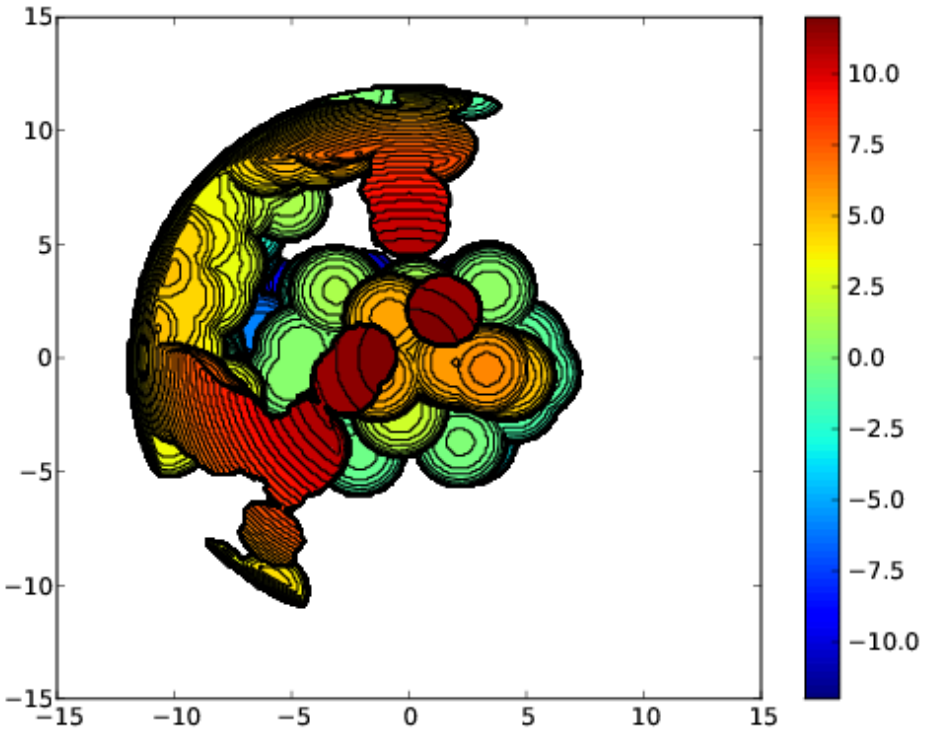
Quadrant	V f	V b	V t	%V f	%V b
SW	794.9	252.0	1046.9	75.9	24.1
NW	731.8	315.2	1046.9	69.9	30.1
NE	830.1	216.8	1046.9	79.3	20.7
SE	811.6	235.4	1046.9	77.5	22.5



At 12.0 Å:

%V Free	%V Buried	% V Tot/V Ex
78.0	22.0	100.0

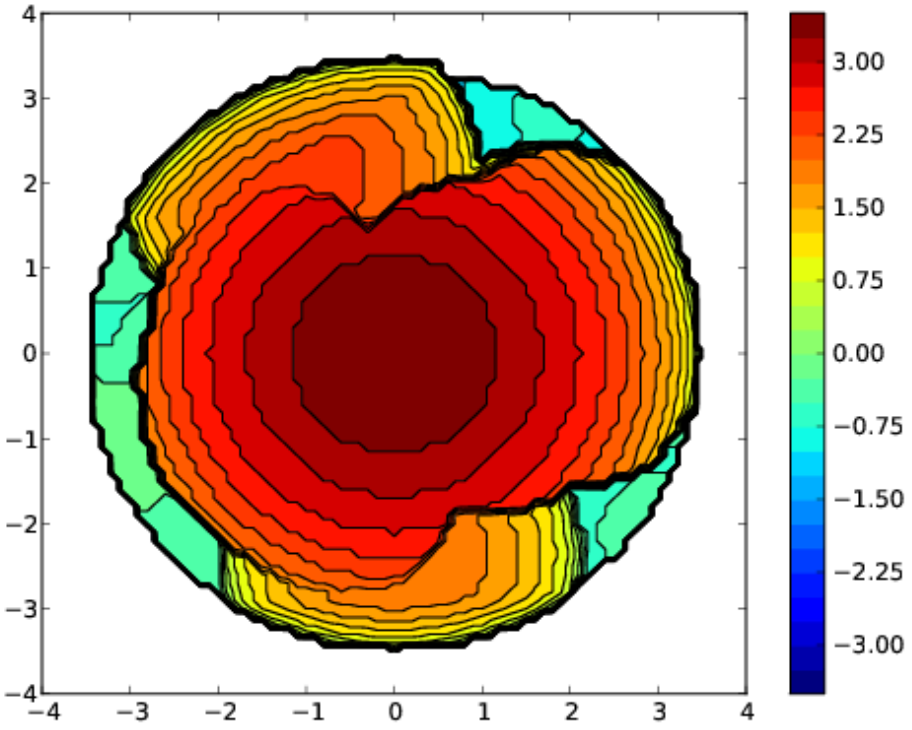
Quadrant	V f	V b	V t	%V f	%V b
SW	1389.5	419.6	1809.1	76.8	23.2
NW	1157.7	651.4	1809.1	64.0	36.0
NE	1525.7	283.5	1809.1	84.3	15.7
SE	1570.3	238.8	1809.1	86.8	13.2



AquaMet^{TM}, including all atoms:

%V Free	%V Buried	% V Tot/V Ex
9.7	90.3	99.9

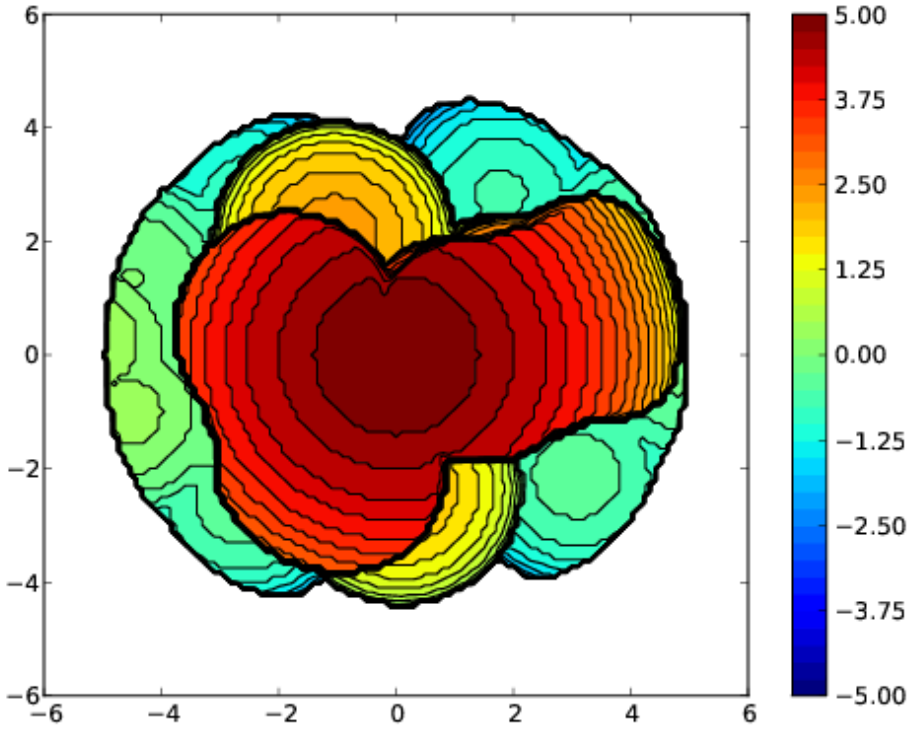
Quadrant	V f	V b	V t	%V f	%V b
SW	5.3	39.5	44.9	11.9	88.1
NW	3.6	41.3	44.9	7.9	92.1
NE	4.2	40.7	44.9	9.3	90.7
SE	4.3	40.5	44.9	9.7	90.3



At 5.0 Å:

%V Free	%V Buried	% V Tot/V Ex
30.0	70.0	99.9

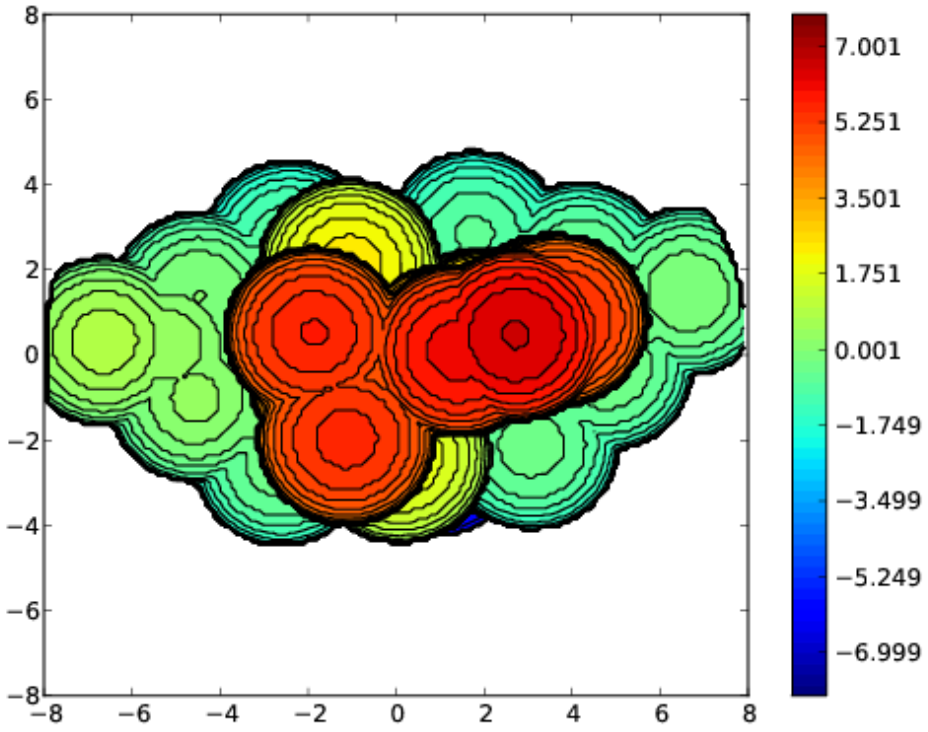
Quadrant	V f	V b	V t	%V f	%V b
SW	37.6	93.2	130.8	28.7	71.3
NW	39.1	91.8	130.8	29.9	70.1
NE	35.5	95.3	130.8	27.2	72.8
SE	44.6	86.2	130.8	34.1	65.9



At 8.0 Å:

%V Free	%V Buried	% V Tot/V Ex
70.1	29.9	100.0

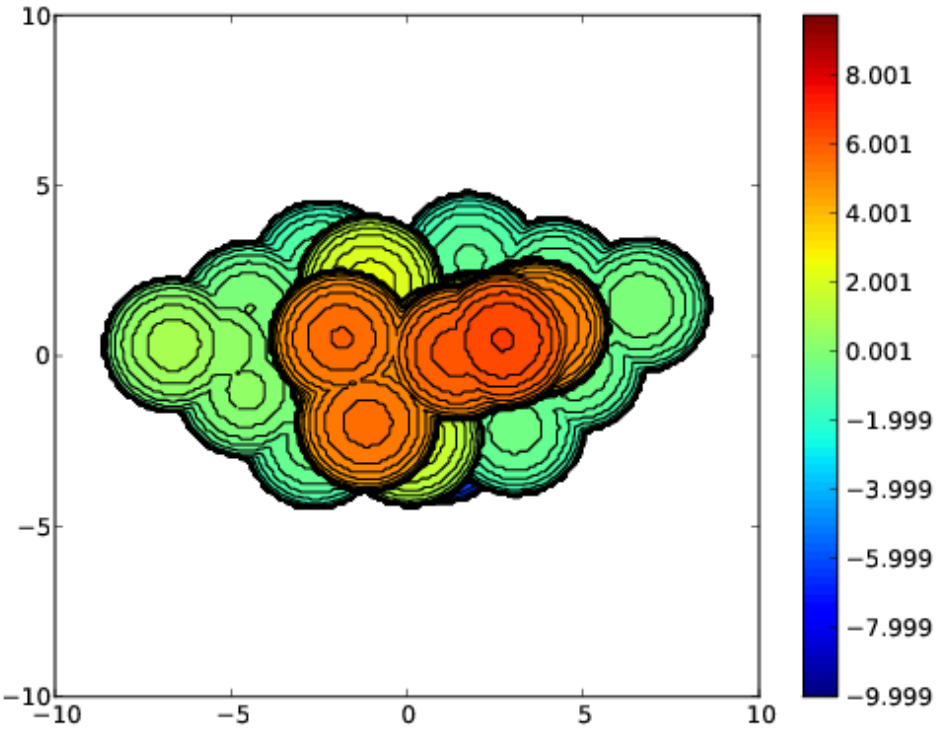
Quadrant	V f	V b	V t	%V f	%V b
SW	386.2	149.7	535.9	72.1	27.9
NW	388.6	147.2	535.8	72.5	27.5
NE	345.2	190.4	535.6	64.4	35.6
SE	381.6	154.2	535.8	71.2	28.8



At 10.0 Å:

%V Free	%V Buried	% V Tot/V Ex
83.2	16.8	100.0

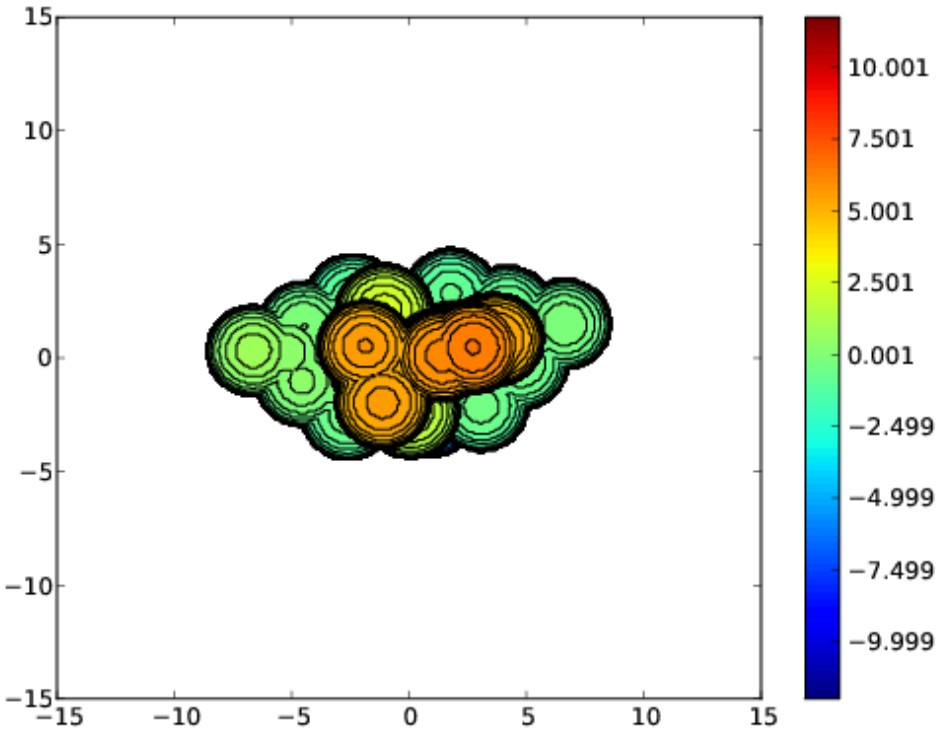
Quadrant	V f	V b	V t	%V f	%V b
SW	883.7	163.3	1047.0	84.4	15.6
NW	893.8	153.0	1046.8	85.4	14.6
NE	838.6	207.9	1046.5	80.1	19.9
SE	867.0	179.7	1046.8	82.8	17.2



At 12.0 Å:

%V Free	%V Buried	% V Tot/V Ex
89.6	**10.4**	100.0

Quadrant	V f	V b	V t	%V f	%V b
SW	1633.9	175.3	1809.2	90.3	**9.7**
NW	1653.6	155.3	1808.9	91.4	**8.6**
NE	1591.8	216.8	1808.6	88.0	**12.0**
SE	1601.5	207.4	1808.9	88.5	**11.5**

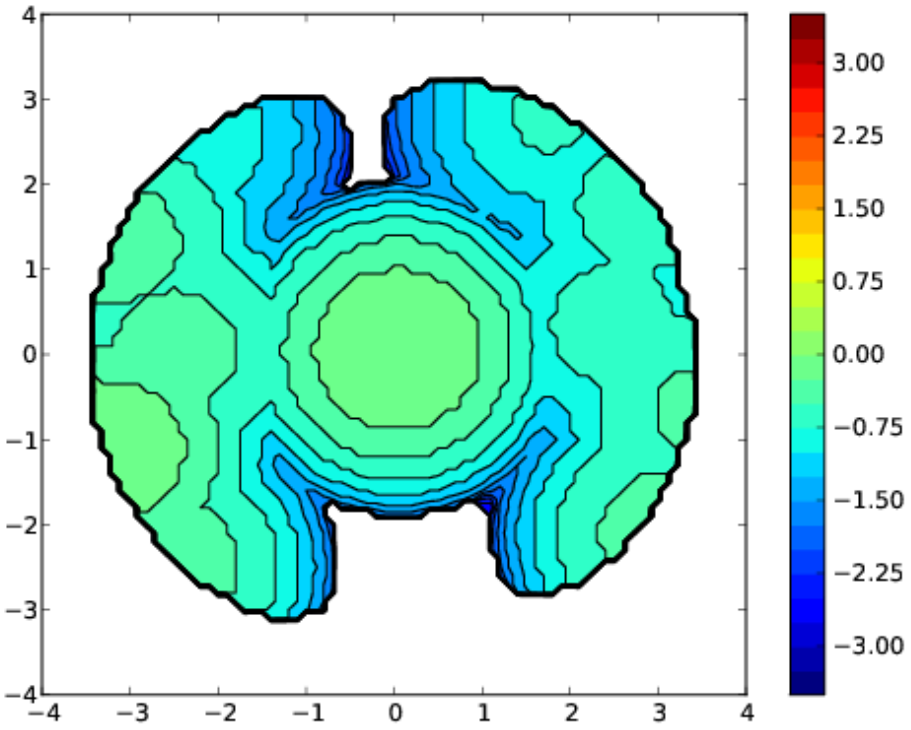


AquaMet™

At 3.5 Å:

%V Free	%V Buried	% V Tot/V Ex
66.7	33.3	99.9

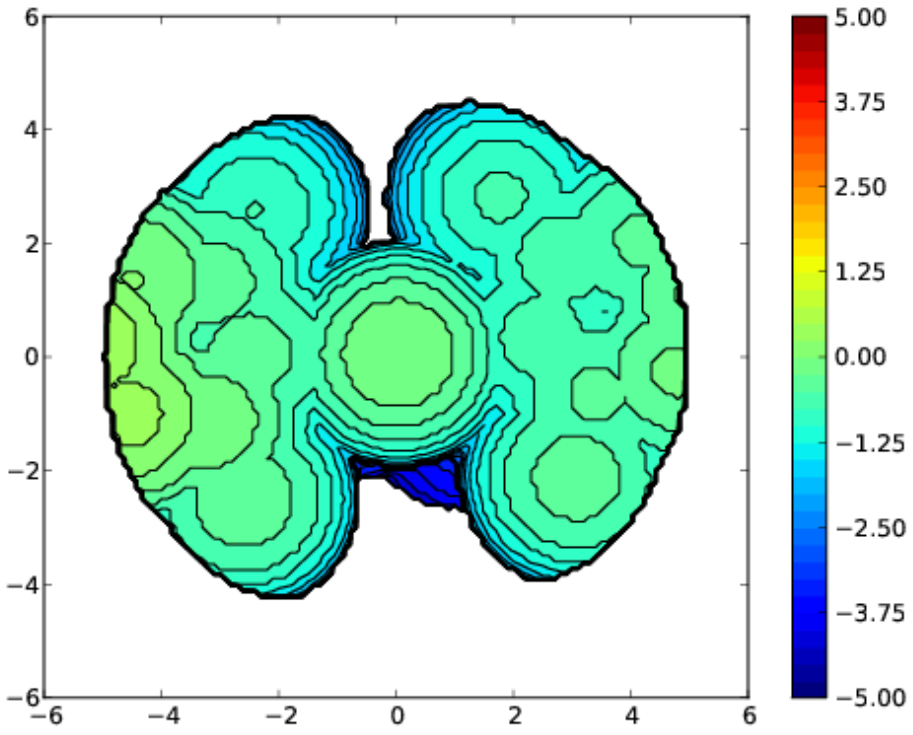
Quadrant	V f	V b	V t	%V f	%V b
SW	29.2	15.7	44.9	65.0	35.0
NW	29.9	15.0	44.9	66.6	33.4
NE	29.2	15.6	44.9	65.2	34.8
SE	31.4	13.4	44.9	70.0	30.0



At 5.0 Å:

%V Free	%V Buried	% V Tot/V Ex
64.4	35.6	99.9

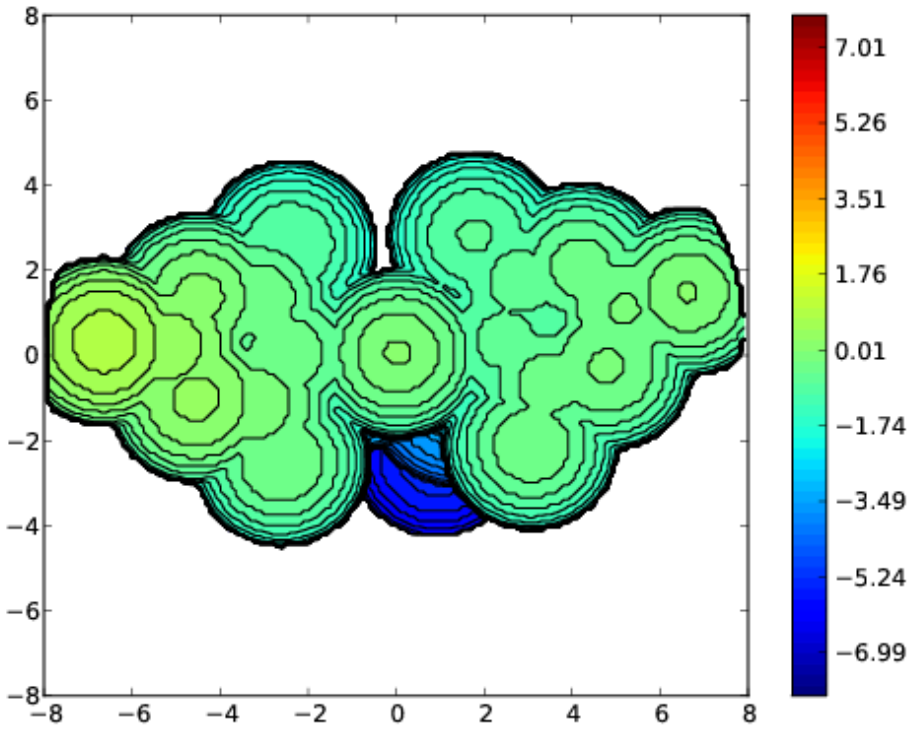
Quadrant	V f	V b	V t	%V f	%V b
SW	82.2	48.6	130.8	62.9	37.1
NW	83.9	46.9	130.8	64.2	35.8
NE	81.4	49.5	130.8	62.2	37.8
SE	89.5	41.4	130.8	68.4	31.6



At 8.0 Å:

%V Free	%V Buried	% V Tot/V Ex
81.3	**18.7**	100.0

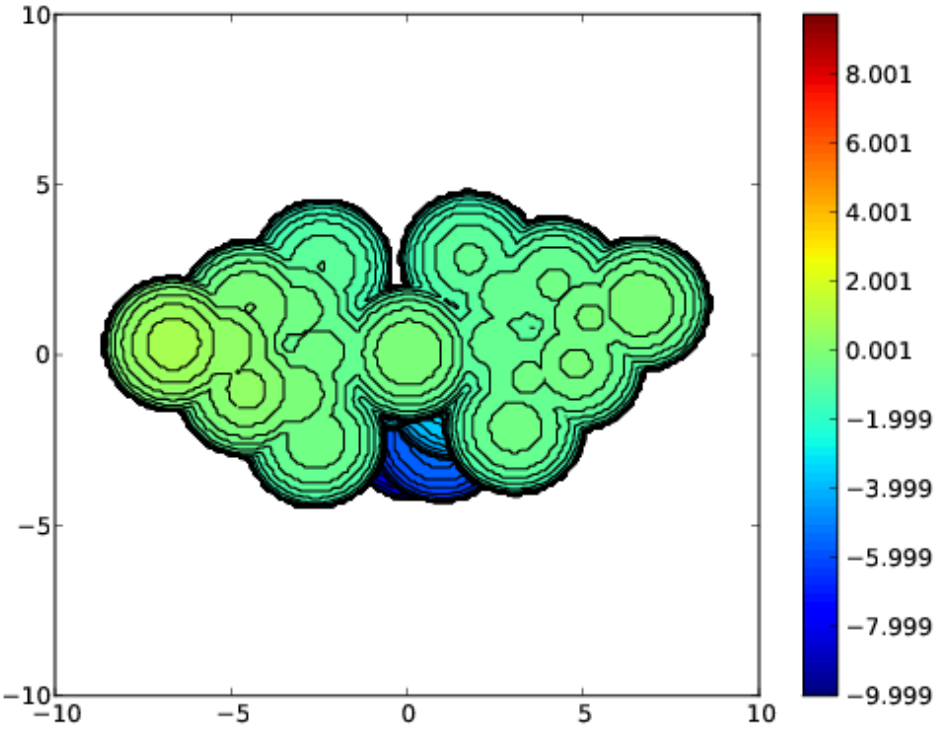
Quadrant	V f	V b	V t	%V f	%V b
SW	443.1	93.0	536.1	82.7	**17.3**
NW	439.9	94.2	534.1	82.4	**17.6**
NE	416.9	115.3	532.2	78.3	**21.7**
SE	437.3	96.8	534.1	81.9	**18.1**



At 10.0 Å:

%V Free	%V Buried	% V Tot/V Ex
89.0	**11.0**	100.0

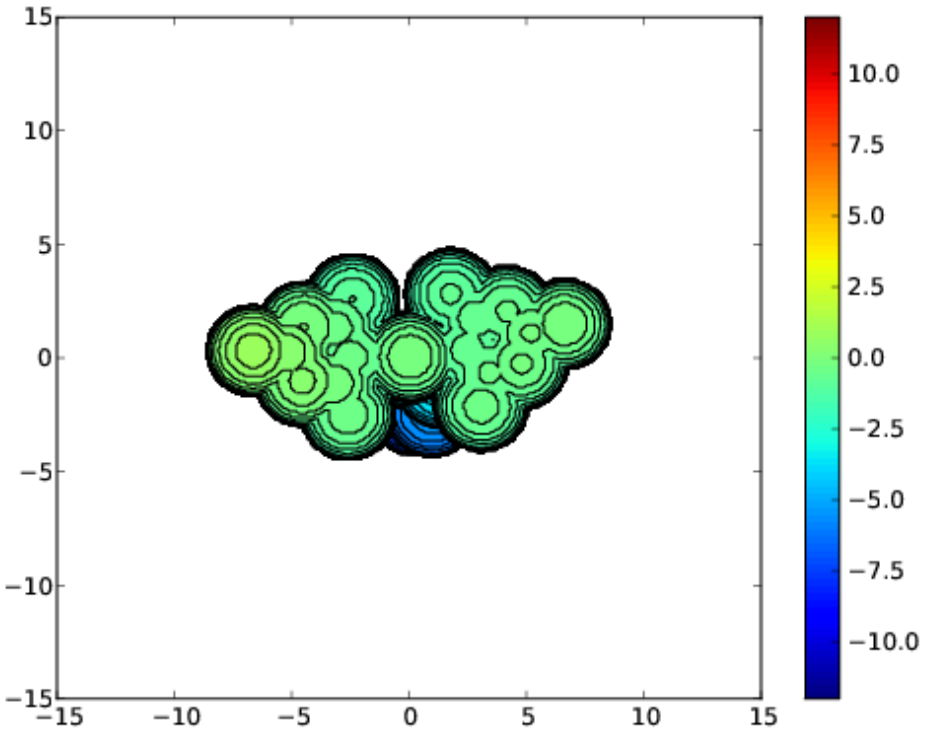
Quadrant	V f	V b	V t	%V f	%V b
SW	941.0	106.1	1047.0	89.9	**10.1**
NW	946.5	100.3	1046.8	90.4	**9.6**
NE	913.2	133.4	1046.5	87.3	**12.7**
SE	924.6	122.2	1046.8	88.3	**11.7**



At 12.0 Å:

%V Free	%V Buried	% V Tot/V Ex
92.9	7.1	100.0

Quadrant	V f	V b	V t	%V f	%V b
SW	1691.2	118.0	1809.1	93.5	6.5
NW	1706.5	102.6	1809.1	94.3	5.7
NE	1666.8	142.3	1809.1	92.1	7.9
SE	1659.3	149.8	1809.1	91.7	8.3



At 15.0 Å:

%V Free	%V Buried	% V Tot/V Ex
96.3	3.7	100.0

Quadrant	V f	V b	V t	%V f	%V b
SW	3414.6	119.7	3534.3	96.6	3.4
NW	3431.0	102.6	3533.6	97.1	2.9
NE	3388.6	144.3	3532.9	95.9	4.1
SE	3376.7	156.8	3533.6	95.6	4.4

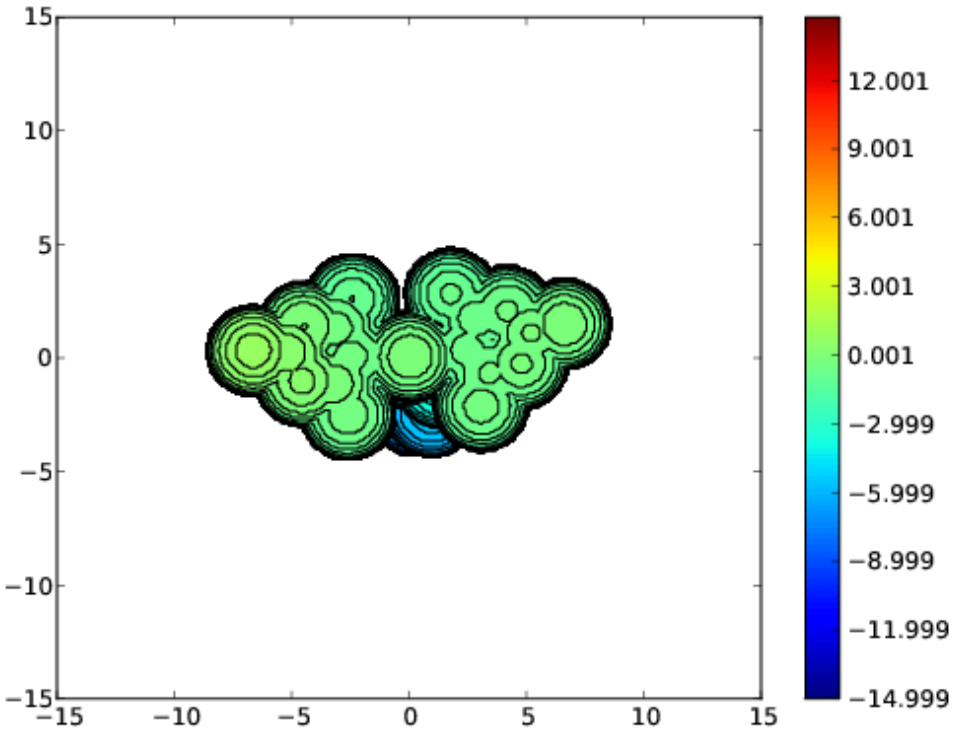


Table S1 NCI plots of the truncated MOF in combination with the Precat. Previously optimised geometries have been evaluated using the promolecular approach suitable for large structures.

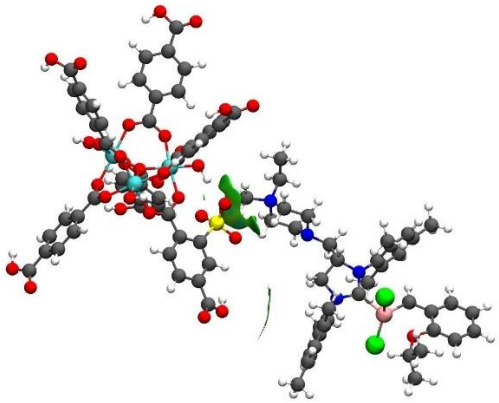
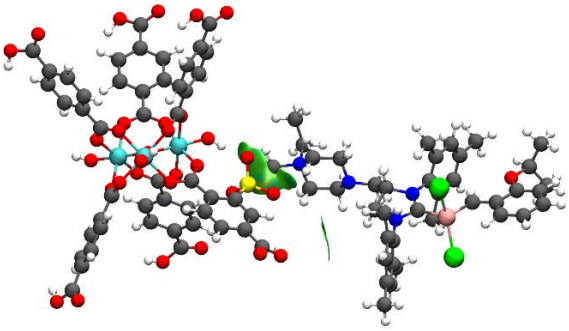
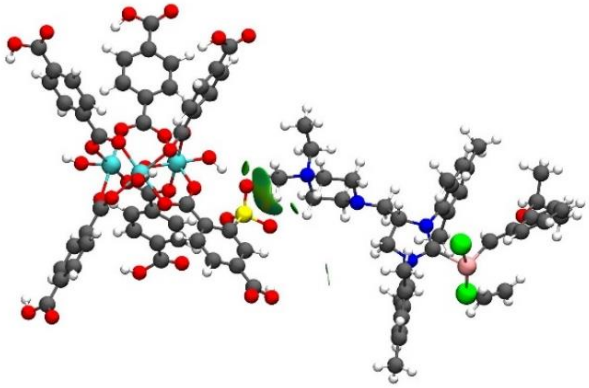
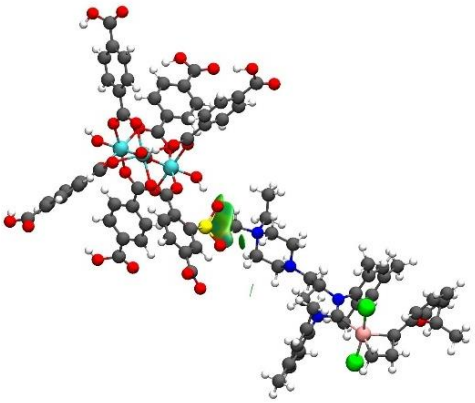
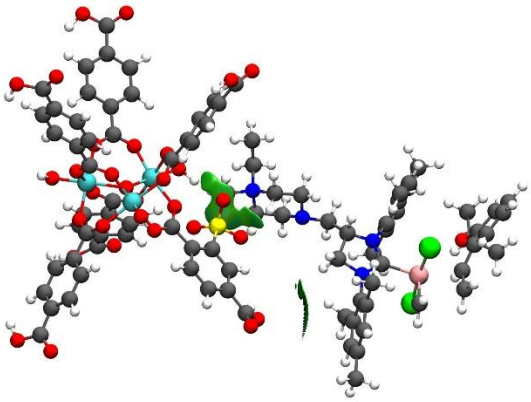
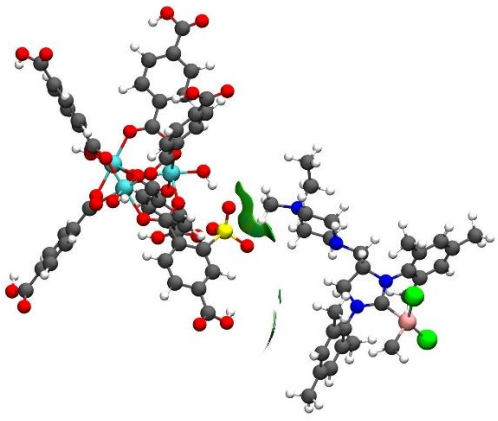
Precat	**Act**
	
CI1	**MCy**
	
CI2	**I14e**
	

Figure S1 NCIplots

Computational Coordinates

Table S2 Coordinates data set, absolute energies (a.u.) for all DFT optimized neutral complexes.

Precat				TS_Open			
75				75			
precat SCF Done: -2403.24318273 A.U.				ts_open SCF Done: -2403.20586043 A.U.			
Ru	0.151733	0.458008	-0.007440	Ru	0.217673	0.504668	-0.183830
C	0.254906	-1.504528	-0.015556	C	0.813487	-1.327998	0.035166
N	1.464220	-2.178459	-0.020183	N	2.143026	-1.697928	-0.051090
N	-0.722276	-2.473184	-0.049902	N	0.088464	-2.492060	0.171349
C	-0.183916	-3.845632	0.034754	C	0.949950	-3.684622	0.301826
C	1.314556	-3.632101	-0.215360	C	2.312892	-3.158994	-0.162390
H	-0.663588	-4.502865	-0.719736	H	0.564896	-4.514084	-0.325535
H	-0.389749	-4.281543	1.039635	H	0.966888	-4.039744	1.358525
H	1.959489	-4.195124	0.490599	H	3.155082	-3.505980	0.470342
H	1.614181	-3.917960	-1.249498	H	2.536120	-3.443030	-1.216111
C	-2.146321	-2.309062	-0.013834	C	-1.325008	-2.661854	0.348717
C	2.785802	-1.605148	-0.003748	C	3.308318	-0.850097	-0.107781
C	3.465329	-1.337784	-1.223055	C	3.875936	-0.491678	-1.359917
C	4.757001	-0.774507	-1.156338	C	5.028345	0.321837	-1.356759
C	5.404507	-0.522148	0.066777	C	5.649890	0.741672	-0.166290
C	4.742655	-0.896593	1.253935	C	5.112146	0.288612	1.055087
C	3.450029	-1.453845	1.247602	C	3.956838	-0.512261	1.112561
C	2.898576	-1.728115	-2.567963	C	3.339896	-1.019956	-2.669985
H	5.277978	-0.543200	-2.100964	H	5.460573	0.621685	-2.326400
C	6.770959	0.124489	0.111650	C	6.856491	1.652822	-0.194128
H	5.254046	-0.765486	2.222597	H	5.610008	0.564286	2.000004
C	2.815337	-1.913040	2.537728	C	3.440718	-1.007785	2.442372
H	1.794071	-1.713326	-2.578825	H	2.233328	-1.041883	-2.694923
H	3.247801	-2.747973	-2.847933	H	3.716138	-2.050585	-2.859598
H	3.244076	-1.036165	-3.360958	H	3.680641	-0.392064	-3.516726
H	7.309577	0.014753	-0.851158	H	7.427775	1.549868	-1.138897
H	7.403295	-0.309419	0.913591	H	7.544320	1.448415	0.651748
H	6.688399	1.214110	0.320490	H	6.548397	2.718674	-0.112199
H	3.548366	-1.882217	3.367754	H	4.175369	-0.810406	3.247643
H	2.432875	-2.952829	2.459202	H	3.234163	-2.098815	2.428345
H	1.954971	-1.263132	2.805832	H	2.493423	-0.490577	2.703770
C	-2.858770	-2.257139	-1.239323	C	-2.132605	-2.942133	-0.784290
C	-2.814364	-2.252852	1.236375	C	-1.871419	-2.632482	1.657531
C	-4.262606	-2.146306	-1.187749	C	-3.505847	-3.179246	-0.577055
C	-4.219756	-2.143555	1.231639	C	-3.252338	-2.874989	1.808613
C	-4.963496	-2.094254	0.034755	C	-4.087599	-3.148774	0.707575
C	-6.474304	-2.017183	0.061021	C	-5.570945	-3.382988	0.887999
H	-4.824424	-2.094349	-2.135704	H	-4.141348	-3.398208	-1.452027
C	-2.041103	-2.251116	2.534604	C	-1.008727	-2.300534	2.854043
H	-4.748316	-2.087708	2.198373	H	-3.686993	-2.845845	2.821970
C	-2.125238	-2.269894	-2.559887	C	-1.541673	-2.961685	-2.173802
H	-1.428316	-1.407237	-2.639859	H	-1.126817	-1.966531	-2.448275

H	-2.834613	-2.225679	-3.409316	H	-2.303885	-3.244269	-2.926207
H	-1.510155	-3.187415	-2.681828	H	-0.702453	-3.685249	-2.255806
H	-1.445744	-3.180371	2.665593	H	-0.501983	-1.319939	2.725857
H	-2.724307	-2.169840	3.402422	H	-0.208701	-3.055148	3.014178
H	-1.323660	-1.402967	2.575521	H	-1.614285	-2.258478	3.780235
H	-6.843561	-1.512951	0.976987	H	-5.835713	-3.537124	1.952941
H	-6.925264	-3.034239	0.044673	H	-5.915976	-4.269481	0.315860
H	-6.872836	-1.472296	-0.818860	H	-6.158841	-2.513771	0.520399
C	-1.667430	0.782448	0.014408	C	-1.561035	0.420585	0.206019
Cl	0.598285	0.673879	-2.315455	Cl	0.167580	0.408181	-2.529104
Cl	0.650646	0.717999	2.287413	Cl	1.152061	1.436872	1.754750
O	0.087510	2.761148	-0.017944	O	-1.302597	3.008355	0.481858
C	1.305614	3.585856	-0.049285	C	-1.086777	4.231404	1.235462
C	1.414925	4.378743	-1.351629	C	-0.798091	5.429296	0.323528
H	2.078952	2.791073	-0.072042	H	-0.147318	3.971294	1.767904
C	1.484690	4.375099	1.247419	C	-2.175730	4.470456	2.285080
H	0.773252	5.218242	1.349975	H	-3.154179	4.743553	1.840638
H	2.510848	4.797155	1.270087	H	-1.866741	5.300703	2.953334
H	1.367206	3.698229	2.116714	H	-2.316332	3.564915	2.908875
H	1.251468	3.703556	-2.214801	H	-0.034835	5.160418	-0.434028
H	2.438594	4.800576	-1.427782	H	-0.396413	6.267471	0.930236
H	0.699489	5.222580	-1.414798	H	-1.698359	5.800442	-0.206466
C	-1.200442	3.218317	0.009266	C	-2.438579	2.690545	-0.211031
C	-2.152519	2.151803	0.024327	C	-2.430687	1.317093	-0.585665
C	-1.621242	4.558719	0.022465	C	-3.444597	3.556687	-0.680788
C	-3.000721	4.842574	0.049817	C	-4.434004	3.048476	-1.544811
C	-3.958169	3.811132	0.063995	C	-4.426902	1.700118	-1.941573
C	-3.532661	2.476086	0.051176	C	-3.445801	0.830102	-1.435484
H	-3.325683	5.895208	0.060285	H	-5.214216	3.729312	-1.921439
H	-0.898320	5.383528	0.012163	H	-3.454473	4.618813	-0.403573
H	-4.263385	1.651288	0.062407	H	-3.463929	-0.241963	-1.685847
H	-5.032024	4.052482	0.085424	H	-5.200918	1.319460	-2.625985
H	-2.447742	-0.001196	0.022009	H	-2.052822	-0.334128	0.854102

Act				TS_Ci1			
75				81			
act SCF Done: -2403.22255201 A.U.				ts_ci1 SCF Done: -2481.74738224 A.U.			
Ru	0.627109	-0.718288	0.465266	Ru	-0.578506	-0.558024	-0.365879
C	1.196552	1.067988	0.019576	C	-1.072999	1.280672	-0.041270
N	2.532158	1.375315	-0.173760	N	-2.394236	1.648533	0.151532
N	0.507331	2.261842	-0.008875	N	-0.344410	2.449143	-0.100110
C	1.379035	3.410058	-0.331032	C	-1.170386	3.646381	0.157067
C	2.786888	2.826047	-0.151334	C	-2.599394	3.102817	0.032910
H	1.171303	4.260055	0.350923	H	-0.941912	4.442531	-0.580669
H	1.190874	3.761513	-1.372407	H	-0.955845	4.055806	1.171569
H	3.487179	3.114951	-0.961892	H	-3.278407	3.471112	0.829243
H	3.243223	3.127667	0.819015	H	-3.058074	3.353545	-0.950833
C	-0.909095	2.495595	0.014208	C	1.078152	2.633756	-0.167100
C	3.625094	0.454025	-0.350208	C	-3.523433	0.784367	0.385268
C	4.464025	0.115198	0.744794	C	-4.365608	0.392880	-0.690322
C	5.534422	-0.772718	0.508884	C	-5.468750	-0.437736	-0.400636

C	5.811115	-1.295085	-0.768152	C	-5.780172	-0.845712	0.909758
C	5.001939	-0.877716	-1.844237	C	-4.972921	-0.366107	1.960868
C	3.916421	-0.001417	-1.665828	C	-3.853575	0.454268	1.729639
C	4.276107	0.719728	2.116326	C	-4.159184	0.898839	-2.098542
H	6.178473	-1.055315	1.358724	H	-6.114603	-0.761100	-1.234443
C	6.934890	-2.284066	-0.981344	C	-6.942863	-1.772503	1.185136
H	5.222836	-1.244410	-2.860778	H	-5.224424	-0.634178	3.000873
C	3.093018	0.446407	-2.849680	C	-3.041981	0.976936	2.890549
H	3.211124	0.731507	2.423783	H	-3.092714	0.882031	-2.398793
H	4.656241	1.765560	2.146753	H	-4.532783	1.942522	-2.200654
H	4.842090	0.148385	2.878254	H	-4.724107	0.281902	-2.824953
H	7.705500	-2.208620	-0.187836	H	-7.698821	-1.735770	0.374997
H	7.431340	-2.135892	-1.962411	H	-7.447012	-1.524442	2.141781
H	6.549577	-3.327530	-0.967776	H	-6.597577	-2.826919	1.265520
H	3.578275	0.152928	-3.801196	H	-3.578968	0.822439	3.847088
H	2.949693	1.547507	-2.862293	H	-2.822108	2.060395	2.789835
H	2.086783	-0.022370	-2.819726	H	-2.069791	0.443205	2.949807
C	-1.528023	2.880621	1.231713	C	1.681831	2.906353	-1.421734
C	-1.641633	2.427813	-1.198483	C	1.833976	2.633357	1.033170
C	-2.900845	3.194721	1.206688	C	3.065447	3.169251	-1.447835
C	-3.011855	2.757609	-1.168566	C	3.213956	2.909003	0.951236
C	-3.659937	3.148408	0.019452	C	3.849708	3.180038	-0.276345
C	-5.124781	3.526910	0.026651	C	5.335988	3.453774	-0.346675
H	-3.391539	3.488078	2.150206	H	3.543928	3.376014	-2.420137
C	-0.988483	1.957642	-2.478137	C	1.190626	2.292917	2.358273
H	-3.589006	2.705892	-2.107353	H	3.808957	2.909102	1.880118
C	-0.743336	2.935607	2.520764	C	0.868540	2.902644	-2.693784
H	-0.298688	1.947066	2.765830	H	0.359815	1.926228	-2.843530
H	-1.389439	3.248556	3.364151	H	1.509386	3.104301	-3.574299
H	0.100023	3.656964	2.458701	H	0.071945	3.678034	-2.675068
H	-0.637094	0.907345	-2.382975	H	0.761932	1.267255	2.344370
H	-0.098907	2.565960	-2.746842	H	0.356936	2.982427	2.610765
H	-1.696879	2.007062	-3.327961	H	1.927889	2.346781	3.182886
H	-5.622921	3.258683	-0.926336	H	5.762099	3.667739	0.653950
H	-5.255997	4.621329	0.173859	H	5.560275	4.317473	-1.006788
H	-5.670611	3.025923	0.853444	H	5.884710	2.581132	-0.764092
C	-1.212821	-0.617475	0.352105	C	1.263300	-0.478554	-0.291435
Cl	1.011697	-0.461072	2.763305	Cl	-0.971026	-0.409153	-2.682484
Cl	1.073855	-1.976926	-1.443404	Cl	-0.969051	-1.507828	1.745710
O	-3.572466	-1.135935	-0.918593	O	3.520125	-1.060702	1.111009
C	-4.729521	-1.211794	-1.789219	C	4.524261	-1.263083	2.137919
C	-4.743984	-2.481982	-2.648773	C	4.356266	-2.596543	2.875258
H	-4.526620	-0.358681	-2.471243	H	4.251050	-0.457067	2.851900
C	-6.046560	-0.902084	-1.065780	C	5.949736	-0.966730	1.653336
H	-6.388243	-1.721757	-0.403922	H	6.365978	-1.757924	0.999258
H	-6.844225	-0.722624	-1.816282	H	6.622815	-0.870513	2.530612
H	-5.940224	0.015484	-0.453020	H	5.975175	-0.008650	1.096514
H	-3.751957	-2.639461	-3.117579	H	3.300116	-2.735419	3.181612
H	-5.492992	-2.366973	-3.459492	H	4.982330	-2.590519	3.791525
H	-5.004114	-3.394936	-2.078131	H	4.657901	-3.471937	2.267393

C	-3.302677	-1.981430	0.111325	C	3.323185	-1.863276	0.030982
C	-2.054897	-1.728412	0.789944	C	2.120228	-1.585464	-0.715483
C	-4.117030	-3.054913	0.531083	C	4.176006	-2.906676	-0.386702
C	-3.716082	-3.879148	1.597412	C	3.856419	-3.675083	-1.520681
C	-2.503220	-3.649530	2.268458	C	2.688225	-3.419358	-2.257621
C	-1.688311	-2.585616	1.862928	C	1.830474	-2.389263	-1.849598
H	-4.371010	-4.710888	1.903404	H	4.540662	-4.482887	-1.826932
H	-5.068945	-3.263477	0.027863	H	5.096952	-3.129928	0.165828
H	-0.755302	-2.365473	2.406515	H	0.923052	-2.156560	-2.428302
H	-2.198866	-4.289518	3.110608	H	2.449072	-4.016037	-3.151295
H	-1.733317	0.201606	-0.176656	C	-2.065625	-3.564043	-1.130294
				C	-0.991201	-4.247533	-0.696548
				H	1.788126	0.347249	0.223308
				H	-0.671006	-4.196447	0.357237
				H	-0.382615	-4.865743	-1.377695
				H	-2.670838	-2.952097	-0.440568
				H	-2.383807	-3.584975	-2.185737

TS_Con				Ci1			
81				81			
ts_con_2 SCF Done: -2481.74092917 A.U.				ci1 SCF Done: -2481.75876594 A.U.			
C	0.686060	-1.308393	0.002036	Ru	0.747112	-0.865237	0.228104
C	0.588520	-3.680114	0.106329	C	1.188578	1.111130	0.049888
H	0.090828	-4.399318	-0.574956	N	2.502051	1.507078	0.007801
H	0.595393	-4.128541	1.125602	N	0.427539	2.242758	0.121644
C	1.983377	-3.267853	-0.369432	C	1.233745	3.483143	0.046082
H	2.801310	-3.712261	0.233091	C	2.669220	2.961872	0.206820
H	2.164475	-3.529630	-1.436436	H	0.934767	4.190366	0.846481
C	-2.174424	-2.646162	1.506884	H	1.065404	3.990175	-0.931326
C	-3.559205	-2.895435	1.569989	H	3.374069	3.380702	-0.540631
H	-4.029420	-3.000617	2.562342	H	3.081736	3.168117	1.219489
C	-4.352242	-3.031733	0.411413	C	-1.002295	2.375506	0.069276
C	-3.720543	-2.910513	-0.841297	C	3.658230	0.667494	-0.194946
H	-4.317002	-3.030151	-1.761271	C	4.433360	0.229669	0.914421
C	-2.338729	-2.650195	-0.964873	C	5.555561	-0.586078	0.658241
C	-1.578270	-2.499040	0.223604	C	5.953907	-0.930626	-0.646897
C	-1.358616	-2.534178	2.772855	C	5.223200	-0.391055	-1.724352
H	-1.998926	-2.666526	3.666840	C	4.089907	0.420834	-1.529655
H	-0.847453	-1.548015	2.848037	C	4.137400	0.674839	2.326212
H	-0.561103	-3.307218	2.818519	H	6.146913	-0.947317	1.516521
C	-5.838148	-3.293648	0.519743	C	7.132299	-1.846606	-0.889448
H	-6.276367	-3.580922	-0.456787	H	5.550135	-0.598392	-2.757196
H	-6.379634	-2.390079	0.875922	C	3.379931	1.026531	-2.715340
H	-6.056444	-4.104081	1.246334	H	3.056553	0.606311	2.565868
C	-1.695732	-2.544021	-2.325331	H	4.464562	1.727284	2.482780
H	-2.438532	-2.714840	-3.128750	H	4.689140	0.053287	3.058758
H	-0.882813	-3.291512	-2.455084	H	7.831639	-1.853841	-0.029147
H	-1.232716	-1.543318	-2.476737	H	7.700319	-1.552942	-1.796116
C	3.218813	-1.106433	-0.216591	H	6.793159	-2.894465	-1.046274
C	3.927517	-0.955035	1.008095	H	3.984835	0.908649	-3.635850
C	5.201268	-0.354207	0.970383	H	3.182708	2.109744	-2.571628

H	5.750631	-0.224684	1.918112	H	2.401210	0.523621	-2.874853
C	5.790777	0.078423	-0.235157	C	-1.721638	2.579913	1.275779
C	5.084029	-0.141188	-1.432975	C	-1.644379	2.421217	-1.194897
H	5.541769	0.154901	-2.391868	C	-3.106129	2.821038	1.187779
C	3.810934	-0.749456	-1.457330	C	-3.031713	2.670061	-1.224775
C	3.335725	-1.410844	2.318587	C	-3.780242	2.875589	-0.049284
H	4.077836	-1.329708	3.136808	C	-5.269348	3.137534	-0.101021
H	2.994118	-2.467051	2.273147	H	-3.674078	2.975773	2.120724
H	2.444910	-0.798481	2.586893	C	-0.873873	2.177784	-2.471979
C	7.136991	0.766867	-0.236601	H	-3.539530	2.711457	-2.203275
H	7.650853	0.663158	-1.213461	C	-1.022990	2.540774	2.613453
H	7.804527	0.362446	0.551644	H	-0.441024	1.602048	2.739659
H	7.024719	1.855876	-0.039065	H	-1.752736	2.619938	3.442858
C	3.133371	-1.036504	-2.776015	H	-0.303066	3.381629	2.724536
H	3.697951	-0.583683	-3.614653	H	-0.455056	1.146516	-2.508634
H	2.093046	-0.645387	-2.803890	H	-0.009397	2.867718	-2.576243
H	3.080894	-2.130195	-2.972184	H	-1.522430	2.317307	-3.358870
C	-1.504054	0.487568	0.365528	H	-5.619367	3.316744	-1.137377
H	-1.891980	-0.094059	1.227338	H	-5.547943	4.021703	0.510286
C	-2.501855	1.317023	-0.323448	H	-5.842555	2.275653	0.304601
C	-3.735156	0.755547	-0.746870	C	-1.115350	-0.709325	0.111814
H	-3.937266	-0.303327	-0.524740	Cl	0.961697	-0.603380	2.626859
C	-4.660979	1.511924	-1.479008	Cl	0.960687	-1.299265	-2.133007
H	-5.597285	1.045280	-1.823646	O	-3.436094	-1.174224	-1.221488
C	-4.389575	2.859820	-1.776946	C	-4.457386	-1.485775	-2.205728
H	-5.108015	3.455948	-2.361805	C	-4.686678	-2.993712	-2.357115
C	-3.204314	3.453348	-1.312587	H	-3.957462	-1.133514	-3.132661
C	-2.271236	2.698915	-0.580119	C	-5.734606	-0.651664	-2.041420
N	-0.146917	-2.395106	0.118862	H	-6.383406	-0.992717	-1.210439
N	1.957240	-1.801326	-0.197028	H	-6.331779	-0.711195	-2.974974
Cl	0.420400	0.651491	2.482731	H	-5.478149	0.412347	-1.867113
Cl	0.021300	0.639189	-2.395484	H	-3.719592	-3.519276	-2.487626
Ru	0.313038	0.629012	0.001772	H	-5.302434	-3.181216	-3.260958
H	-2.981385	4.512423	-1.511275	H	-5.212838	-3.443029	-1.491900
O	-1.130718	3.310832	-0.096305	C	-3.483594	-1.484976	0.098400
C	-1.169119	3.864729	1.276359	C	-2.246782	-1.287724	0.820960
C	1.886420	2.326484	-0.707853	C	-4.614798	-1.988474	0.777660
C	2.307735	2.109346	0.578046	C	-4.541685	-2.299479	2.145716
H	1.124305	3.084998	-0.950840	C	-3.344645	-2.121166	2.862238
H	2.394419	1.859561	-1.564827	C	-2.213007	-1.634435	2.198481
H	3.155102	1.445708	0.802897	H	-5.438227	-2.693258	2.651715
H	1.897834	2.671675	1.429767	H	-5.559392	-2.144988	0.243004
C	-0.108724	4.961068	1.314551	H	-1.264186	-1.475032	2.735259
H	0.875796	4.584128	0.976108	H	-3.294129	-2.365944	3.934419
H	0.009493	5.339753	2.350498	C	1.578020	-2.942028	0.645789
H	-0.397346	5.810375	0.660398	C	0.245901	-3.219625	0.401750
C	-2.545374	4.382364	1.691565	H	-1.428648	-0.121229	-0.773918
H	-0.874756	3.030070	1.954487	H	-0.109970	-3.454114	-0.613345
H	-2.887846	5.217712	1.045486	H	-0.456025	-3.380061	1.233219
H	-2.477309	4.761191	2.732323	H	2.316636	-2.989535	-0.174952

H	-3.317172	3.587835	1.674903	H	1.969071	-2.907778	1.675441
TS_MCy				MCy			
81				81			
ts_mcy SCF Done: -2481.75565653 A.U.				mcy SCF Done: -2481.76698777 A.U.			
Ru	0.689004	-0.806804	0.259894	Ru	0.612952	-0.761675	-0.040240
C	1.354959	1.037650	-0.301871	C	1.386553	1.099518	-0.097620
N	2.673566	1.339157	-0.489237	N	2.708579	1.412666	-0.163184
N	0.620946	2.143698	-0.600341	N	0.658780	2.246598	-0.093933
C	1.451796	3.272284	-1.079044	C	1.517394	3.453266	-0.084152
C	2.887332	2.745033	-0.899530	C	2.925429	2.871654	-0.307601
H	1.246264	4.184938	-0.481131	H	1.418428	3.981724	0.889878
H	1.208147	3.504986	-2.138965	H	1.205425	4.157115	-0.883099
H	3.484099	2.790286	-1.834381	H	3.324622	3.097468	-1.320794
H	3.452720	3.293579	-0.114384	H	3.667617	3.228746	0.435721
C	-0.805607	2.310826	-0.522327	C	-0.770136	2.379953	0.055961
C	3.807450	0.469482	-0.281219	C	3.838391	0.512800	-0.156574
C	4.430018	0.425856	0.996911	C	4.484954	0.240819	1.079261
C	5.548126	-0.417439	1.161710	C	5.606994	-0.611454	1.067393
C	6.080719	-1.175081	0.101274	C	6.109493	-1.173681	-0.122080
C	5.489680	-1.039264	-1.170354	C	5.478969	-0.830515	-1.333860
C	4.369617	-0.214854	-1.395138	C	4.356531	0.020887	-1.384908
C	3.946828	1.271545	2.149162	C	4.002031	0.839236	2.377872
H	6.027205	-0.464975	2.154198	H	6.107728	-0.834035	2.024689
C	7.252512	-2.105922	0.318303	C	7.287734	-2.121718	-0.097549
H	5.920778	-1.582965	-2.027845	H	5.880394	-1.225243	-2.282519
C	3.816458	-0.052593	-2.789128	C	3.756383	0.403841	-2.715287
H	2.948204	0.932276	2.503405	H	3.024505	0.395620	2.669394
H	3.847236	2.340447	1.864068	H	3.854757	1.937672	2.304755
H	4.654636	1.215103	2.999274	H	4.728507	0.649728	3.192181
H	6.902041	-3.136121	0.549961	H	7.979734	-1.894108	0.738702
H	7.885875	-1.778797	1.167751	H	7.863861	-2.085290	-1.044402
H	7.892865	-2.177157	-0.584586	H	6.948449	-3.172623	0.037817
H	4.428697	-0.614229	-3.521578	H	4.333056	-0.044299	-3.548047
H	3.808201	1.012282	-3.107815	H	3.759853	1.505361	-2.865632
H	2.770736	-0.426761	-2.844077	H	2.698533	0.068263	-2.799540
C	-1.364823	2.841080	0.669639	C	-1.334324	2.415889	1.361106
C	-1.601913	2.055889	-1.667963	C	-1.560684	2.609770	-1.100382
C	-2.749957	3.089954	0.698343	C	-2.722314	2.624944	1.473442
C	-2.984758	2.320114	-1.581095	C	-2.942977	2.823754	-0.924472
C	-3.579103	2.833440	-0.412415	C	-3.545401	2.826619	0.347777
C	-5.068092	3.087879	-0.335998	C	-5.033981	3.036728	0.513153
H	-3.193982	3.499812	1.621012	H	-3.170238	2.643961	2.481024
C	-0.997180	1.525882	-2.945827	C	-0.952577	2.626930	-2.480859
H	-3.613775	2.127869	-2.466783	H	-3.564434	3.004090	-1.817739
C	-0.502491	3.124950	1.876911	C	-0.488454	2.255713	2.601376
H	-0.017212	2.197630	2.254139	H	-0.054455	1.233743	2.676617
H	-1.103260	3.562926	2.697987	H	-1.091800	2.440776	3.511508
H	0.315620	3.840665	1.644161	H	0.365131	2.967009	2.616183
H	-0.230455	2.218275	-3.356729	H	-0.129008	3.368602	-2.563816
H	-1.773966	1.395042	-3.724684	H	-1.712858	2.883836	-3.244303

H	-0.490007	0.547616	-2.787172	H	-0.518882	1.632788	-2.730462
H	-5.572449	2.300859	0.266220	H	-5.255011	3.781230	1.306605
H	-5.536572	3.091544	-1.340703	H	-5.535874	2.090867	0.812193
H	-5.292427	4.059772	0.151140	H	-5.507286	3.386019	-0.426264
C	-1.189563	-1.036042	0.084541	C	-1.171096	-1.728946	-0.185586
Cl	0.900230	-0.287292	2.612870	Cl	1.014993	-0.976059	2.324912
Cl	0.792700	-1.534919	-2.060050	Cl	0.427303	-0.648842	-2.460129
O	-3.604462	-1.924327	-0.794749	O	-3.682523	-1.229584	-1.151093
C	-4.725240	-2.551653	-1.473185	C	-4.831675	-1.520122	-1.990048
C	-5.289434	-3.753662	-0.705870	C	-5.391151	-2.929024	-1.769519
H	-4.214784	-2.950352	-2.375421	H	-4.363382	-1.499172	-2.997480
C	-5.774469	-1.545364	-1.962750	C	-5.885704	-0.405259	-1.965415
H	-6.418152	-1.147729	-1.153735	H	-6.513651	-0.415849	-1.051854
H	-6.435939	-2.041295	-2.702997	H	-6.564954	-0.518570	-2.836049
H	-5.280587	-0.690205	-2.465905	H	-5.394870	0.585576	-2.040169
H	-4.470890	-4.435434	-0.399018	H	-4.579318	-3.682253	-1.822124
H	-5.973455	-4.321894	-1.369678	H	-6.126377	-3.162010	-2.567219
H	-5.859467	-3.468436	0.199921	H	-5.903426	-3.040330	-0.793449
C	-3.646800	-1.291006	0.404769	C	-3.627140	-1.429882	0.196323
C	-2.375068	-0.817960	0.913319	C	-2.318708	-1.653455	0.751576
C	-4.820530	-1.089558	1.165616	C	-4.755653	-1.401673	1.047424
C	-4.758020	-0.456490	2.417332	C	-4.613557	-1.603065	2.429066
C	-3.530707	-0.006583	2.934207	C	-3.341995	-1.824216	2.985750
C	-2.364077	-0.184880	2.183046	C	-2.217312	-1.839844	2.151250
H	-5.687988	-0.320987	2.993561	H	-5.508053	-1.575580	3.072346
H	-5.790586	-1.436256	0.790427	H	-5.752031	-1.210636	0.629282
H	-1.389142	0.146006	2.570800	H	-1.213269	-1.966075	2.584953
H	-3.484678	0.482493	3.919325	H	-3.224385	-1.972337	4.070432
C	1.277149	-2.846915	0.711549	C	1.402802	-2.562348	-0.270457
C	-0.118321	-2.922475	0.909822	C	-0.110410	-2.916226	-0.031543
H	-1.456800	-1.436790	-0.914154	H	-1.513707	-1.653223	-1.231148
H	-0.744144	-3.438566	0.163678	H	-0.389408	-3.590455	-0.866773
H	-0.538498	-2.810205	1.921518	H	-0.236098	-3.389408	0.959094
H	1.725661	-3.277706	-0.198926	H	1.773018	-2.802253	-1.284727
H	1.929423	-2.720677	1.593432	H	2.058453	-2.892957	0.557129

TS_Ci2				Ci2			
81				81			
ts_ci2 SCF Done: -2481.74740294 A.U.				ci2 SCF Done: -2481.75117097 A.U.			
Ru	0.560189	-0.789672	0.062175	Ru	0.271097	-0.103196	0.934492
C	1.345739	1.076579	-0.047282	C	1.339054	1.051165	-0.420273
N	2.670023	1.403375	-0.105605	N	2.597895	0.867690	-0.905126
N	0.622640	2.231076	-0.059121	N	0.823479	2.178464	-0.981962
C	1.472030	3.442301	-0.067498	C	1.731300	2.781154	-1.985373
C	2.889651	2.863292	-0.223282	C	3.022596	1.968219	-1.803486
H	1.339383	4.008217	0.880656	H	1.865345	3.864276	-1.787117
H	1.182341	4.114500	-0.902177	H	1.294325	2.674354	-3.002543
H	3.344445	3.102184	-1.209791	H	3.417860	1.559808	-2.755686
H	3.590023	3.216079	0.562304	H	3.836110	2.553594	-1.321698
C	-0.810465	2.370005	0.019964	C	-0.473910	2.775750	-0.763552
C	3.809945	0.526321	-0.172919	C	3.548507	-0.176370	-0.614399

C	4.526874	0.234392	1.019116	C	4.467582	-0.009866	0.457660
C	5.674144	-0.577643	0.921214	C	5.417306	-1.027875	0.679483
C	6.131550	-1.085953	-0.311231	C	5.498760	-2.171903	-0.137906
C	5.419084	-0.740449	-1.475918	C	4.614243	-2.268355	-1.230455
C	4.266298	0.071379	-1.439751	C	3.644097	-1.283414	-1.501645
C	4.079424	0.768637	2.357604	C	4.461488	1.224526	1.326282
H	6.232088	-0.811998	1.843589	H	6.124839	-0.909638	1.517408
C	7.347042	-1.984116	-0.376543	C	6.500640	-3.267023	0.151769
H	5.776323	-1.102247	-2.454910	H	4.684096	-3.136328	-1.907508
C	3.554079	0.442315	-2.717576	C	2.752479	-1.403907	-2.712738
H	3.075336	0.369655	2.625481	H	3.476598	1.382023	1.819171
H	3.999307	1.877103	2.356859	H	4.676607	2.140323	0.732884
H	4.795156	0.486155	3.154300	H	5.238562	1.153974	2.112346
H	7.811366	-1.973557	-1.383231	H	7.404820	-2.872729	0.658357
H	7.075828	-3.039261	-0.151022	H	6.820584	-3.785750	-0.774709
H	8.117749	-1.684611	0.363103	H	6.061987	-4.039011	0.822163
H	4.100484	0.053054	-3.598960	H	2.965056	-2.339076	-3.266983
H	3.470217	1.543986	-2.838173	H	2.904322	-0.559077	-3.420001
H	2.516266	0.038407	-2.742028	H	1.680503	-1.403309	-2.417716
C	-1.434858	2.471606	1.294558	C	-0.583334	3.856220	0.158629
C	-1.547024	2.554000	-1.180673	C	-1.567513	2.400604	-1.590651
C	-2.826204	2.686234	1.332827	C	-1.839277	4.475654	0.307433
C	-2.935615	2.777989	-1.078534	C	-2.798399	3.063505	-1.399868
C	-3.596647	2.835722	0.162787	C	-2.963200	4.088054	-0.449727
C	-5.089830	3.059619	0.249982	C	-4.302250	4.761271	-0.246166
H	-3.318942	2.756545	2.316977	H	-1.931684	5.306303	1.027277
C	-0.879248	2.517820	-2.533154	C	-1.437785	1.353327	-2.668693
H	-3.512918	2.927262	-2.006546	H	-3.651800	2.771061	-2.033555
C	-0.646569	2.381342	2.578195	C	0.604290	4.360481	0.940180
H	-0.199940	1.371296	2.716284	H	0.974688	3.581451	1.642481
H	-1.294237	2.597147	3.450298	H	0.335605	5.263603	1.522222
H	0.194833	3.106975	2.598211	H	1.452546	4.630007	0.274837
H	-0.017009	3.215884	-2.592782	H	-0.619668	1.595407	-3.380689
H	-1.593235	2.796883	-3.332786	H	-2.375722	1.276321	-3.252079
H	-0.487553	1.498367	-2.748468	H	-1.206758	0.351322	-2.243328
H	-5.339111	3.867370	0.969972	H	-4.799471	4.388547	0.676308
H	-5.607439	2.142480	0.606072	H	-4.990649	4.570229	-1.093646
H	-5.523921	3.330727	-0.733056	H	-4.194131	5.859666	-0.129629
C	-1.151930	-2.321227	-0.021221	C	-1.659097	-1.250011	1.756619
Cl	0.888590	-0.787815	2.467902	Cl	1.176790	1.408294	2.632707
Cl	0.239582	-0.829965	-2.342011	Cl	-0.307211	-1.492972	-0.988752
O	-3.488128	-1.540932	-1.182473	O	-2.887745	-3.449016	0.690235
C	-4.640927	-1.665549	-2.055493	C	-2.999005	-4.659407	-0.105688
C	-5.485079	-2.907919	-1.751725	C	-4.264012	-5.461658	0.228873
H	-4.139562	-1.830484	-3.032923	H	-2.133312	-5.241336	0.278173
C	-5.443192	-0.363953	-2.180687	C	-2.762715	-4.421761	-1.599724
H	-6.102847	-0.168756	-1.311566	H	-3.615777	-3.919340	-2.097283
H	-6.088676	-0.415098	-3.082248	H	-2.604754	-5.397810	-2.103710
H	-4.755533	0.497188	-2.296467	H	-1.859221	-3.795858	-1.744564
H	-4.844260	-3.811213	-1.701243	H	-4.393019	-5.539229	1.327399

H	-6.224766	-3.058073	-2.565150	H	-4.170013	-6.489920	-0.178653
H	-6.043421	-2.826404	-0.798078	H	-5.186096	-5.017946	-0.197647
C	-3.524114	-1.559663	0.177733	C	-3.503399	-2.268596	0.403038
C	-2.291598	-1.909739	0.830258	C	-2.890890	-1.097326	0.958699
C	-4.663488	-1.253207	0.956662	C	-4.711842	-2.148380	-0.319027
C	-4.601000	-1.292705	2.358239	C	-5.314451	-0.892951	-0.497883
C	-3.402013	-1.633235	3.008254	C	-4.727690	0.261589	0.047262
C	-2.268091	-1.936790	2.245076	C	-3.530802	0.147663	0.767932
H	-5.502380	-1.049017	2.943649	H	-6.258792	-0.824656	-1.061622
H	-5.604132	-0.973858	0.466222	H	-5.198879	-3.042715	-0.727674
H	-1.320041	-2.172438	2.750062	H	-3.066954	1.056495	1.183670
H	-3.348755	-1.659072	4.107483	H	-5.200528	1.246341	-0.085623
C	1.956531	-1.968620	-0.120442	C	1.571071	-1.295638	1.356529
C	-0.022130	-3.067663	0.385643	C	-1.147889	-0.307923	2.657070
H	-1.390780	-2.339321	-1.095546	H	-1.295413	-2.286340	1.818465
H	0.422914	-3.755617	-0.351135	H	-0.498377	-0.620956	3.487484
H	0.166235	-3.294627	1.446906	H	-1.638658	0.669287	2.803482
H	2.245438	-2.382077	-1.113154	H	1.679528	-2.247090	0.790414
H	2.558646	-2.302353	0.754926	H	2.261224	-1.117946	2.210736

TS_I14e				I14e			
81				55			
ts_I14e SCF Done: -2481.74389163 A.U.				I14e SCF Done: -1979.31478192 A.U.			
Ru	-0.409997	-0.120105	-0.826076	Ru	0.091304	-0.062519	-1.461499
C	-1.489486	0.951817	0.454007	C	-0.085405	0.063361	0.459131
N	-2.756637	0.742310	0.920731	N	-1.210029	0.152327	1.247084
N	-1.004488	2.087419	1.041473	N	1.004148	0.099519	1.307570
C	-1.934925	2.650249	2.042466	C	0.625830	0.366802	2.706547
C	-3.212692	1.821635	1.823328	C	-0.894398	0.148635	2.690274
H	-2.085961	3.735638	1.867684	H	0.900553	1.408336	2.989011
H	-1.516697	2.528259	3.066464	H	1.156735	-0.321210	3.396604
H	-3.619821	1.396193	2.763769	H	-1.191130	-0.823316	3.146978
H	-4.025320	2.407302	1.338699	H	-1.454820	0.949584	3.215332
C	0.281539	2.708138	0.831791	C	2.398042	0.049647	0.944403
C	-3.674872	-0.308603	0.577903	C	-2.588736	0.077811	0.856269
C	-4.571666	-0.127388	-0.511136	C	-3.303592	1.284697	0.649826
C	-5.511950	-1.144808	-0.770603	C	-4.670981	1.199774	0.318281
C	-5.596775	-2.307758	0.020155	C	-5.333144	-0.038373	0.193669
C	-4.717150	-2.433940	1.114705	C	-4.586371	-1.216711	0.401806
C	-3.757143	-1.450528	1.422272	C	-3.217858	-1.188503	0.735406
C	-4.522965	1.109772	-1.374251	C	-2.602601	2.621136	0.727464
H	-6.205955	-1.014822	-1.618023	H	-5.233467	2.132883	0.146384
C	-6.591922	-3.399106	-0.305020	C	-6.808631	-0.105436	-0.132078
H	-4.782710	-3.326141	1.759963	H	-5.082806	-2.196169	0.296233
C	-2.836631	-1.615094	2.605354	C	-2.437691	-2.470656	0.907736
H	-3.541090	1.212965	-1.890222	H	-1.784871	2.685370	-0.022341
H	-4.665339	2.035830	-0.776275	H	-2.137089	2.790590	1.721966
H	-5.320273	1.084821	-2.142510	H	-3.309574	3.452927	0.541430
H	-6.136782	-4.165338	-0.971030	H	-7.166284	0.829243	-0.608449
H	-7.482941	-2.999450	-0.830168	H	-7.413458	-0.259132	0.788870
H	-6.934817	-3.926428	0.608390	H	-7.038599	-0.950141	-0.813392

H	-3.091926	-2.525304	3.182681	H	-3.098408	-3.353123	0.802844
H	-2.894331	-0.748898	3.299206	H	-1.952272	-2.533692	1.905141
H	-1.775673	-1.690354	2.274616	H	-1.627392	-2.553219	0.151105
C	0.375568	3.789576	-0.091256	C	3.120530	1.255079	0.732362
C	1.381417	2.346081	1.656163	C	3.059512	-1.210398	0.942606
C	1.619327	4.433063	-0.234215	C	4.484536	1.161005	0.391575
C	2.602912	3.027113	1.465783	C	4.425307	-1.243479	0.601594
C	2.748377	4.061894	0.524165	C	5.151275	-0.075123	0.296524
C	4.067991	4.778035	0.339420	C	6.601873	-0.147679	-0.123739
H	1.699047	5.266823	-0.952159	H	5.044853	2.092394	0.203357
C	1.265688	1.292918	2.730256	C	2.344652	-2.483669	1.326777
H	3.463492	2.743287	2.093732	H	4.940239	-2.218744	0.585772
C	-0.816283	4.258709	-0.887569	C	2.499833	2.616667	0.945660
H	-1.124287	3.481442	-1.621991	H	1.411997	2.619703	0.750311
H	-0.579178	5.190380	-1.437609	H	2.956878	3.370084	0.274843
H	-1.695012	4.462605	-0.239417	H	2.673529	2.960083	1.990708
H	0.429168	1.508371	3.428999	H	1.746326	-2.358332	2.253639
H	2.196005	1.242322	3.328951	H	3.070177	-3.303149	1.497278
H	1.072821	0.285501	2.297579	H	1.644521	-2.802627	0.525668
H	4.825370	4.439361	1.074034	H	7.110112	-1.034501	0.306320
H	3.951874	5.877103	0.451552	H	7.164522	0.757849	0.181881
H	4.481140	4.604924	-0.677914	H	6.687974	-0.226723	-1.230037
C	1.893721	-1.394586	-1.867651	Cl	0.864954	2.078650	-1.926201
Cl	-1.129813	1.293146	-2.658440	Cl	0.558716	-2.337906	-1.652329
Cl	0.357315	-1.573976	0.958961	C	-1.607842	0.029259	-2.075066
O	3.385273	-3.284189	-0.576208	H	-1.679703	-0.040820	-3.192039
C	3.618151	-4.339214	0.398446	H	-2.561940	0.158018	-1.529198
C	4.944596	-5.070087	0.153360				
H	2.801067	-5.045990	0.138241				
C	3.389206	-3.885797	1.842268				
H	4.203645	-3.239798	2.225934				
H	3.329088	-4.778493	2.498819				
H	2.434684	-3.326794	1.917992				
H	5.060966	-5.311082	-0.922589				
H	4.952365	-6.023824	0.721181				
H	5.829172	-4.484474	0.475701				
C	3.876341	-2.019514	-0.480724				
C	3.127875	-1.008165	-1.167411				
C	5.082966	-1.672055	0.169165				
C	5.545862	-0.347393	0.148146				
C	4.819835	0.653801	-0.521635				
C	3.625767	0.315128	-1.170513				
H	6.491006	-0.100571	0.658190				
H	5.677352	-2.443158	0.675443				
H	3.042584	1.101904	-1.674812				
H	5.180474	1.693281	-0.533330				
C	-1.709974	-1.324532	-1.222454				
C	1.246546	-0.673320	-2.840233				
H	1.539551	-2.411793	-1.640610				
H	0.419701	-1.118797	-3.411661				

H	1.598924	0.309430	-3.189224
H	-1.805588	-2.282508	-0.663254
H	-2.393276	-1.175825	-2.089179

Table S3 Coordinates data set, absolute energies (a.u.) for DFT all the optimized ammonium tagged complexes (AquaMet^{TM}).

Precat				TS_Open			
103				103			
PENJOLL-precat SCF Done: -3287.58987447 A.U.				PENJOLL-TSopenFFall SCF Done: -3287.55982492 A.U.			
Ru	-2.211045	0.191413	-0.104445	Ru	-2.095474	0.500935	-0.401998
C	-0.249587	0.134430	-0.218149	C	-0.174935	0.236599	-0.373055
N	0.508955	1.281724	-0.279198	N	0.709572	1.287424	-0.458265
N	0.636532	-0.925386	-0.337063	N	0.586913	-0.922335	-0.320113
C	2.053832	-0.477633	-0.264688	C	2.029721	-0.612464	-0.124214
C	1.929351	1.019671	-0.563035	C	2.105729	0.840829	-0.598600
H	2.611141	1.630666	0.070325	H	2.267265	-0.650693	0.967101
H	2.143791	1.235276	-1.638780	H	2.810738	1.450105	0.010814
C	0.346830	-2.313902	-0.110387	H	2.412412	0.900239	-1.672497
C	0.052658	2.646009	-0.170383	C	0.122915	-2.261062	-0.092944
C	-0.319621	3.369422	-1.335344	C	0.409397	2.696675	-0.507757
C	-0.757454	4.702083	-1.179375	C	0.185634	3.334050	-1.755912
C	-0.781925	5.339919	0.074265	C	-0.098901	4.716357	-1.754850
C	-0.307680	4.622576	1.190638	C	-0.112983	5.475727	-0.571513
C	0.131639	3.288356	1.097836	C	0.208452	4.825164	0.637241
C	-0.159847	2.795417	-2.724328	C	0.487421	3.447935	0.698852
H	-1.066802	5.262304	-2.078271	C	0.356506	2.614325	-3.074262
C	-1.292495	6.756305	0.223762	H	-0.296704	5.213474	-2.719749
H	-0.267258	5.119249	2.174748	C	-0.460432	6.947864	-0.587673
C	0.733123	2.600427	2.297988	H	0.250376	5.410396	1.571290
H	-0.528547	1.753533	-2.798320	C	0.926436	2.816559	1.996948
H	0.910893	2.810678	-3.029117	H	0.090106	1.543357	-3.013616
H	-0.716297	3.401400	-3.466763	H	1.412393	2.696968	-3.418623
H	-1.327125	7.285364	-0.750106	H	-0.279120	3.067880	-3.860362
H	-0.657763	7.348373	0.915593	H	-0.371923	7.380236	-1.604802
H	-2.322568	6.767738	0.644003	H	0.195120	7.529426	0.093521
H	0.540506	3.185744	3.218771	H	-1.506617	7.113940	-0.247809
H	1.838374	2.498931	2.188349	H	0.714831	3.491108	2.849922
H	0.301579	1.591192	2.441773	H	2.023928	2.616867	1.989342
C	0.077986	-3.156239	-1.222200	H	0.399537	1.860626	2.181844
C	0.362917	-2.829512	1.214643	C	-0.148565	-3.096798	-1.210178
C	-0.139395	-4.528605	-0.982557	C	-0.017295	-2.743807	1.235626
C	0.147363	-4.211528	1.395724	C	-0.538043	-4.428750	-0.967816
C	-0.095680	-5.081001	0.313527	C	-0.404147	-4.087974	1.420657
C	-0.287256	-6.565800	0.533498	C	-0.666608	-4.948103	0.337005
H	-0.357257	-5.185521	-1.841777	C	-1.111376	-6.377074	0.558295
C	0.510631	-1.919121	2.412509	H	-0.751899	-5.081018	-1.831646
H	0.151633	-4.614926	2.422707	C	0.157344	-1.827876	2.426093
C	-0.023528	-2.597774	-2.621906				

H	-0.772038	-1.777708	-2.675318	H	-0.521692	-4.466246	2.450286
H	-0.315152	-3.388437	-3.341022	C	-0.067508	-2.564868	-2.621276
H	0.940239	-2.167055	-2.967162	H	-0.786908	-1.731438	-2.776686
H	1.463889	-1.349638	2.406814	H	-0.288209	-3.361446	-3.358804
H	0.471881	-2.498007	3.355947	H	0.936941	-2.153405	-2.853473
H	-0.306291	-1.165057	2.436384	H	-0.489789	-0.929713	2.330004
H	-0.669471	-6.783970	1.551320	H	1.199819	-1.459017	2.535319
H	0.674561	-7.114403	0.421886	H	-0.111799	-2.346835	3.366643
H	-0.994436	-7.001345	-0.201715	H	-2.195070	-6.495708	0.339262
C	-2.677594	-1.563635	0.235568	H	-0.947678	-6.700757	1.605560
Cl	-2.500632	0.293215	-2.451600	H	-0.570661	-7.081037	-0.108454
Cl	-2.313410	1.066997	2.079832	C	-2.789967	-1.151729	-0.028632
O	-4.517033	0.323130	-0.033151	Cl	-2.355897	0.560803	-2.725239
C	-5.238458	1.596286	-0.171492	Cl	-2.313925	1.704964	1.574403
C	-6.094989	1.620388	-1.438026	O	-4.908789	-0.212620	1.620470
H	-4.383637	2.286720	-0.323162	C	-5.707299	0.796129	2.294638
C	-5.937478	1.993957	1.128628	C	-6.274817	1.844393	1.334081
H	-6.829444	1.376186	1.354483	H	-4.926523	1.297349	2.903885
H	-6.271198	3.049194	1.046364	C	-6.732185	0.183257	3.258489
H	-5.224163	1.918836	1.973036	H	-7.612550	-0.252551	2.743903
H	-5.491432	1.288053	-2.305644	H	-7.105605	0.968361	3.948792
H	-6.429835	2.661919	-1.624406	H	-6.258730	-0.611295	3.869977
H	-7.000226	0.984986	-1.366497	H	-5.463813	2.253212	0.698871
C	-5.069617	-0.900913	0.218410	H	-6.705216	2.683005	1.919722
C	-4.080311	-1.923788	0.361429	H	-7.073118	1.446381	0.676228
C	-6.437305	-1.201534	0.333737	C	-5.294389	-0.902839	0.516116
C	-6.828063	-2.529441	0.595112	C	-4.229502	-1.422249	-0.284584
C	-5.874499	-3.554169	0.740690	C	-6.633327	-1.199659	0.166151
C	-4.511594	-3.248731	0.623474	C	-6.918925	-2.002162	-0.949610
H	-7.901794	-2.759214	0.685457	C	-5.879716	-2.540771	-1.727855
H	-7.200599	-0.421630	0.224025	C	-4.550789	-2.254355	-1.385705
H	-3.746775	-4.034511	0.734114	H	-7.969976	-2.217301	-1.201487
H	-6.197473	-4.586566	0.945562	H	-7.457768	-0.820905	0.783918
H	-1.957766	-2.392155	0.372200	H	-3.725167	-2.657042	-1.993728
C	3.027196	-1.231894	-1.194063	H	-6.102485	-3.176528	-2.598770
H	2.430661	-0.611888	0.778622	H	-2.169490	-2.024110	0.259724
N	4.405370	-0.885060	-0.881193	C	3.010174	-1.565916	-0.836125
H	2.811799	-0.975963	-2.254542	H	2.719448	-2.626583	-0.644208
H	2.863893	-2.330485	-1.096813	H	2.947872	-1.416543	-1.935628
C	5.225277	-0.115022	-1.781283	C	4.874466	-1.972703	0.777711
C	5.149634	-1.671671	0.071703	C	5.399275	-0.875874	-1.311593
C	6.057599	-0.771467	0.908163	C	5.856002	-1.072116	1.529096
H	5.730633	-2.511074	-0.409922	H	5.323029	-2.981191	0.540943
H	4.450601	-2.157446	0.783601	H	4.042073	-2.173417	1.484301
C	6.156841	0.809885	-0.991433	C	6.373032	0.067636	-0.603208
H	4.586884	0.548798	-2.400211	H	5.944699	-1.737107	-1.797222
H	5.803336	-0.754231	-2.511201	H	4.946631	-0.292846	-2.139793
N	7.008946	0.055584	0.039251	H	6.325620	-1.587294	2.391756
H	5.438010	0.003651	1.435484	H	5.328150	-0.131942	1.845572
H	6.676983	-1.339957	1.628793	H	7.200163	0.399451	-1.260326

H 5.546340 1.516842 -0.369798	H 5.811438 0.948041 -0.190855
H 6.864594 1.354998 -1.648983	N 4.370083 -1.296078 -0.392843
C 7.652917 1.092878 0.927466	N 7.000913 -0.571352 0.638250
H 8.325395 1.717607 0.308737	C 7.713241 0.520569 1.400795
H 8.226584 0.582777 1.722377	H 8.156680 0.079545 2.314035
H 6.817560 1.697625 1.365676	H 8.503519 0.952730 0.760514
C 8.059783 -0.780574 -0.676904	H 6.937720 1.288966 1.651498
C 8.947527 -1.649300 0.207256	C 7.945860 -1.720657 0.318552
H 8.667927 -0.051590 -1.250853	H 8.323400 -2.067219 1.302432
H 7.520554 -1.406784 -1.413538	H 7.326151 -2.537737 -0.098421
H 9.511724 -1.066056 0.961823	C 9.101201 -1.401196 -0.623082
H 9.694026 -2.148665 -0.443298	H 9.755015 -0.588832 -0.248224
H 8.382776 -2.448353 0.726558	H 9.730362 -2.310044 -0.712548
Cl 4.536856 2.115094 1.619830	H 8.761458 -1.140112 -1.644623
	Cl 4.727693 2.051531 1.533478
Act	TS_Ci1
103	109
PENJOLL-Act SCF Done: -3287.57212486 A.U.	PENJOLL-TS1FFllqst3 SCF Done: -3366.09107456 A.U.
Ru 1.936656 1.362824 0.484197	
C 0.082674 0.812713 0.413269	Ru 1.593471 1.114867 0.408198
N -0.932690 1.720496 0.213937	C 0.013667 0.309301 -0.366062
N -0.511405 -0.411331 0.670537	N -1.076116 1.066967 -0.711070
C -1.995519 -0.367524 0.511344	N -0.361763 -1.023144 -0.463570
C -2.271316 1.139560 0.389910	C -1.804260 -1.178020 -0.788858
H -2.288224 -0.855602 -0.447782	C -2.254475 0.267076 -1.088753
H -2.917682 1.356801 -0.487224	H -1.894159 -1.822102 -1.692369
H -2.746369 1.558418 1.310550	H -2.491565 0.423231 -2.165182
C 0.105182 -1.711204 0.627129	H -3.163622 0.568984 -0.521016
C -0.817670 3.114998 -0.132257	C 0.494159 -2.171759 -0.598996
C -0.825291 4.101219 0.890111	C -1.137088 2.506927 -0.794937
C -0.757154 5.456647 0.506240	C -1.693464 3.256810 0.275807
C -0.719570 5.850391 -0.844410	C -1.728866 4.661671 0.148820
C -0.784991 4.845806 -1.830088	C -1.291654 5.324279 -1.012181
C -0.844655 3.476725 -1.507557	C -0.843046 4.538619 -2.092889
C -0.953160 3.737023 2.351438	C -0.769326 3.136146 -2.016862
H -0.746676 6.227264 1.295661	C -2.344669 2.597967 1.465868
C -0.598572 7.308041 -1.230060	H -2.144571 5.251127 0.983297
H -0.789450 5.133659 -2.894955	C -1.308133 6.833870 -1.104264
C -0.938925 2.438018 -2.597737	H -0.547958 5.031487 -3.034568
H -0.157999 3.035221 2.679076	C -0.335004 2.336942 -3.222787
H -1.931051 3.250980 2.564149	H -1.803633 1.687807 1.788723
H -0.892328 4.642693 2.986745	H -3.393382 2.325768 1.198685
H -0.958282 7.978754 -0.423446	H -2.385944 3.293612 2.327711
H -1.171022 7.536984 -2.152622	H -2.066792 7.277753 -0.428222
H 0.461816 7.577178 -1.432355	H -1.521272 7.178402 -2.137100
H -1.007763 2.923672 -3.591121	H -0.321689 7.260980 -0.816911
H -1.818933 1.766424 -2.488067	H -0.300334 2.979814 -4.124430
H -0.031573 1.799586 -2.597964	H -1.027485 1.495316 -3.433054
C 0.525095 -2.335217 1.834127	H 0.679546 1.915031 -3.066336
C 0.215239 -2.381259 -0.623490	C 0.787250 -3.010198 0.509249

C	1.020869	-3.652846	1.765820	C	1.004338	-2.472047	-1.893403
C	0.712850	-3.702171	-0.628076	C	1.557054	-4.170688	0.278397
C	1.109194	-4.361275	0.550888	C	1.760938	-3.645736	-2.067670
C	1.613051	-5.788068	0.524982	C	2.038441	-4.519258	-0.996770
H	1.350975	-4.138673	2.699885	C	2.818673	-5.797355	-1.212181
C	-0.113172	-1.690634	-1.927190	H	1.795524	-4.819506	1.138534
H	0.803205	-4.224772	-1.595598	C	0.792561	-1.520389	-3.048034
C	0.491077	-1.610235	3.158085	H	2.154932	-3.877288	-3.071889
H	1.190337	-0.746818	3.161502	C	0.337812	-2.690520	1.916975
H	0.769634	-2.290356	3.987186	H	0.205414	-1.602555	2.079170
H	-0.509780	-1.187152	3.379988	H	1.086946	-3.053724	2.649001
H	0.436338	-0.729090	-2.010068	H	-0.620832	-3.197322	2.163583
H	-1.193093	-1.448073	-2.052085	H	1.255324	-0.533334	-2.833253
H	0.181687	-2.324285	-2.786737	H	-0.282729	-1.327714	-3.249183
H	1.796938	-6.140213	-0.509847	H	1.243566	-1.917311	-3.978444
H	0.878508	-6.483828	0.987170	H	2.135682	-6.660385	-1.376552
H	2.557756	-5.896806	1.098195	H	3.447137	-6.046421	-0.332667
C	2.833654	-0.238362	0.294405	H	3.478312	-5.731488	-2.101079
Cl	1.966540	1.757725	2.796195	C	2.774602	-0.303442	0.398833
Cl	2.385084	2.303537	-1.593941	Cl	0.628017	0.992773	2.556190
O	4.277394	-2.005350	-1.201598	Cl	2.536671	2.299300	-1.389962
C	4.791470	-2.921148	-2.199651	O	5.044219	-1.415364	-0.632327
C	5.620738	-2.215000	-3.279354	C	6.128243	-1.807200	-1.512289
H	3.845305	-3.252911	-2.677903	C	7.101652	-0.658163	-1.797262
C	5.445516	-4.169902	-1.592887	H	5.568725	-2.005565	-2.451288
H	6.449346	-3.978678	-1.165337	C	6.791683	-3.128863	-1.100425
H	5.559386	-4.944128	-2.380019	H	7.468466	-3.029656	-0.228874
H	4.802178	-4.587373	-0.792547	H	7.394300	-3.517349	-1.947769
H	5.077106	-1.327259	-3.659990	H	6.019708	-3.885384	-0.854579
H	5.784787	-2.909092	-4.129614	H	6.543998	0.252498	-2.094288
H	6.613810	-1.882645	-2.918390	H	7.770138	-0.942590	-2.636142
C	5.030730	-1.260079	-0.349199	H	7.739761	-0.404615	-0.927955
C	4.284928	-0.320446	0.451583	C	5.193022	-0.921610	0.626586
C	6.433126	-1.334417	-0.210181	C	4.007985	-0.318745	1.185417
C	7.104343	-0.498226	0.699691	C	6.379658	-0.961348	1.388806
C	6.394154	0.421446	1.489491	C	6.411098	-0.417884	2.685844
C	5.001832	0.503805	1.359772	C	5.264930	0.169584	3.246961
H	8.200106	-0.576338	0.787481	C	4.082397	0.221160	2.496792
H	7.015717	-2.042457	-0.812158	H	7.350593	-0.463083	3.260290
H	4.424717	1.193794	1.996746	H	7.288831	-1.418514	0.979352
H	6.921390	1.066216	2.209212	H	3.165271	0.657654	2.923112
H	2.340401	-1.142612	-0.105863	H	5.290714	0.582711	4.267160
C	-2.742982	-1.083695	1.665406	C	2.524108	4.007914	1.890664
H	-2.187445	-2.013705	1.910558	C	3.828517	3.715828	1.735545
H	-2.707962	-0.450007	2.582416	H	2.683489	-1.121734	-0.340414
C	-4.460128	-2.742200	0.822089	H	4.287352	3.670968	0.734141
C	-5.211722	-0.516219	1.435935	H	4.479886	3.492201	2.597087
C	-5.157475	-2.621268	-0.540687	H	1.880700	4.235456	1.024432
H	-5.082807	-3.355602	1.529284	H	2.045995	4.032888	2.883588
H	-3.536547	-3.331626	0.649409	C	-2.567469	-1.844774	0.387871

C	-5.893074	-0.345952	0.071227
H	-5.971439	-0.800701	2.214785
H	-4.835005	0.482014	1.737429
H	-5.525850	-3.600819	-0.909662
H	-4.477119	-2.143740	-1.292082
H	-6.771390	0.327546	0.116160
H	-5.165118	0.018305	-0.697834
N	-4.121440	-1.461033	1.393832
N	-6.374405	-1.684103	-0.496660
C	-6.819129	-1.450601	-1.919964
H	-7.150375	-2.416746	-2.346704
H	-7.650936	-0.722864	-1.925186
H	-5.934522	-1.044369	-2.472167
C	-7.491016	-2.323499	0.318098
H	-7.737487	-3.262702	-0.218180
H	-7.053546	-2.611581	1.292795
C	-8.740037	-1.474769	0.528373
H	-9.217996	-1.164415	-0.421670
H	-9.481059	-2.087899	1.080486
H	-8.546453	-0.571401	1.139586
Cl	-3.716423	-0.343550	-2.534280

H	-2.256477	-2.921115	0.456712
H	-2.231917	-1.349852	1.322042
C	-4.708190	-2.272239	-0.811246
C	-4.748774	-1.801236	1.542089
C	-6.063961	-1.591032	-0.998265
H	-4.801038	-3.393877	-0.717164
H	-4.149198	-2.096162	-1.753873
C	-6.097133	-1.099399	1.418282
H	-4.858929	-2.874271	1.876741
H	-4.197958	-1.280651	2.353433
H	-6.654557	-2.051093	-1.816150
H	-5.903129	-0.491923	-1.168268
H	-6.706084	-1.182709	2.338569
H	-5.926854	-0.022359	1.138698
N	-4.006614	-1.670819	0.303502
N	-6.936042	-1.643526	0.260802
C	-8.086816	-0.688762	0.047048
H	-8.688986	-1.047341	-0.809894
H	-8.704027	-0.655727	0.963114
H	-7.627688	0.313264	-0.159004
C	-7.433670	-3.063588	0.485427
H	-8.018807	-3.314591	-0.423198
H	-6.539903	-3.717205	0.489353
C	-8.263125	-3.293829	1.743987
H	-9.174125	-2.664271	1.782697
H	-8.597059	-4.351319	1.745552
H	-7.682909	-3.134826	2.674249
Cl	-5.709361	1.645946	-0.353548

TS_Conc

109

PENJOLL-TSconc SCF Done: -3366.08812308 A.U.

C	0.181844	0.249948	0.183002
C	-1.981981	-0.689529	-0.044232
H	-2.244434	-0.629092	-1.127142
C	-2.108962	0.703385	0.571237
H	-2.863787	1.334130	0.048931
H	-2.372818	0.652827	1.656974
C	-0.090201	-3.030616	-1.170534
C	0.263994	-4.395044	-1.143603
H	0.226139	-4.965807	-2.087107
C	0.659772	-5.045843	0.041334
C	0.693528	-4.288064	1.228439
H	0.982264	-4.779132	2.173256
C	0.355328	-2.918550	1.262015
C	-0.028994	-2.290462	0.044281
C	-0.519064	-2.388864	-2.468812
H	-0.252684	-3.031871	-3.330886
H	-0.037424	-1.396208	-2.607473
H	-1.620330	-2.232920	-2.509453
C	1.060668	-6.504557	0.032897

Ci1

109

PENJOLL-CI1 SCF Done: -3366.10527741 A.U.

Ru	1.874612	1.534905	0.238952
C	0.023227	0.693813	0.262365
N	-1.073239	1.507479	0.211509
N	-0.432213	-0.597323	0.383732
C	-1.913274	-0.677383	0.212502
C	-2.337284	0.779382	0.429676
H	-2.139485	-0.971571	-0.840769
H	-3.140838	1.096840	-0.271937
H	-2.688559	0.947101	1.476891
C	0.339396	-1.809724	0.320524
C	-1.079220	2.936218	-0.000251
C	-1.041501	3.822597	1.111053
C	-1.037878	5.209921	0.852910
C	-1.128956	5.729971	-0.451308
C	-1.279623	4.820063	-1.516731
C	-1.282737	3.425561	-1.322740
C	-1.110515	3.327813	2.536462
H	-0.987563	5.903041	1.709812
C	-1.081366	7.220224	-0.706329

H	0.902748	-6.979141	1.022725	H	-1.413992	5.204976	-2.541566
H	2.138619	-6.621695	-0.216776	C	-1.573724	2.499728	-2.477043
H	0.490582	-7.082544	-0.723024	H	-0.367110	2.531792	2.745283
C	0.398954	-2.163292	2.566107	H	-2.123674	2.925485	2.760697
H	0.528587	-2.856733	3.420141	H	-0.925174	4.157316	3.247286
H	-0.527337	-1.574198	2.732309	H	-1.297862	7.801388	0.212763
H	1.234427	-1.426101	2.583032	H	-1.808943	7.524275	-1.487316
C	-0.547194	2.658175	0.548424	H	-0.075357	7.531370	-1.065138
C	-0.759570	3.486182	-0.589160	H	-1.542291	3.054141	-3.435626
C	-0.638845	4.880670	-0.420270	H	-2.590138	2.051241	-2.381618
H	-0.790228	5.528633	-1.300001	H	-0.827485	1.683751	-2.535651
C	-0.357652	5.467196	0.829245	C	0.781078	-2.418552	1.526926
C	-0.229322	4.618106	1.945189	C	0.565871	-2.426348	-0.939572
H	-0.055486	5.057553	2.942053	C	1.427092	-3.667662	1.444181
C	-0.338573	3.216068	1.838871	C	1.210760	-3.680801	-0.961190
C	-1.155992	2.912418	-1.927054	C	1.641019	-4.323453	0.215155
H	-1.081861	3.685457	-2.717787	C	2.333310	-5.668183	0.171701
H	-2.217830	2.570154	-1.903340	H	1.771406	-4.143503	2.378031
H	-0.515664	2.054010	-2.220702	C	0.188433	-1.740722	-2.233102
C	-0.199742	6.965302	0.964534	H	1.386064	-4.165452	-1.936795
H	-0.902305	7.511506	0.301918	C	0.578457	-1.750742	2.864966
H	0.827605	7.284771	0.681080	H	1.028680	-0.733889	2.882914
H	-0.372539	7.303799	2.006208	H	1.030810	-2.352424	3.677689
C	-0.259413	2.357590	3.078293	H	-0.498750	-1.619066	3.102078
H	-0.208711	2.988533	3.987539	H	0.641784	-0.725797	-2.303114
H	0.639197	1.701876	3.058051	H	-0.908806	-1.601592	-2.340008
H	-1.146990	1.696755	3.177479	H	0.532525	-2.330683	-3.105204
C	2.686924	-1.063082	-0.378598	H	2.305233	-6.112818	-0.843409
H	2.219986	-1.706978	-1.153828	H	1.862851	-6.390486	0.872234
C	3.937200	-1.579024	0.195816	H	3.399760	-5.581362	0.473006
C	4.018258	-2.897995	0.712525	C	2.867427	-0.041006	0.064354
H	3.123127	-3.537126	0.667708	Cl	1.871940	1.646681	2.661549
C	5.195638	-3.370809	1.309839	Cl	1.765189	1.837921	-2.148810
H	5.225067	-4.388528	1.730489	O	4.435210	-1.695419	-1.417125
C	6.331999	-2.544095	1.376971	C	5.172260	-2.321142	-2.499088
H	7.255511	-2.904960	1.857223	C	6.450436	-1.557799	-2.862771
C	6.291988	-1.255447	0.819754	H	4.456923	-2.183684	-3.337574
C	5.113498	-0.776950	0.220309	C	5.355886	-3.832950	-2.311227
N	-0.513836	-0.939830	0.077828	H	6.135295	-4.094224	-1.568380
N	-0.741525	1.234830	0.415648	H	5.652605	-4.288690	-3.278840
Cl	1.610287	0.531138	-2.510798	H	4.402153	-4.298749	-1.992029
Cl	2.651196	0.600881	2.276392	H	6.229994	-0.479776	-2.995735
Ru	2.097842	0.674343	-0.079153	H	6.848340	-1.946612	-3.822929
H	7.172426	-0.595830	0.847947	H	7.248552	-1.658289	-2.101272
O	5.090950	0.479908	-0.349247	C	4.910394	-1.450889	-0.168804
C	5.515255	0.639362	-1.758202	C	4.113976	-0.543389	0.626240
C	3.034163	2.848777	0.303245	C	6.095590	-1.996611	0.371724
C	2.640679	2.898271	-1.012211	C	6.506757	-1.655085	1.671270
H	4.054213	2.555734	0.596135	C	5.750527	-0.765137	2.454462
H	2.389020	3.242275	1.104486	C	4.577693	-0.211593	1.927471

H	1.675664	3.329931	-1.310440	H	7.437452	-2.092175	2.068537
H	3.325438	2.642955	-1.834013	H	6.707877	-2.690700	-0.217133
C	6.216888	1.992886	-1.840058	H	3.960079	0.481554	2.520893
H	5.585758	2.798048	-1.415380	H	6.077533	-0.500878	3.472055
H	6.434094	2.249396	-2.897588	C	3.041026	3.479251	0.422675
H	7.174854	1.974041	-1.279084	C	4.034943	2.599103	0.037107
C	6.386754	-0.499586	-2.284706	H	2.474301	-0.697314	-0.737182
H	4.573503	0.663357	-2.354865	H	4.264657	2.430776	-1.026330
H	7.354948	-0.571421	-1.747219	H	4.726909	2.174173	0.779092
H	6.603664	-0.304580	-3.355357	H	2.483493	4.060143	-0.334979
H	5.876999	-1.480960	-2.218046	H	2.942607	3.799611	1.472287
C	-2.893351	-1.753237	0.599356	C	-2.627408	-1.689818	1.130043
N	-4.287570	-1.451153	0.304804	H	-2.094342	-2.669569	1.103106
H	-2.740191	-1.767020	1.700150	H	-2.584737	-1.336865	2.182863
H	-2.613390	-2.769263	0.236298	C	-4.372650	-2.824738	-0.260098
C	-5.228192	-1.124684	1.348507	C	-5.106123	-1.458043	1.596236
C	-4.899510	-2.019800	-0.871293	C	-5.531832	-2.323057	-1.121688
C	-6.262764	-0.127502	0.824032	H	-4.589929	-3.835770	0.192210
H	-4.701440	-0.617848	2.183042	H	-3.521672	-2.984725	-0.954909
H	-5.726465	-2.032006	1.799861	C	-6.271285	-0.911090	0.768213
C	-5.941932	-1.058840	-1.444098	H	-5.444266	-2.293407	2.277033
H	-5.329215	-3.047321	-0.687929	H	-4.784333	-0.632174	2.263656
H	-4.135968	-2.150670	-1.666447	H	-5.883977	-3.088657	-1.842846
N	-7.002455	-0.651309	-0.410737	H	-5.225003	-1.375164	-1.641487
H	-6.488376	-1.492621	-2.306173	H	-7.146246	-0.641537	1.391015
H	-5.444276	-0.089195	-1.716801	H	-5.923294	-0.032263	0.162491
H	-7.026620	0.131087	1.582711	N	-4.018733	-1.834110	0.727603
H	-5.744155	0.794363	0.448645	N	-6.752595	-1.908578	-0.288788
C	-7.916156	-1.831504	-0.113510	C	-7.693505	-1.173985	-1.213917
C	-8.995963	-1.595972	0.936817	H	-8.042625	-1.878644	-1.992983
H	-7.263324	-2.674023	0.185470	H	-8.550348	-0.790547	-0.630743
H	-8.368812	-2.101094	-1.089790	H	-7.105483	-0.329541	-1.656950
H	-8.579032	-1.405555	1.945319	C	-7.416877	-3.142313	0.303218
H	-9.611505	-2.515653	1.007692	H	-7.691206	-3.771631	-0.568182
H	-9.679763	-0.765300	0.672692	H	-6.633333	-3.686575	0.864398
C	-7.780518	0.499938	-1.002700	C	-8.629476	-2.893692	1.193327
H	-7.030925	1.293090	-1.255690	H	-9.451806	-2.369391	0.667824
H	-8.505765	0.870279	-0.255741	H	-9.024553	-3.878499	1.515720
H	-8.308445	0.138345	-1.905849	H	-8.378609	-2.328175	2.112529
Cl	-4.839008	2.073677	-1.263929	Cl	-5.126846	0.900851	-1.808296
TS_MCy				MCy			
109				109			
PENJOLL-TSMCy SCF Done: -3366.10238633 A.U.				PENJOLL-MCy SCF Done: -3366.11455475 A.U.			
Ru	1.771061	1.627781	0.003773	Ru	1.779185	1.462610	0.123671
C	-0.074028	0.820485	0.327050	C	-0.112862	0.801682	0.335753
N	-1.231683	1.533035	0.263924	N	-1.240458	1.549370	0.257586
N	-0.398719	-0.505821	0.446508	N	-0.460066	-0.513395	0.475683
C	-1.850426	-0.721938	0.182031	C	-1.918170	-0.695475	0.219017
C	-2.424389	0.676035	0.437154	C	-2.453001	0.722804	0.458751
C	-2.506729	-1.847039	1.000884	C	-2.596339	-1.793684	1.057243

H	-1.979213	-0.969779	-0.898791	H	-2.056979	-0.956036	-0.857518
H	-3.250458	0.938512	-0.260882	H	-3.279060	0.996620	-0.235454
H	-2.809770	0.776577	1.482190	H	-2.819785	0.850334	1.506787
C	0.512930	-1.605391	0.598040	C	0.454077	-1.621466	0.603622
C	-1.357288	2.967587	0.167414	C	-1.334091	2.983033	0.113440
C	-1.269426	3.753193	1.347587	C	-1.218250	3.807656	1.263810
C	-1.396049	5.153444	1.224364	C	-1.322611	5.203321	1.091007
C	-1.645763	5.774902	-0.012000	C	-1.570197	5.784940	-0.166645
C	-1.817383	4.953134	-1.144951	C	-1.757925	4.926861	-1.268090
C	-1.704518	3.551116	-1.085239	C	-1.665734	3.525210	-1.158740
C	-1.088327	3.131341	2.711581	C	-1.030549	3.230198	2.646825
H	-1.314281	5.771516	2.134443	H	-1.225908	5.851785	1.978296
C	-1.762832	7.278667	-0.130416	C	-1.638534	7.286947	-0.334774
H	-2.066713	5.414950	-2.115319	H	-2.000044	5.357876	-2.254195
C	-2.016198	2.710789	-2.297706	C	-1.968807	2.647640	-2.347179
H	-0.042510	2.783779	2.861328	H	-1.181577	4.011310	3.417983
H	-1.748954	2.250329	2.851691	H	-0.012355	2.803362	2.783797
H	-1.325208	3.864253	3.508127	H	-1.753474	2.411880	2.850274
H	-1.606509	7.781778	0.844602	H	-0.680227	7.688162	-0.733033
H	-2.762097	7.578827	-0.513002	H	-1.833887	7.799692	0.628814
H	-1.014305	7.684252	-0.844911	H	-2.433198	7.582303	-1.050848
H	-2.063862	3.343582	-3.206095	H	-2.024774	3.254999	-3.272269
H	-3.006499	2.209516	-2.189856	H	-2.951646	2.134477	-2.228093
H	-1.241146	1.935212	-2.460894	H	-1.181222	1.879874	-2.488474
C	0.985475	-1.922774	1.901333	C	0.902395	-1.990498	1.903717
C	0.867929	-2.397434	-0.525932	C	0.821830	-2.379534	-0.542389
C	1.816134	-3.049546	2.053190	C	1.764440	-3.098425	2.020739
C	1.702400	-3.515061	-0.313242	C	1.676784	-3.485350	-0.359371
C	2.188061	-3.859949	0.961966	C	2.169690	-3.856214	0.905621
C	3.109738	-5.043063	1.157469	C	3.127820	-5.014637	1.064670
H	2.183535	-3.301102	3.062298	H	2.123379	-3.380682	3.024709
C	0.383155	-2.064848	-1.917819	C	0.328868	-2.031655	-1.926634
H	1.980044	-4.135671	-1.182423	H	1.967613	-4.073731	-1.245869
C	0.624804	-1.073826	3.096135	C	0.485642	-1.231725	3.139029
H	1.114096	-0.074486	3.039160	H	1.041374	-0.269662	3.214008
H	0.940917	-1.561795	4.039140	H	0.689675	-1.824407	4.052629
H	-0.466467	-0.879716	3.153605	H	-0.591780	-0.969454	3.123761
H	-0.693757	-2.310099	-2.055031	H	-0.759754	-2.228484	-2.045518
H	0.943677	-2.646244	-2.676378	H	0.853189	-2.639563	-2.689884
H	0.507739	-0.983513	-2.148156	H	0.501786	-0.958208	-2.163744
H	2.874169	-5.594697	2.091199	H	2.943853	-5.574230	2.005053
H	4.167721	-4.708778	1.237016	H	4.176533	-4.646332	1.104855
H	3.048922	-5.756456	0.310731	H	3.057777	-5.727307	0.217940
C	3.131613	0.354749	-0.384204	C	3.610056	0.771242	-0.428512
Cl	2.199441	2.150337	2.330804	Cl	2.165873	1.787490	2.484288
Cl	1.255762	1.504693	-2.368048	Cl	1.333165	1.383185	-2.259359
O	4.781805	-1.366128	-1.704520	O	4.578907	-1.463020	-1.700946
C	5.599568	-2.077187	-2.668280	C	5.394936	-1.997134	-2.777146
C	7.043209	-1.561668	-2.719200	C	6.799978	-1.389164	-2.819095
H	5.108866	-1.767389	-3.615306	H	4.839839	-1.628459	-3.666585

C	5.455683	-3.602023	-2.573794	C	5.370618	-3.530752	-2.838854
H	6.009970	-4.048067	-1.725153	H	6.015206	-4.008521	-2.073569
H	5.841697	-4.063604	-3.506151	H	5.730128	-3.868340	-3.833372
H	4.386974	-3.876962	-2.471995	H	4.335285	-3.902520	-2.704606
H	7.052542	-0.455791	-2.795854	H	6.746179	-0.281844	-2.808418
H	7.548113	-1.968954	-3.619542	H	7.309344	-1.698726	-3.754964
H	7.644157	-1.851046	-1.834914	H	7.429273	-1.712789	-1.966154
C	4.975415	-1.327618	-0.361202	C	5.005475	-1.308641	-0.412205
C	4.109951	-0.428758	0.374830	C	4.473432	-0.185370	0.309237
C	5.944478	-2.087143	0.333761	C	5.893263	-2.202138	0.229402
C	6.078978	-1.970276	1.726740	C	6.264713	-2.001964	1.568185
C	5.250721	-1.100594	2.456269	C	5.742544	-0.915010	2.290663
C	4.281394	-0.350949	1.780773	C	4.855878	-0.030343	1.663441
H	6.847863	-2.570557	2.240463	H	6.958470	-2.711080	2.048522
H	6.608727	-2.771263	-0.207796	H	6.287517	-3.067156	-0.319440
H	3.626532	0.345197	2.327709	H	4.406786	0.796902	2.234205
H	5.359886	-1.007139	3.547752	H	6.018183	-0.761265	3.345632
C	2.828279	3.441330	-0.511116	C	2.566505	3.252391	-0.178473
C	3.892283	2.507685	-0.509018	C	3.848177	2.340977	-0.247872
H	3.167419	0.118899	-1.466851	H	3.564877	0.508484	-1.499056
H	4.319549	2.181021	-1.471006	H	4.354186	2.619355	-1.194623
H	4.532768	2.406714	0.381110	H	4.482813	2.514666	0.640066
H	2.419974	3.802602	-1.469645	H	2.300600	3.741193	-1.134074
H	2.690005	4.081863	0.377201	H	2.553582	3.914441	0.707775
N	-3.876034	-2.048657	0.545876	N	-3.963340	-1.987342	0.594765
H	-2.520105	-1.570835	2.076889	H	-2.615084	-1.493391	2.126410
H	-1.898622	-2.780789	0.923218	H	-1.997974	-2.735633	1.005929
C	-4.990072	-1.969748	1.459927	C	-5.085885	-1.860827	1.493042
C	-4.112000	-2.923582	-0.578648	C	-4.204825	-2.887732	-0.508175
C	-6.234182	-1.472635	0.720729	C	-6.306889	-1.350982	0.724925
H	-4.774312	-1.218676	2.247773	H	-4.862416	-1.097211	2.266486
H	-5.196157	-2.939481	2.001127	H	-5.321614	-2.812677	2.053241
C	-5.343572	-2.463527	-1.358048	C	-5.414681	-2.419950	-1.316267
H	-4.180481	-4.009944	-0.279924	H	-4.303517	-3.963087	-0.180063
H	-3.260898	-2.861211	-1.288706	H	-3.343139	-2.865419	-1.207646
N	-6.593320	-2.357428	-0.474676	N	-6.672578	-2.255940	-0.453350
H	-5.597625	-3.151330	-2.190001	H	-5.676503	-3.125188	-2.131000
H	-5.181309	-1.413447	-1.725860	H	-5.219043	-1.385914	-1.711308
H	-7.125355	-1.425902	1.375821	H	-7.205841	-1.263497	1.364971
H	-6.025000	-0.472612	0.255189	H	-6.062968	-0.369103	0.238247
C	-7.066621	-3.749255	-0.080398	C	-7.190828	-3.623321	-0.029873
C	-8.258389	-3.809737	0.868677	C	-8.399013	-3.624612	0.900595
H	-6.196061	-4.270231	0.362411	H	-6.341901	-4.155691	0.440669
H	-7.297855	-4.258609	-1.038464	H	-7.421618	-4.152268	-0.977347
H	-8.027498	-3.395890	1.870105	H	-8.176652	-3.179490	1.890446
H	-8.529476	-4.875600	1.011003	H	-8.695056	-4.678719	1.076653
H	-9.155291	-3.295858	0.469948	H	-9.278157	-3.106976	0.468138
C	-7.648586	-1.634018	-1.277954	C	-7.695610	-1.525185	-1.290453
H	-7.190362	-0.662678	-1.599517	H	-7.213713	-0.567061	-1.614838
H	-8.532779	-1.457709	-0.638917	H	-8.591209	-1.326178	-0.674513

H -7.921461 -2.262867 -2.147114	H -7.958914 -2.160631 -2.157682
Cl -5.437487 0.853613 -1.555257	Cl -5.393784 0.888794 -1.590270
TS_Ci2	Ci2
109	109
PENJOLL-TS2 SCF Done: -3366.09225128 A.U.	PENJOLL-CI2 SCF Done: -3366.09868040 A.U.
Ru 1.653322 1.419209 0.235439	Ru -1.903775 0.830631 -1.035166
C -0.051437 0.679886 -0.551171	C 0.132365 0.672602 -0.645949
N -1.242116 1.328635 -0.658702	N 1.022692 1.661758 -0.378300
N -0.237122 -0.630573 -0.905892	N 0.807480 -0.512252 -0.718919
C -1.677654 -0.947870 -1.098355	C 2.257634 -0.363748 -0.381311
C -2.312943 0.452213 -1.191043	C 2.411834 1.163240 -0.287982
H -1.794874 -1.512018 -2.048723	H 2.449147 -0.795493 0.627876
H -2.543404 0.743572 -2.240469	H 2.874154 1.456625 0.678685
H -3.260880 0.540332 -0.614640	H 3.007432 1.585786 -1.130517
C 0.770430 -1.617279 -1.212631	C 0.228411 -1.839216 -0.736932
C -1.489215 2.740343 -0.508877	C 0.795132 3.065699 -0.145567
C -2.213124 3.210461 0.619810	C 0.992281 3.996831 -1.202272
C -2.450631 4.595543 0.721128	C 0.817904 5.366713 -0.920695
C -2.024990 5.508904 -0.263305	C 0.492839 5.832853 0.368159
C -1.364612 4.998611 -1.397067	C 0.375923 4.885794 1.403889
C -1.097880 3.622680 -1.553920	C 0.538453 3.502272 1.185040
C -2.772961 2.268251 1.654467	C 1.403717 3.557539 -2.586952
H -3.003820 4.967222 1.600195	H 0.952179 6.092119 -1.741081
C -2.278031 6.991897 -0.103751	C 0.268409 7.305577 0.630166
H -1.060197 5.688413 -2.202412	H 0.163558 5.230175 2.430110
C -0.436844 3.118542 -2.813521	C 0.459599 2.533008 2.336573
H -2.060245 1.448557 1.874882	H 0.743905 2.750225 -2.972006
H -3.738777 1.843208 1.290914	H 2.447940 3.172080 -2.595703
H -2.981462 2.806287 2.600716	H 1.366725 4.408338 -3.295713
H -2.133137 7.537701 -1.057702	H 0.552934 7.585846 1.664957
H -1.585727 7.439109 0.643345	H -0.804193 7.573688 0.504306
H -3.309539 7.192377 0.253854	H 0.846292 7.940427 -0.072160
H -0.380991 3.922234 -3.573984	H 0.319751 3.076790 3.291634
H -1.000934 2.271967 -3.259215	H 1.378538 1.912740 2.433541
H 0.595871 2.748377 -2.623270	H -0.394134 1.831532 2.208203
C 1.309619 -2.465408 -0.211332	C 0.017625 -2.508012 -1.977260
C 1.134892 -1.779839 -2.582312	C 0.006238 -2.508820 0.505537
C 2.184482 -3.499684 -0.616919	C -0.462273 -3.836318 -1.944973
C 1.993941 -2.836514 -2.928115	C -0.457496 -3.839052 0.465215
C 2.517713 -3.722695 -1.962972	C -0.697945 -4.523548 -0.741164
C 3.387104 -4.889862 -2.377336	C -1.159704 -5.964341 -0.735358
H 2.606110 -4.159276 0.160381	H -0.636299 -4.351747 -2.904747
C 0.655224 -0.815093 -3.638966	C 0.214426 -1.842101 1.842358
H 2.269531 -2.966223 -3.988545	H -0.643774 -4.352426 1.423481
C 0.979837 -2.329676 1.258072	C 0.323683 -1.875830 -3.314723
H 0.569520 -1.336309 1.523971	H -0.126668 -0.866322 -3.425115
H 1.892641 -2.479416 1.870147	H -0.047743 -2.517398 -4.138387
H 0.248796 -3.106215 1.575097	H 1.417727 -1.752163 -3.466346
H -0.447151 -0.683771 -3.635788	H 1.242757 -1.452369 2.006163
H 0.954416 -1.153871 -4.650225	H -0.004641 -2.553144 2.663045

H	1.109090	0.184518	-3.455683	H	-0.479932	-0.979360	1.944995
H	2.770521	-5.716292	-2.795597	H	-0.313738	-6.655413	-0.523694
H	3.955095	-5.304822	-1.520660	H	-1.591330	-6.262629	-1.712020
H	4.112375	-4.603224	-3.167086	H	-1.922614	-6.144145	0.050091
C	3.831647	1.377819	0.969533	C	-4.204211	0.182349	-1.015547
Cl	0.581302	1.096289	2.396218	Cl	-1.135891	1.267572	-3.331447
Cl	2.710351	1.647185	-1.927715	Cl	-2.294768	0.512056	1.343593
O	5.359204	-0.620389	-0.076525	O	-5.948124	0.063063	1.092045
C	6.558842	-1.157349	-0.690413	C	-6.426340	0.389039	2.423980
C	7.823073	-0.869494	0.125869	C	-7.876291	-0.063707	2.646150
H	6.607110	-0.545803	-1.616543	H	-6.435459	1.499750	2.378472
C	6.401842	-2.618714	-1.129394	C	-5.451284	-0.014349	3.533090
H	6.497915	-3.340770	-0.293461	H	-5.430459	-1.107717	3.711972
H	7.186744	-2.867003	-1.873973	H	-5.753511	0.477837	4.480846
H	5.412597	-2.764430	-1.606292	H	-4.424985	0.313910	3.272928
H	7.886320	0.207986	0.379347	H	-8.506078	0.216168	1.777461
H	8.718041	-1.133601	-0.474667	H	-8.289326	0.438728	3.545904
H	7.864512	-1.449929	1.068961	H	-7.969924	-1.157324	2.803339
C	4.974556	-0.833149	1.211539	C	-5.417944	-1.140052	0.730358
C	4.115396	0.169495	1.778094	C	-4.510467	-1.112949	-0.378098
C	5.341777	-1.958834	1.984668	C	-5.769625	-2.376901	1.315814
C	4.879486	-2.099432	3.302918	C	-5.231579	-3.577260	0.824989
C	4.040652	-1.123968	3.870076	C	-4.340903	-3.564087	-0.261659
C	3.669021	-0.008295	3.109138	C	-3.994444	-2.340225	-0.850186
H	5.179954	-2.984445	3.887043	H	-5.522187	-4.530047	1.296378
H	5.985242	-2.736132	1.553640	H	-6.484064	-2.406734	2.148490
H	2.990842	0.741192	3.541738	H	-3.284223	-2.334372	-1.692704
H	3.674738	-1.232124	4.902755	H	-3.919138	-4.502244	-0.652129
C	1.386552	3.232836	0.350326	C	-2.061317	2.621927	-0.797308
C	3.309654	2.598903	1.453146	C	-3.686064	0.353136	-2.304797
H	4.392358	1.419756	0.023023	H	-4.678343	1.043332	-0.522080
H	3.647705	3.525849	0.962679	H	-3.858959	1.285672	-2.861338
H	2.941577	2.695353	2.486866	H	-3.431598	-0.514984	-2.936300
H	1.758995	3.927562	-0.436480	H	-2.365969	3.037770	0.188344
H	0.839429	3.693479	1.203948	H	-1.891051	3.334631	-1.633878
C	-2.195403	-1.803935	0.088174	C	3.194133	-1.073410	-1.391049
H	-1.697342	-2.808830	0.050079	H	2.742983	-2.056152	-1.644818
H	-1.857197	-1.311723	1.023295	H	3.230866	-0.493080	-2.342100
C	-4.324818	-2.588811	-0.925577	C	4.902165	-2.537708	-0.228557
C	-4.225157	-2.180848	1.436231	C	5.575184	-0.310291	-0.919370
C	-5.795805	-2.173755	-0.965618	C	5.425873	-2.277529	1.191783
H	-4.197177	-3.709155	-0.860181	H	5.644172	-3.145482	-0.815665
H	-3.900810	-2.295477	-1.908477	H	4.006437	-3.182888	-0.119727
C	-5.686014	-1.745228	1.462188	C	6.078986	0.000608	0.495848
H	-4.098473	-3.262107	1.736734	H	6.435846	-0.592897	-1.585848
H	-3.705574	-1.582248	2.213654	H	5.174764	0.635841	-1.336046
H	-6.365737	-2.723074	-1.742141	H	5.812372	-3.200764	1.670809
H	-5.859853	-1.061069	-1.110775	H	4.633036	-1.802668	1.824847
H	-6.177495	-1.959965	2.430208	H	6.911613	0.731218	0.500689
H	-5.746111	-0.650252	1.208992	H	5.242478	0.361508	1.147675

N	-3.644146	-1.884771	0.141143	N	4.548432	-1.323988	-0.924336
N	-6.517518	-2.413428	0.365251	N	6.574683	-1.257682	1.215251
C	-7.840386	-1.688207	0.293568	C	6.827424	-0.894547	2.658559
H	-8.442840	-2.134154	-0.520965	H	7.157805	-1.803998	3.196144
H	-8.363409	-1.795810	1.261119	H	7.610568	-0.116165	2.703028
H	-7.598134	-0.613302	0.088397	H	5.860144	-0.508448	3.068620
C	-6.721875	-3.905765	0.579117	C	7.821230	-1.865179	0.585915
H	-7.348176	-4.239109	-0.273879	H	8.063438	-2.745642	1.215903
H	-5.730100	-4.383498	0.461123	H	7.525899	-2.250236	-0.408585
C	-7.351233	-4.315650	1.905953	C	9.028135	-0.941992	0.457799
H	-8.349342	-3.863115	2.070295	H	9.369868	-0.537643	1.431106
H	-7.490165	-5.415823	1.893718	H	9.867445	-1.532638	0.037675
H	-6.707375	-4.078953	2.775774	H	8.848252	-0.095443	-0.233890
Cl	-5.973619	1.055996	-0.239873	Cl	3.603429	0.035207	2.804848

TS_I14e

109

PENJOLL-TS3FFfprovarCll SCF Done: -3366.09257217 A.U.

Ru	-1.650780	-0.786407	-0.238408
C	0.205730	-0.227864	-0.440500
N	0.761054	1.018440	-0.472902
N	1.237231	-1.148921	-0.434006
C	2.531610	-0.479341	-0.146718
C	2.232977	0.961794	-0.582590
H	2.711828	-0.486247	0.955112
H	2.736698	1.716664	0.062691
H	2.540390	1.136460	-1.644158
C	1.054528	-2.578145	-0.403258
C	0.075936	2.276563	-0.553700
C	-0.340926	2.762957	-1.822835
C	-0.940466	4.037473	-1.880391
C	-1.113007	4.833585	-0.731355
C	-0.665382	4.327205	0.506447
C	-0.059719	3.061950	0.626340
C	-0.158132	1.941121	-3.075788
H	-1.271646	4.422020	-2.859924
C	-1.748557	6.204248	-0.814474
H	-0.781363	4.940932	1.415714
C	0.438320	2.562393	1.958667
H	-0.780361	1.017644	-3.055666
H	0.895555	1.612080	-3.200277
H	-0.437330	2.525245	-3.974795
H	-2.663638	6.264588	-0.186799
H	-2.032849	6.463453	-1.853905
H	-1.056905	6.991710	-0.445244
H	0.106801	3.234286	2.774908
H	1.552553	2.534432	1.984925
H	0.057664	1.540380	2.172407
C	0.885828	-3.268441	-1.638832
C	1.117735	-3.293627	0.827679

I14e

83

PENJOLL-14e2 SCF Done: -2863.66506662 A.U.

Ru	3.154852	0.752716	-0.029989
C	1.347074	0.070751	-0.195657
N	0.888154	-1.219899	-0.253813
N	0.255488	0.904730	-0.386180
C	-1.031169	0.154056	-0.429687
C	-0.554344	-1.301438	-0.547600
H	-1.566330	0.264031	0.541894
H	-1.072849	-1.949783	0.190665
H	-0.703725	-1.714145	-1.574982
C	0.212530	2.316006	-0.078229
C	1.602090	-2.453416	-0.078724
C	2.151821	-3.114221	-1.205479
C	2.791307	-4.354898	-1.000535
C	2.884500	-4.947264	0.273391
C	2.310735	-4.266143	1.367470
C	1.661850	-3.024082	1.221773
C	2.079755	-2.504245	-2.585448
H	3.229342	-4.872982	-1.870471
C	3.590669	-6.270329	0.474567
H	2.368105	-4.713991	2.374129
C	1.080883	-2.308547	2.417874
H	2.584707	-1.515096	-2.618328
H	1.029529	-2.337031	-2.909167
H	2.558469	-3.164554	-3.335070
H	2.970895	-6.976196	1.066801
H	4.543529	-6.136253	1.031634
H	3.835173	-6.756202	-0.491130
H	1.253104	-2.891020	3.344195
H	-0.015387	-2.133447	2.328293
H	1.552683	-1.311463	2.550187
C	0.366203	3.271191	-1.120848
C	-0.087334	2.725716	1.255056
C	0.253210	4.640090	-0.793566

C	0.697567	-4.665490	-1.604393	C	-0.197735	4.104846	1.514783
C	0.929540	-4.690393	0.797024	C	-0.022478	5.080084	0.512855
C	0.703840	-5.395530	-0.400976	C	-0.100619	6.553702	0.844489
C	0.521510	-6.897552	-0.398042	H	0.379915	5.383976	-1.598356
H	0.550749	-5.198363	-2.559037	C	-0.246477	1.738958	2.387869
C	1.391317	-2.605668	2.142882	H	-0.413295	4.425842	2.547995
H	0.956741	-5.242527	1.751885	C	0.643134	2.877261	-2.552884
C	0.907041	-2.549135	-2.963883	H	1.683299	2.508187	-2.679210
H	-0.072441	-2.051740	-3.150006	H	0.497035	3.741466	-3.230804
H	1.101185	-3.257662	-3.793389	H	-0.011682	2.051817	-2.896876
H	1.677550	-1.752282	-2.988620	H	-1.128192	1.067576	2.290742
H	2.451415	-2.277084	2.222754	H	-0.343783	2.274562	3.352405
H	1.199896	-3.293207	2.990057	H	0.648015	1.088277	2.460900
H	0.740000	-1.715844	2.275671	H	-0.253729	7.172142	-0.062871
H	0.046633	-7.249169	0.540472	H	0.839815	6.901166	1.326183
H	1.499410	-7.421716	-0.484445	H	-0.924776	6.771296	1.555407
H	-0.104956	-7.234978	-1.248466	Cl	3.583787	0.931978	-2.320167
C	-4.577899	-1.759155	0.071007	Cl	3.157763	1.994175	1.929478
Cl	-2.209080	-1.114388	-2.549321	C	4.107560	-0.708018	0.452355
Cl	-1.543395	-0.754131	2.146599	H	5.213436	-0.537020	0.517867
O	-5.904055	0.539942	-0.543654	H	3.749518	-1.721291	0.719562
C	-6.563938	1.668469	-1.169977	C	-1.979446	0.643222	-1.553651
C	-8.084921	1.492272	-1.262662	H	-1.903535	1.750424	-1.605950
H	-6.161724	1.591898	-2.202649	H	-1.624688	0.261217	-2.539218
C	-6.101884	3.019744	-0.609262	C	-4.286231	1.165885	-0.656915
H	-6.510428	3.242170	0.395829	C	-3.932848	-0.975348	-1.750408
H	-6.429680	3.830502	-1.292599	C	-4.924248	0.463984	0.550053
H	-4.995612	3.051292	-0.548640	H	-5.080010	1.594815	-1.328277
H	-8.331783	0.494439	-1.678012	H	-3.731204	2.038155	-0.254860
H	-8.502499	2.259645	-1.947064	C	-4.539643	-1.714435	-0.550685
H	-8.598847	1.596756	-0.286730	H	-4.694811	-0.880034	-2.572768
C	-6.066117	0.138999	0.747822	H	-3.133375	-1.626293	-2.158882
C	-5.347881	-1.052021	1.102723	H	-5.708571	1.085763	1.028910
C	-6.840394	0.804977	1.724154	H	-4.140582	0.168185	1.293158
C	-6.897798	0.314707	3.039312	H	-5.025872	-2.666849	-0.840246
C	-6.186729	-0.840564	3.405732	H	-3.766669	-1.898499	0.238852
C	-5.424543	-1.507860	2.438789	N	-3.383299	0.306465	-1.383775
H	-7.507232	0.851486	3.784138	N	-5.592339	-0.866233	0.169672
H	-7.395195	1.715930	1.469663	C	-5.955330	-1.572725	1.453111
H	-4.873904	-2.419225	2.716425	H	-6.696771	-0.955612	1.995958
H	-6.229093	-1.219805	4.438172	H	-6.382571	-2.563313	1.213146
C	-2.349846	0.894733	-0.274313	H	-5.009938	-1.681755	2.040847
C	-3.695194	-2.787454	0.263022	C	-6.835617	-0.599114	-0.668779
H	-4.757530	-1.427438	-0.964217	H	-7.497958	0.006599	-0.016922
H	-3.258487	-3.302533	-0.607486	H	-6.524971	0.051017	-1.508522
H	-3.436859	-3.169343	1.263175	C	-7.569194	-1.827769	-1.194668
H	-2.531892	1.465683	0.663980	H	-7.903754	-2.510741	-0.388972
H	-2.708499	1.357615	-1.220673	H	-8.478640	-1.481344	-1.726353
C	3.758552	-1.117783	-0.822663	H	-6.967996	-2.406591	-1.923145
H	3.761582	-2.219260	-0.638975	Cl	-2.691200	-1.360419	2.264132

H	3.693619	-0.988161	-1.924180
C	5.601292	-0.984123	0.865375
C	5.885242	0.197135	-1.224980
C	6.261338	0.161570	1.633678
H	6.321281	-1.830303	0.668160
H	4.828473	-1.400312	1.544769
C	6.527278	1.381213	-0.499358
H	6.670397	-0.479453	-1.672880
H	5.322358	0.622616	-2.081192
H	6.819590	-0.193103	2.523817
H	5.482651	0.922538	1.910901
H	7.256305	1.923541	-1.131923
H	5.729185	2.075246	-0.123852
N	4.977979	-0.487444	-0.337464
N	7.259248	0.951046	0.774376
C	7.616978	2.202039	1.541073
H	8.125400	1.905210	2.478319
H	8.285632	2.827666	0.922319
H	6.652159	2.732681	1.749203
C	8.495188	0.103687	0.506640
H	8.922915	-0.109323	1.507884
H	8.140741	-0.860391	0.093462
C	9.546022	0.718599	-0.411466
H	9.932907	1.687718	-0.038761
H	10.407202	0.021568	-0.460731
H	9.181342	0.857460	-1.448338
Cl	4.338234	2.875149	1.565679

Table S4 Coordinates data set, absolute energies (a.u.) for DFT all the optimized ammonium tagged complexes (AquaMet^{TM+}).

Precat				TS_Open			
102				102			
precatnocl_2 SCF Done: -2827.27562574 A.U.				PENJOLL-TSopen+ SCF Done: -2827.24323473 A.U.			
Ru	-2.060265	0.144218	-0.093212	Ru	-1.992635	0.608443	-0.145316
C	-0.130029	0.287434	0.165466	C	-0.070178	0.545674	-0.148280
N	0.517680	1.505660	0.264766	N	0.702837	1.682489	0.027551
N	0.870381	-0.678845	0.111124	N	0.813004	-0.528879	-0.163593
C	2.225674	-0.112459	0.286404	C	2.169955	-0.124673	0.271797
C	1.975508	1.399977	0.170586	C	2.138598	1.388891	0.026369
H	2.467494	1.989911	0.972210	H	2.266426	-0.328062	1.367479
H	2.340886	1.798061	-0.805573	H	2.663349	1.969840	0.811522
C	0.707005	-2.092842	0.336437	H	2.599296	1.652545	-0.956943
C	-0.064410	2.821792	0.385524	C	0.498938	-1.922069	-0.321048
C	-0.295220	3.612365	-0.772506	C	0.278120	3.057834	-0.094992
C	-0.846094	4.899462	-0.597565	C	0.206064	3.654828	-1.382164
C	-1.120648	5.434749	0.674999	C	-0.194729	5.001703	-1.468896
C	-0.789678	4.656924	1.802890	C	-0.492599	5.771187	-0.327835
C	-0.253583	3.360957	1.688580				

C	0.104986	3.153702	-2.155864	C	-0.332513	5.168506	0.935705
H	-1.047230	5.510093	-1.493896	C	0.064802	3.825033	1.083168
C	-1.749927	6.800324	0.831872	C	0.612545	2.916565	-2.638019
H	-0.952581	5.072377	2.811516	H	-0.277051	5.463300	-2.467074
C	0.105473	2.580356	2.930059	C	-0.981180	7.195747	-0.454757
H	-0.177406	2.099707	-2.352001	H	-0.516628	5.765152	1.844774
H	1.205090	3.254017	-2.300477	C	0.292347	3.249150	2.460443
H	-0.375805	3.780992	-2.932108	H	0.392525	1.834243	-2.581517
H	-1.598384	7.429712	-0.067804	H	1.701718	3.046648	-2.833889
H	-1.339951	7.342302	1.708592	H	0.075393	3.314473	-3.520439
H	-2.847131	6.712959	0.991938	H	-0.584803	7.687454	-1.366028
H	0.134679	3.242325	3.817651	H	-0.696754	7.808576	0.424368
H	1.092965	2.080251	2.841467	H	-2.090803	7.223740	-0.526460
H	-0.652905	1.788389	3.110834	H	0.122122	4.017581	3.239549
C	0.680628	-2.989476	-0.763257	H	1.333805	2.877075	2.581330
C	0.595446	-2.565456	1.674624	H	-0.385924	2.392546	2.658978
C	0.582302	-4.371436	-0.489843	C	0.398003	-2.453270	-1.637199
C	0.506749	-3.954099	1.888514	C	0.336225	-2.750622	0.820139
C	0.508903	-4.878210	0.821717	C	0.154948	-3.832904	-1.783331
C	0.435287	-6.365449	1.085353	C	0.094270	-4.124974	0.614397
H	0.545736	-5.073944	-1.339484	C	0.001844	-4.689371	-0.672795
C	0.480000	-1.606518	2.838013	C	-0.300173	-6.158335	-0.863212
H	0.412056	-4.324323	2.923358	H	0.070849	-4.249711	-2.801081
C	0.701148	-2.506064	-2.196068	C	0.376650	-2.188093	2.222775
H	0.137466	-1.558737	-2.319405	H	-0.044971	-4.772317	1.496454
H	0.247520	-3.263636	-2.865201	C	0.471012	-1.560032	-2.854776
H	1.737559	-2.339770	-2.565021	H	-0.411621	-0.884987	-2.901828
H	1.325027	-0.886970	2.890606	H	0.495255	-2.156895	-3.787086
H	0.445140	-2.152262	3.800665	H	1.360586	-0.896389	-2.845284
H	-0.445701	-0.996247	2.754081	H	-0.227485	-1.259761	2.307831
H	-0.264559	-6.599629	1.913475	H	1.413256	-1.948093	2.551265
H	1.429005	-6.768113	1.381593	H	-0.024409	-2.921547	2.949125
H	0.107375	-6.925924	0.187435	H	-1.386737	-6.317522	-1.038452
C	-2.394396	-1.656546	0.170803	H	-0.022109	-6.755096	0.028251
Cl	-1.827385	0.269170	-2.443636	H	0.232150	-6.575922	-1.742068
Cl	-2.747563	0.977685	1.998223	C	-2.513570	-1.091909	-0.589363
O	-4.309097	0.023157	-0.540661	Cl	-2.465185	1.717374	-2.130895
C	-5.107153	1.204887	-0.921898	Cl	-2.131793	0.737131	2.183705
C	-5.675609	1.071657	-2.334344	O	-4.458222	-1.369341	1.473001
H	-4.307254	1.973089	-0.946667	C	-5.253074	-1.036422	2.647088
C	-6.101330	1.586540	0.173750	C	-6.042542	0.263456	2.476176
H	-6.957735	0.887786	0.249501	H	-4.446067	-0.838861	3.382996
H	-6.510455	2.593157	-0.051039	C	-6.069430	-2.227527	3.165129
H	-5.586853	1.630245	1.153858	H	-6.976425	-2.438434	2.563733
H	-4.878116	0.770439	-3.041621	H	-6.402932	-2.018905	4.202936
H	-6.066168	2.060097	-2.653276	H	-5.446263	-3.144354	3.186781
H	-6.509788	0.346257	-2.405205	H	-5.370369	1.072651	2.127325
C	-4.778205	-1.249222	-0.366392	H	-6.463808	0.567445	3.456530
C	-3.744540	-2.161634	0.013369	H	-6.885218	0.171105	1.762873
C	-6.103067	-1.689274	-0.522489	C	-4.935147	-1.456283	0.206582

C -6.401883 -3.047714 -0.302908	C -3.949306 -1.371508 -0.828188
C -5.402139 -3.967130 0.068409	C -6.284241 -1.698833 -0.146411
C -4.083468 -3.523302 0.224662	C -6.652525 -1.869200 -1.489369
H -7.442264 -3.387956 -0.425675	C -5.687463 -1.819987 -2.511175
H -6.904710 -0.998022 -0.809099	C -4.349874 -1.580935 -2.173264
H -3.284345 -4.223707 0.516277	H -7.709811 -2.057451 -1.735072
H -5.657476 -5.024534 0.235662	H -7.049827 -1.779283 0.635079
H -1.634971 -2.401715 0.472622	H -3.585196 -1.521230 -2.964173
C 3.236507 -0.635313 -0.749425	H -5.976414 -1.962379 -3.563587
H 2.594145 -0.375166 1.309460	H -1.797727 -1.888100 -0.875838
N 4.566028 -0.027329 -0.561042	C 3.290356 -0.859626 -0.478497
H 2.871956 -0.356540 -1.759029	H 3.175576 -1.965093 -0.351079
H 3.284111 -1.751631 -0.712986	H 3.182277 -0.649486 -1.562688
C 5.356995 0.085516 -1.775545	C 5.049985 -0.895569 1.236041
C 5.351851 -0.622765 0.510962	C 5.662302 -0.639999 -1.062245
C 6.558008 0.251580 0.834222	C 6.329027 -0.198907 1.694987
H 5.668305 -1.678117 0.286563	H 5.166377 -2.013482 1.254821
H 4.744126 -0.680903 1.437754	H 4.279289 -0.663259 1.999990
C 6.582846 0.967017 -1.534496	C 6.949210 0.086306 -0.680742
H 4.760194 0.589275 -2.564678	H 5.857823 -1.732810 -1.240891
H 5.655531 -0.909094 -2.206300	H 5.340672 -0.224212 -2.040060
N 7.461861 0.474401 -0.379318	H 6.693614 -0.598366 2.661955
H 6.215573 1.259568 1.140633	H 6.144851 0.888176 1.800021
H 7.182356 -0.174079 1.641978	H 7.758158 -0.079842 -1.416550
H 6.254798 1.986040 -1.249914	H 6.752691 1.174102 -0.606565
H 7.230573 1.032218 -2.431133	N 4.627786 -0.397302 -0.066044
C 8.464913 1.547781 -0.050385	N 7.479327 -0.332370 0.690462
H 9.106401 1.726137 -0.933639	C 8.582931 0.608171 1.095885
H 9.083442 1.226200 0.806175	H 8.960547 0.313824 2.092946
H 7.924430 2.475487 0.212643	H 9.399565 0.559980 0.353942
C 8.198163 -0.804769 -0.811572	H 8.181200 1.637142 1.136575
C 9.041651 -1.486238 0.257735	C 8.001785 -1.778538 0.705841
H 8.820384 -0.494088 -1.675220	H 8.354553 -1.941287 1.744430
H 7.424156 -1.494942 -1.196056	H 7.120260 -2.428465 0.553449
H 9.839502 -0.838857 0.672041	C 9.092954 -2.108997 -0.303865
H 9.549393 -2.347593 -0.221933	H 10.009766 -1.499362 -0.180839
H 8.439346 -1.897806 1.091415	H 9.388964 -3.164421 -0.135803
	H 8.750150 -2.039913 -1.355100
Act	TS_Ci1
102	108
PENJOLL-Act+ SCF Done: -2827.25391155 A.U.	PENJOLL-TS1+ SCF Done: -2905.77972796 A.U.
Ru -1.774054 1.201615 -0.576155	Ru -1.513141 1.093843 -0.434447
C -0.002532 0.776953 0.018710	C 0.123678 0.529143 0.389743
N 0.920441 1.753686 0.340005	N 1.091971 1.431855 0.796629
N 0.674020 -0.440331 0.049646	N 0.690092 -0.738141 0.508032
C 2.090980 -0.293777 0.446618	C 2.129439 -0.671052 0.842584
C 2.269563 1.232880 0.568552	C 2.306571 0.783188 1.304987
H 2.241177 -0.790695 1.435577	H 2.347311 -1.392263 1.660921
H 2.651114 1.549835 1.563372	H 2.377005 0.877366 2.413083
H 2.982699 1.623300 -0.193805	H 3.221596 1.242283 0.874081

C	0.097720	-1.759522	0.133209	C	0.031114	-2.017040	0.600967
C	0.695594	3.174370	0.468817	C	0.974907	2.869022	0.883931
C	0.942957	4.033146	-0.636593	C	1.446254	3.674138	-0.188718
C	0.747197	5.417336	-0.456855	C	1.341941	5.074809	-0.067604
C	0.353459	5.967116	0.778675	C	0.827302	5.691405	1.089004
C	0.191163	5.091189	1.869904	C	0.449687	4.863445	2.164895
C	0.364226	3.699655	1.746874	C	0.522002	3.459217	2.096001
C	1.436536	3.509458	-1.965418	C	2.090956	3.072097	-1.415153
H	0.921835	6.088377	-1.314497	H	1.690999	5.703302	-0.904069
C	0.103806	7.450222	0.927265	C	0.680702	7.192996	1.176425
H	-0.081172	5.503185	2.855944	H	0.084232	5.325083	3.097359
C	0.180346	2.809998	2.953069	C	0.115882	2.627115	3.288904
H	0.714019	2.804460	-2.428914	H	1.389716	2.414244	-1.972234
H	2.401837	2.966221	-1.859180	H	2.976425	2.454443	-1.141929
H	1.605210	4.343006	-2.674733	H	2.441346	3.866529	-2.102962
H	0.703819	8.043146	0.207867	H	1.360179	7.715488	0.473633
H	0.335820	7.805780	1.951585	H	0.884618	7.565970	2.200805
H	-0.965496	7.688483	0.735039	H	-0.356897	7.501224	0.920914
H	0.255331	3.395313	3.890528	H	0.016692	3.258942	4.192958
H	0.928227	1.991521	2.996704	H	0.847453	1.824224	3.515460
H	-0.824597	2.336840	2.922828	H	-0.866726	2.144917	3.098367
C	-0.024921	-2.568718	-1.027208	C	-0.114641	-2.860276	-0.529456
C	-0.303530	-2.242759	1.409792	C	-0.411193	-2.439542	1.889140
C	-0.513789	-3.882884	-0.868774	C	-0.672169	-4.144275	-0.333145
C	-0.773759	-3.566260	1.510407	C	-0.957873	-3.726813	2.026248
C	-0.874991	-4.410421	0.385795	C	-1.085973	-4.605184	0.927991
C	-1.351739	-5.839155	0.519973	C	-1.650712	-5.995470	1.113550
H	-0.626677	-4.511753	-1.768023	H	-0.796625	-4.800699	-1.211105
C	-0.304657	-1.339037	2.622525	C	-0.339103	-1.509275	3.078956
H	-1.088969	-3.942055	2.498409	H	-1.303354	-4.051937	3.022201
C	0.314340	-2.058710	-2.409398	C	0.255812	-2.432246	-1.931203
H	0.045598	-0.990474	-2.534357	H	0.450673	-1.346301	-2.007279
H	-0.231544	-2.639496	-3.178814	H	-0.576657	-2.658347	-2.628549
H	1.397494	-2.167992	-2.639332	H	1.140515	-2.991892	-2.308660
H	-0.955907	-0.454718	2.454827	H	-0.919873	-0.580307	2.897352
H	0.705094	-0.945511	2.870623	H	0.701538	-1.194489	3.310865
H	-0.678482	-1.874865	3.516340	H	-0.746867	-1.994756	3.986712
H	-1.978849	-5.981019	1.422771	H	-0.927042	-6.654474	1.641407
H	-0.492011	-6.539994	0.606576	H	-1.891000	-6.474493	0.143874
H	-1.939663	-6.158960	-0.364136	H	-2.574363	-5.981635	1.728635
C	-2.677204	-0.406872	-0.423619	C	-2.493919	-0.475455	-0.392375
Cl	-1.186555	1.282653	-2.846964	Cl	-0.541378	1.053160	-2.587865
Cl	-2.752423	2.318642	1.214238	Cl	-2.625161	2.184912	1.311484
O	-4.461963	-2.054647	0.824420	O	-4.547667	-1.940784	0.644273
C	-5.236821	-2.837416	1.774435	C	-5.515773	-2.625232	1.488141
C	-6.288472	-1.999985	2.510244	C	-6.680936	-1.719297	1.899747
H	-4.447116	-3.096369	2.511489	H	-4.900055	-2.802974	2.395237
C	-5.752865	-4.157719	1.188433	C	-5.922746	-4.000720	0.944761
H	-6.620428	-4.032072	0.511431	H	-6.629481	-3.948815	0.093497
H	-6.072965	-4.823791	2.016249	H	-6.417635	-4.579542	1.751843

H	-4.947710	-4.673232	0.627366
H	-5.837204	-1.063048	2.893851
H	-6.673023	-2.575864	3.377121
H	-7.155470	-1.730607	1.875919
C	-4.965512	-1.409985	-0.258943
C	-4.033780	-0.540145	-0.938231
C	-6.287906	-1.519043	-0.739953
C	-6.699468	-0.786198	-1.866087
C	-5.806218	0.064251	-2.541317
C	-4.492028	0.180532	-2.076783
H	-7.738056	-0.890395	-2.218657
H	-7.010031	-2.174662	-0.238723
H	-3.769724	0.812301	-2.618644
H	-6.131339	0.625122	-3.430462
H	-2.313189	-1.241175	0.203423
C	3.049806	-0.934199	-0.575705
H	2.770512	-2.004572	-0.736957
H	2.918304	-0.412380	-1.545711
C	4.866963	-1.752307	0.855341
C	5.405480	-0.802423	-1.273919
C	6.247380	-1.401259	1.406020
H	4.833529	-2.816143	0.493438
H	4.167308	-1.709570	1.715795
C	6.793425	-0.396899	-0.785978
H	5.446255	-1.783949	-1.821242
H	5.098635	-0.046532	-2.026704
H	6.598158	-2.143105	2.150488
H	6.216881	-0.400130	1.879163
H	7.539923	-0.388214	-1.602269
H	6.746527	0.613891	-0.334821
N	4.459291	-0.799511	-0.167156
N	7.322171	-1.315689	0.316450
C	8.560265	-0.702147	0.913660
H	8.928715	-1.353756	1.727873
H	9.334245	-0.598852	0.132857
H	8.307981	0.295345	1.317642
C	7.643194	-2.729995	-0.194742
H	8.026700	-3.271435	0.693725
H	6.674989	-3.190344	-0.466231
C	8.623545	-2.815412	-1.357090
H	9.615061	-2.374281	-1.133458
H	8.794544	-3.890932	-1.566378
H	8.230816	-2.369329	-2.291798
TS_Con			

H	-5.027547	-4.566979	0.617738
H	-6.300684	-0.750599	2.281214
H	-7.252713	-2.208219	2.715215
H	-7.387919	-1.512061	1.072632
C	-4.799896	-1.428452	-0.586117
C	-3.728210	-0.639769	-1.149106
C	-5.993857	-1.597637	-1.319474
C	-6.140636	-1.007826	-2.586629
C	-5.106677	-0.240345	-3.151333
C	-3.920265	-0.057400	-2.432536
H	-7.082944	-1.158065	-3.137564
H	-6.820765	-2.188926	-0.908708
H	-3.088895	0.518548	-2.867647
H	-5.224395	0.206910	-4.150028
C	-2.688900	3.900597	-1.988593
C	-3.975060	3.526774	-1.860335
H	-2.280590	-1.272043	0.344657
H	-4.453079	3.450977	-0.869904
H	-4.595812	3.275880	-2.736759
H	-2.078965	4.164144	-1.107991
H	-2.196183	3.966028	-2.972520
C	2.990389	-1.008747	-0.398410
H	2.707033	-2.015809	-0.787292
H	2.737511	-0.273970	-1.190514
C	4.978603	-2.077271	0.565836
C	5.243279	-0.596214	-1.296837
C	6.408584	-1.809662	1.030526
H	4.919964	-3.018756	-0.045492
H	4.387645	-2.282501	1.482771
C	6.670227	-0.255760	-0.876521
H	5.239156	-1.404829	-2.077725
H	4.831349	0.307676	-1.792405
H	6.860453	-2.697699	1.515201
H	6.416743	-0.964383	1.746026
H	7.314394	-0.003975	-1.739885
H	6.656144	0.605397	-0.179550
N	4.435575	-0.920037	-0.129489
N	7.344827	-1.395705	-0.110850
C	8.631140	-0.890534	0.486656
H	9.114972	-1.710835	1.049270
H	9.300389	-0.538470	-0.318191
H	8.403765	-0.051967	1.170068
C	7.631570	-2.614992	-1.002417
H	8.112397	-3.352391	-0.328161
H	6.646913	-3.027140	-1.291435
C	8.487761	-2.358177	-2.235121
H	9.493493	-1.958501	-1.999590
H	8.643771	-3.334437	-2.737503
H	7.998593	-1.695643	-2.976053
Ci1			

108			
PENJOLL-TSconc+ SCF Done: -2905.77136054 A.U.			
C	-0.071550	0.459862	0.006261
C	2.212074	-0.055549	0.382874
H	2.393523	0.013017	1.483307
C	2.111143	1.350763	-0.216099
H	2.660823	2.116059	0.366763
H	2.492654	1.382382	-1.265739
C	0.752642	-2.752826	1.338986
C	0.676867	-4.158231	1.251675
H	0.761259	-4.747530	2.180231
C	0.494326	-4.827040	0.025078
C	0.387094	-4.044110	-1.142518
H	0.254087	-4.544695	-2.116308
C	0.447780	-2.635217	-1.117134
C	0.624148	-1.995744	0.141558
C	0.965660	-2.088091	2.679530
H	0.743336	-2.791441	3.505922
H	0.312985	-1.195279	2.796323
H	2.022365	-1.761661	2.817161
C	0.383296	-6.333635	-0.034436
H	-0.676925	-6.656132	0.061019
H	0.944259	-6.820823	0.788353
H	0.757652	-6.735571	-0.997663
C	0.318620	-1.851267	-2.398963
H	0.354279	-2.521808	-3.279349
H	1.121942	-1.091619	-2.509882
H	-0.637088	-1.279563	-2.434434
C	0.201884	2.967391	-0.321248
C	0.104690	3.788093	0.836707
C	-0.289790	5.129987	0.667529
H	-0.381776	5.768826	1.561933
C	-0.552993	5.680584	-0.603514
C	-0.372423	4.856071	-1.731520
H	-0.530454	5.277593	-2.738244
C	0.018412	3.505243	-1.623984
C	0.438686	3.256576	2.210202
H	0.286163	4.036121	2.982014
H	1.502504	2.935347	2.273639
H	-0.179915	2.369691	2.476173
C	-1.017177	7.111567	-0.749302
H	-0.747017	7.532668	-1.738363
H	-0.588079	7.764968	0.037228
H	-2.123637	7.177708	-0.657271
C	0.234672	2.678883	-2.867785
H	0.160347	3.308240	-3.775804
H	-0.527641	1.870717	-2.938960
H	1.233609	2.192270	-2.877156
C	-2.335515	-1.277435	0.342109

108			
PENJOLL-CI1+ SCF Done: -2905.79069465 A.U.			
Ru	-1.813609	1.408301	-0.312015
C	0.080675	0.857063	0.094935
N	1.045974	1.819424	0.248030
N	0.717490	-0.364539	0.117143
C	2.168602	-0.241574	0.408494
C	2.408021	1.273178	0.279304
H	2.346413	-0.580930	1.458578
H	2.983591	1.702405	1.125354
H	2.956334	1.520888	-0.659372
C	0.107201	-1.664457	0.257291
C	0.848344	3.249404	0.329785
C	0.989494	4.060705	-0.830826
C	0.788190	5.449728	-0.695031
C	0.510320	6.053470	0.546527
C	0.489900	5.230157	1.689919
C	0.673769	3.836174	1.615076
C	1.428663	3.496794	-2.161535
H	0.871867	6.081224	-1.595328
C	0.248784	7.538264	0.651624
H	0.333968	5.686759	2.681509
C	0.704792	3.010238	2.877142
H	0.882793	2.567952	-2.425965
H	2.520835	3.277141	-2.152603
H	1.257011	4.229924	-2.973900
H	0.753878	8.103852	-0.157118
H	0.585200	7.946736	1.626042
H	-0.839614	7.752318	0.568935
H	0.792535	3.660358	3.769468
H	1.557066	2.297872	2.887161
H	-0.230430	2.415320	2.967974
C	-0.094830	-2.481499	-0.888282
C	-0.218064	-2.128759	1.561181
C	-0.586939	-3.787275	-0.689746
C	-0.696631	-3.447583	1.698936
C	-0.877591	-4.298197	0.590983
C	-1.395434	-5.709430	0.757078
H	-0.757075	-4.423433	-1.574673
C	-0.140705	-1.220215	2.767138
H	-0.949806	-3.814306	2.707843
C	0.175360	-1.985782	-2.290832
H	-0.138631	-0.929797	-2.429052
H	-0.370380	-2.605618	-3.029001
H	1.253706	-2.053365	-2.555923
H	-0.885541	-0.394056	2.693915
H	0.850345	-0.731736	2.882520
H	-0.346208	-1.781853	3.699132
H	-1.543953	-5.970985	1.823446
H	-0.696135	-6.453168	0.318951

H	-1.788252	-1.858646	1.114658	H	-2.367188	-5.843311	0.235673
C	-3.407836	-2.006230	-0.344540	C	-2.602339	-0.291389	-0.203499
C	-3.157484	-3.301488	-0.872278	Cl	-1.225770	1.402386	-2.657738
H	-2.160208	-3.744591	-0.730577	Cl	-2.364890	1.863429	1.992389
C	-4.135779	-3.990167	-1.601595	O	-4.290412	-2.037327	1.022233
H	-3.906893	-4.979641	-2.027446	C	-5.236566	-2.641771	1.950976
C	-5.404864	-3.413098	-1.791907	C	-6.631293	-2.016409	1.857223
H	-6.174811	-3.942389	-2.375120	H	-4.795240	-2.326185	2.919725
C	-5.697038	-2.163854	-1.222226	C	-5.212622	-4.174761	1.921787
C	-4.719714	-1.466842	-0.489026	H	-5.737814	-4.608266	1.047873
N	0.833107	-0.572745	0.175368	H	-5.710618	-4.564716	2.833463
N	0.666797	1.609090	-0.169377	H	-4.167749	-4.544171	1.919630
Cl	-1.651829	0.396943	2.589508	H	-6.563946	-0.911148	1.904747
Cl	-2.390034	0.489938	-2.249112	H	-7.242391	-2.357287	2.718109
Ru	-2.032351	0.545393	0.136205	H	-7.171985	-2.293493	0.930828
H	-6.689752	-1.704533	-1.340696	C	-4.439221	-1.968886	-0.323070
O	-5.037038	-0.263236	0.099644	C	-3.577413	-1.020638	-0.995718
C	-5.623454	-0.262363	1.459121	C	-5.358015	-2.730079	-1.079561
C	-3.411312	2.482031	-0.229278	C	-5.441081	-2.565698	-2.471542
C	-3.166007	2.528145	1.120520	C	-4.617087	-1.641470	-3.140727
H	-4.303129	1.985466	-0.642135	C	-3.710061	-0.873364	-2.404119
H	-2.801370	3.062417	-0.939671	H	-6.169457	-3.169305	-3.036844
H	-2.360390	3.146851	1.540724	H	-6.017648	-3.454526	-0.586443
H	-3.846712	2.068958	1.852706	H	-3.048374	-0.145110	-2.899510
C	-6.560634	0.941105	1.515270	H	-4.689748	-1.517594	-4.232067
H	-6.047530	1.869444	1.196305	C	-3.194081	3.131891	-0.921877
H	-6.929627	1.091560	2.550519	C	-4.097497	2.099684	-0.769576
H	-7.435750	0.786199	0.850592	H	-2.352020	-0.810971	0.743511
C	-6.328399	-1.562938	1.839870	H	-4.585596	1.909865	0.198854
H	-4.766067	-0.110787	2.156013	H	-4.473186	1.546965	-1.643510
H	-7.207190	-1.766449	1.194038	H	-2.976443	3.812861	-0.079420
H	-6.689149	-1.470071	2.884903	H	-2.853363	3.439462	-1.923646
H	-5.650851	-2.438317	1.795424	C	3.044563	-1.081913	-0.535118
C	3.299692	-0.929194	-0.260638	H	2.715779	-2.150484	-0.510682
N	4.632160	-0.310236	-0.141426	H	2.890756	-0.715568	-1.570677
H	3.071650	-1.036183	-1.341206	C	4.900273	-1.730502	0.938306
H	3.278998	-1.958505	0.174407	C	5.368652	-1.172096	-1.340265
C	5.587277	-0.764516	-1.142560	C	6.313952	-1.343644	1.366478
C	5.211743	-0.401932	1.191436	H	4.817282	-2.837560	0.761549
C	6.831993	0.117247	-1.121937	H	4.242199	-1.518677	1.806850
H	5.141541	-0.663816	-2.154207	C	6.787710	-0.736868	-0.984723
H	5.863698	-1.848826	-1.033300	H	5.357539	-2.233654	-1.710871
C	6.460504	0.470877	1.298293	H	5.048807	-0.545301	-2.198773
H	5.428388	-1.461584	1.497424	H	6.676801	-1.966341	2.208119
H	4.495552	-0.014497	1.945557	H	6.334564	-0.278718	1.670434
N	7.520723	0.133894	0.243315	H	7.497566	-0.889463	-1.819273
H	6.947455	0.378571	2.289208	H	6.785056	0.336192	-0.709231
H	6.189678	1.531065	1.126573	N	4.476474	-0.945704	-0.212363
H	7.581961	-0.197537	-1.871637	N	7.340790	-1.475101	0.235160
H	6.544974	1.167920	-1.324554	C	8.620202	-0.811088	0.669843

C	8.173527	-1.214378	0.592495	H	9.012607	-1.331430	1.563574
C	9.190944	-1.744800	-0.408819	H	9.359550	-0.858997	-0.149318
H	7.345460	-1.935020	0.726997	H	8.409956	0.246139	0.914670
H	8.636037	-1.055236	1.587603	C	7.599267	-2.965058	-0.042229
H	8.744063	-2.005666	-1.388338	H	8.020026	-3.359793	0.904602
H	9.607573	-2.683461	0.009679	H	6.605807	-3.430888	-0.179266
H	10.048166	-1.062394	-0.571696	C	8.508074	-3.280583	-1.222433
C	8.564631	1.218688	0.250901	H	9.518437	-2.834924	-1.135345
H	8.075103	2.189045	0.049189	H	8.647608	-4.380463	-1.246750
H	9.315568	1.015228	-0.532893	H	8.068851	-2.995260	-2.198441
H	9.052420	1.244509	1.243329				
TS_MCy				MCy			
108				108			
PENJOLL-TSMCy+ SCF Done: -2905.78835366 A.U.				PENJOLL-MCy+ SCF Done: -2905.79854839 A.U.			
Ru	1.715351	1.508086	-0.045422	Ru	1.745369	1.355763	0.042698
C	-0.204639	0.888602	-0.252727	C	-0.228033	0.990815	0.030420
N	-1.227948	1.770000	-0.463051	N	-1.215384	1.908473	-0.151164
N	-0.695752	-0.377596	-0.429786	N	-0.788860	-0.256585	0.080609
C	-2.143046	-0.379159	-0.757792	C	-2.225289	-0.221653	-0.289415
C	-2.426989	1.113173	-1.012203	C	-2.548645	1.281534	-0.181068
H	-2.300317	-0.977798	-1.681247	C	-3.098610	-1.119681	0.599865
H	-2.533708	1.343655	-2.094889	H	-2.322238	-0.557995	-1.349760
H	-3.348036	1.461865	-0.498717	H	-3.138573	1.663388	-1.037757
C	0.016362	-1.624589	-0.313079	H	-3.113210	1.519021	0.751858
C	-1.197853	3.200260	-0.258639	C	-0.074257	-1.494793	0.291314
C	-1.513104	3.702369	1.034683	C	-1.098335	3.350514	-0.148335
C	-1.496709	5.095477	1.232054	C	-1.110378	4.044378	1.091344
C	-1.203170	5.996268	0.188406	C	-1.024462	5.451121	1.062204
C	-0.967858	5.465710	-1.094270	C	-0.954308	6.175298	-0.143461
C	-0.977091	4.079229	-1.353887	C	-1.011297	5.453410	-1.352489
C	-1.866293	2.779461	2.176074	C	-1.098452	4.047785	-1.386599
H	-1.724987	5.488810	2.236787	C	-1.213088	3.324212	2.413820
C	-1.137121	7.484689	0.443322	H	-1.022917	5.997123	2.020487
H	-0.778419	6.153341	-1.935428	C	-0.815220	7.680554	-0.141572
C	-0.808596	3.578921	-2.768345	H	-0.996112	6.001686	-2.309360
H	-0.966005	2.221329	2.514522	C	-1.204049	3.325004	-2.706978
H	-2.637696	2.034786	1.880625	H	-1.459569	4.033209	3.228102
H	-2.260041	3.352682	3.038167	H	-0.250989	2.824940	2.668103
H	-1.326778	8.069574	-0.478884	H	-1.994846	2.535285	2.403799
H	-0.129928	7.775559	0.814995	H	0.256704	7.977357	-0.158252
H	-1.868792	7.802123	1.214028	H	-1.263322	8.133671	0.765629
H	-0.451417	4.391594	-3.430696	H	-1.292100	8.138719	-1.031575
H	-1.778857	3.228145	-3.187102	H	-1.176952	4.041751	-3.550697
H	-0.081816	2.740755	-2.831595	H	-2.156216	2.754853	-2.790265
C	0.335940	-2.139499	0.974622	H	-0.371682	2.598064	-2.831024
C	0.318763	-2.354525	-1.493883	C	0.225735	-1.893478	1.625051
C	0.948903	-3.405530	1.047967	C	0.246421	-2.327259	-0.816827
C	0.921009	-3.622408	-1.355946	C	0.897850	-3.117152	1.814253
C	1.242054	-4.169578	-0.099505	C	0.907475	-3.544882	-0.561118
				C	1.256997	-3.953922	0.740302

C	1.910514	-5.520537	0.022507	C	2.017777	-5.236959	0.980602
H	1.206406	-3.805489	2.042848	H	1.145122	-3.425438	2.843560
C	0.049750	-1.790638	-2.869603	C	-0.096040	-1.941936	-2.236704
H	1.158058	-4.193008	-2.269743	H	1.165029	-4.190315	-1.417437
C	0.042767	-1.371371	2.242292	C	-0.143403	-1.053333	2.822611
H	0.480537	-0.350240	2.224189	H	0.535603	-0.175310	2.917681
H	0.453155	-1.902893	3.122348	H	-0.072971	-1.645958	3.755485
H	-1.048172	-1.245762	2.413719	H	-1.170920	-0.640798	2.750424
H	-1.037080	-1.722491	-3.103747	H	-1.189907	-2.007969	-2.437884
H	0.504112	-2.431321	-3.650353	H	0.400812	-2.622207	-2.955529
H	0.477369	-0.767344	-2.963734	H	0.234019	-0.904107	-2.463637
H	1.432627	-6.143765	0.806971	H	1.713545	-5.723341	1.929755
H	2.978477	-5.410365	0.310304	H	3.107344	-5.028639	1.057882
H	1.877734	-6.083506	-0.931441	H	1.876530	-5.963301	0.155148
C	3.025549	0.123396	-0.040572	C	3.524646	0.407444	-0.280110
Cl	1.508995	2.072015	2.289931	Cl	1.903866	1.752801	2.409488
Cl	1.848759	1.334672	-2.477952	Cl	1.553481	1.197434	-2.380770
O	4.809311	-1.764770	-0.858787	O	4.385068	-1.946054	-1.389778
C	5.898292	-2.438616	-1.555318	C	5.228937	-2.660239	-2.338691
C	7.277468	-1.905465	-1.157029	C	6.707193	-2.280119	-2.225487
H	5.701635	-2.108165	-2.597006	H	4.848046	-2.254523	-3.300326
C	5.764975	-3.966065	-1.537193	C	4.960358	-4.170628	-2.350823
H	6.064359	-4.425279	-0.574194	H	5.419287	-4.704433	-1.494400
H	6.415392	-4.397959	-2.325540	H	5.378725	-4.613230	-3.278585
H	4.720214	-4.263178	-1.757772	H	3.869523	-4.366808	-2.341148
H	7.299073	-0.798749	-1.215982	H	6.829971	-1.178555	-2.246068
H	8.037270	-2.296944	-1.864270	H	7.261423	-2.701383	-3.089174
H	7.583833	-2.204751	-0.135424	H	7.180642	-2.664375	-1.300460
C	4.655225	-1.682887	0.484761	C	4.653262	-1.813965	-0.060241
C	3.702278	-0.698381	0.959802	C	4.168611	-0.616488	0.574928
C	5.341630	-2.492680	1.419128	C	5.342263	-2.783179	0.705042
C	5.122474	-2.336337	2.795844	C	5.563033	-2.585453	2.076656
C	4.214232	-1.374038	3.275156	C	5.089215	-1.423549	2.711965
C	3.517772	-0.576142	2.363152	C	4.397926	-0.463151	1.964382
H	5.675962	-2.977743	3.500820	H	6.105736	-3.353266	2.651318
H	6.054924	-3.250535	1.073733	H	5.707552	-3.700132	0.225204
H	2.815370	0.195536	2.714843	H	3.991162	0.430573	2.461540
H	4.055790	-1.245643	4.356853	H	5.253340	-1.269657	3.789570
C	3.022777	3.218967	-0.276367	C	2.790955	3.015055	-0.236034
C	3.958999	2.208889	0.043541	C	3.936381	1.943763	-0.115883
H	3.327586	-0.151225	-1.070815	H	3.560880	0.108652	-1.341075
H	4.614216	1.814016	-0.749921	H	4.578402	2.106150	-1.005254
H	4.308323	2.091833	1.081165	H	4.483077	2.076794	0.834935
H	2.939109	3.571797	-1.317575	H	2.701465	3.479398	-1.235397
H	2.689377	3.901525	0.524593	H	2.771666	3.723073	0.613651
C	-2.987789	-0.980729	0.385732	N	-4.503784	-1.120647	0.154480
N	-4.409483	-1.097471	0.019116	H	-3.069509	-0.729558	1.637972
H	-2.913686	-0.307617	1.264712	H	-2.670948	-2.152396	0.632711
H	-2.556538	-1.966903	0.688134	C	-5.472986	-1.347817	1.216935
C	-5.328881	-1.037946	1.146455	C	-4.765287	-2.002609	-0.974174

C	-4.704583	-2.248934	-0.822062	C	-6.883723	-1.051288	0.714642
C	-6.765846	-0.897747	0.651695	H	-5.279431	-0.644925	2.053924
H	-5.111994	-0.134856	1.754605	H	-5.416437	-2.379801	1.659546
H	-5.232523	-1.911992	1.847334	C	-6.160924	-1.756067	-1.542956
C	-6.128200	-2.171211	-1.369340	H	-4.615946	-3.087286	-0.720052
H	-4.524563	-3.226322	-0.296738	H	-4.050920	-1.788719	-1.796234
H	-4.031064	-2.258992	-1.704160	N	-7.269701	-1.903723	-0.493930
N	-7.186755	-2.045427	-0.267436	H	-6.400127	-2.453179	-2.370286
H	-6.390034	-3.063871	-1.971294	H	-6.234137	-0.715156	-1.914241
H	-6.238324	-1.266274	-1.998625	H	-7.650149	-1.211014	1.496202
H	-7.493972	-0.849007	1.483068	H	-6.939882	-0.000033	0.369491
H	-6.859452	0.022386	0.041821	C	-7.437643	-3.390333	-0.139362
C	-7.307124	-3.384791	0.477128	C	-8.437401	-3.709344	0.964011
C	-8.249487	-3.404992	1.673155	H	-6.430710	-3.760975	0.128349
H	-6.281493	-3.661718	0.783969	H	-7.725043	-3.877574	-1.092978
H	-7.626844	-4.111459	-0.296965	H	-8.134661	-3.316242	1.954444
H	-7.907981	-2.761875	2.507985	H	-8.479644	-4.813266	1.060964
H	-8.268555	-4.443893	2.060543	H	-9.468089	-3.371558	0.739186
H	-9.295142	-3.142550	1.417793	C	-8.553349	-1.373722	-1.075868
C	-8.505437	-1.701722	-0.907017	H	-8.401532	-0.322369	-1.381679
H	-8.393970	-0.760908	-1.476486	H	-9.352697	-1.423884	-0.315402
H	-9.272849	-1.569712	-0.123878	H	-8.829924	-1.983113	-1.956534
H	-8.799541	-2.520404	-1.590149				

TS_Ci2				Ci2			
108				108			
PENJOLL-TS2+ SCF Done: -2905.78053899 A.U.				PENJOLL-CI2+ SCF Done: -2905.78910674 A.U.			
Ru	1.542377	1.397409	0.300703	Ru	-1.441567	-0.648451	-0.152995
C	-0.204385	0.856811	-0.516028	C	0.367956	-0.157399	0.486504
N	-1.312373	1.643506	-0.671663	N	0.867764	1.040679	0.912069
N	-0.540959	-0.425464	-0.874135	N	1.405502	-1.064988	0.463601
C	-1.999111	-0.557746	-1.109643	C	2.705650	-0.428850	0.767467
C	-2.429524	0.904858	-1.290715	C	2.277196	0.938905	1.331775
H	-2.168127	-1.161042	-2.027535	H	3.240038	-1.037475	1.529756
H	-2.539783	1.193848	-2.360603	H	2.357345	0.989947	2.441490
H	-3.390713	1.118574	-0.779497	H	2.886092	1.766784	0.912101
C	0.341656	-1.536202	-1.157882	C	1.260028	-2.500861	0.358117
C	-1.423817	3.072809	-0.514790	C	0.146423	2.261953	1.154318
C	-2.087202	3.594617	0.628199	C	0.204673	3.296289	0.184787
C	-2.227787	4.991730	0.737417	C	-0.460797	4.507063	0.463132
C	-1.746128	5.874205	-0.251000	C	-1.164314	4.714617	1.666393
C	-1.135097	5.317827	-1.391371	C	-1.180831	3.671393	2.614648
C	-0.972151	3.926689	-1.558319	C	-0.532052	2.440623	2.391305
C	-2.627725	2.689451	1.709089	C	0.930778	3.101167	-1.124937
H	-2.732741	5.402196	1.628115	H	-0.427495	5.313667	-0.288416
C	-1.873151	7.371351	-0.083686	C	-1.894736	6.011603	1.932893
H	-0.780835	5.986665	-2.193493	H	-1.712639	3.818966	3.569594
C	-0.340202	3.382691	-2.815197	C	-0.573774	1.352114	3.436627
H	-1.814113	2.063115	2.138950	H	0.502135	2.243197	-1.691891
H	-3.410128	2.001715	1.314233	H	2.012280	2.886546	-0.969069
H	-3.088361	3.281132	2.524419	H	0.860756	4.009620	-1.754876

H	-1.842707	7.897748	-1.058531	H	-1.740327	6.360031	2.974963
H	-1.038490	7.773418	0.531870	H	-2.991179	5.886015	1.796647
H	-2.815466	7.648547	0.431365	H	-1.566739	6.817612	1.246803
H	-0.196405	4.187080	-3.562417	H	-1.053823	1.716725	4.365396
H	-0.966291	2.595608	-3.286840	H	0.443186	0.993615	3.704768
H	0.651264	2.917958	-2.609785	H	-1.140957	0.462332	3.080443
C	0.736988	-2.450882	-0.147526	C	1.281778	-3.156565	-0.903459
C	0.722016	-1.735568	-2.518267	C	1.136528	-3.245954	1.568741
C	1.486638	-3.583978	-0.537515	C	1.132798	-4.561808	-0.921330
C	1.455387	-2.888302	-2.847013	C	1.013007	-4.643514	1.486312
C	1.834862	-3.838038	-1.874636	C	0.995368	-5.324515	0.251143
C	2.571097	-5.098773	-2.268949	C	0.808886	-6.823503	0.198102
H	1.802683	-4.293214	0.245880	H	1.131947	-5.074387	-1.898053
C	0.398790	-0.714276	-3.581504	C	1.079359	-2.566383	2.914975
H	1.748485	-3.044333	-3.898774	H	0.908698	-5.218733	2.421464
C	0.396436	-2.285048	1.316720	C	1.493877	-2.436937	-2.216934
H	0.027487	-1.273960	1.573918	H	1.112619	-1.396607	-2.210615
H	1.299817	-2.458297	1.936947	H	0.971678	-2.969372	-3.036862
H	-0.356065	-3.038507	1.640771	H	2.572199	-2.423503	-2.494059
H	-0.680667	-0.454747	-3.621074	H	1.881031	-1.811479	3.057243
H	0.693385	-1.079374	-4.584444	H	1.162101	-3.306076	3.734822
H	0.959294	0.224766	-3.373012	H	0.101415	-2.043973	3.018733
H	1.857757	-5.890168	-2.589586	H	1.067694	-7.236381	-0.797006
H	3.160133	-5.512510	-1.426289	H	-0.248305	-7.097239	0.407114
H	3.259038	-4.923807	-3.120894	H	1.429071	-7.339319	0.960154
C	3.715858	1.074716	1.014238	C	-3.739875	-1.226168	-1.275039
Cl	0.445850	1.105844	2.461004	Cl	-0.842032	0.168379	-2.362932
Cl	2.606410	1.606850	-1.854347	Cl	-2.148659	-1.623165	1.929084
O	5.003284	-1.012910	-0.164808	O	-5.230914	1.012983	-1.660719
C	6.154937	-1.626200	-0.812413	C	-5.922674	2.133945	-2.281310
C	7.430537	-1.524522	0.027746	C	-7.135415	1.695650	-3.108025
H	6.272627	-0.957937	-1.691421	H	-5.143543	2.483334	-2.991469
C	5.854128	-3.028906	-1.352447	C	-6.188016	3.284398	-1.302068
H	5.853713	-3.810525	-0.566193	H	-7.021439	3.083040	-0.600902
H	6.627718	-3.309497	-2.096949	H	-6.448327	4.198396	-1.874954
H	4.868737	-3.038182	-1.858935	H	-5.278028	3.502756	-0.707849
H	7.601236	-0.479393	0.355680	H	-6.857673	0.874089	-3.798442
H	8.299827	-1.834227	-0.588075	H	-7.488444	2.550641	-3.720498
H	7.407841	-2.171245	0.927473	H	-7.986166	1.353336	-2.486820
C	4.595623	-1.259774	1.106351	C	-5.786922	0.121697	-0.797782
C	3.853687	-0.204491	1.742923	C	-4.987602	-1.042975	-0.533039
C	4.832780	-2.465483	1.807294	C	-7.026859	0.279445	-0.139382
C	4.358303	-2.633062	3.117190	C	-7.467464	-0.687535	0.778307
C	3.634235	-1.606676	3.751624	C	-6.685897	-1.821647	1.063455
C	3.389909	-0.411737	3.064675	C	-5.460079	-1.987894	0.410196
H	4.560210	-3.579059	3.645081	H	-8.437668	-0.544067	1.280323
H	5.386466	-3.280434	1.324826	H	-7.650482	1.161669	-0.326991
H	2.802762	0.381479	3.549369	H	-4.846293	-2.874832	0.623694
H	3.264880	-1.736671	4.780350	H	-7.034658	-2.572477	1.788311
C	1.486591	3.222087	0.500312	C	-2.347544	0.895714	0.193930

C	3.342358	2.322400	1.561354	C	-2.794897	-2.232644	-1.085962
H	4.262990	1.099171	0.058695	H	-3.590801	-0.544175	-2.127420
H	3.782758	3.226354	1.110957	H	-2.086325	-2.436461	-1.908188
H	2.993825	2.412144	2.602376	H	-2.935631	-3.022479	-0.331755
H	1.927548	3.903692	-0.261633	H	-3.110487	0.936119	1.004155
H	1.006527	3.702632	1.383012	H	-2.225341	1.802701	-0.437366
C	-2.666886	-1.232814	0.113056	C	3.570023	-0.309109	-0.510177
H	-2.201210	-2.233444	0.282706	H	3.735705	-1.325094	-0.942772
H	-2.433496	-0.613776	1.003952	H	2.989069	0.269354	-1.257842
C	-4.584418	-2.414528	-0.863889	C	5.854973	-0.412173	0.390368
C	-4.828372	-1.355048	1.271191	C	5.397796	1.041056	-1.453888
C	-6.084499	-2.304671	-1.130966	C	7.029525	0.456580	0.836655
H	-4.319563	-3.428379	-0.456381	H	6.205070	-1.274683	-0.239814
H	-4.085901	-2.353706	-1.853945	H	5.437765	-0.868039	1.312368
C	-6.330063	-1.187919	1.061973	C	6.534316	1.977093	-1.053574
H	-4.610298	-2.277520	1.875204	H	5.737743	0.313041	-2.240384
H	-4.493666	-0.498071	1.892413	H	4.618559	1.668965	-1.934102
H	-6.460392	-3.150831	-1.739616	H	7.838422	-0.145496	1.296137
H	-6.301043	-1.355197	-1.658928	H	6.679983	1.210209	1.569278
H	-6.891529	-1.209647	2.014889	H	6.983552	2.493305	-1.922915
H	-6.530467	-0.224912	0.552201	H	6.152375	2.738822	-0.345558
N	-4.130660	-1.328600	-0.007766	N	4.841510	0.393744	-0.273772
N	-6.920661	-2.267240	0.153541	N	7.659085	1.252670	-0.312297
C	-8.331966	-1.887217	-0.204507	C	8.596352	2.275478	0.272329
H	-8.758237	-2.662070	-0.868879	H	9.396107	1.755431	0.831965
H	-8.936300	-1.804638	0.715978	H	9.036798	2.880660	-0.539685
H	-8.319951	-0.912548	-0.725720	H	8.028792	2.933066	0.955911
C	-6.909442	-3.658486	0.807472	C	8.446184	0.292488	-1.220714
H	-7.358588	-4.331728	0.049434	H	9.244207	-0.119378	-0.570513
H	-5.845908	-3.942711	0.911316	H	7.759528	-0.539347	-1.464679
C	-7.629103	-3.778232	2.144681	C	9.027441	0.897815	-2.491076
H	-8.706772	-3.526700	2.091965	H	9.713926	1.746910	-2.303233
H	-7.565859	-4.839814	2.459038	H	9.627094	0.108927	-2.988947
H	-7.156352	-3.180922	2.949146	H	8.251789	1.211929	-3.216685
TS_I14e				I14e			
108				82			
PENJOLL-TS3+ SCF Done: -2905.76875751 A.U.				PENJOLL-14e2+ SCF Done: -2403.34511303 A.U.			
Ru	1.854666	-0.044646	-0.192670	Ru	2.856638	0.390341	-0.916519
C	-0.046002	-0.453910	-0.166615	C	1.239334	-0.011777	0.030316
N	-0.634707	-1.688559	0.007163	N	0.736590	-1.210314	0.479859
N	-1.078517	0.471985	-0.217828	N	0.256120	0.952236	0.246161
C	-2.370994	-0.125968	0.190802	C	-1.004058	0.352780	0.734462
C	-2.099818	-1.624433	0.003152	C	-0.564156	-1.061041	1.151655
H	-2.536679	0.092287	1.274916	H	-1.370101	0.941275	1.603793
H	-2.526962	-2.248400	0.813817	H	-0.453316	-1.170963	2.254853
H	-2.513656	-2.000032	-0.964946	H	-1.282147	-1.836199	0.810181
C	-0.980480	1.898136	-0.402926	C	0.457757	2.383192	0.342495
C	-0.011240	-2.982243	0.019474	C	1.371021	-2.501323	0.500722
C	0.216044	-3.666020	-1.209389	C	1.126990	-3.410014	-0.558852
C	0.718899	-4.980818	-1.150134	C	1.719696	-4.687414	-0.488505

C	0.978316	-5.631853	0.072729	C	2.531056	-5.078967	0.594752
C	0.705034	-4.937143	1.270689	C	2.742819	-4.149352	1.635027
C	0.202213	-3.623689	1.274489	C	2.177879	-2.859345	1.613390
C	-0.035974	-3.000696	-2.539777	C	0.279849	-3.019694	-1.747680
H	0.908756	-5.515168	-2.095986	H	1.541357	-5.398434	-1.312493
C	1.552504	-7.029286	0.105113	C	3.181524	-6.442994	0.632862
H	0.888035	-5.435553	2.237344	H	3.375905	-4.433971	2.492080
C	-0.070260	-2.898905	2.569212	C	2.477503	-1.869901	2.715991
H	0.707426	-2.193565	-2.734718	H	0.702938	-2.137446	-2.275444
H	-1.036116	-2.520074	-2.585212	H	-0.756185	-2.749574	-1.442631
H	0.026085	-3.734188	-3.367048	H	0.206073	-3.854617	-2.471353
H	2.653904	-6.998577	0.257177	H	3.152366	-6.881289	1.651471
H	1.367798	-7.572932	-0.842733	H	4.252461	-6.378869	0.340600
H	1.129952	-7.627074	0.938328	H	2.691971	-7.151852	-0.063899
H	0.157077	-3.543098	3.440684	H	3.096133	-2.333412	3.508437
H	-1.134198	-2.585525	2.652411	H	1.555705	-1.479783	3.197627
H	0.540895	-1.970049	2.644181	H	3.030489	-0.990379	2.321532
C	-0.986087	2.418497	-1.728804	C	0.192114	3.246823	-0.751502
C	-1.021447	2.763801	0.725898	C	0.870035	2.909913	1.602754
C	-1.001758	3.819012	-1.893974	C	0.378328	4.635390	-0.563183
C	-1.048490	4.155023	0.496980	C	1.024428	4.298829	1.734825
C	-1.030618	4.706690	-0.799259	C	0.793259	5.184675	0.660665
C	-1.009555	6.203276	-1.010367	C	1.018902	6.669988	0.822806
H	-0.999063	4.226608	-2.918719	H	0.189814	5.307969	-1.416914
C	-1.005822	2.235411	2.141015	C	1.186837	2.004101	2.769047
H	-1.069977	4.830152	1.369154	H	1.355317	4.703172	2.706006
C	-0.961929	1.520110	-2.940506	C	-0.300824	2.770017	-2.099580
H	0.035240	1.035423	-3.052070	H	0.237385	3.293150	-2.915778
H	-1.175649	2.093345	-3.863533	H	-1.380085	3.007548	-2.234441
H	-1.697468	0.692617	-2.865001	H	-0.146022	1.687132	-2.255651
H	-1.955868	1.723151	2.415064	H	0.358442	1.304941	3.013001
H	-0.870036	3.062472	2.865060	H	1.403572	2.594746	3.680060
H	-0.177575	1.506092	2.291779	H	2.085710	1.392935	2.541559
H	-1.495211	6.744443	-0.173524	H	0.548110	7.250753	0.005083
H	-1.514605	6.492968	-1.954036	H	2.105530	6.905345	0.814089
H	0.036215	6.576174	-1.075893	H	0.618349	7.041320	1.788701
C	3.427942	2.459548	-0.365182	Cl	1.883585	0.195256	-3.029845
Cl	2.180902	-0.048464	-2.571900	Cl	3.947694	1.821972	0.541511
Cl	1.937854	0.173432	2.188770	C	3.841939	-1.121494	-0.790828
O	4.619063	0.059838	-0.165790	H	4.808093	-1.068570	-1.356195
C	5.424255	-0.758186	-1.084973	H	3.642410	-2.060309	-0.239578
C	6.479039	0.074066	-1.811690	C	-2.077392	0.343491	-0.379520
H	4.651355	-1.066261	-1.820353	H	-2.220042	1.380445	-0.766230
C	5.983722	-2.009649	-0.401862	H	-1.686184	-0.262785	-1.222551
H	6.849161	-1.787588	0.255264	C	-4.171530	0.662785	0.850429
H	6.330721	-2.726940	-1.174765	C	-4.137913	-0.839444	-1.012355
H	5.203443	-2.511609	0.204681	C	-5.360748	-0.067022	1.470622
H	6.017515	0.943882	-2.320168	H	-4.510654	1.556769	0.259534
H	6.968613	-0.551641	-2.585939	H	-3.581062	1.072420	1.696285
H	7.268298	0.444603	-1.126233	C	-5.304808	-1.638133	-0.438245

C	5.177607	1.026023	0.645977
C	4.513476	2.278539	0.618718
C	6.246652	0.799733	1.531869
C	6.660730	1.831059	2.393184
C	6.000126	3.072387	2.392196
C	4.927363	3.288657	1.513068
H	7.499486	1.651961	3.084392
H	6.733928	-0.183538	1.572603
H	4.418298	4.265226	1.486422
H	6.325893	3.873622	3.073338
C	2.343301	-1.801655	-0.075993
C	2.235460	3.053126	-0.111655
H	3.615992	2.076119	-1.384173
H	1.502617	3.214521	-0.916281
H	1.977548	3.412633	0.897387
H	2.542380	-2.284473	0.906538
H	2.644461	-2.384570	-0.976075
C	-3.571845	0.405583	-0.605496
H	-3.554709	1.523396	-0.619027
H	-3.479534	0.071656	-1.659682
C	-5.298665	0.576248	1.127186
C	-5.918123	-0.154513	-1.064386
C	-6.492791	-0.141294	1.749384
H	-5.527333	1.661479	0.944252
H	-4.494633	0.567605	1.892196
C	-7.121944	-0.914066	-0.512001
H	-6.223651	0.862916	-1.433192
H	-5.574966	-0.713288	-1.960118
H	-6.877669	0.392259	2.640811
H	-6.201858	-1.169324	2.041449
H	-7.955267	-0.962833	-1.237622
H	-6.818348	-1.945851	-0.245976
N	-4.848531	-0.110738	-0.076682
N	-7.667055	-0.299347	0.777097
C	-8.670233	-1.243635	1.384389
H	-9.050086	-0.809428	2.328122
H	-9.504905	-1.398663	0.678036
H	-8.175488	-2.210572	1.589677
C	-8.325026	1.071676	0.546879
H	-8.687888	1.383388	1.547193
H	-7.510610	1.763981	0.263130
C	-9.445874	1.110407	-0.483372
H	-10.295096	0.441712	-0.240164
H	-9.848587	2.143580	-0.494729
H	-9.098637	0.894161	-1.512980
H	-4.501302	-0.084414	-1.761626
H	-3.508936	-1.555486	-1.581616
H	-6.024457	0.624220	2.026633
H	-5.001503	-0.854651	2.161547
H	-5.925685	-2.103091	-1.226626
H	-4.916543	-2.434201	0.227382
N	-3.351904	-0.247878	0.062963
N	-6.228601	-0.786284	0.432891
C	-7.190626	-1.691661	1.155509
H	-7.842701	-1.080035	1.806711
H	-7.802723	-2.242791	0.419633
H	-6.616799	-2.409725	1.769554
C	-7.017711	0.254791	-0.380962
H	-7.674873	0.753121	0.360186
H	-6.282481	1.006182	-0.724316
C	-7.821652	-0.286259	-1.555761
H	-8.571159	-1.048544	-1.264910
H	-8.385426	0.563897	-1.990639
H	-7.186082	-0.693810	-2.366405

Table S5 Coordinates data set, absolute energies (a.u.) for DFT optimized ionic complex (Cluster (Cr)Mil-101-AquaMet^{TM}).

Precat				Act			
217				217			
i =	23, E =	-1494.8902351452		i =	35, E =	-1494.8869603544	
Cr	25.9581117390	15.1123496912	17.2249211851	Cr	26.2350053249	15.0232330053	17.2103892519
Cr	22.6555799042	15.8258554551	17.5411141837	Cr	22.9488399220	15.7428922288	17.5391488394
Cr	24.9369341985	17.4449566438	19.4176482615	Cr	25.1802400524	17.3798048867	19.4298083870
O	24.5053460519	16.1686661675	18.1271417049	O	24.7199311967	16.1099847309	18.1282674957
O	25.1149495996	13.3773448835	17.7338241388	O	25.3591266146	13.3017690199	17.7332432076
O	25.1177221428	15.0913510514	15.4261228066	O	25.3618465164	15.0137333071	15.4164065848
O	26.8423664693	16.8048429489	16.7038022144	O	27.1455662537	16.7233746967	16.7140035758
O	26.9953246749	14.9376097809	18.9050289019	O	27.2308220053	14.8600407208	18.9092483136
O	23.1773150802	16.2472742430	15.7064518709	O	23.4183496222	16.1666208143	15.6987758204
O	22.1765590747	15.4064460082	19.4400065558	O	22.4747617481	15.3189658528	19.4414890307
O	22.9278870151	13.8677348250	17.3331201695	O	23.1714037545	13.7848632903	17.3333059573
O	25.8951160724	16.0950077613	20.5296426524	O	26.1306279903	16.0227082467	20.5298084394
O	26.5962141928	18.0467012485	18.5902928794	O	26.8365650718	17.9729223477	18.5880111155
O	23.3296071214	17.0328676964	20.5375511377	O	23.5721294509	16.9757343022	20.5423559453
C	23.8868828627	13.0690205297	17.6158777065	C	24.1352518858	12.9883387876	17.6169307070
C	23.5223256959	11.6311099158	17.8112260484	C	23.7759773554	11.5515396872	17.8156345775
C	22.1775808745	11.2319401845	17.7432928730	C	22.4310794980	11.1500539368	17.7770981524
C	24.5200684778	10.6798386960	18.0732809235	C	24.7840254508	10.6034989354	18.0488586101
C	24.1746586782	9.3416868818	18.2619421945	C	24.4485497685	9.2632216925	18.2364529134
C	22.8294494114	8.9376653023	18.1944283254	C	23.1035245899	8.8576362743	18.1978942660
C	21.8350698899	9.8982503079	17.9405803406	C	22.0988289160	9.8146978471	17.9752391496
H	25.5556439251	11.0074070625	18.1291835918	H	25.8188656979	10.9367118475	18.0811729760
H	21.4208454218	11.9859747385	17.5388267997	H	21.6671362512	11.9026017124	17.5949217558
C	27.3905992567	14.3763204450	21.1612618070	C	27.6445162092	14.3156987098	21.1636600355
C	28.1424246516	13.2603391648	20.7655216975	C	28.4072648329	13.2072550404	20.7658580832
C	27.2506333826	14.6804865887	22.5253324596	C	27.5042875648	14.6175905289	22.5281047571
C	28.7552021187	12.4590693060	21.7247476499	C	29.0220970737	12.4060478051	21.7237998596
C	28.6147666020	12.7581374811	23.0899712123	C	28.8719316900	12.6966374296	23.0901179375
C	27.8511066856	13.8696131710	23.4836526893	C	28.1066016127	13.8061791936	23.4849612941
C	29.2207574950	11.9093356497	24.1571984298	C	29.4636942125	11.8375407754	24.1572920741
H	26.6645908336	15.5507056508	22.8118938482	H	26.9147820350	15.4845814026	22.8170707404
C	26.7088771368	15.2012529764	20.1205799875	C	26.9533092995	15.1306927124	20.1215830307
C	22.4803551378	16.0791378058	20.4812780308	C	22.7537670297	15.9950646666	20.4821043280
C	21.7614868096	15.7085651434	21.7409087697	C	22.0492278150	15.6088709317	21.7415711207
C	22.1090562823	16.3019211244	22.9637682085	C	22.4106812013	16.1971209830	22.9621598591
C	21.4413237533	15.9363137198	24.1329339331	C	21.7519671931	15.8295571167	24.1343731897
C	20.4108999845	14.9798278441	24.0960521263	C	20.7178219325	14.8784582375	24.0986618962
C	20.0535279478	14.4038812938	22.8651771816	C	20.3498139207	14.3031682085	22.8707799808
C	20.7278720571	14.7566537011	21.7003752995	C	21.0166270277	14.6567013128	21.7024223877
H	22.9014318687	17.0460184969	22.9853276965	H	23.2054711722	16.9385144231	22.9773604568
H	20.4681662116	14.3080149226	20.7446247606	H	20.7508995253	14.2119819638	20.7461807408
C	19.6499571293	14.5486786734	25.3129625481	C	19.9571731802	14.4602546827	25.3167497364
O	22.1590313976	17.7176011544	17.7339239960	O	22.3948111423	17.6274472081	17.7331747582
O	23.9591671265	18.8944019550	18.4332304509	O	24.1875658594	18.8199854120	18.4317919978

H	28.2191405160	13.0279428999	19.7065334730	H	28.4889277905	12.9787141231	19.7061138467
C	24.0996463227	15.7146681112	14.9916773772	C	24.3458711072	15.6377493295	14.9828502878
C	23.9626965921	15.8211895332	13.5100636900	C	24.2072176782	15.7489144704	13.5027131358
C	24.9603981896	15.2615243231	12.6962198700	C	25.1984441835	15.1780626665	12.6888629472
C	24.8323975458	15.3103141064	11.3104923853	C	25.0677784401	15.2247143642	11.3037145301
C	23.7014704385	15.9062018547	10.7251823798	C	23.9411306292	15.8306345070	10.7207104384
C	22.7060411811	16.4626817099	11.5475194665	C	22.9545307998	16.4020919048	11.5426990096
C	22.8375463467	16.4351321977	12.9344206637	C	23.0884762216	16.3761257539	12.9290602828
H	22.0846302207	16.8779436729	13.5875803113	H	22.3422414104	16.8300966226	13.5823553545
H	25.8164330225	14.7841024436	13.1686912174	H	26.0502229665	14.6939550315	13.1625022525
C	22.7807408332	18.8044419036	17.9441512341	C	23.0079648035	18.7182269575	17.9421452307
C	22.0617650067	20.0855603906	17.6395546165	C	22.2749181913	19.9940523305	17.6347149570
C	20.7919817602	20.1823016934	17.0092611308	C	20.9965807091	20.0930268583	17.0142054985
C	20.2414419535	21.4580239187	16.8246010703	C	20.4473202046	21.3714871549	16.8400996778
C	20.8929472526	22.6265274237	17.2422192570	C	21.1090953612	22.5398470255	17.2457205023
C	22.1378234919	22.5221196776	17.8783414993	C	22.3620739441	22.4330056386	17.8635325840
C	22.7067173229	21.2679320544	18.0597459042	C	22.9257212048	21.1766728794	18.0443069181
S	19.7480886510	18.8189994453	16.3523186356	S	19.9568444151	18.7398392977	16.3138378092
C	27.0895658931	17.8175693238	17.4322203849	C	27.3611689378	17.7417673622	17.4406868453
C	28.0493647965	18.8295455551	16.9087413436	C	28.3237841023	18.7652345312	16.9307321817
C	28.3491922622	19.9711012759	17.6709150618	C	28.5979745370	19.9198449165	17.6834934684
C	29.2315610152	20.9230714602	17.1733540819	C	29.4697916496	20.8847970008	17.1868175814
C	29.8318016276	20.7423153799	15.9159039193	C	30.0889355591	20.7091179053	15.9372081582
C	29.5266676171	19.6000716657	15.1566674406	C	29.8168045242	19.5475705431	15.1922738767
C	28.6391073140	18.6462725383	15.6494504173	C	28.9413637227	18.5806362912	15.6841262189
H	28.3838014297	17.7597131655	15.0738005204	H	28.7157086717	17.6817069528	15.1146188369
H	27.8769625752	20.0922864781	18.6435139043	H	28.1132999600	20.0432258365	18.6498635196
O	20.9252661243	15.5561148917	17.1148490649	O	21.2240006706	15.4772292393	17.1204376757
O	27.3287080897	14.1546618269	16.4149823679	O	27.6159599997	14.0734501155	16.4023281614
O	25.3469815400	18.6719291182	20.6981290585	O	25.5802236382	18.6600839671	20.6862332648
H	24.6205019183	18.7773104691	21.3385378933	H	24.8315188664	18.7742837795	21.3006686093
H	28.1120721968	14.1529524600	16.9916685406	H	28.3739342818	14.0162996279	17.0063218156
H	20.4033624452	16.3980239942	17.2378818124	H	20.6847007350	16.3160066764	17.2135365484
H	27.7441501758	14.0748134751	24.5467118512	H	27.9974701275	14.0074588718	24.5485180682
H	29.3020173351	11.5734094182	21.4020251406	H	29.5762451928	11.5259425240	21.3978098993
O	28.7778522556	11.8219223315	25.2852397309	O	29.0115884677	11.7451082308	25.2816805357
O	30.3407272048	11.1949821005	23.8036565663	O	30.5785031059	11.1154546310	23.8056875728
H	30.6322480083	11.4666415879	22.9141557701	H	30.8831987770	11.3936073222	22.9226337624
H	29.4729004988	21.8216450842	17.7370723090	H	29.6860011906	21.7915320386	17.7478499004
H	29.9447948405	19.4624368280	14.1594782536	H	30.2508255500	19.4007806609	14.2029989299
C	30.7510592638	21.8159488417	15.4379482254	C	30.9883755615	21.8011822503	15.4490060005
O	30.7273942148	22.9536974765	15.8650975602	O	30.9555834579	22.9432517586	15.8671022313
O	31.6588964982	21.4690094891	14.4645287878	O	31.8911933448	21.4669285535	14.4653106933
H	31.6203919367	20.5069915766	14.3129989674	H	31.8689462186	20.5039391311	14.3159665792
C	23.4983661901	15.9366781641	9.2454294581	C	23.7341897969	15.8589298136	9.2427126031
H	21.8370201471	16.9150107256	11.0750153124	H	22.0909529752	16.8643146691	11.0698409518
H	25.5958760701	14.8379778455	10.6922772033	H	25.8247984166	14.7427710218	10.6850859885
O	22.4050768516	15.9477634640	8.7102308530	O	22.6394967109	15.8701998207	8.7096447558
O	24.6416006308	15.9445274712	8.4749167812	O	24.8766690061	15.8667211754	8.4723127667
H	25.4186506895	16.0427578350	9.0555933057	H	25.6541111741	15.9605176372	9.0532972836

H	20.7988430049	9.5698483044	17.9050243653	H	21.0641795421	9.4796102231	17.9648272513
H	24.9628049743	8.6271337041	18.5008679544	H	25.2445282534	8.5491623578	18.4495332585
C	22.3798950912	7.5262872810	18.4074854745	C	22.6568442197	7.4481909168	18.4096688851
O	21.2471449808	7.2289032660	18.7400873710	O	21.5276184729	7.1507552635	18.7475158688
O	23.3190609749	6.5371852310	18.2027948184	O	23.5798932698	6.4530325128	18.1988202571
H	24.1357191790	6.9352245774	17.8491750497	H	24.4046634964	6.8387297299	17.8497562886
H	21.7089328648	16.4329507591	25.0657071470	H	22.0272754138	16.3216077843	25.0671745067
H	19.2448862102	13.6764543816	22.8496773675	H	19.5379220722	13.5791059453	22.8612992786
O	20.2934020541	14.6985438648	26.5212415082	O	20.6006130550	14.6194914622	26.5232519809
H	21.2167241172	14.9708972459	26.3673623600	H	21.5272657083	14.8782914581	26.3664765871
O	18.5257968386	14.0830205337	25.2789088423	O	18.8300068446	14.0024997292	25.2816458634
C	20.3028441296	23.9895668501	17.0490928876	C	20.5290773189	23.9078624885	17.0500214089
H	19.2551172933	21.4844698448	16.3631598788	H	19.4559172727	21.4039389878	16.3895940325
H	22.6400569288	23.4258234619	18.2169501662	H	22.8760875086	23.3354738085	18.1877528113
O	19.3733844201	24.1153002642	16.0368158946	O	19.6050672164	24.0374232495	16.0341690159
H	19.3106306754	23.2678716366	15.5573120848	H	19.5410430955	23.1905086071	15.5538939490
O	20.6059248333	24.9588464588	17.7213698386	O	20.8383318484	24.8769166087	17.7199947395
O	19.3687867999	17.9563394150	17.4984629205	O	19.6045828718	17.8069925223	17.4170122151
O	20.5389239724	18.1289908361	15.3173865474	O	20.7671106119	18.1266286657	15.2443087569
O	18.5683081849	19.5294529487	15.7845220603	O	18.7491803171	19.4443668332	15.7907223236
H	23.6754101489	21.1667020613	18.5435465106	H	23.8995412560	21.0732880966	18.5171549875
Ru	9.6145881558	23.5839923346	14.6205048109	Ru	10.0939425619	23.5507920020	14.7080076611
H	8.0432926419	25.6314098322	17.8341559319	Cl	10.2063042760	23.2941631688	16.9954491288
H	8.1354617223	27.4061691617	17.7060945600	C	13.5181811659	23.9251266829	16.9565634305
Cl	9.8022865934	23.1840123374	16.9034435638	C	9.8489100066	19.5142149690	16.3544595672
C	7.7099612270	26.5000230427	17.2511388736	H	16.0587867328	16.8105120562	16.2857794612
C	13.1290468631	23.9941022283	16.9101130056	H	15.4663268190	14.6877981005	16.0965039771
C	9.6059760204	19.5957710053	16.3246614675	H	17.1171956319	14.1970995463	15.6361083398
H	6.6192217684	26.5765854244	17.3199610850	C	16.0937770068	14.3365613337	15.2686964947
H	15.7263440252	16.9156910875	16.3009975913	H	14.1410657555	18.3503816299	15.9313247188
H	15.1706855460	14.7867144368	16.0647882906	C	15.9618897778	17.4168491732	15.3784510303
H	16.8496992897	14.3522554833	15.6519796726	H	18.2705249112	16.0801593061	15.4687507966
C	15.8347088442	14.4654523643	15.2535300675	H	16.5781427625	18.3191421797	15.5100981688
H	13.7977865683	18.4386484762	15.9217831135	H	14.3976036797	26.3850047531	16.3812499422
C	15.6455276611	17.5363889520	15.4022097206	H	15.7145343156	13.3474349292	14.9718700770
H	17.9735756065	16.2380502288	15.5267242960	C	14.5039650150	17.7542710022	15.0815293278
H	16.2433229580	18.4452238714	15.5631824562	H	12.5927846510	19.8364538941	15.5349751748
H	14.0506716448	26.4486566982	16.3691987001	H	7.9090584865	17.9775412243	15.3294007365
H	15.4961458186	13.4692486642	14.9327126184	C	13.6414551519	24.5392422443	15.5852400113
C	14.1936930276	17.8636435820	15.0720543817	C	18.0928521495	16.5385027202	14.4913808459
H	12.3332958612	19.9613947226	15.5264651582	C	9.4985766052	19.3568090743	14.8950995271
H	7.6570840943	18.0840136734	15.2778571991	H	13.8794071861	16.8389576467	15.0535266461
C	8.2174450328	26.3929688393	15.8171506398	C	14.1627082171	25.8375331276	15.4696949566
C	13.2686828697	24.6296506447	15.5462893829	H	14.3827656933	21.3637353825	15.1577623935
C	17.8108844416	16.7112091318	14.5540494632	H	18.5161191457	17.5487960022	14.5046650061
C	9.2603131780	19.4447942725	14.8606417633	C	8.4338995470	18.5133997843	14.5393473733
H	13.5789360700	16.9435765890	15.0052219496	N	16.6087976753	16.6403643071	14.2383709715
H	9.3138824399	26.3588299488	15.8405255046	C	16.0190458708	15.2455783104	14.0496783434
C	13.8122912119	25.9170255450	15.4498180193	C	12.6437023602	20.1808709051	14.4890823038
H	5.4058711515	26.1501720790	15.6245126096	C	13.6274042258	21.3502901738	14.3631988772

H	14.0553163233	21.5694770593	15.1652277268	N	12.7487226351	22.5229220101	14.4684070373
O	7.9433718903	25.0507559780	15.2433393390	C	11.4180446868	22.1994815369	14.3413508420
H	18.2091409999	17.7313254065	14.5983153510	N	11.3449481892	20.8336786082	14.1592231987
C	8.1930164571	18.6160319297	14.4938525460	N	14.3824664779	18.5416136639	13.8498773380
C	5.4699788533	25.1687763199	15.1691219227	C	13.3098983541	23.8499796268	14.4004405175
N	16.3318955874	16.7898924545	14.2659802455	H	18.5435736809	15.9375470178	13.6951630544
C	15.7723410281	15.3882304030	14.0439150240	C	10.1768105883	20.0490561561	13.8700756253
C	6.7016598194	24.5516502461	14.9421153383	H	14.9802022208	15.3739301551	13.7304547480
C	12.3736197245	20.3115821455	14.4819233364	C	13.0073870993	19.0005197204	13.5805398434
C	4.2968919285	24.4988908488	14.7968133568	C	14.4040537708	26.4357391381	14.2298199954
H	3.3373103472	24.9816607948	14.9713609650	H	16.5755767634	14.8187759170	13.2058288858
C	13.3218054299	21.5027472898	14.3531897847	H	12.2629228955	18.1897319146	13.6783590819
C	7.7946910780	27.5082071027	14.8676681101	C	8.0225127967	18.3507599567	13.2123386817
N	12.4007050948	22.6493664576	14.4023224372	C	16.4048388199	17.4610074580	12.9732356688
H	8.2212610688	28.4546131228	15.2302561427	C	14.9528550457	27.8386906155	14.1406170473
C	6.7815412129	23.2649335041	14.3464302858	H	16.9875697979	18.3784071920	13.1232314978
C	11.0831027212	22.3019449439	14.2793710213	C	14.9420541922	17.8060967534	12.7174812385
N	11.0645139011	20.9344345827	14.1539116056	H	14.1509697058	21.3331930289	13.3947447895
N	14.1053818219	18.6743140084	13.8544444487	C	6.8860409860	17.4199504123	12.8589236122
C	4.3444170893	23.2289176419	14.2095167742	C	13.6016885991	24.3997239732	13.1306619416
C	12.9569463196	23.9633134357	14.3470655420	C	9.7666587725	19.9292094380	12.5217396226
H	18.2936156974	16.1343850107	13.7592058486	H	14.3558077472	16.9033944768	12.4565839133
C	8.0823634462	22.6668487083	14.1329587139	C	14.1397905794	25.6887160569	13.0744665713
C	9.9399244842	20.1281151409	13.8357161118	Cl	10.2710173510	24.9541527184	12.9025031849
H	14.7399184312	15.5011660523	13.6987560344	C	8.6931884158	19.0799769340	12.2223184305
C	5.5775586137	22.6187349897	13.9886479806	H	12.9740467446	19.3450864006	12.5379550020
H	6.7085199883	27.6366893441	14.8066423161	H	16.8383037288	16.8913203968	12.1418201021
C	12.7432203001	19.1456779042	13.5644893524	H	14.9207545691	18.4556902145	11.8291766833
C	14.0854260920	26.5162919425	14.2164200080	C	13.3628534888	23.6361781846	11.8523300462
H	16.3597488624	14.9834990195	13.2103407130	C	10.4368242851	20.7023044530	11.4134945250
H	11.9884815908	18.3408230883	13.6328452508	H	14.3524889665	26.1239521260	12.0997218959
H	3.4232182495	22.7246283536	13.9279948306	H	8.3784768032	18.9821888556	11.1844634235
C	7.7924155422	18.4665999844	13.1615346333	H	4.4123839477	20.1937981352	15.7634787869
C	16.1489834650	17.6245150631	13.0070652279	H	6.3002578182	26.6466629179	15.8669373652
H	8.0822827598	21.6767579232	13.6697060508	C	6.1989140735	25.6299266418	15.4964586774
H	5.6346488867	21.6309897073	13.5345283839	C	7.3258781771	24.8735640853	15.2037250837
C	14.6772196736	27.8990740819	14.1494937860	H	3.2524511849	21.4637196176	15.3215278841
H	16.7188071034	18.5454307572	13.1817749582	C	4.9325119787	25.0649527450	15.3037687537
C	14.6905528975	17.9605857549	12.7230905064	H	8.3084698220	25.3286318017	15.3478719857
H	13.8704949773	21.4864217536	13.3993908519	C	3.8149512899	20.6051284546	14.9392774816
C	6.6421842713	17.5633334511	12.8024526962	H	4.0371461104	25.6444379705	15.5200048084
H	8.1887354151	27.3148554233	13.8612073569	C	7.2440056935	23.5432452049	14.7185006848
C	13.2898046432	24.4975990301	13.0847335083	C	4.7984806470	23.7543650621	14.8412373345
C	9.5651667622	20.0128529236	12.4793694728	C	5.9334175144	22.9800934434	14.5573038694
H	14.1149567438	17.0584084295	12.4375455250	H	3.0871282765	19.8411598814	14.6310833235
C	13.8366414109	25.7820176925	13.0501716331	H	3.8066279837	23.3383860817	14.7128241000
Cl	9.9625468993	24.9796524845	12.8117579967	O	5.9177452927	21.6813084280	14.1503271388
C	8.4849753687	19.1782825831	12.1737521444	C	4.7173556467	20.9471303422	13.7516944377
H	12.7327642243	19.5095119705	12.5276604625	C	4.0103815224	21.5736690367	12.5496216639
H	16.6069525058	17.0697741145	12.1791996651	H	3.4634212210	22.4900561603	12.7956585457

H	14.6818795038	18.6244124176	11.8451382320	H	3.2884496268	20.8521551081	12.1417012307
C	13.1276111804	23.7293231799	11.7923936419	H	4.7382154038	21.8094646026	11.7621105812
C	10.2525363115	20.7699369814	11.3636711837	C	8.4351189062	22.7826103774	14.3994909808
H	14.0790224945	26.2153700905	12.0822539613	H	8.2975004301	21.7788090451	13.9937458205
H	8.1804778908	19.0839496873	11.1332786987	H	5.1785023099	20.0106495794	13.4098913902
H	12.6659264331	23.0035065214	16.8758372343	H	13.0809737086	22.9232273683	16.9270372821
H	12.5057784200	24.6062687596	17.5767690990	H	12.8723404352	24.5330912695	17.6045936853
H	14.1209256987	23.9060185516	17.3775393579	H	14.5090543142	23.8691267193	17.4293673777
H	13.4340030297	24.3566198036	10.9442968562	H	10.6200577657	20.2721257392	16.5250261649
H	12.0920848078	23.4090925117	11.6173005526	H	10.1782466505	18.5594114459	16.7888849762
H	13.7667480124	22.8340045154	11.7686936567	H	8.9631391375	19.8385108391	16.9196804663
H	14.8301277623	28.2205452167	13.1130419184	H	15.0965621810	28.1487537382	13.0981592618
H	15.6481359809	27.9352714813	14.6619480276	H	15.9209109418	27.9214018504	14.6556109153
H	14.0256255697	28.6350320219	14.6390567035	H	14.2714298197	28.5598307955	14.6150052379
H	10.4153813545	20.3092839408	16.5089766254	H	6.6799582605	17.4263820015	11.7811409098
H	9.8734280324	18.6258169531	16.7682324832	H	5.9590337830	17.6999400976	13.3808436640
H	8.7372095653	19.9780886068	16.8808250233	H	7.1120074497	16.3838231310	13.1509083807
H	6.4581529130	17.5575895510	11.7220918600	H	9.9847522028	20.4557774703	10.4450830182
H	5.7165585482	17.8800900397	13.3016869368	H	11.5117211799	20.4839061037	11.3477336740
H	6.8379528009	16.5294739887	13.1172562775	H	10.3436780695	21.7874205837	11.5702300590
H	9.7959548663	20.5112423710	10.3986773213	H	13.6034010637	24.2612712019	10.9836603457
H	11.3243617520	20.5385567791	11.2897023176	H	12.3153991778	23.3205859980	11.7618056252
H	10.1745708485	21.8600724098	11.4926802329	H	13.9957885152	22.7384782224	11.7921243232
Ci1				MCy			
223				223			
i =	66, E =	-1508.6173620635		i =	40, E =	-1508.6074468406	
Cr	26.4516294192	15.2706332079	17.2080594825	Cr	26.7537230533	15.3414571315	17.2160271641
Cr	23.1440442119	16.0135506291	17.5362960339	Cr	23.4785661466	16.0178292064	17.5495297196
Cr	25.3896483224	17.6367247548	19.4225648940	Cr	25.7141530047	17.6875625950	19.4495648839
O	24.8954734109	16.3936507094	18.1199600818	O	25.2058108713	16.3900153398	18.0797152423
O	25.5726972210	13.5373849566	17.7318836056	O	25.8962775099	13.6038577575	17.7358492373
O	25.5760566954	15.2452754130	15.4141674399	O	25.8991451691	15.3242028499	15.4210196345
O	27.3628862921	16.9677417642	16.7197033781	O	27.6848097078	17.0286097984	16.7172032658
O	27.4492901254	15.1563610383	18.9103345401	O	27.7704287541	15.1677968243	18.9064270023
O	23.6306825026	16.3971787419	15.6992810070	O	23.8956813004	16.3927304124	15.6726021837
O	22.7002764706	15.5594404385	19.4487081047	O	23.0243622274	15.5690934115	19.4534181875
O	23.3931471700	14.0707695679	17.3339395777	O	23.7133449762	14.0800449739	17.3346510038
O	26.2793424817	16.2408332129	20.5291795566	O	26.6780916986	16.3234957867	20.5333451939
O	27.0495738254	18.2570131337	18.5791464729	O	27.3787028079	18.2824878251	18.5886868809
O	23.7723599452	17.2535466097	20.5377487131	O	24.1017871791	17.2587583439	20.5414984215
C	24.3395083128	13.2533680092	17.6158921948	C	24.6725027577	13.2800451750	17.6200490606
C	23.9461745444	11.8228027168	17.8120753640	C	24.3043472667	11.8410910057	17.8223365907
C	22.5957811863	11.4338266106	17.7761012076	C	22.9559295799	11.4451334265	17.7826673142
C	24.9416894738	10.8636519113	18.0457308260	C	25.2996715075	10.8805957671	18.0623882945
C	24.5918889315	9.5299338882	18.2386853285	C	24.9485107147	9.5440005766	18.2552668856
C	23.2444163837	9.1332367114	18.2005209706	C	23.6000585545	9.1438608889	18.2148184906
C	22.2487227596	10.1000838419	17.9763623627	C	22.6083852709	10.1118203404	17.9838407436
H	25.9794785819	11.1840049217	18.0750377467	H	26.3397814066	11.1970253046	18.0963679835
H	21.8356807086	12.1903396277	17.5934703766	H	22.1968535972	12.2009906549	17.5945687281
C	27.8014042204	14.5276105796	21.1574471066	C	28.1662878393	14.5812641149	21.1591696025

C	28.5548348261	13.4132260339	20.7540050756	C	28.9196235243	13.4657492718	20.7586503488
C	27.6603179640	14.8130428214	22.5253937411	C	28.0252953559	14.8700820045	22.5269675157
C	29.1700969464	12.6037110840	21.7069110179	C	29.5366068194	12.6584419259	21.7125347228
C	29.0364469814	12.8921050140	23.0758410918	C	29.4003901222	12.9488972539	23.0797315901
C	28.2652554966	13.9960704270	23.4765952744	C	28.6304432355	14.0546483238	23.4787777030
C	29.6610518498	12.0516997027	24.1456512842	C	30.0037168972	12.1031885171	24.1524952529
H	27.0739224037	15.6797025666	22.8209574212	H	27.4350254750	15.7338529009	22.8236036723
C	27.1274411264	15.3725864429	20.1232503969	C	27.4884412797	15.4241615273	20.1246100909
C	22.9648551099	16.2589437248	20.4788827179	C	23.2949840557	16.2641941318	20.4863765935
C	22.2501903260	15.8771696003	21.7366355438	C	22.5805444356	15.8834944774	21.7465983832
C	22.5986399920	16.4703863977	22.9583803158	C	22.9292094720	16.4735197063	22.9701924248
C	21.9342452699	16.1019529078	24.1280829082	C	22.2561924445	16.1126280570	24.1374478539
C	20.9087290063	15.1427078786	24.0927802315	C	21.2166968296	15.1667613033	24.0980482317
C	20.5498707792	14.5642863851	22.8634879612	C	20.8616220758	14.5887634137	22.8673756042
C	21.2207861918	14.9197528243	21.6971683099	C	21.5434599840	14.9349546603	21.7045402848
H	23.3887890839	17.2170346157	22.9785552967	H	23.7249250810	17.2139168398	22.9928540231
H	20.9602396457	14.4696412325	20.7413293629	H	21.2839417333	14.4880350491	20.7476511110
C	20.1494956514	14.7224010278	25.3101553747	C	20.4397068057	14.7635723350	25.3129924489
O	22.6158745326	17.8963052690	17.7299132036	O	22.9463762667	17.9072245368	17.7362050942
O	24.4124524015	19.0698945006	18.4314593383	O	24.7319492576	19.1191617662	18.4327265618
H	28.6373164152	13.1849077472	19.6943027342	H	28.9978402798	13.2356349333	19.6991313131
C	24.5505929537	15.8572228056	14.9806780008	C	24.8562323977	15.9050906052	14.9776653917
C	24.3928445622	15.9515283307	13.5023434557	C	24.7304878911	16.0034911843	13.4958313065
C	25.3770687678	15.3775939734	12.6830084684	C	25.7258129283	15.4344062559	12.6857637063
C	25.2505943665	15.4421888669	11.2984169185	C	25.6013739243	15.4876240750	11.2997711561
C	24.1337295783	16.0688185889	10.7206793611	C	24.4787392412	16.1003500127	10.7163643979
C	23.1396881825	16.6221297676	11.5474909087	C	23.4848341114	16.6632277644	11.5348012413
C	23.2705021832	16.5783628583	12.9341057462	C	23.6116993258	16.6278890382	12.9203941643
H	22.5205714636	17.0258865722	13.5875421443	H	22.8626655491	17.0758769272	13.5739180017
H	26.2255469763	14.8839318775	13.1508501449	H	26.5760563349	14.9497318071	13.1615425598
C	23.2330021004	18.9846795226	17.9426658482	C	23.5518529256	19.0055947856	17.9526274074
C	22.5155815510	20.2760093817	17.6474854691	C	22.8210449862	20.2900706303	17.6707832264
C	21.2449121412	20.3896577700	17.0175532232	C	21.5427301232	20.4017484074	17.0631109466
C	20.6974808828	21.6697303711	16.8476238453	C	21.0007495269	21.6807034611	16.8770715138
C	21.3509765014	22.8352892651	17.2742972940	C	21.6690287970	22.8464219876	17.2765212420
C	22.5962739194	22.7139273675	17.9084960243	C	22.9193671093	22.7301034708	17.9002537277
C	23.1608565271	21.4541310009	18.0806415145	C	23.4781544234	21.4705164119	18.0810967538
S	20.2093625514	19.0466139073	16.3244343477	S	20.5066449041	19.0545125368	16.3817636489
C	27.5646111407	18.0038521924	17.4298002176	C	27.9009223779	18.0504458016	17.4456812195
C	28.5046749523	19.0321937089	16.8961322187	C	28.8615312639	19.0711148085	16.9242480487
C	28.7637105926	20.1973329217	17.6374084642	C	29.1339293116	20.2277630427	17.6736031896
C	29.6371221639	21.1580183206	17.1393398218	C	30.0034307631	21.1931033298	17.1743194397
C	30.2694092006	20.9642907144	15.8996617370	C	30.6232110102	21.0170603923	15.9251401709
C	29.9958212911	19.8039348340	15.1554024190	C	30.3490685792	19.8550369521	15.1804561428
C	29.1186619014	18.8407110961	15.6495718995	C	29.4745397975	18.8876261348	15.6751273449
H	28.8943342356	17.9376787161	15.0857374628	H	29.2461302885	17.9895502034	15.1053015482
H	28.2704961498	20.3257773249	18.5989888037	H	28.6488260242	20.3513997512	18.6396335615
O	21.3894060575	15.7774083273	17.1922260131	O	21.7309261231	15.7915542358	17.1996309118
O	27.8337755347	14.3067792371	16.4097532258	O	28.1346766079	14.3942883408	16.4066675803
O	25.8041543698	18.8924144582	20.6884661127	O	26.0640252321	18.9829117964	20.6968269932

H	25.0618070789	19.0019724062	21.3103364360	H	25.3243973110	19.0317207627	21.3281709363
H	28.5883379889	14.2580771209	17.0198819229	H	28.9076828673	14.3580380998	16.9940530459
H	20.8907216756	16.6445382807	17.2631209025	H	21.2040370014	16.6389600718	17.2849702902
H	28.1553241893	14.1925435975	24.5405579047	H	28.5218964611	14.2500499786	24.5435963360
H	29.7158724432	11.7195472051	21.3770327653	H	30.0849660412	11.7756207359	21.3836018019
O	29.2312227280	11.9722861040	25.2793809504	O	29.5614793560	12.0501856775	25.2835429709
O	30.7906759720	11.3476160266	23.7964922210	O	31.1089339809	11.3562314879	23.8069336489
H	31.0647480890	11.5983586643	22.8949494874	H	31.4079080536	11.6105795073	22.9147342567
H	29.8477044572	22.0708324480	17.6928775212	H	30.2179827508	22.1013051609	17.7332589554
H	30.4331273496	19.6543296550	14.1677412254	H	30.7796668855	19.7071415796	14.1897211051
C	31.1961148600	22.0394061238	15.4307676187	C	31.5285248253	22.1096502100	15.4446377805
O	31.1805206766	23.1743767595	15.8627669165	O	31.4995358468	23.2502063185	15.8670748365
O	32.1122000636	21.6924795037	14.4623739872	O	32.4356950180	21.7761160180	14.4647404389
H	32.0559379191	20.7336677156	14.2934743364	H	32.4092433465	20.8140686021	14.3093706348
C	23.9456985639	16.1416048042	9.2411110561	C	24.2787548054	16.1542657818	9.2393610073
H	22.2754514325	17.0896379965	11.0796989340	H	22.6223524262	17.1256505067	11.0601711588
H	26.0046476686	14.9648640258	10.6724565381	H	26.3591186288	15.0072708148	10.6803073011
O	22.8555734521	16.1757249640	8.7034528279	O	23.1848892368	16.1804659483	8.7064008974
O	25.0932293778	16.1709473597	8.4761448129	O	25.4243885436	16.1767615853	8.4733472401
H	25.8672573768	16.2378197122	9.0652191677	H	26.1989013490	16.2479938044	9.0617481038
H	21.2103727348	9.7747463520	17.9633691020	H	21.5698044170	9.7883349900	17.9654593085
H	25.3806768072	8.8106578701	18.4571268000	H	25.7393876358	8.8258021128	18.4742346121
C	22.8175137049	7.7147970175	18.4066097772	C	23.1580871650	7.7255455481	18.4149737161
O	21.6944748750	7.3843685593	18.7393012947	O	22.0314142485	7.3963126194	18.7401029791
O	23.7800432786	6.7541232656	18.1991765717	O	24.1106865752	6.7579997209	18.2004532902
H	24.5811377882	7.1678494807	17.8294654424	H	24.9228241112	7.1672695590	17.8498647568
H	22.1998860943	16.5986435206	25.0614296490	H	22.5241959033	16.6078760604	25.0705476482
H	19.7423910394	13.8346829729	22.8514208738	H	20.0467640298	13.8681834172	22.8499362698
O	20.7596287473	14.9277921913	26.5239525345	O	21.0729437252	14.9305319690	26.5237877789
H	21.6809654834	15.2131104221	26.3838012871	H	22.0063301496	15.1692050355	26.3740924405
O	19.0390870470	14.2248253830	25.2752418183	O	19.3082056130	14.3153486625	25.2781759975
C	20.7636690294	24.2051251294	17.0855912395	C	21.0865345274	24.2133547519	17.0768387304
H	19.7104608807	21.6960919797	16.3871458770	H	20.0115780956	21.7096759172	16.4221331190
H	23.1044999466	23.6125026296	18.2534684677	H	23.4375578567	23.6286774284	18.2288580259
O	19.8176762311	24.3360732807	16.0965117686	O	20.1457869341	24.3376880815	16.0803180483
H	19.7301437104	23.4918448613	15.6149014707	H	20.0899718178	23.4970857664	15.5860785422
O	21.0757852028	25.1857676373	17.7356602093	O	21.3922718828	25.1918165304	17.7325115313
O	19.8991591228	18.1103816476	17.4425856226	O	20.1535776871	18.1236298305	17.4957966038
O	20.9869361283	18.4345303563	15.2408645314	O	21.3097152647	18.4344756280	15.3174457866
O	18.9739837233	19.7456917202	15.8655438870	O	19.2934180709	19.7574778565	15.8718099831
H	24.1285793187	21.3475949398	18.5645347034	H	24.4519109632	21.3630794644	18.5532942912
H	15.5172077157	15.2109835652	17.8857170621	Ru	9.2382494606	22.4880133808	14.7479610958
H	15.8537517300	17.3479992375	17.4955912931	C	11.0373655620	21.5508531312	14.7211796072
H	17.1668412668	14.7216034473	17.4197703886	N	12.2663528517	22.1120860017	14.7109447555
C	16.1133233505	14.7052962355	17.1166647969	N	11.1652919592	20.2035916342	14.8624303954
H	18.1022229725	16.6142999778	16.8330637017	C	12.5720493788	19.8212384371	15.1832753043
H	5.0484998633	23.7255149001	17.8621202844	C	13.3399216446	21.1025259830	14.8335469607
C	9.6093313307	19.5914782850	17.1603232056	H	14.0527463798	21.4051728481	15.6096234742
H	15.7941558860	13.6530238651	17.0991281320	H	13.8860514743	21.0074099998	13.8835140164
C	15.7182437919	17.7087299088	16.4702400289	C	10.1340073206	19.1933543237	14.8644439085

C	12.8099047705	24.2526044747	16.4409885469	C	12.6193356661	23.4782526515	14.4105837701
Cl	9.6526288098	23.3560813788	16.6805742492	C	12.7610990662	23.8574053069	13.0570766899
H	13.8617897945	18.6687248660	16.8242764410	C	13.1348883419	25.1777499106	12.7782744119
H	16.2821984907	18.6443771070	16.3582397550	C	13.4081023654	26.1037997901	13.7927359227
C	5.1673917070	23.0287078664	17.0355430418	C	13.3373516074	25.6673194679	15.1202834208
C	17.8804632203	16.7691235165	15.7749404817	C	12.9634071009	24.3579222372	15.4577496716
C	14.2453335065	17.9063497375	16.1306317850	C	12.5916633452	22.8710487819	11.9292994658
H	7.2232449452	23.5587439508	16.6648670768	H	13.2325274559	25.4833570369	11.7380326039
H	3.1316141607	22.3024857103	17.1186420594	H	13.5967590439	26.3567408919	15.9226506157
H	13.6627058785	16.9841980611	16.3261774461	C	13.0172358753	23.9315241403	16.9037375245
H	18.2220673061	17.7754872629	15.5060635887	C	9.6838912226	18.6867891331	13.6207428474
C	4.0991094030	22.2229906956	16.6256872732	C	9.7341858627	18.5958373619	16.0801275614
C	15.8947512129	15.2845949143	15.7252272070	C	8.8696041852	17.5460428941	13.6268760428
C	6.3786394563	22.9433569914	16.3601239886	C	8.9263702516	17.4498551938	16.0223814508
H	12.2199234241	19.8864975092	16.1415176322	C	8.5196340403	16.8850718274	14.8100627023
N	16.3946920345	16.7130971995	15.5408510180	H	8.5350967762	17.1442719209	12.6717300780
H	8.0231892621	17.4694728407	16.7194182507	C	10.1595030488	19.1040932481	17.4357880879
C	9.2849468027	18.9627956273	15.8273622244	H	8.6303408079	16.9765095173	16.9576514161
H	13.4949461318	26.5521288139	15.2737273776	C	10.0818126026	19.3003149788	12.3045275427
H	18.3718900125	16.0087729087	15.1590283454	C	7.3087818342	21.9045381694	14.8652019655
H	13.7726927936	21.5411982006	15.4298587291	Cl	9.0255673376	22.6362734545	12.3855297262
C	8.4230390439	17.8553380723	15.7822030382	Cl	9.7447587173	22.6366067210	17.0846322886
H	8.9441377173	25.6317661104	15.5394450525	O	5.7601869372	19.6048976897	14.6249557578
C	12.8268246091	24.5358705932	14.9603858105	C	4.6502414782	18.8011265614	14.1048388376
H	14.8330713452	15.2723561563	15.4590810389	C	4.6425571068	17.3722721561	14.6507847637
C	12.2353498711	20.0027035274	15.0467270313	H	4.9373470078	18.7409838516	13.0468088796
H	16.4361267824	14.7012840927	14.9701727717	C	3.3043851318	19.5163461701	14.1873262845
C	13.2634265674	25.7962181638	14.5243800500	H	2.9435549778	19.6262301436	15.2159387045
C	4.2550251904	21.3085035955	15.5832227476	H	2.5585418902	18.9323026919	13.6298035152
N	14.0873558501	18.3773727268	14.7520145478	H	3.3663415469	20.5136172158	13.7331628874
C	6.5821523233	22.0431275325	15.2827200286	H	5.6436218813	16.9379083472	14.5654694596
C	13.0838022085	21.2126174857	14.6424278989	H	3.9511613825	16.7589781160	14.0557597957
C	8.8114176255	25.3492435874	14.4968133498	H	4.3258504297	17.3028730579	15.6970701731
N	10.8655269054	20.4278208568	14.6262810690	C	5.7520903240	20.1924226675	15.8643015847
C	16.1384093092	17.1867022654	14.1179260417	C	6.5922785785	21.3349697936	16.0276874772
N	12.0679438902	22.2518189878	14.3894805827	C	4.9889682867	19.7348895413	16.9542359700
C	12.6945655762	18.6930422294	14.3972467166	C	5.0421301539	20.3838954701	18.1883787170
Ru	9.2639198920	23.1449086873	14.3338536856	C	5.8598626111	21.5045224442	18.3620983147
C	10.7940252874	21.7693597076	14.3861254996	C	6.6149634608	21.9619962878	17.2890075396
C	9.8131480496	19.4485286411	14.6134316766	H	4.4400821719	20.0106151916	19.0142056316
C	5.4869045885	21.1800511463	14.9235875180	H	4.3466667621	18.8701833246	16.8421392645
H	6.7698142431	24.7181049264	14.7010610935	H	7.2721499815	22.8169181054	17.4234876172
C	7.8143522359	21.9732210903	14.5343240708	H	5.9094233262	22.0165806251	19.3199191802
H	11.9992454214	17.8730155842	14.6530228049	H	7.0508389434	21.4101907269	13.9251979479
C	12.5066214546	23.5671562421	13.9841704199	C	13.0426511124	18.5906757720	14.4020331230
H	3.4084064370	20.7036121477	15.2854456160	H	12.6230783424	19.6189730897	16.2643773940
H	16.6877328615	18.1314763865	14.0221099450	N	14.4713130307	18.3240287070	14.6304452813
H	5.2316914796	18.0761233210	15.2411307431	H	12.9161995103	18.7993632197	13.3309837546
H	3.5668849496	18.6934584041	15.2410225134	H	12.4036452272	17.7208954719	14.6399315552
C	8.0767262180	17.2306932734	14.5787758500	C	15.0258362587	17.4821434137	13.5698232643

C	14.6620655018	17.4066895579	13.8203689198	C	14.7522620440	17.7147251684	15.9360022926
C	7.6110222172	24.8612359438	14.0287335032	C	16.2564856142	17.5887420893	16.1612163153
C	4.3693571955	18.3082739698	14.6037068869	H	14.2470385062	16.7351338488	16.0532107450
H	13.6727210944	21.0167108819	13.7338913117	H	14.3629766543	18.3610628228	16.7359108532
C	13.4402145452	26.0970791384	13.1703018235	C	16.5306608660	17.3374274424	13.7415895263
H	14.1069317887	16.4489305530	13.8060068115	H	14.8614145496	17.9786061593	12.6015773050
C	7.2221087599	15.9847125050	14.5653070974	H	14.5293017023	16.4944449496	13.5054069942
H	9.5761031022	25.7022708852	13.7981091138	N	16.9286245130	16.7460552688	15.0852388720
H	16.5861409583	16.4463371584	13.4435762017	H	16.7512388513	18.5688603596	16.1227622380
H	7.8928246887	21.0923978188	13.8886681162	H	16.4871091883	17.1328549967	17.1301745251
O	5.7384687186	20.2961098104	13.9187585553	H	17.0050542739	18.3261568289	13.7079048535
C	13.9118786353	27.4640618347	12.7368964526	H	16.9739609955	16.7036361652	12.9639556003
C	9.4333822751	18.8824068610	13.3738871428	C	18.4228864434	16.8856677024	15.2088235757
H	12.6576418698	18.8198526768	13.3065478590	H	18.9029089452	16.2392217185	14.4683059764
H	4.0116205928	17.3710355474	14.1530020291	H	18.7418153740	16.6266019180	16.2218029394
C	8.5657967528	17.7819448789	13.3871407189	H	18.6798904086	17.9387168162	15.0420494661
C	12.7638507902	23.8070036007	12.6127946024	C	16.5489918222	15.2715317900	15.1555121823
C	4.7843337377	19.2664556567	13.4838489339	C	16.8921911351	14.5866192615	16.4724390510
H	14.6017288420	17.8178538805	12.8011632428	H	17.0909688386	14.8074299370	14.3220385387
C	13.2074209662	25.0801377393	12.2355453489	H	15.4779634828	15.1959691820	14.9421506579
H	7.4124553319	24.7791325091	12.9633814915	H	17.9546148332	14.6726511795	16.7304376066
H	2.8879916105	20.3753879665	13.2994990096	H	16.6670569683	13.5156529170	16.3646533699
Cl	9.2839349241	23.2025446247	11.9635861004	H	16.2946074019	14.9598293222	17.3126452414
C	3.6191629970	19.8444717621	12.6794296702	C	13.8030827318	27.5234473068	13.4648156907
H	5.4252486756	18.7063616985	12.7913705074	C	7.7875984678	15.5643880962	14.7805270246
C	9.9333437853	19.4264653463	12.0596543204	C	8.5152332701	24.3407294701	14.8768742270
C	12.6406086721	22.7256087100	11.5698068216	C	7.2128120298	23.5036371917	14.6860497053
H	8.2847549854	17.3291418683	12.4372938028	H	8.7288052580	25.0007281951	14.0339302316
H	13.3914706219	25.2759504380	11.1805277586	H	8.6213920613	24.7927602266	15.8660676414
H	3.0905749526	19.0210159084	12.1762782123	H	6.8508927356	23.6634090413	13.6650609884
H	3.9843107207	20.5358496762	11.9088738568	H	6.5029415883	23.8132922667	15.4601556742
H	12.4112695855	23.2616009256	16.6736931040	H	13.8194975975	27.6962154010	12.3815670728
H	12.1806601182	24.9769331277	16.9757746224	H	14.8015456024	27.7608088368	13.8601048408
H	13.8303542074	24.3363526813	16.8428015930	H	13.1012387466	28.2432841226	13.9103490248
H	10.1905596139	20.5151265819	17.0607789916	H	12.6483694760	22.9127371950	17.0546178297
H	10.1498717645	18.8884580900	17.8107993328	H	12.4002953553	24.5871975860	17.5333775423
H	8.6805405786	19.8634970030	17.6828014997	H	14.0519234153	23.9987144989	17.2721209170
H	6.9648984607	15.6845678187	13.5417315727	H	10.7231685335	20.0409195407	17.3851977497
H	6.2849478566	16.1248530361	15.1210013894	H	10.7519394264	18.3443772582	17.9663922344
H	7.7476633356	15.1419963761	15.0379188996	H	9.2725188169	19.3117807421	18.0526031760
H	14.0185742425	27.5268907102	11.6470019279	H	12.7240354266	23.3709512160	10.9618211615
H	14.8849358871	27.7093505143	13.1867463114	H	11.5986250736	22.4008880759	11.9366944089
H	13.2059393264	28.2458858546	13.0523206497	H	13.3501690519	22.0755145248	11.9882733953
H	12.8419567366	23.1345482870	10.5718652751	H	9.6370311508	18.7408902516	11.4727025898
H	11.6345974417	22.2862185680	11.5592778752	H	11.1716987796	19.3000708209	12.1637015215
H	13.3718495723	21.9223415022	11.7454946786	H	9.7532128480	20.3489467942	12.2243170516
H	9.5227192893	18.8461257623	11.2242539822	H	7.3633858241	15.3563402667	13.7898500761
H	11.0294704697	19.3861603968	11.9865352132	H	6.9747302499	15.5279165866	15.5184099945
H	9.6511857419	20.4830987320	11.9192003073	H	8.4735991517	14.7393573455	15.0246597645
Ci2				I14e			

223				197			
i =	16, E =	-1508.6061006353		i =	112, E =	-1421.7167583376	
Cr	26.1593888107	15.0119937981	17.2143948774	Cr	24.9697534923	15.0979232345	17.2067523356
Cr	22.8383848657	15.7220288634	17.5462033639	Cr	21.6544235467	15.7919158778	17.5408426571
Cr	25.1026255887	17.3608651752	19.4279042608	Cr	23.9264329623	17.4508571926	19.4227619827
O	24.6020440042	16.0975985747	18.1296228530	O	23.4154808682	16.1893891248	18.1237182771
O	25.2383063377	13.3015432795	17.7364799960	O	24.0461862832	13.3819879066	17.7312296119
O	25.3131368564	15.0042103069	15.4164875564	O	24.1111827691	15.0918563710	15.4105004627
O	27.0831475395	16.7085193519	16.7246568792	O	25.8951770039	16.7976552526	16.7135215127
O	27.1675207955	14.8527547685	18.9149994355	O	25.9756248163	14.9359748424	18.9044235016
O	23.3338405948	16.0867517459	15.6991448371	O	22.0940560776	16.1067729114	15.6906574985
O	22.3480301513	15.3141728157	19.4473084897	O	21.2262235966	15.3922897545	19.4490334707
O	23.0424899705	13.7674609835	17.3425382287	O	21.8542413041	13.8504787349	17.3376228802
O	26.0720508320	16.0149131685	20.5345965838	O	24.8790053380	16.1006128236	20.5252182726
O	26.7667958209	17.9644325787	18.5941899596	O	25.5864001400	18.0492934832	18.5846182704
O	23.4957505638	16.9499740684	20.5445413587	O	22.3228702482	17.0529419360	20.5435435419
C	24.0169922825	12.9791489352	17.6227572841	C	22.8254720836	13.0598928841	17.6166894374
C	23.6665679078	11.5416317815	17.8229476854	C	22.4637755644	11.6246366393	17.8117630244
C	22.3207093864	11.1451013510	17.7895109808	C	21.1161450829	11.2311514050	17.7827151095
C	24.6709100241	10.5882555077	18.0535719804	C	23.4693386992	10.6729385480	18.0353617816
C	24.3278962858	9.2492046113	18.2427300997	C	23.1271713405	9.3345993242	18.2232167331
C	22.9801526012	8.8502845856	18.2085105811	C	21.7799666587	8.9354370509	18.1940285325
C	21.9802925203	9.8126817091	17.9885421677	C	20.7782141793	9.8977000847	17.9806168539
H	25.7083628502	10.9135872618	18.0847173316	H	24.5060321963	11.0008503312	18.0607980365
H	21.5616977112	11.9034362331	17.6110156967	H	20.3552357326	11.9885427513	17.6088617067
C	27.5565469606	14.2803779226	21.1676896458	C	26.3524872388	14.3629716184	21.1578330185
C	28.3137704403	13.1691689750	20.7675468237	C	27.1028089973	13.2472027021	20.7582950229
C	27.4100191469	14.5703800597	22.5335584836	C	26.2030605074	14.6585230261	22.5220378776
C	28.9396995441	12.3699011095	21.7219862096	C	27.7152429972	12.4436512266	21.7157655208
C	28.8029336910	12.6603475119	23.0894987679	C	27.5756852171	12.7396037591	23.0819703254
C	28.0230867489	13.7609393563	23.4865325778	C	26.8036951715	13.8449820197	23.4777816845
C	29.4164647072	11.8169390542	24.1568736052	C	28.1977803172	11.9025026322	24.1518416099
H	26.8158760608	15.4321154988	22.8310265749	H	25.6131181564	15.5254543994	22.8107415255
C	26.8862499271	15.1151423229	20.1274209285	C	25.6888886338	15.1970798455	20.1166670897
C	22.6549329511	15.9850048746	20.4849329612	C	21.5011680106	16.0741597373	20.4860908282
C	21.9411682323	15.6064258802	21.7433629554	C	20.7876254910	15.6927389140	21.7437350455
C	22.2990541928	16.1909199092	22.9660644450	C	21.1439608300	16.2793210495	22.9668483974
C	21.6395137773	15.8211492403	24.1386044138	C	20.4799872167	15.9115641217	24.1367397571
C	20.6039765349	14.8701630034	24.1026120424	C	19.4449991182	14.9619283660	24.0979402806
C	20.2386533018	14.2987998119	22.8719838108	C	19.0793715201	14.3903592754	22.8670110832
C	20.9058191214	14.6555131061	21.7040527566	C	19.7508744107	14.7441295956	21.7008466745
H	23.0947429250	16.9317841388	22.9799846899	H	21.9394055107	17.0198837182	22.9869150932
H	20.6380079827	14.2117447081	20.7478554812	H	19.4851714189	14.3021767126	20.7431396269
C	19.8330262483	14.4529747486	25.3176344523	C	18.6783579329	14.5411559047	25.3127864832
O	22.3138732617	17.6099775949	17.7352533340	O	21.1468574472	17.6716795356	17.7303026259
O	24.1100713229	18.8092990134	18.4309654051	O	22.9280490142	18.8915214134	18.4271878234
H	28.3928656615	12.9427394300	19.7072607550	H	27.1818202303	13.0189914738	19.6982981407
C	24.2748215694	15.5915592727	14.9849959512	C	23.0561459442	15.6449290052	14.9749614372
C	24.1279650155	15.7109059435	13.5063961497	C	22.9135925345	15.7604661476	13.4963435381
C	25.1103648531	15.1427818244	12.6811444887	C	23.9085421893	15.1950760999	12.6832683108

C	24.9671245710	15.1916372883	11.2965925271	C	23.7894352207	15.2612018207	11.2983835317
C	23.8348134920	15.7995389941	10.7246695431	C	22.6732842415	15.8846737939	10.7165009224
C	22.8604724224	16.3758540253	11.5584405207	C	21.6802805076	16.4479631319	11.5366487102
C	23.0074333610	16.3450432866	12.9439544476	C	21.8004331023	16.3991531984	12.9234134344
H	22.2677708570	16.8017597441	13.6029374351	H	21.0507654667	16.8494917784	13.5754076783
H	25.9641786479	14.6568401210	13.1482169816	H	24.7550666901	14.7020390507	13.1564371553
C	22.9269537985	18.7005160995	17.9469552739	C	21.7468336981	18.7705648521	17.9402118204
C	22.1881351418	19.9789231416	17.6532066070	C	20.9951871689	20.0361199816	17.6372895506
C	20.9157268033	20.0834204660	17.0227261963	C	19.7174959110	20.1254050638	17.0121980308
C	20.3661090361	21.3621407845	16.8506813903	C	19.1662765399	21.4018132079	16.8232498899
C	21.0214547095	22.5280004200	17.2742990910	C	19.8236019672	22.5700082679	17.2337670130
C	22.2631740032	22.4152949001	17.9153726410	C	21.0668796719	22.4713256192	17.8706060623
C	22.8264641949	21.1578016324	18.0890645567	C	21.6360954431	21.2207512803	18.0552695425
S	19.8949735196	18.7304300116	16.3132014054	S	18.6967978583	18.7630928509	16.3021891290
C	27.2850597909	17.7323989400	17.4445399506	C	26.1029571214	17.8231468835	17.4317861750
C	28.2235299242	18.7656456759	16.9228368137	C	27.0475051731	18.8569485312	16.9105073124
C	28.4805813062	19.9225228575	17.6748390610	C	27.3079969286	20.0203607007	17.6539870766
C	29.3475362659	20.8872205256	17.1776029432	C	28.1784717851	20.9855662712	17.1554466445
C	29.9659189043	20.7061964241	15.9299029806	C	28.8105212018	20.8018259066	15.9131123511
C	29.7034369181	19.5452780928	15.1820121849	C	28.5415096764	19.6373005578	15.1720680657
C	28.8329987800	18.5773107567	15.6739575866	C	27.6672088874	18.6700272838	15.6653993248
H	28.6054684790	17.6755854677	15.1104891240	H	27.4473994396	17.7679468978	15.0990940742
H	27.9893512355	20.0428948925	18.6379033090	H	26.8169786054	20.1500846187	18.6162013479
O	21.1029299963	15.4736608428	17.1238695134	O	19.9153164051	15.5553735918	17.1982077044
O	27.5476007018	14.0622300616	16.4111160953	O	26.3558120734	14.1500825935	16.4030773164
O	25.4564992051	18.6508903076	20.6915176848	O	24.3234675241	18.7317396743	20.6773619879
H	24.6980530140	18.7475151646	21.2959784259	H	23.5788270917	18.8335636347	21.2988927786
H	28.2952344966	14.0005022854	17.0276145153	H	27.1024119456	14.0979904634	17.0201061352
H	20.5686046779	16.3182388714	17.2236952270	H	19.3707423850	16.4071380815	17.2561309059
H	27.9145670903	13.9577824297	24.5518459979	H	26.6924524160	14.0453733544	24.5410429316
H	29.4947597580	11.4914945718	21.3910382641	H	28.2640609843	11.5604716842	21.3897190446
O	28.9601693445	11.7320397560	25.2830672379	O	29.3244787408	11.1973668838	23.7997675752
O	30.5549962773	11.1186760477	23.8165914901	H	29.6035663879	11.4579373436	22.9027220802
H	30.8301811363	11.3738240863	22.9169068875	H	28.3870080591	21.8974575182	17.7109827307
H	29.5632052094	21.7967346919	17.7319465191	H	28.9805503598	19.4865842940	14.1855287136
H	30.1405934659	19.3993238288	14.1945816013	C	29.7303531997	21.8846003319	15.4385526933
C	30.8549678947	21.8021184270	15.4440263740	O	29.7096279660	23.0226432076	15.8661040288
O	30.8223174161	22.9416348005	15.8668739269	O	30.6431897624	21.5446095259	14.4654699325
O	31.7588875185	21.4702529343	14.4636393416	H	30.6026468151	20.5848233247	14.3003280986
H	31.7490967552	20.5070913005	14.3223195953	C	22.4798067961	15.9317507562	9.2388508115
C	23.6124084950	15.8424972660	9.2487020688	H	20.8238358162	16.9226656936	11.0631337675
H	21.9932545997	16.8388168748	11.0914931531	H	24.5463478709	14.7829894437	10.6770165314
H	25.7167225357	14.7027796051	10.6726415687	O	21.3868967353	15.9488364356	8.7039741319
O	22.5153394368	15.8637286009	8.7181716270	O	23.6248176290	15.9448427411	8.4724328549
O	24.7476574046	15.8607558349	8.4709472223	H	24.4000843805	16.0382111327	9.0561925098
H	25.5308234006	15.9400686964	9.0455054925	H	19.7416449247	9.5694905245	17.9775432997
H	20.9437034213	9.4841671154	17.9806334526	H	23.9208501194	8.6162813154	18.4292734536
H	25.1203328101	8.5302992792	18.4540957975	C	21.3305219419	7.5263195619	18.4068557092
C	22.5249398290	7.4420576218	18.4159799024	O	20.2008832039	7.2297437210	18.7462535707
O	21.3922249865	7.1466618870	18.7505869605	O	22.2528842718	6.5310010385	18.1976100753

O	23.4445364106	6.4427400528	18.2022380135	H	23.0753007659	6.9153299823	17.8419574915
H	24.2708889489	6.8294920791	17.8572467893	H	20.7529888540	16.4019270979	25.0709500235
H	21.9168506690	16.3132319693	25.0709540373	H	18.2650536116	13.6690681518	22.8523913301
H	19.4276032860	13.5736527822	22.8602575873	O	19.2959009381	14.7022870916	26.5275878364
O	20.4688209580	14.6119879343	26.5291049360	H	20.2217209062	14.9767193311	26.3939773787
H	21.3984549728	14.8662909226	26.3829491256	O	17.5576487666	14.0733978432	25.2730963575
O	18.7029135273	14.0011899680	25.2820464317	C	19.2639478225	23.9428616235	17.0427111820
C	20.4446314109	23.8970959671	17.0621886746	H	18.1814080887	21.4317914680	16.3578353888
H	19.3795796008	21.3941585090	16.3908041267	H	21.5655087511	23.3785329807	18.2040725440
H	22.7751167301	23.3117100485	18.2568472694	O	18.3528361677	24.1104905637	16.0245125481
O	19.5449040852	24.0297678981	16.0263132858	H	18.2590116518	23.2706764756	15.5363039019
H	19.4860995850	23.1828927463	15.5465387519	O	19.5922047793	24.8934729251	17.7272379532
O	20.7285404677	24.8711657925	17.7343492445	O	18.3611547754	17.8110439120	17.4014776371
O	19.5423222079	17.7980384485	17.4202112685	O	19.5271697740	18.1898058489	15.2324745292
O	20.7108374301	18.1194049597	15.2494190949	O	17.4810864857	19.4460983123	15.7893959044
O	18.6875285987	19.4336400985	15.7908943631	H	22.6056329185	21.1236954626	18.5368201483
H	23.7921835814	21.0469894074	18.5767111789	Ru	8.5357477772	23.4849204244	14.4920743920
Ru	9.6463188641	23.2916307770	14.3809285770	Cl	7.9316504813	22.8257960914	16.6024350462
Cl	9.4814305915	22.7652466509	16.6902734235	C	12.1982438925	23.8771878778	16.9440108528
C	13.2739390484	23.9334207205	16.9626584182	C	8.4269407397	19.5638642292	16.3485624184
C	9.8242242114	19.4479916530	16.3853605231	H	14.5085970123	16.7457164248	16.2410382163
H	15.9833959174	16.8200200914	16.2911483188	H	13.8558504879	14.6379051738	16.0730347310
H	15.3784301716	14.6998902791	16.1316389867	H	15.4669388227	14.0577042609	15.5731563393
H	17.0157514817	14.1864572855	15.6488100108	C	14.4452335616	14.2574516255	15.2302870191
C	15.9887665807	14.3366409257	15.2964835322	H	12.6259430066	18.3350968790	15.9124623489
H	14.0846414651	18.3847034819	15.9446859993	C	14.4094332904	17.3495478790	15.3323496317
C	15.8878171763	17.4226451457	15.3810961328	H	16.6768099700	15.9173676606	15.3860448253
H	18.1826230716	16.0609196271	15.4582934349	H	15.0442088214	18.2402344528	15.4451720373
H	16.5178109431	18.3168001137	15.5023656228	H	13.3358024882	26.2552017939	16.3853449627
H	14.2866348874	26.3663059024	16.4180022037	H	14.0038323579	13.2920585393	14.9392070728
H	15.5928373463	13.3504927954	15.0116367598	C	12.9568138661	17.7250560125	15.0594405525
C	14.4334585463	17.7814356646	15.0941165646	H	11.1066596667	19.8730170235	15.5324509016
H	12.4910896837	19.8317617214	15.5547001465	H	6.3682451072	18.2139127504	15.3555074249
H	7.9210737895	17.8794945813	15.4003340248	C	12.4455982141	24.4719403437	15.5797243775
C	13.4760321759	24.5507932376	15.6012060977	C	16.5067792108	16.4198730061	14.4289030757
C	17.9993979251	16.5146835258	14.4794470058	C	8.0142627809	19.5137408761	14.8978430842
C	9.4472310082	19.3141598073	14.9315348839	H	12.3065070638	16.8275655418	15.0468853384
H	13.7935547847	16.8760659769	15.0720199305	C	13.0499023848	25.7337115348	15.4728114778
C	14.0395310377	25.8321700019	15.5016389681	H	12.9665689723	21.3160115673	15.1497706709
H	14.2342857346	21.4301988178	15.2547243721	H	16.9530180075	17.4220720833	14.4790629787
H	18.4338208638	17.5209700815	14.4818088006	C	6.8997268213	18.7316893943	14.5580879475
C	8.4162511329	18.4241875261	14.5973935671	N	15.0209570099	16.5525703595	14.1875227282
N	16.5129608567	16.6297710296	14.2409059826	C	14.3902784872	15.1701867304	14.0135188626
C	15.9057409408	15.2382607317	14.0727280319	C	11.1734444828	20.2151248879	14.4864818412
C	12.5624940475	20.1904327755	14.5154726799	C	12.2071045843	21.3368215920	14.3588673682
C	13.5188219683	21.3863457896	14.4251169274	N	11.3853552820	22.5527025344	14.4673781814
N	12.6024938433	22.5452434878	14.4708558736	C	10.0442186196	22.2992789280	14.3122548989
C	11.3049775158	22.1788788772	14.2820927759	N	9.9134827575	20.9248700772	14.1489140018
N	11.2603256763	20.8177909609	14.1587679404	N	12.8417648725	18.5105834909	13.8276938802
N	14.3171507791	18.5669235548	13.8591340755	C	12.0475438267	23.8240992771	14.3939245327

C	13.1505613437	23.8723965743	14.4073408143	H	16.9412738898	15.8371014383	13.6096819286
H	18.4350851474	15.9029242334	13.6826222635	C	8.7029745483	20.1918236388	13.8665173620
C	10.0896579129	20.0186509644	13.8881347381	H	13.3521441257	15.3322073040	13.7072448343
H	14.8635393350	15.3757078374	13.7682090397	C	11.4804474532	19.0187557211	13.5785091964
C	12.9448674377	19.0290271064	13.5940828999	C	13.2681168882	26.3499351965	14.2346721403
C	14.3024741265	26.4344956239	14.2660517195	H	14.9199637865	14.7243316191	13.1621999608
H	16.4443392263	14.7991709905	13.2235351807	H	10.7076953644	18.2368801194	13.6901528809
H	12.1990961357	18.2164573472	13.6768893804	C	6.4555484031	18.5964643473	13.2395518221
C	8.0206788767	18.2013808446	13.2753082112	C	14.8111429740	17.3606570263	12.9135769895
C	16.3045953788	17.4368937730	12.9683651688	C	13.8527518330	27.7389991825	14.1528941831
C	14.8882879564	27.8236896461	14.1882379766	H	15.4269068121	18.2609238105	13.0287399683
H	16.9015695663	18.3480182015	13.0979841247	C	13.3522437440	17.7470095592	12.6905332637
C	14.8446891088	17.8021947037	12.7293878674	H	12.7263800604	21.2971264134	13.3881178038
H	14.0880042655	21.3786069389	13.4831614076	C	5.2630574996	17.7319698968	12.9067910824
C	6.9645879567	17.1698217702	12.9565796819	C	12.3116014382	24.3852463251	13.1262663836
C	13.4590343853	24.4250765415	13.1426222143	C	8.2904743870	20.0567560853	12.5166815573
C	9.6885537370	19.8439619078	12.5394340710	H	12.7326903262	16.8599523377	12.4530845485
H	14.2366064843	16.9058376465	12.4960439047	C	12.9136671955	25.6481920833	13.0748667698
C	14.0194743353	25.7066907402	13.1025118287	Cl	7.7160355229	23.6874031668	12.3586250040
Cl	9.6120534794	23.9217966897	12.0793032542	C	7.1634996157	19.2716825355	12.2387838459
C	8.6521662379	18.9394188110	12.2677015130	H	11.4438220317	19.3608470178	12.5356598620
H	12.9130964147	19.3888701470	12.5566092291	H	15.2014457662	16.7614405824	12.0811828779
H	16.7173547433	16.8501859422	12.1382291527	H	13.3281856262	18.3861896458	11.7947237139
H	14.8168805477	18.4358857371	11.8299007856	C	11.9470637491	23.6706531184	11.8486200053
C	13.2224174908	23.6686931256	11.8609658121	C	9.0263736446	20.7021380227	11.3701209558
C	10.3459123265	20.5711443796	11.3957997401	H	13.0987426322	26.1005555910	12.1019211625
H	14.2468100480	26.1462304349	12.1327876166	H	6.8406925761	19.1743503360	11.2035963162
H	8.3530416249	18.7923286566	11.2308171043	C	9.2796511923	25.1092025959	14.7852341476
H	5.5809408937	19.0269599392	11.6892984086	H	8.5396406583	25.8981545332	15.0113139857
H	4.8082123315	21.9692715400	17.7935132821	H	10.3270718565	25.4152557851	14.7679970565
C	5.0048005632	21.9034841424	16.7267166245	H	11.6754897137	22.9169568560	16.8853167471
C	6.0623504700	22.6067312288	16.1634857451	H	11.5769002865	24.5484667288	17.5540782226
H	3.9384829668	19.4100655982	12.2502579646	H	13.1460308285	23.7317565667	17.4820596859
C	4.1737655317	21.1402810245	15.8975366925	O	27.7641229523	11.8223309120	25.2838733390
H	6.7043432493	23.2165836142	16.7938535579	H	9.2263174360	20.2847554710	16.5399889914
C	4.7105400090	19.6701687015	11.5174217505	H	8.7423373512	18.5694978954	16.6966302664
H	3.3021010735	20.6350919703	16.3094166112	H	7.5758798681	19.8758041165	16.9701005051
C	6.3339704984	22.5537963108	14.7803911452	H	5.0582947168	17.7255263759	11.8289226327
C	4.4623551762	21.0003365786	14.5394670517	H	4.3568594645	18.0857221372	13.4196300325
C	5.5713414538	21.6532182241	13.9730038385	H	5.4258472418	16.6916790559	13.2246088123
H	4.3047674409	19.4406077964	10.5210901471	H	8.5618460669	20.4221414731	10.4165893619
H	3.8257437320	20.3787363254	13.9210079633	H	10.0820790965	20.4021493097	11.3319865676
O	6.0061456861	21.4728196439	12.6873431437	H	8.9968447998	21.7975593956	11.4474996487
C	5.1247163197	21.1438775519	11.5613542065	H	12.2009236349	24.2864621690	10.9770824712
C	3.9647706548	22.1244902662	11.4333105525	H	10.8733158934	23.4394754476	11.8031791922
H	3.2411028064	22.0247371465	12.2505373498	H	12.4943923752	22.7215581428	11.7469119130
H	3.4335431762	21.9356430508	10.4904685499	H	13.9810636736	28.0597205805	13.1116479828
H	4.3327038851	23.1585509433	11.4153082165	H	14.8313295184	27.7947781673	14.6504930739
C	7.1965180914	23.5354390013	14.1139837922	H	13.1959676911	28.4689579254	14.6488086487
H	7.2464086965	23.4446108630	13.0291490374				

H	5.8163392642	21.3110137486	10.7251516966	
C	10.3461910353	24.9209438901	14.8178226216	
C	7.6700716800	24.7143773873	14.6617352799	
H	10.5233864621	25.6951350186	14.0608644568	
H	10.5386549403	25.1828253409	15.8662651144	
H	7.9415828083	25.5287963179	13.9945730830	
H	7.5376815608	24.9530801249	15.7153504958	
H	12.7547756020	22.9710091710	16.9105412893	
H	12.6765944672	24.5896322897	17.6111353647	
H	14.2451080136	23.7873105564	17.4592585623	
H	10.5724548830	20.2247564135	16.5633021101	
H	10.1838219676	18.4882803157	16.7829661632	
H	8.9413337299	19.7394265137	16.9725667911	
H	13.4937852181	24.2871694809	10.9963956067	
H	12.1675678436	23.3779929798	11.7527350564	
H	13.8368100830	22.7572135228	11.8137806203	
H	15.0305410679	28.1408562892	13.1479677680	
H	15.8626539482	27.8750118698	14.6946363465	
H	14.2314543734	28.5572763447	14.6770292574	
H	9.9181555472	20.2440546740	10.4402254505	
H	11.4291601881	20.3933185998	11.3586477603	
H	10.2023167559	21.6609227292	11.4751281867	
H	6.7988157419	17.0796980924	11.8759426962	
H	6.0036882185	17.4206218585	13.4281074781	
H	7.2572449701	16.1795361737	13.3327167980	

Table S6 Coordinates data set, absolute energies (a.u.) for DFT optimized cluster (Cr)Mil-101 and (Cr)Mil-101-$SO3^{-}$.

Cluster Mil-101				Cluster Mil-101-SO_3^-			
112				115			
E = -1002.2448612961				E = -1060.0288698801			
Cr	13.294580566200	11.840878504300	12.233590096600	Cr	18.323338812000	16.878326438700	17.232930761300
Cr	10.018140883000	12.602137834100	12.579580672900	Cr	15.033753755100	17.563226109100	17.544046393200
Cr	12.331837884600	14.189934393000	14.465127952200	Cr	17.299960111900	19.223559243500	19.416295780200
O	12.033161594100	12.893742129000	13.129382907100	O	17.031112951400	17.895332026600	18.117330255000
O	12.488413965800	10.160136294600	12.735243530400	O	17.503629616700	15.161741738000	17.738326436300
O	12.440680202600	11.861618107800	10.480679812200	O	17.491823235600	16.880877935300	15.469873687400
O	14.218974514500	13.526216258600	11.714521599300	O	19.287301555600	18.574152354500	16.715138989400
O	14.376895703300	11.645410791700	13.903110477700	O	19.441678119000	16.723201197000	18.900333163100
O	10.470314069100	12.975804003200	10.696490252700	O	15.487192095200	17.959231301700	15.654494534600
O	9.539372644600	12.189033692500	14.453155090300	O	14.623862957500	17.124319567300	19.457085115600
O	10.302292864300	10.641838535300	12.337812407800	O	15.317309269000	15.616229137400	17.333579549200
O	13.284170149300	12.803777738600	15.539938106200	O	18.276731782500	17.819254944600	20.530059262800
O	13.989220349000	14.772130832100	13.605514738200	O	18.982947260800	19.836876851000	18.586769953000
O	10.762543769600	13.756333677200	15.556872567400	O	15.709553245900	18.815545626100	20.534191029300
C	11.244170836500	9.839014716800	12.594948987500	C	16.267721739800	14.831974426200	17.612293057800
C	10.903150188600	8.407509552800	12.766016802600	C	15.920265422500	13.390809370100	17.812803599800
C	9.560414117800	8.009354585600	12.653848148200	C	14.571431186000	12.995449806900	17.771762741800

C	11.903550800600	7.472144705400	13.066253916600	C	16.920615240900	12.438487164300	18.055462851400
C	11.559903006600	6.136802347200	13.256903130800	C	16.575244087500	11.101731222400	18.246298498800
C	10.218617544400	5.735532030100	13.153136379200	C	15.228770007900	10.698890388500	18.203207178800
C	9.221082367700	6.678320924200	12.854967004300	C	14.229449168500	11.661274723500	17.974195416200
H	12.933299564000	7.807189847000	13.158118227400	H	17.957786796000	12.761876124400	18.094575251300
H	8.807462297800	8.759057103100	12.419256666400	H	13.812649840800	13.753182282200	17.582063267800
C	14.755488987400	11.071894619600	16.162650268600	C	19.797606221100	16.125909336200	21.158373034300
C	15.508859196100	9.954072048400	15.775655491900	C	20.554063365800	15.012670128400	20.765043282700
C	14.604370713700	11.383282474600	17.524231311500	C	19.648804583200	16.421976955300	22.523468988900
C	16.122423788500	9.163008525300	16.742777113400	C	21.158821618800	14.205151179000	21.725087495800
C	15.980951198600	9.477079280900	18.104251030000	C	21.007481019500	14.494261999000	23.092004198100
C	15.206083445100	10.583133877000	18.489227963700	C	20.242301256800	15.606535629000	23.483384948000
C	16.609907957300	8.658917208300	19.184376370900	C	21.600074121300	13.632096573800	24.156382362000
H	14.012738100500	12.251846568500	17.803444792200	H	19.058553474800	17.289986094400	22.808464414400
C	14.088065648000	11.904461678300	15.124549293800	C	19.116906947400	16.959883099900	20.116809098700
C	9.878202505900	12.821163605200	15.498959862900	C	14.892695760100	17.818111399200	20.481753498100
C	9.174086494300	12.459087955800	16.754670977000	C	14.183360880500	17.450454651600	21.746784409600
C	9.498019447600	13.081802516000	17.968019395300	C	14.535751557700	18.037459661000	22.970913135600
C	8.828594200400	12.714069165100	19.132796953500	C	13.867607425200	17.670818345500	24.138884470300
C	7.828755672100	11.729077086100	19.087023059200	C	12.831858538900	16.720493379300	24.098185770800
C	7.490641226100	11.125455137400	17.865742710700	C	12.468498162100	16.151737301400	22.865349077600
C	8.165435522100	11.481059332100	16.706209689200	C	13.142432057100	16.506412946600	21.701190523600
H	10.267728530100	13.848559383200	17.985529850000	H	15.330458178200	18.778654247800	22.992381264600
H	7.928309676800	11.018075577500	15.751366297800	H	12.874963109400	16.073086804800	20.739631535900
C	7.068207971300	11.294274684100	20.293972930900	C	12.069553935300	16.291758065400	25.310038483100
O	9.531506700400	14.524891750600	12.810473115600	O	14.531855324200	19.453521911400	17.731965176900
O	11.401278308400	15.615471266700	13.506095284600	O	16.333964512100	20.615491070900	18.430538137900
H	15.592825733400	9.712159771900	14.719599829300	H	20.638605087500	14.784460609800	19.705815948900
C	11.407125618800	12.463927134200	10.009822429700	C	16.452485701300	17.476853782500	14.991906415400
C	11.301283085300	12.529949802300	8.529215664500	C	16.354896248300	17.574917670900	13.506784764400
C	12.317860155000	11.984982777800	7.730623479400	C	17.348997243400	17.011527481000	12.693649247100
C	12.198801959800	12.022990009800	6.343789175900	C	17.215062323700	17.057879950700	11.307674525900
C	11.063716043700	12.597466934500	5.748429821400	C	16.085564710000	17.659611318500	10.723756310700
C	10.041482529200	13.126072343000	6.553730720000	C	15.094365967000	18.222480528800	11.546333552600
C	10.161419840500	13.100109669500	7.938096322800	C	15.228483606500	18.190279553300	12.931358013200
H	9.380566950000	13.500709120900	8.580408426000	H	14.469963830100	18.623180657600	13.584852074100
H	13.179107220200	11.526591165400	8.210647550400	H	18.201721100800	16.528119329800	13.165476446100
C	10.204177829300	15.579529083100	13.036388222600	C	15.137095138000	20.538848619500	17.947313349900
C	9.558832752000	16.887853915100	12.755122738700	C	14.436876955700	21.838451745500	17.661968298900
C	8.279291548800	16.919483159600	12.179859773900	C	13.164735981300	21.958744881500	17.036904931600
C	7.663242042600	18.142738873500	11.929100515800	C	12.626724657800	23.240859995800	16.858260893900
C	8.316464337200	19.340986515500	12.260917359800	C	13.292359209000	24.402324009500	17.270783810700
C	9.589187596300	19.304458483700	12.853608220000	C	14.540509237700	24.278182172600	17.898779927800
C	10.214071450900	18.085348099800	13.089430652900	C	15.096113949000	23.015666304000	18.077601926800
H	11.203725282100	18.040387972800	13.537876226400	S	12.114657082700	20.618523051300	16.356833027200
H	7.782471627300	15.982409283300	11.941581359400	C	19.498587306500	19.595249026200	17.445520078400
C	14.471815519600	14.539977182700	12.445310609700	C	20.459752817200	20.615926691300	16.920294526800
C	15.433533514600	15.538465856100	11.908895709000	C	20.733005320800	21.770686777100	17.671182906900
C	15.774224645500	16.660776049700	12.681941521900	C	21.602667753500	22.735772954100	17.172473659700
C	16.664859930200	17.599743819900	12.177131454800	C	22.221118545800	22.560877113500	15.922375572200

C	17.230955619900	17.421958221500	10.904021644500
C	16.884073650200	16.300972066800	10.132874313200
C	15.987058750500	15.359922822800	10.632303492700
H	15.698579847800	14.490011778400	10.047211984300
H	15.330185908700	16.777496971200	13.668072405200
O	8.256169219600	12.324266715900	12.105088719700
O	14.687372597100	11.018015217800	11.406653555900
O	12.742727089400	15.383963534600	15.777615361900
H	12.015742991800	15.428890107500	16.427297033200
H	15.443778590000	10.915682019700	12.014881607000
H	7.691957325700	13.043409324000	12.434535652800
H	15.094737415800	10.794149035100	19.550759872600
H	16.675264663000	8.277943031900	16.428999419900
O	16.173241646300	8.592119474400	20.315869485600
O	17.740614940800	7.962919731900	18.835640180500
H	18.022415446700	8.220033508500	17.938825086700
H	16.938867363000	18.485633159700	12.746005636700
H	17.277062266300	16.172612330700	9.124470229200
C	18.159633465000	18.486606314000	10.422663809800
O	18.134982603200	19.621856988200	10.853944831400
O	19.064885956200	18.130808301400	9.452248521600
H	19.022774085400	17.168979772700	9.300738179700
C	10.868639948900	12.639260472600	4.269340980200
H	9.162713131100	13.545277328500	6.068425251800
H	12.973594368800	11.560289745400	5.732931569500
O	9.773344190800	12.658415878500	3.742672682200
O	12.014374246500	12.656169015200	3.506346760600
H	12.789925839500	12.749207803300	4.089251581500
H	8.188818446000	6.340168081700	12.795143921400
H	12.337121562000	5.423894361500	13.530740567700
C	9.774894213300	4.333460191800	13.396210999900
O	8.650021703400	4.050984233300	13.754559338400
O	10.707128946300	3.346520390600	13.202356367200
H	11.512493268900	3.727299957400	12.807035153200
H	9.063718983800	13.225601808700	20.065774629800
H	6.698522628600	10.379775754600	17.855632145400
O	7.723926308400	11.404080404100	21.495801928400
H	8.652801311100	11.654583094300	21.339546354800
O	5.935722302200	10.857785960400	20.242367287200
C	7.698295250500	20.683292479800	12.046311047700
H	6.655889887800	18.154377706700	11.513481480100
H	10.064554469600	20.245953760800	13.120571022900
O	6.794690685200	20.786908336000	11.016699145000
H	6.781432653200	19.956271083200	10.506601684200
O	7.964871925800	21.650195786000	12.731580874400

C	21.945458051600	21.399441326500	15.176257098100
C	21.069848226700	20.432633808400	15.670434900800
H	20.835194726900	19.536658504200	15.099470934500
H	20.246215083000	21.891974151200	18.636682410100
O	13.286082219200	17.188028291000	17.112440503400
O	19.686635878600	15.951513038000	16.411714510200
O	17.733437149200	20.452271301200	20.706307448900
H	16.985443174200	20.547673369600	21.323903816800
H	20.453247982900	15.895817055700	17.010502657900
H	12.735803126200	18.002001655800	17.128495348700
H	20.125986053300	15.809322730000	24.545939693100
H	21.705285909800	13.320005075800	21.400519187000
O	21.155405778200	13.535059245400	25.283317881000
O	22.716604564000	12.908174607100	23.801830084900
H	23.011130809500	13.186040939000	22.915267486500
H	21.818430628000	23.643144231800	17.731995144600
H	22.373008307100	21.252200657500	14.184011933300
C	23.125617068400	23.653623305800	15.443510567900
O	23.100609189400	24.795289557500	15.865609672500
O	24.035246690900	23.318016018100	14.464348098400
H	23.995416454600	22.355380574400	14.308945608300
C	15.877128596900	17.690289853800	9.246699011200
H	14.222371364100	18.676778571800	11.080640377800
H	17.970244955800	16.574165476900	10.688715877900
O	14.786607726700	17.735528099200	8.708991847700
O	17.024113470900	17.657002968900	8.474030890500
H	17.797239350800	17.747054424900	9.060644438200
H	13.190451622900	11.338454738000	17.956907060000
H	17.365059364900	10.384447122300	18.468986411100
C	14.805305097600	9.281086406300	18.409987240000
O	13.686059333200	8.943654898200	18.744641844000
O	15.769201453100	8.315864762600	18.200720128600
H	16.565772380800	8.733175122400	17.827207705800
H	14.137341668200	18.164413323300	25.072525024700
H	11.653048474200	15.432028073000	22.846798819000
O	12.682391794400	16.489279205400	26.527708936300
H	13.601005106300	16.781059300700	26.382182374900
O	10.963707145600	15.787307294400	25.277131831200
C	12.714075903800	25.769137854000	17.061727170400
H	11.639017239000	23.274199565000	16.398733530900
H	15.059412807600	25.175411309600	18.229765882300
O	11.819844031700	25.899621056100	16.023982772300
H	11.722712138200	25.040486890400	15.569673117200
O	12.995062547500	26.747260492400	17.731820202300
O	11.746352045900	19.753547048700	17.496013620400
O	12.935723353900	19.979303669100	15.315642213900
O	10.948609486300	21.324569909700	15.789096666400
H	16.067975208300	22.907669052000	18.551651778000

Annex 1: Computational chemistry

In general terms computational chemistry is based on electronic structure calculations generally aimed at calculating the physical and chemical properties while knowing only the atomic composition and positions of the atoms of the system under study. Basically, one can optimize a structure from a geometry with a particular connectivity. In other words, it is possible to compute its more stable geometry. Beyond simple geometry optimizations, computational chemistry allows us to explore the reaction pathways for a given chemical process by analysing potential energy surfaces (PESs). The PES is the hypersurface defined by the potential energy of a group of atoms over all the possible atomic arrangements. A PES is composed of local minima and saddle points, which in chemical terms are defined as intermediates and transition states (TSs), respectively. PES is an essential model to study chemical transformations. Moreover, chemical properties such as NMR, IR, UV-Vis and EPR spectra can also be computed as well as reactivity data for example, equilibrium constants, rate constants, heats of formation and pK_a values. Finally, different properties which are not measurable can be studied, among other the more relevant ones are atomic charges, and bond order.

All the computable properties mentioned before can be calculated with different computational numerical technics, techniques by which mathematical problems are formulated and solved with arithmetic operations. Those techniques are basically numerical methods, depending on the accuracy of the model implied one can define three main categories.

Molecular Mechanics (MM) uses classical mechanics methods to model chemical systems. They have been broadly used to study very large systems such as proteins. Basically, force fields are used in order to calculate the potential energy of a system. For example, it is well known that considering all the vibrational spectroscopy data one is able to reconstruct the vibrational energy levels with a high degree of accuracy. The spacing between the different vibrational energy levels depends on the potential energy associated with bond stretching. The function associated to its potential energy would be easily resolved using data from the spectroscopic experimentation permitting the derivation of the potential energy function. However, assuming that the dissociation energy for the bond is positive,

defining the minimum of the function to have a potential energy zero and calling the bond length at the minimum r_{eq}, one can determine the value of the potential energy at an arbitrary point by taking a Taylor expansion about r_{eq}

$$U(r) = U(r_{eq}) + \left.\frac{dU}{dr}\right|_{r=r_{eq}} (r - r_{eq}) + \left.\frac{1}{2!}\frac{d^2U}{dr^2}\right|_{r=r_{eq}} (r - r_{eq})^2 + \left.\frac{1}{3!}\frac{d^3U}{dr^3}\right|_{r=r_{eq}} (r - r_{eq})^3 + \cdots \quad (1.1)$$

the first two terms of the equation are zero, the first by arbitrary choice, the second because r_{eq} was considered being the minimum. By truncating after the first non-zero term, one obtains the simplest expression (harmonic approximation) for the vibrational potential energy

$$U(r_{AB}) = \frac{1}{2} k_{AB} (r_{AB} - r_{AB,eq})^2 \quad (1.2)$$

where the second derivative of *U* has been replaced by the symbol *k*. This simplified equation is the Hooke's equation for a spring, where *k* is the "force constant" for the spring; the same term is used both for spectroscopy and molecular mechanics. It has been added A and B subscripts to emphasize that force constant and bond lengths could vary from one pair of atoms to the other. Even though a new set of parameters is needed when using a different pair of atoms, such technique has the characteristic of transferability, one can use a set of parameters to calculate molecules containing similar bonds, including that the data obtained for small molecules can be used to large systems (for instance from C-C in ethene to C-C bonds in proteins). Summarizing, molecular mechanics expresses the total energy by applying force fields, that is written as a sum of Taylor series expansion for stretches for every pair of bonded atoms (as described above), adding additional potential energy terms coming from bending, torsion energy, van der Waals energy, electrostatics, and cross terms.

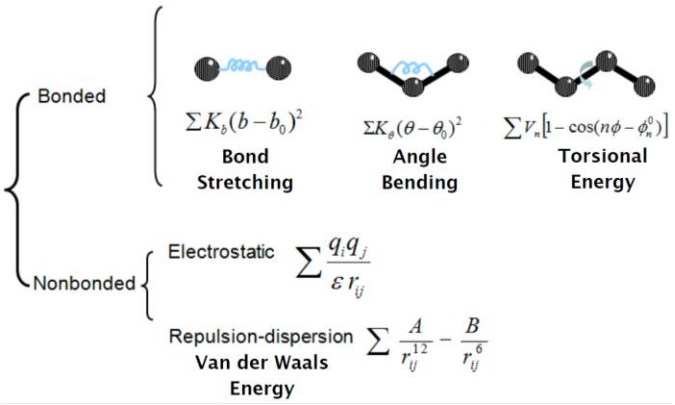


Figure 7.1 Representation of the different parameters set within a force field.

Semi-empirical quantum chemistry methods combine experimental data with quantum chemistry methods to reduce computational cost. Numerical approximations are used to calculate the Hartree-Fock (HF) energy for a system, as the simple resolution of the HF theory is very expensive in terms of computational costs (this aspect will be further discussed below). Here, in semi-empirical calculations these approximations involve the adoption of a parametric form for some aspect of the calculation where the parameters involved are chosen so as best to reproduce experimental data. The most computationally expensive is the calculation of the two electron integrals. For example, one of the most radical implementations is the *zero-differential overlapping* (ZDO) which considers the S matrix equal to the unit matrix. One of the first implementations in order to replace matrix elements in the secular equation to solve HF theory was the complete neglected of differential overlap (CNDO) described by Pople and co-workers in 1965.[1,2] The secular determinant overlap matrix elements are defined by

$$S_{\mu\nu} = \delta_{\mu\nu} \tag{1.3}$$

Considering only s and p orbitals the two-electron integrals are parameterized as

$$(\mu\nu|\lambda\sigma) = \delta_{\mu\nu}\delta_{\lambda\sigma}(\mu\mu|\lambda\lambda) \tag{1.4}$$

where δ is the Kronecker delta. Considering that the two integrals which are non-zero have μ and ν as identical orbitals on the same atom and λ and σ also as identical orbitals on the same atom, but the second atom being different than the first atom (all the integrals being zero are the ones involving overlap of the orbitals rising the name of the model). It is obtained the two-electron integrals

$$(\mu\mu|\lambda\lambda) = \gamma_{AB} \tag{1.5}$$

where A and B are the atoms on which the orbitals μ and λ reside, respectively. The term γ can be computed explicitly from s-type Slater Type Orbitals (STOs), or it can be treated as a parameter. One possible parametric form is the so called Pariser-Parr approximation for the one-centre term[3,4]

$$\gamma_{AA} = IP_A - EA_A \tag{1.6}$$

where IP and EA are the atomic ionization potential and electron affinity, respectively. Adopting the approximation for a two-centre term

$$\gamma_{AB} = \frac{\gamma_{AA} + \gamma_{BB}}{2 + r_{AB}(\gamma_{AA} + \gamma_{BB})} \tag{1.7}$$

where r_{AB} is the interatomic distance. The one-electron integral for diagonal matrix elements looks like:

$$\left\langle \mu \middle| -\frac{1}{2}\nabla^2 - \sum_k \frac{Z_k}{r_k} \middle| \mu \right\rangle = -IP_\mu - \sum_k (Z_k - \delta_k)\gamma_{Ak} \tag{1.8}$$

The full Fock matrix $F_{\mu\mu}$ is composed by the sum of the one-electron integral and a series of two-electron integrals. If the number of valence atoms is exactly the same of the valence nuclear charge, the repulsive two-electron terms will cancel the attractive nuclear terms appearing at the end of Eq. 1.8 obtaining that the energy associated with the diagonal matrix elements is the ionization potential of the orbital (IP_μ).

Finally, the one-electron terms for the off-diagonal matrix elements are the terms remaining to be defined:

$$\left\langle \mu \middle| -\frac{1}{2}\nabla^2 - \sum_k \frac{Z_k}{r_k} \middle| \nu \right\rangle = \frac{(\beta_A + \beta_B)S_{\mu\nu}}{2} \tag{1.9}$$

where μ and ν are centred on atoms A and B, respectively, the β values are the semiempirical parameters, and $S_{\mu\nu}$ is the overlap matrix elements computed by using STO, here the computation is carried out for every combination of orbitals. There are so two different S matrices, one for each purpose. β values provide a measure of the strength of through space interactions between atoms. They are intended for completely general use and originally adjusted to reproduce certain experimental quantities.

CNDO method represent a vast simplification of HF theory. For instance, the number of two-electron integrals having non-zero values are reduced from formally N^4 to simply N^2 Eq. (1.4). Moreover, those N^2 integrals are computed by trivial algebraic equations. However, such simplification come with a chemical cost as CNDO cannot predict molecular properties at a quantitative level of accuracy. Nevertheless, this is one of the first parametrizations performed, nowadays improved semi-empirical methods have been developed and they are very useful when studying larger systems in a cost-effective manner, always losing some accuracy. It is important to remark that the main difference between the different semi-empirical methods resides on the level of implementation of the number of integrals that have been considered zero and then not computed as well as, the surviving integrals which have been pre-set to some parameters and then they have not been computed either.

Ab initio quantum chemistry methods. HF theory assumes that each electron sees all the other electrons as an average field allow for a tremendous progress when performing molecular orbital calculations (MO). However, the electron correlation (described below) is being neglected having chemical consequences when it comes to determining accurate properties. The development of semi-empirical methods commented before were motivated, in part, to compensate these consequences by judicious parameterizations. *Ab initio* methods intends to reduce the correlation energy to the minimum as possible by developing mathematical and computational techniques to reach the HF limit, basically solving the HF equations with no additional approximations. Obviously solving the Schrödinger equation would be the most rigorous way to describe a chemical system however, that equation is insoluble in a practical sense for all but the simplest of systems. Since all the calculations in this thesis are based on this method, in the following sub-sections *ab initio* approaches will be accurately described and, being redundant, from the beginning.

The Schrödinger equation

If one recalls at the start of the section 4 it was mentioned that the principal aim of the computational chemistry is to study the physical and chemical properties while knowing only the atomic composition and positions of the atoms of the system. A system which only the atomic composition and positions are known is

described by the body time-independent (it is considered the absence of time dependent external fields) Schrödinger equation

$$\hat{H}\Psi = E\Psi \tag{1.10}$$

where E is the total energy for the system, a caret that indicates a differential operator and Ψ is the wave function, which contains all the information that can be extracted relative to the system within the limits set by Heisenberg uncertainty principle. The Hamiltonian, $\hat{H}$, includes the kinetic energies of the nuclei, $\hat{T}_n$, and electrons, $\hat{T}_e$, as well as the Coulomb interactions (potential energies) between the electrons and nuclei, V_{ne}, between electrons, V_{ee}, and between nuclei, V_{nn}

$$\hat{H} = \hat{T}_e + \hat{T}_n + V_{ne} + V_{ee} + V_{nn} \tag{1.11}$$

The mathematical notion for the Hamiltonian looks like

$$\hat{H} = -\sum_i \frac{\hbar^2}{2m_e}\nabla_i^2 - \sum_k \frac{\hbar^2}{2m_k}\nabla_k^2 - \sum_i \sum_k \frac{e^2 Z_k}{r_{ik}} + \sum_{i<j} \frac{e^2}{r_{ij}} + \sum_{k<l} \frac{e^2 Z_k Z_l}{r_{kl}} \tag{1.12}$$

where i and j represent the electrons, k and l the nuclei, ħ is the Planck's constant divided by 2π, m_e is the mass of the electron, m_k is the mass of the nucleus k, ∇^2 is the Laplacian operator, e is the charge on the electron, Z is an atomic number, and r_{ab} is the distance between particles a and b. As mentioned before the Hamiltonian operator is composed of kinetic energy and potential energy parts. The potential energy terms are calculated as they do in classical mechanics. However, the kinetic energy for a quantum mechanics (QM) particle is not expressed as $|P|^2/2m$ (where P is the momentum and m is the mass of the body), but rather as the eigenvalue of the kinetic energy operator

$$T = -\frac{\hbar^2}{2m}\nabla^2 \tag{1.13}$$

The Ψ is a function of 3_n coordinates where n is the total number of particles (nuclei and electrons, for instance, x, y and z Cartesian coordinates specific to each particle). If one is working in Cartesian coordinates, the Laplacian looks like

$$\nabla_i^2 = \frac{\partial^2}{\partial x_i^2} + \frac{\partial^2}{\partial y_i^2} + \frac{\partial^2}{\partial z_i^2} \tag{1.14}$$

In general, the term Ψ in Schrödinger equation has many acceptable eigenfunctions for a given molecule, each associated to a different eigenvalue E. One can say there is almost an infinity of Ψ_i with eigenvalues E_i. For this reason, it is assumed that these wave functions are orthonormal without losing generality, i.e., for a one particle system where the wave function depends on only three coordinates

$$\int\int\int \Psi_i \Psi_j dxdydz = \delta_{ij} \tag{1.15}$$

the Kronecker delta (δ_{ij}) is equal to one when $i = j$ and equal to 0 when $i \neq j$. Matter of fact, this characteristic of the Kronecker delta is directly related to the definition of orthonormal as this last implies two qualities at the same time: "orthogonal" meaning that the integral in Eq. (1.15) is equal to zero if $i \neq j$ and "normal" meaning that vale of the integral is equal to one when $i = j$.

Now, if we consider the Schrödinger equation for a specific wave function (Ψ_i), multiplying on left by Ψ_j and integrating one obtains

$$\int \Psi_j H \Psi_i dr = \int \Psi_j E_i \Psi_i dr \tag{1.16}$$

the dr is a simplification of all multiple integrals over Cartesian space, which is now considered a single integral over a generalized 3n-dimensional volume element. The energy E is a scalar value, it is removed out from the integral, and then considering that $\int \Psi_j \Psi_i dr = \delta_{ij}$ one can write

$$\int \Psi_j H \Psi_i dr = E_i \delta_{ij} \tag{1.17}$$

However, by considering the equation is Orthonormal seems it has been simplified, this equation can only be solved exactly for very small systems, when working with larger systems it becomes to complicate to be solved (including MOFs). For this particular reason, modern computational approaches intend to adopt a number of simplifying approximations in order to "solve" it.

The Born-Oppenheimer approximation

The Born-Oppenheimer approximation[5–7] is indeed the first step in most of the computational approaches. Schrödinger equation can be solved with the two following steps: first, the nuclei is treated as a stationary (under typical physical conditions the nuclei of molecular systems are moving much more slowly than

electrons). As such it is convenient to couple these two motions, can compute energies for "fixed" nuclear positions. The kinetic energy of the nuclei is taken to be independent of the electrons and then $\hat{T}_n$drops from Eq. (1.11) and it can be solved of a set of nuclei positions (R) as,

$$\hat{H}_{B-O}(R_1 R_2 \dots R_n) = \hat{T}_e + V_{ne} + V_{ee} + V_{nn} \tag{1.18}$$

Now Schrödinger equation eigenvalue corresponds only to the sum of electronic energies and the nuclear repulsion, this sum is denoted as H_{el} where are included only the first, third and four terms of the Hamiltonian ($\hat{T}_e$, V_{ne} and V_{ee}). Correlation in the attractive electron-nuclear potential energy term is eliminated, and the repulsive nuclear-nuclear potential energy becomes a simply evaluated constant for a given geometry. Finally obtaining the "electronic" Schrödinger equation

$$(H_{el} + V_N)\Psi_{el}(q_i; q_k) = E_{el}\Psi_{el}(q_i; q_k) \tag{1.19}$$

where the term "el" refers to the invocation of the Born-Oppenheimer approximation. The term H_{el} is the electronic energy mentioned before, V_N is the nuclear-nuclear repulsion energy and the electronic coordinates q_i are independent variables however, the nuclear coordinates q_k are parameters. Here the eigenvalue of the electronic Schrödinger equation is called "electronic energy".

The Born-Oppenheimer approximation is an extremely mild one, however it has profound consequences from a conceptual point of view, and it can be considered as a Dogma. From the Born-Oppenheimer approximation it is defined the concept of potential energy surface (PES) which indeed is the surface defined by E_{el} over all possible nuclear coordinates. The local minima of the PES are the equilibrium structures, and the saddle points are transition structures for chemical transformations (chemical reactions or conformational isomerizations) from one equilibrium structure to another.

Taking the advantages of the Born-Oppenheimer approximations there have been developed many approaches to solve the Schrödinger equation, which one can say, it is the key step in quantum-chemical characterization of properties and reactivities of MOFs as well as other molecular or solid-state systems. These methods can be divided into two general branches: wave functional theory (WFT) and density functional theory (DFT) approaches. In general terms, WFT uses

variational methods, perturbation theory or many-body theory to achieve an approximate solution, while DFT exploits one-to-one mapping between the electron density and the wave function. Only DFT will be further discussed as all the calculations in this manuscript are computed using DFT approaches.

Hartree-Fock theory

Hartree-Fock (HF) theory[5–7] was one of the earliest methods developed for solving the Schrödinger equation. Here, the wave function is taken as a Slater determinant of orthonormal single-particle wave functions, typically referred to as orbitals, they are indeed spin-orbitals. Each electron interacts only with the mean field of all of the other electrons, basically the electronic motion is treated by a mean-field approximation. The Slater determinant represents a convenient many-body wave function that satisfies the Pauli requirements (the wave function change sign with an exchange of particle indices called antisymmetry). In essence the calculation of an HF theory is a variational optimization of the before mentioned Slater determinant wave function by finding the spin orbitals that give the lowest energy.

The HF equations that determine the set of spin-orbitals that minimize the energy of the Slater operator look like a simple set of one-electron Schrödinger equation for the set of spin-orbitals

$$\hat{f}\chi_i = \varepsilon_i \chi_i \tag{1.20}$$

where $\hat{f}$ is the Fock operator, χ_i is the spin-orbital and ε_i the energy of the spin-orbitals. it is worth to mention that in this equation the spin-orbitals act as eigenfunctions and the energy of the spin-orbitals acts as eigenvalue.

The one-electron Fock operator is then defined for each electron i as

$$f_i = -\frac{1}{2}\nabla_i^2 - \sum_{k}^{nuclei} \frac{Z_k}{r_{ij}} + v_i^{HF}\{j\} \tag{1.21}$$

where the first two terms are associated to the kinetic energy of the electrons and the electrostatic interactions between the electrons and the nuclei ($\hat{h}$). The v_i^{HF} is a one-electron potential operator obtained by averaging the interaction of the other $n-1$ electrons with the electron i. Then, the instantaneous correlation between the electrons due to the two-electron operator is replaced by an averaging interaction.

The Hartree-Fock potential operator is divided in two terms, the coulomb potential operator and the exchange potential operator

$$v_i^{HF} = \sum_j^n (\hat{J}_j - \hat{k}_j) \tag{1.22}$$

the j term of coulomb potential operator gives the average electrostatic repulsion between the electron in the occupied spin-orbital χ_i and another electron in the spin-orbital χ_j.

$$\hat{J}_j\chi_i = \chi_j \frac{1}{r_{ij}} \chi_j\chi_i \tag{1.23}$$

the coulomb potential is called local averaged potential since it gives one value for each value of the coordinates of electron i and such value does not depend on the shape of χ_i.

The exchange potential operator has a similar form than the coulomb potential operator however now it is involved an exchange of electrons i and j

$$\hat{k}_j\chi_i = \chi_j \frac{1}{r_{ij}} \chi_i\chi_j \tag{1.24}$$

the exchange potential is called a nonlocal averaged potential since, although it gives one value for each value of coordinates of electron i, this value depends on the shape of χ_i.

Hartree-Fock equations have the form of an eigenvalue equation, however one could consider them pseudo-eigenvalue equations since the Fock operator depend on the wavefunction. As a result, this pseudo-eigenvalue equations must be solved by iterating until the orbitals are consistent with the operator and the operator is consistent with the orbitals. This is indeed called self-consistency, and the mean-field determined self-consistency is called self-consistent field (SCF).

In this subsection it has been mentioned for first time the term Slater determinant, which its mathematical notation looks like

$$\Psi_{SD} = \frac{1}{\sqrt{2}} \begin{vmatrix} \psi_a(1)\alpha(1) & \psi_b(1)\alpha(1) \\ \psi_a(2)\alpha(2) & \psi_b(2)\alpha(2) \end{vmatrix} \tag{1.25}$$

where molecular orbital (MO) products are expressed as a determinant. On a term-by-term basis, Slater determinantal wave functions are tedious to write down, but they can be expressed compactly

$$\Psi_{SD} = \frac{1}{\sqrt{N!}} \begin{vmatrix} \chi_1(1) & \chi_2(1) & \cdots & \chi_N(1) \\ \chi_1(2) & \chi_2(2) & \cdots & \chi_N(2) \\ \vdots & \vdots & \ddots & \vdots \\ \chi_1(N) & \chi_2(N) & \cdots & \chi_N(N) \end{vmatrix} \tag{1.26}$$

where N is the total number of electrons and χ is a spin-orbital, the product of the spatial orbital and an electron spin eigenfunction. Practically, the spatial parts of the spin-orbitals are expanded in a set of basis functions, they are referred as one-electron or single-particle basis functions.

The HF equations are very powerful but still chemical flawed. Thus, many approximations have been introduced to simplify their solution, and at the same time improve the accuracy. The most justified ones have been described above and they are based in adding some parameterization to reproduce key experimental quantities. In fact those approximations refer to the semiempirical methodologies described at the beginning of the section 4.

However, HF provides a very well-defined energy, which can be converged in the limit of an infinite basis set. The difference between the HF energy and the so-called accurate solution to the electronic Schrödinger equation is usually called the correlation energy

$$E_{corr} = E_0 - E_{HF} \tag{1.27}$$

Developing a methodology to achieve the limit would not only permit the evaluation of the chemical utility of the HF limit itself, but also probably facilitate to approximate to a possible solution of the Schrödinger equation. By the motivation of finding a technology to achieve the HF limit with no further approximations was the foundation for further research on *ab initio* HF theory.

Post-Hartree-Fock methods

Hartree-Fock theory, even though its fundamental assumption that each electron sees all of the others as an average field, was adopted as useful in the *ab initio* philosophy because it provides a very well-defined steppingstone on the way

to more sophisticated theories, theories which come closer to an accurate solution of the Schrödinger equation. The methods born from the Hartree-Fock theory are called Post-Hartree-Fock methodologies. As mentioned before, HF theory assumes that each electron sees all the others as an average field, however neglecting the electron correlation (physically it corresponds to correlate the motion of the electrons) can have profound chemical consequences when it comes to determining accurate wave functions and properties derived from them. All the efforts have been expended on developing mathematical and computational technics to solve the HF equations with the equivalent of an infinite basis set, in other words with no additional approximations. Basis sets are the mathematical functions used to construct the HF wave functions, which availability made possible the testing of how useful such wave functions might be for the prediction of properties beyond the energy. As described in the previous subsection, each MO is expressed as a linear combination of basis functions, the coefficient for which are determined from the iterative solution of the HF SCF equations. All the basis functions are represented as a Slater determinant formed for the individual occupied MOs. Generally, HF orbitals are used to make many-electron basis functions termed configuration state functions (CSFs), with each HF orbital having a definite integer occupancy. Basically, post-HF methods modify the HF wave functions to obtain a lower electronic energy considering the electron correlation.

Møller-Plesset Second-Order Perturbation theory attempts to recover dynamical correlation by adding a perturbation $\lambda\widehat{H}'$, that is equal to the difference between the full Hamiltonian and the Hamiltonian of which the HF wave function is an eigenfunction. The perturbation method expresses the Hamiltonian of the exact (or perturbed) system $\widehat{H}$ as the sum of a zero-order unperturbed Hamiltonian $\widehat{H}^0$ and a perturbation operator $\widehat{H}'$

$$\widehat{H} = \lambda\widehat{H}' + \widehat{H}^0 \tag{1.28}$$

the last term in the previous equation is the zeroth-order Hamiltonian, which is the sum of the one-electron Fock operators. The main purpose of the perturbation method is to express the approximate perturbed wavefunction of the system as a linear combination of the complete basis set formed by the zero-order wavefunctions. Both the wave function and $\widehat{H}$ can then be expanded as a power series in λ

$$\Psi_i = \Psi_i^{(0)} + \lambda\Psi_i^{(1)} + \lambda\Psi_i^{(2)} + \cdots \quad (1.29)$$

these equations are then inserted into the electronic Schrödinger equation which is then solved order by order. The first order is the HF energy, and the following orders are called MP2, MP3, etc. in recognition of the original derivation by Møller and Plesset.[8,9] Although it exists *MPn* methods, MP2 is the most used post-Hartree-Fock method to introduce dynamic correlation. However, it is only efficient when the HF wavefunctions properly describes the studied chemical system, otherwise energies converge very slowly, or they even diverge.

Coupled-Cluster theory (cc) expresses the energy as a many-body theory exponential functions of cluster operators which is defined as the sum of the excitation operators

$$\hat{T} = \hat{T}_1 + \hat{T}_2 + \hat{T}_3 + \cdots + \hat{T}_n \quad (1.30)$$

that generate excited-state determinants excited by one, two, three, …, n electrons from the reference ground-state HF wave function. The application of the $\hat{T}_i$operators on the ground state Slater determinant generates a linear combination of all the excitations of i order

$$\hat{T}_1\Psi_0 = \sum_i^{occ}\sum_a^{virt} t_i^a\Psi_i^a \quad (1.31)$$

$$\hat{T}_2\Psi_0 = \sum_{j>i}^{occ}\sum_{b>a}^{virt} t_{ij}^{ab}\Psi_{ij}^{ab} \quad (1.32)$$

where $t_{ij\ldots}^{ab\cdots}$ are the CC coefficients also called CC amplitudes. If the number of electrons n would be the total number of electrons in the system (also called full configuration interaction (CI)) the results would be exact, but, in practice even a of $n = 3$ is usually too computational expensive. However, the main advantage of CC methods is that the truncated CC wavefunctions are size consistent. Truncation of the included cluster operators at double and triple excitations leads to the coupled single and doubles (CCSD) theory and the coupled cluster singles, doubles, and triples (CCSDT) method. At a CCSD level, some triple, quadruple, and higher excitations are already included due to those some higher order excitations can be expresses as products of linked double excitations

$$e^{\hat{T}_1+\hat{T}_2} = 1 + \hat{T}_1 + \hat{T}_2 + \frac{\hat{T}_1^2}{2} + \frac{\hat{T}_2^2}{2} + \hat{T}_1\hat{T}_2 + \cdots \quad (1.33)$$

CCSD(T) method is regarded as the best compromise between speed and accuracy. In this method, triple excitations are incorporated into the CCSD wave function in a perturbative manner rather than evaluated explicitly by full cc theory. CCSD(T) is not only more accurate than CCSD but also is very accurate for closed-shell systems and is often referred as the gold standard of computational chemistry. However, the errors can be larger than expected when the system cannot be reasonably described by a single Slater determinant which is the reference wave function.[10,11]

Density Functional Theory (DFT)

The post-HF methods presented in posterior subsection introduce the electron correlation expanding the wavefunction as a linear combination of the ground state and excited Slater determinants. Density Functional Theory (DFT) is a completely different approach for introducing the electron correlation. Until now all the approaches are based on working with wave functions which are essentially uninterpretable, (in the book *Essentials of Computational Chemistry Theories and Models* written by Christopher J. Cramer the wave function is defined as "an inscrutable oracle that returns valuably accurate answers when questioned by quantum mechanical operators, but it offers little by way of sparking intuition").[6] DFT proposes a simpler method, rather than having to work with a wave function, working with a physical observable to determine the energy and other properties of a molecule. The Hamiltonian depends only on the positions and atomic numbers of the nuclei and the total number of electrons, such dependence on the total number of electrons makes obvious that the perfect candidate is the electron density ρ, since when it is integrated over all space one obtains the total number of electrons N

$$N = \int \rho(r) dr \quad (1.34)$$

The main difference with the wavefunction is that this one depends on $3n$ spatial variables and n spin variables, while the one-electron density function only depends on three spatial variables. Moreover, the complexity of the wavefunction increases exponentially with the number of electrons, the electron density however has the same number of variables independent of the system size.

Early DFT models found widespread use in the solid-state physics community since the enormous system size required to mimic the properties of solids put a premium on simplicity. However, large errors in molecular calculations and the failure of the theories to be rigorously founded lead DFT to have a little impact on chemistry, basically that errors were related to normal functions that did not deal with the electron correlation. Is not until 1964 that Hohenberg and Kohn proved two theorems that revolution the used of DFT methods.

The first Hohenberg-Kohn theorem (Existence Theorem)

The first theorem is based in that the energy and any observable of a non-degenerate ground state of a chemical system is uniquely determined by the electron density, reducing the number of variables, while the wavefunction depends on 4n variables, the electron density only depends on three spatial variables.

The Hamiltonian of a system with n electrons and M nuclei in atomic units can be expressed as

$$\begin{aligned}\widehat{H} &= -\frac{1}{2}\sum_{i=1}^{n}\widehat{\nabla}_i^2 - \sum_{J=1}^{m}\sum_{i=1}^{n}\frac{Z_j}{r_{ij}} + \sum_{i<j}^{n-1}\frac{1}{r_{ij}} \\ &= -\frac{1}{2}\sum_{i=1}^{n}\widehat{\nabla}_i^2 - \sum_{i=1}^{n}v(r_i) + \sum_{i<j}^{n-1}\frac{1}{r_{ij}}\end{aligned} \tag{1.35}$$

where $v(r_i)$ only depends on the coordinates of one electron as it contains the electron-nuclei attraction potential, and it is called external potential. Moreover, if the molecule also interacts with an external electrical or magnetic field, the external electric or magnetic potential must be added to the external potential. Thus, the external potential includes all the potentials that interact with the n-electron system but the electron-electron potential.

If one assumes that two different (v_a and v_b) external potential can each be consistent with the same nondegenerate ground-state density ρ_0, thus, these two external potentials appear in their corresponding Hamiltonian operators H_a and H_b, with the corresponding associated ground-state wave function Ψ_0 and its associated eigenvalue E_0. One can write the following expression considering that the value of the Hamiltonian a over the wavefunction b must be higher than the ground-state energy (variational theorem)

$$E_{0,a} < \langle \Psi_{0,b} | H_a | \Psi_{0,b} \rangle \tag{1.36}$$

and it can be rewritten as

$$\begin{aligned} E_{0,a} &< \langle \Psi_{0,b} | H_a - H_b + H_b | \Psi_{0,b} \rangle \\ E_{0,a} &< \langle \Psi_{0,b} | H_a - H_b | \Psi_{0,b} \rangle + \langle \Psi_{0,b} | H_b | \Psi_{0,b} \rangle \\ E_{0,a} &< \langle \Psi_{0,b} | v_a - v_b | \Psi_{0,b} \rangle + E_{0,b} \end{aligned} \tag{1.37}$$

this last equation can be rewritten in terms of the ground-state density since the potentials v are one-electron operators

$$E_{0,a} < \int [v_a(r) - v_b(r)]\, \rho(r) dr + E_{0,b} \tag{1.38}$$

where $E_{0,a}$ and $E_{0,b}$ are the ground state energies determined by H_a and H_b respectively. Since it has not made any distinction between a and b the equation can be also written as

$$E_{0,b} < \int [v_b(r) - v_a(r)]\, \rho(r) dr + E_{0,a} \tag{1.39}$$

and by adding the two previous equations one obtains

$$\begin{aligned} E_{0,a} + E_{0,b} &< E_{0,a} + E_{0,b} + \int \rho(r)[0] dr \\ E_{0,a} + E_{0,b} &< E_{0,a} + E_{0,b} \end{aligned} \tag{1.40}$$

by assuming that the ground-state densities associated with wavefunctions a and b are the same permits to eliminate the integrals as they must sum to zero. However, that assumption leads to an impossible result, the sum of the two energies is less than itself, indicating that the initial assumption was incorrect. Which implies that $v(r)$, and then the Hamiltonian, the wavefunction, the energy and all the other expected values are determined only by $\rho(r)$. Thus, the ground state energy is functional of $\rho(r)$

$$E_0 = E_v[\rho] \tag{1.41}$$

The second Hohenberg-Kohn theorem (Variational Theorem)

The first theorem explained how the electron density has a tremendous amount of information coded, however, it is unhelpful in providing any indication of how to predict the density of a system, it is then needed a means to optimize the fundamental quantity. Hohenberg and Kohn showed in a second theorem that the density obeys a variational principle; If the energy functional is applied to a one-

electron density different of the exact one-electron density, the energy obtained is higher or equal than the exact energy.

$$E_0 = E_v[\rho] \leq E_v[\rho'] \tag{1.42}$$

where ρ' is an approximate one-electron density of the chemical system, therefore there is an approximate wavefunction Ψ' of the molecule described by the Hamiltonian $\widehat{H}$. The energy functional applied to any electron density different from the exact electron density functional leads to an energy value higher than the exact one

$$E_v[\rho] = \langle \Psi' | \widehat{H} | \Psi' \rangle \geq E_0 = E_v[\rho] \tag{1.43}$$

the minimum of the energy functional is obtained when the functional is applied to the exact one-electron density. By applying the vibrational approach one can determine the exact one electron considering that first derivative of the energy functional respect to the one-electron density functional should be equal to zero

$$\frac{\delta E_v[\rho]}{\delta \rho} = 0 \tag{1.44}$$

The trial one-electron density function that leads to the minimum value of the energy functional is the trail function most similar to the exact one electron density.[12]

Kohn-Sham Method (Self-Consistent Methodology)

In order to find the exact electron density, it is needed to find the electron density that minimizes the energy of the chemical system (second theorem of Hohenberg-Kohn). The energy functional can be split in to

$$E_0 = E_v[\rho] = T[\rho] + V_{Ne}[\rho] + V_{ee}[\rho] \tag{1.45}$$

where $T[\rho]$ is the kinetic energy functional, $V_{Ne}[\rho]$ is the electron-nuclei attraction potential energy functional and $V_{ee}[\rho]$ is the electron-electron interaction potential energy functional. The exact expression to obtain the electron-nuclei attraction potential energy from the one-electron density is given by

$$V_{Ne}[\rho] = \int \rho(r) v(r) dr \tag{1.46}$$

and the sum of the kinetic energy functional and electron-electron interaction potential energy functional defines the Hohenberg-Kohn functional. The energy functional can be also written as

$$E_0 = E_v[\rho] = +V_{Ne}[\rho] + F_{HK}[\rho] \tag{1.47}$$

Even though the expression of $V_{Ne}[\rho]$ is known Eq. (1.46) the expression for the $F_{HK}[\rho]$ it is still unknown. Kohn and Sham developed a method to calculate $T[\rho]$ taking into account that the Hohenberg-Kohn functional is the sum of the kinetic energy functional, and the electron-electron interaction functional

$$F_{HK}[\rho] = T[\rho] + V_{ee}[\rho] \tag{1.48}$$

The approximation proposed by Kohn-Sham is to define a fictitious reference system formed by n electrons that do not interact with each other, but they interact with an external potential $v_s(r)$, which is defined in order to generate a ground state electron density identical to the exact electron density of the ground state of the chemical system under study. Since the density determines the position and atomic number of the nuclei, these quantities are necessarily identical in the non-interacting system and in the real system. So now considering the non-interacting system the energy functional looks like

$$E_v[\rho] = T_{ni}[\rho] + V_{Ne}[\rho] + V_{ee}[\rho] + \Delta T[\rho] + \Delta V_{ee}[\rho] \tag{1.49}$$

where the terms refer respectively to the kinetic energy of the non-interacting system, the nuclear-electron interaction, the classical electron-electron repulsion, the correction to the kinetic energy deriving from the interacting nature of the electrons, and all non-classical corrections to the electron-electron repulsion energy. For a non-interacting system, the kinetic energy is only the sum of the individual electronic kinetic energies. Considering now the orbital expression for the density, the energy functional can be rewritten as

$$\begin{aligned} E_v[\rho(r)] = \sum_i^N \left(\left\langle \chi_i \right| -\frac{1}{2}\nabla_i^2 \left| \chi_i \right\rangle - \left\langle \chi_i \right| \sum_k^{nuclei} \frac{Z_k}{|r_i - r_k|} \left| \chi_i \right\rangle \right) \\ + \sum_i^N \left\langle \chi_i \right| -\frac{1}{2} \int \frac{\rho(r')}{|r_i - r'|} dr' \left| \chi_i \right\rangle + E_{xc}[\rho(r)] \end{aligned} \tag{1.50}$$

where N is the number of electrons. The exact wavefunction can be expressed as the product of the one electron wavefunctions (i.e., the orbitals), the Slater

determinant is then the exact wavefunction of the reference system, thus the density can be simply defined as

$$\rho = \sum_{i=1}^{N} \langle \chi_i | \chi_i \rangle \tag{1.51}$$

Terms ΔT and ΔV_{ee} have been merged under the term E_{xc}, known as the exchange-correlation energy which includes not only the effects of quantum mechanical exchange and correlation, but also the correction for the classical self-interaction energy and for the difference in kinetic energy between the fictitious non-interacting system and the real one. The orbitals χ_i are then the n eigenfunctions of the one electron Hamiltonian operator h_i^{KS} with the lowest energy satisfying the eigenvalue equations

$$h_i^{KS} \chi_i = \varepsilon_i \chi_i \tag{1.52}$$

where the Kohn-Sham (KS) one-electron operator is defined as

$$h_i^{KS} = -\frac{1}{2}\nabla_i^2 - \sum_{k}^{nuclei} \frac{Z_k}{|r_i - r_k|} + \int \frac{\rho(r')}{|r_i - r'|} dr' + V_{XC} \tag{1.53}$$

where

$$V_{XC} = \frac{\delta E_{XC}}{\delta \rho} \tag{1.54}$$

the V_{XC} is described as the one-electron operator for which the expectation value of the KS Slater determinant is E_{XC} and it is a so-called functional derivative.

Since it was considered that the E which is being minimized is exact, the orbitals χ must provide the exact density, being these orbitals the ones that form the Slater-determinant eigenfunction for the separable non-interacting Hamiltonian defined as the sum of the Kohn-Sham operators i.e.

$$\sum_{i=1}^{N} h_i^{KS} |\chi_1 \chi_2 \dots \chi_n\rangle = \sum_{i=1}^{N} \varepsilon_i |\chi_1 \chi_2 \dots \chi_n\rangle \tag{1.55}$$

the previous equality corroborates that there is an internal consistency in the Kohn-Sham approach by considering a non-interacting system with a density identical to the one for the real system.

Basically, if one works with the exact exchange-correlation term would be able to predict the exact energy from the DFT calculation. However, the actual form of the functional corresponding to $E_{XC}[\rho]$ is not known. Thus, Hohenberg and Kohn proved the existence of an exact, unique density functional, however there is no prescription for how to find that functional. Various approximations to this energy functional have been developed, and their varying strength and weakness are the subject of many benchmarking studies in literature. These approximations are so-called density functionals, or more accurately exchange-correlation functionals. These density functionals can be approximated using not only explicit functions of the density but also functions of the gradients of the density and functions of the KS spin-orbitals. Moreover, the functions of the orbitals can be local if the energy is computed exclusively from the density at that position. On the other hand, they can be nonlocal when the energy at a point in space depend not only on the local value of the density, but on the extent to which the density is locally changing (i.e., the gradient of the density) Indeed, it has been demonstrated that the unknown exact function is nonlocal.[13]

Local Density Approximations (LDA)

In the Local Density Approximation (LDA) the density is treated as a uniform electron gas, or equivalently the density is considered a slowly varying function. In LDA the exchange-correlation energy functional can be decomposed into the exchange functional $E_x[\rho(r)]$ and the correlation functional $E_c[\rho(r)]$

$$E_{xc}[\rho(r)] = E_x[\rho(r)] + E_c[\rho(r)] \tag{1.56}$$

The earliest LDA method was proposed by Slater in 1951[14] and it is called $X\alpha$. This model is based on the electron gas model or uniform density, where the exchange energy functional is given by

$$E_x[\rho(r)] = -\frac{3}{2}\left(\frac{3}{4\pi}\right)^{\frac{1}{3}} \int \rho^{\frac{4}{3}}(r)dr \tag{1.56}$$

and, that the energy correlation functional is equal to zero being

$$E_{xc}[\rho(r)] = E_x^{LDA}[\rho(r)] = -\frac{3}{2}\left(\frac{3}{4\pi}\right)^{\frac{1}{3}} \int \rho^{\frac{4}{3}}(r)dr \tag{1.57}$$

This is indeed one of the simplest LDA methods, however posteriorly Vosko, Wilska and Nusair (VWN)[15] derived an expression for the $E_c[\rho(r)]$ functional for uniform density. DFT-LDA method that combines both Slater exchange functional (S) and the VWN correlation functional is called SVWN. As mentioned before, in LDA the density depends on a uniform electron gas, matter of fact this would mean that LDA is suitable for solid-state systems where the electron density varies only slowly. However, it shows a poor performance when working with molecular systems, LDA often overestimates bonding energies and underestimates bond lengths.

Generalized Gradient Approximation (GGA) and Hybrid Functionals

The electron density in molecular systems is rather uniform, for this reason LDA approaches have some limitations. A possible solution to this problem is consider that the correlation functional depends not only on the local value of the density, but on the extent to which the density is locally changing, i.e., the gradient of the density. The generalized gradient approximation GGA improves LDA approaches including in the formulas of $E_x[\rho(r)]$ and $E_c[\rho(r)]$ terms that depend on the module of the gradient of the one electron density $\nabla\rho(r)$

$$E_{xc}^{GGA}[\rho(r)] = E_{xc}^{LDA}[\rho(r)] + \Delta E_{xc}\left[\frac{|\nabla\rho(r)|}{\rho^{\frac{4}{3}}(r)}\right] \qquad (1.58)$$

where the dependence of the correction terms is on the dimensionless reduced gradient and not the absolute gradient.

The first widely popular GGA exchange functional was developed by Becke (abbreviated as "B").[16] This functional incorporates a single empirical parameter optimized by fitting to the exactly known exchange energies of the six noble gas atoms. Alternative GGA exchange functionals have been developed based on rational function expansions of the reduced gradient, these functionals do not contain empirically optimized parameters (such as PBE,[17] B86,[18] LG[19] and *m*PBE[20]). The most popular GGA correlation energy functionals are the ones developed by Perdew and Wang (PW91)[21] that use a different expression for the LDA correlation energy and do not contain empirical parameters. Another correlation energy functional also widely used is the one developed by Lee, Yang and Parr (LYP),[22] which does not correct the LDA expression but instead computes

the correlation energy *in toto* (in total). It contains however four empirical parameters that fit to the helium atom. Typically, in literature one works with a complete specification of the exchange and correlation functionals leading to the BLYP and BPW91 DFT methods.

Finally, GGA exchange functional expression can include part of the exact HF exchange energy, these functionals are named hybrid functionals. The most commonly used hybrid method was proposed by Becke, B3, in 1993.[23] Which expression is

$$\begin{aligned} E_{xc}^{B3}[\rho(r)] = E_x^{LDA}[\rho(r)] + \alpha_0(E_x^{HF}[\rho(r)] - E_x^{LDA}[\rho(r)]) \\ + \alpha_x(E_x^{B}[\rho(r)] - E_x^{LDA}[\rho(r)]) + E_c^{LDA}[\rho(r)] \\ + \alpha_c(E_c^{GGA}[\rho(r)] - E_c^{LDA}[\rho(r)]) \end{aligned} \quad (1.59)$$

where α_0, α_x and α_c parameters are fitted to reproduce the experimental data.

B3 method uses correlation functionals such as PW91 functional and LYP functional obtaining the correspondent B3PW91[23] and B3LYP,[24] this last one indeed is the method most used in DFT approaches.

Summarizing, DFT includes the electron correlation effects in the electronic structure and expected values with a low computational cost, one can determine geometries, frequencies, activation barriers and dipole moments much more accurate than HF with a similar computational cost as well as one can correctly describe organometallic complexes which are not properly described by HF method. However, DFT method also present some disadvantages. The main drawback is that does not exist a systematic procedure to improve DFT results. Moreover, DFT incorrectly describe systems with weak interactions for instance systems presenting van der Waals interactions, the dissociation of molecules in radical ionic species and the one-electron systems like the hydrogen atom. Even though DFT presents some disadvantages, it is particularly advantageous for studying large molecular and periodic systems such as MOFs as well as systems containing heavy atoms, because the computational cost for solving the KS equation is low compared to HF methods, and the cost of DFT computations scales much more slowly as the system size increases.

In the previous annex it has been described in *grosso modo* the basics of the computational chemistry in order to contextualize the methodology applied on this

manuscript. All the contents discussed above are based on recent editions of excellent quantum chemistry, computational chemistry and molecular modelling textbooks.[5–7]

References

1. Pople, J. A., Santry, D. P. & Segal, G. A. *J. Chem. Phys.* **43**, S129–S135 (1965).
2. Pople, J. A. & Segal, G. A. *J. Chem. Phys.* **43**, S136–S151 (1965).
3. Pariser, R. & Parr, R. G. *J. Chem. Phys.* **21**, 466–471 (1953).
4. Pariser, R. & Parr, R. G. *J. Chem. Phys.* **21**, 767–776 (1953).
5. Szabo, A. & Ostlund, N. L. *Modern Quantum Chemistry: Introduction to Advanced Electronic Structure Theory*; Dover Publishing: Mineaola, NY, 1996.
6. Cramer, C. J. *Essentials of Computational Chemistry Theories and Models Second Edition*; Wiley: Chichester, 2004.
7. Strich, A. *Quantum Chemistry, 4th ed.*; Prentice Hall: Englewood Cliffs, NJ, 1992.
8. Binkley, J. S. & Pople, J. A. *Int. J. Quantum Chem.* **9**, 229–236 (1975).
9. Møller, C. & Plesset, M. S. *Phys. Rev.* **46**, 618–622 (1934).
10. Raghavachari, K. & Anderson, J. B. *J. Phys. Chem.* **100**, 12960–12973 (1996).
11. Raghavachari, K., Trucks, G. W., Pople, J. A. & Head-Gordon, M. *Chem. Phys. Lett.* **157**, 479–483 (1989).
12. Hohenberg, P. & Kohn, W. *Phys. Rev.* **136**, B864 (1964).
13. Kohn, W. & Sham, L. J. *Phys. Rev.* **140**, A1133 (1965).
14. Slater, J. C. *Phys. Rev.* **81**, 385–390 (1951).
15. Vosko, S. H., Wilk, L. & Nusair, M. *Can. J. Phys.* **58**, 1200–1211 (1980).
16. Becke, A. D. *Phys. Rev. A* **38**, 3098–3100 (1988).

17. Perdew, J. P., Burke, K. & Ernzerhof, M. *Phys. Rev. Lett.* **77**, 3865–3868 (1996).

18. Becke, A. D. *J. Chem. Phys.* **84**, 4524–4529 (1986).

19. Lacks, D. J. & Gordon, R. G. *Phys. Rev. A* **47**, 4681–4690 (1993).

20. Adamo, C. & Barone, V. *J. Chem. Phys.* **116**, 5933–5940 (2002).

21. Perdew, J. P. *Electronic Structure of Solids '91*; Aka- demie Verlag, Berlin, 1991.

22. Lee, C., Yang, W. & Parr, R. G. *Phys. Rev. B* **37**, 785–789 (1988).

23. Becke, A. D. *J. Chem. Phys.* **98**, 1372–1377 (1993).

24. Stephens, P. J., Devlin, F. J., Chabalowski, C. F. & Frisch, M. J. *J. Phys. Chem.* **98**, 11623–11627 (1994).